Abstract Book

17th Biometal

25-30 AUGUST, 2025

Grand Hôtel San Michele,
Cetraro, CS, Italy

BIODEGRADABLE METALS

17th Biometal

25-30 AUGUST, 2025

Grand Hôtel San Michele, Cetraro, CS, Italy

Symposium Co-Chairs:

Diego Mantovani
Laval University, Canada

Frank Witte
Berlin Charité, Germany

Chris Hyung-Seop Han
Korean Institute of Science and Technology, South Korea

Sofia Gambaro
National Research Council, Italy

Yufeng Zheng
Peking University, China

Mark Staiger
University of Canterbury, New Zealand

Abstract Book Committee:

Carlos Henrique Michelin Beraldo
Laval University, Canada

Alexis Levasseur
Conferium

Carlos Andrés Cuao Moreu
Laval University, Canada

Iria Lucena Araujo
Laval University, Canada

For any changes, corrections, updates or any other matter that you would like to make in your abstract, please contact carlos-henrique.michelin-beraldo.1@ulaval.ca no later than September 15, 2025. After that date, this abstract book will be archived online on Biometal website (/past editions).

elecell Hope for Healing

BioActiveMetals Innovation in Metallic Biomaterials

meo. Inspiring Materials.

medical magnesium

UNIVERSITÉ LAVAL

CHARITÉ UNIVERSITÄTSMEDIZIN BERLIN

KeAi CHINESE ROOTS GLOBAL IMPACT

PEKING UNIVERSITY

Informations about the Abstract book, please contact:
carlos-henrique.michelin-beraldo.1@ulaval.ca

Biometal2025 was proudly sponsored by

elecell

Hope for Healing

BioActiveMetals

Innovation in Metallic Biomaterials

meo.

Inspiring Materials.

medical magnesium

Informations about the Abstract book, please contact:
carlos-henrique.michelin-beraldo.1@ulaval.ca

Cooperating Organizations

Informations about the Abstract book, please contact:
carlos-henrique.michelin-beraldo.1@ulaval.ca

Workshop

Tuesday,
August 26th, 2025

elecell
Hope for Healing

BioActiveMetals
Innovation in Metallic Biomaterials

meo.
Inspiring Materials.

medical magnesium

UNIVERSITÉ LAVAL

CHARITÉ
UNIVERSITÄTSMEDIZIN BERLIN

KeAi
CHINESE ROOTS GLOBAL IMPACT

PEKING UNIVERSITY

European Cells and Materials Vol. NN. Suppl. N, 20xx (page htu) ISSN 1473-2262

Development of bioabsorbable metals for endovascular medical devices: a presentation of the BIOMEND Doctoral Network

A Mainguy[1,2,3], K Mashoufi[1,2,3], J Cruz[1,4,5], M Thiel[6,7], S Schmidt[1,6], V Squartecchia[1,2,3], D Blunda[1,6,8], J Sygor[1,9,10], A Di Lorenzo[5,7,11], M Bittner[6,7], M Rodrigues[5,7,11], S O'Connell[6,12], A Fathy[13,14], A Panagi[15,16], T Vaughan[6], A Kopp[1,7,16]

[1]Meotec GmbH, Aachen, Germany, [2]IMDEA Materials Institute, Getafe, Spain, [3]Universitat Politecnica de Madrid, Madrid, Spain, [4]Lehrstuhl für Lasertechnik, Aachen, Germany, [5]RWTH University, Aachen, Germany, [6]University of Galway, Galway, Ireland, [7]Fibrothelium GmbH, Aachen, Germany, [8]B. Braun, Melsungen, Germany, [9]University of Eastern Finland, Kuopio, Finland, [10]Abiomed GmbH, Aachen, German, [11]BioTex – Biohybrid & Medical Textiles, Aachen, Germany, [12]Hydrumedical SA, Guimarães, Portugal, [13]Embocraft GmbH, Aachen, Germany, [14]OVGU, Magdeburg, Germany, [15]MERLN, Maastricht University, Maastricht, Netherlands, [16]Medical Magnesium GmbH, Aachen, Germany

INTRODUCTION: BIOMEND is a Doctoral Network focused on three major axes in bioresorbable devices. The first axis (WP1) is the development of alloying systems and manufacturing methods for the production of endovascular medical devices (EMD). The second axis (WP2) is focused on the design of EMD prototypes using experimental and analytical approaches. The third axis (WP3) consists in the preclinical validation of afore-mentioned EMD prototypes.

METHODS: PhD candidates of WP1 are focused on producing stent preforms. To achieve this, they are using gravity permanent mold casting of magnesium (Mg) and zinc (Zn) alloys are considered for their biocompatibility and favorable corrosion properties. This is followed by double extrusion of the cast material. After rods are produced with the first extrusion, the second extrusion is either a wire extrusion to achieve thin wires for wire-braided devices, or a microtube extrusion to produce laser-cut devices. Laser cutting and wire braiding are also explored within the scope of the BIOMEND project. Within WP1, the degradation behavior of these materials is also investigated, both in *in silico* simulations and in experimental setups.

Fig. 1: Graphical representation of WP1 workflow

In WP2, the devices developed by the PhD students are strongly interconnected with the methods investigated in WP1. A coronary stent, aortic stent-graft and large bore access closure will all benefit from the development of laser-cut preforms. A flow-diverting stent, intracranial stent and urethral stent will take advantage of the latest advances in wire braiding methods. A device for anastomosis, along with other devices, will also gain from the development of Mg alloys with increased corrosion resistance.

On one hand, some of these devices are developed with the help of simulations for mechanical performance, e.g. radial strength, crimping and crush resistance. On the other hand, experimental methods are used to validate simulations and conduct in-vitro biocompatibility studies. Bench testing will assess mechanical performance and corrosion behavior of devices.

WP3 focuses on testing the in-vivo biocompatibility and functional performance of devices developed within WP2. Small animal models will be used to assess the performance of endovascular devices and their bioresorbability. Histology and imaging techniques such as intravascular ultrasound (IVUS) and angiography are in the scope of the BIOMEND project.

RESULTS: Preliminary results will be presented individually by the PhD students present at the Biometals conference.

ACKNOWLEDGEMENTS: This project has received funding from the European Union's EU Framework Programme for Research and Innovation Europe Horizon. Grant Agreement n°101120006.

European Cells and Materials Vol. NN. Suppl. N, 20xx (page htu) ISSN 1473-2262

Resorbable magnesium alloy implants for cranial applications

J Skoch[1,2], B Owen[2], A Raut[3], B Kraus[4], V Shanov[3,4]

[1]Division of Neurosurgery, Cincinnati Children's Hospital Medical Center, Ohio, USA. [2]Department of Neurosurgery, University of Cincinnati, Ohio, USA. [3]Department of Mechanical and Materials Engineering, University of Cincinnati, Ohio, USA. [4]Department of Chemical and Environmental Engineering, University of Cincinnati, Ohio, USA.

INTRODUCTION: Craniosynostosis is a congenital condition characterized by the premature fusion of cranial sutures in newborns. It can cause significant cosmetic deformity and impact normal brain growth. This disease occurs with an incidence of 1/2500 live births. An increasingly popular FDA approved surgical treatment involves implantation of stainless steel (SS) springs within a minimally invasive craniotomy to expand the skull. This necessitates additional surgery to remove these scarred implants from just above the brain surface[1]. We have developed prototypes of magnesium alloy biodegradable springs that match the opening force and expansion distance of conventional SS implants with the goal of avoiding secondary surgeries[2].

METHODS: WE43 magnesium alloy springs were made using precision manufacturing methods which included controlled rod bending, waterjet, Electric Discharge Machining (EDM), milling, and 3D printing of PLLA to produce resorbable skull attachments for the springs. The obtained implants were compressed to 1.5 cm distance between the endpoints of the spring arms to ensure mechanical stability and match the compression of the gold standard SS cranial springs.

RESULTS: Multiple implant designs have been achieved that match or exceed the spring force (4-10N) and post compressive opening width (3.5-5.5cm) of comparative conventional stainless-steel implants. A variety of spring shapes that meet these comparative criteria have been fashioned for in vitro stress and degradation testing (***Fig. 1***)[3]

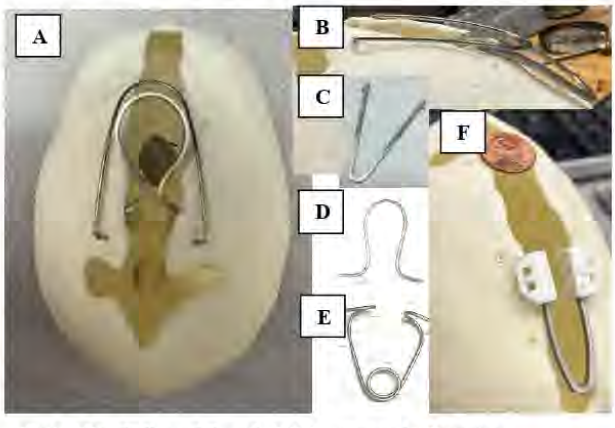

Fig1: (A) skull model with FDA approved SS spring (outer) and WE43 spring(inner) (B) side view of SS spring (left) and WE43 spring on curved skull model (C-E) additional spring shapes tested (F) WE43 with attached PLLA skull clamps for safety and stability

DISCUSSION & CONCLUSIONS: While the surgical results for spring augmented craniosynostosis surgery are excellent, the risks, family stress, cost, and inconvenience of secondary surgery limit widespread adoption of this technique. We now have met sufficient criteria for a potentially clinically applicable prototype of a WE43 resorbable implant, have designed a live large animal (*Ovis Aries*) survival surgery protocol and are awaiting approval to evaluate for safety and *in vivo* degradation parameters.

REFERENCES: [1]Campbell C, Lin K. (2009) Complications of rigid internal fixation. Craniomaxillofac Trauma Reconstr. 2:41–7. [2]Zhao, D., Witte, F., Lu, F., Wang, J., Li, J., Qin, L. (2017). Current Status on Clinical Applications of Magnesium-Based Orthopaedic Implants: A Review from Clinical Translational Perspective. *Biomaterials 112 287-302.* [3]ASTM G0031-21. Standard Guide for Laboratory Immersion Corrosion Testing of Metals.

ACKNOWLEDGEMENTS: The authors appreciate the financial support of the Cincinnati Children's Hospital Medical Center Junior Cooperative Society. This template was modified with kind permission from eCM Journal.

European Cells and Materials Vol. NN. Suppl. N, 20xx (page htu) ISSN 1473-2262

Engineering biodegradable WE43 springs for craniosynostosis repair

B Kraus[1], A Raut[1], J Skoch[2], V Shanov[1], B Owen[2]

[1] *Nanoworld Laboratory, University of Cincinnati, Cincinnati, OH.* [2] *Department of Neurosurgery, Cincinnati Children's Hospital Medical Center, Cincinnati, OH*

INTRODUCTION: Craniosynostosis is a congenital condition characterized by the premature fusion of cranial sutures in newborns. Such birth defects are frequently treated surgically, often requiring inert medical implants [1]. Utilizing biodegradable implants allows for controlled mechanical support while naturally degrading over time. By leveraging the unique properties of WE43 and applying tailored biomechanical design, we aim to improve both the effectiveness and biocompatibility of springs used in these procedures.

METHODS: Variety of fabricating methods were employed to process different forms of WE43 alloy and create optimal springs mimicking the stainless-steel commercial implants. Besides rod bending, WE43 plates were formed into springs using computer-aided manufacturing. Waterjet Machining (WM) and Electric Discharge Machining (EDM) following AutoCAD-generated designs were utilized due to the material's flammability. However, with proper safety procedures, dry milling was employed thus avoiding the rapid oxidation of the WE43 alloy in aqueous mediums. 3D printing techniques were used with biodegradable PLLA filaments to produce skull attachments for the springs. Springs were compressed to 1.5 cm to determine their corrosion under stress and force degradation over time in custom-designed apparatuses. Fluorination of the magnesium alloy in 0.1M KF and deposition of Parylene-C coating on the springs were applied as separate approaches to delaying corrosion. Finite Elemental Analysis (FEA) via Siemens NX and Siemens Simcenter software were employed to refine the spring designs.

RESULTS: Springs produced through WM and EDM methods were more susceptible to early corrosion due to the water exposure compared to dry-milled springs. Application of Parylene-C and fluorinated films inhibited corrosion to varying degrees. The V-Leaf design cut from 2 mm plates (***Fig. 1a)*** balanced force output with minimal plastic deformation. Springs with various designs exhibited a 1.5–2 N force loss and ~62% reduction in opening width after pre-conditioning, however remained stable thereafter.

Fig. 1: (A) Two springs machined with a Waterjet: one 2.3-2.3-1.4 WE43 Short V-Leaf and another 2.4-2.4-1.4 WE43 Long V-Leaf. (B) Apparatus for quantifying corrosion of V-Leaf spring under applied compressive stress. (C) Von Mises stress plot of a 2.3-2.3-1.4 Short V-Leaf spring.

FEA simulations ***(Fig. 1c)*** revealed stress concentrations at the bend origins of the springs. Furthermore, a correlation between localized corrosion and areas of high stress was observed repeatedly using the in-house made apparatus ***(Fig. 1b)***. Adding a taper along the spring legs reduced weight without compromising structural integrity and force output at 1.5 cm compression. Scaled springs maintained proportional opening widths post-conditioning, supporting adaptability to different skull shapes and sizes.

DISCUSSION & CONCLUSIONS: The tapered V-Leaf design effectively reduces spring weight without compromising force output. The final geometry was inspired by observations of plastic deformation, and its scalable design can be utilized for a range of skull anatomies. FEA simulations refined the final spring designs. Parylene-C and fluorinated films delay corrosion without compromising force output. Finally, 3D-printed PLLA skull attachments provided a stable interface between the spring and skull.

REFERENCES: [1]Division of Plastic, Reconstructive and Oral Surgery. (2025). *Craniosynostosis surgery*. Children's Hospital of Philadelphia.

ACKNOWLEDGEMENTS: The authors appreciate the financial support of the Cincinnati Children's Hospital Medical Center Junior Cooperative Society. This template was modified with kind permission from eCM Journal.

European Cells and Materials Vol. NN. Suppl. N, 20xx (page htu)
ISSN 1473-2262

Biocompatible therapeutic platform: plant-derived nanovesicles for ROS modulation in chronic inflammatory diseases

Yuna Jung[1], Sun Hee Lee[1], Hyung-Seop Han[1*]

[1]*Biomaterials Research Center, Biomedical Research Division, Korea Institute of Science and Technology (KIST), Seoul, Republic of Korea*

INTRODUCTION: Chronic inflammatory pathologies, such as diabetic foot ulcers (DFU), are predominantly governed by persistent oxidative stress and impaired mechanisms of tissue regeneration.[1] Recently, plant-derived extracellular nanovesicles (PDEVs) have gained the spotlight as natural nanocarriers with the highly biocompatible manner and intrinsic therapeutic effects. These vesicles typically include various antioxidants, anti-inflammatory and bioactive molecules such as polyphenols, flavonoids, proteins, and membrane structures that facilitate cellular internalization. This study proposes a new therapeutic platform for chronic wounds, highlighting their capacity to regulate reactive oxygen species (ROS), augment angiogenesis, and promote tissue repair within diabetic microenvironments.

METHODS: The vesicles were separated from edible plants (*Petroselinum crispum*.) and purified using ultrafiltration and size exclusion chromatography. After the purification step, the basic properties of PDEVs such as the size, concentration, morphology, and protein content were analyzed. The ROS scavenging ability toward H2O2 was tested via a peroxidase (POD) kit and DCF-DA assays. Wound closure effects were observed in a high-glucose Human Umbilical Vein Endothelial Cells (HUVEC) model simulating diabetic conditions. The cellular uptake and protective potential of PDEVs were examined in both normal and ischemic conditions. Furthermore, the antibacterial properties of PDEVs were assessed by a minimal inhibitory concentration (MIC) test against representative bacteria (8 strains) linked to diabetic infections.

RESULTS: Isolated PDEVs showed uniform size distribution from 130 to 150 nm and a negative surface charge (-28 mV), with circular vesicular morphology. SEC fractionation between F1 and F7 exhibited vesicle-rich peaks with elevated particle-to-protein ratios. In high-glucose HUVECs, PDEVs significantly enhanced cell proliferation and declined intracellular ROS levels by up to 73%. Also, efficient cellular uptake was confirmed through the fluorescent labeling method. Finally, rapid wound closure (~6 h) in fibroblasts was observed in a dose-dependent manner under diabetic conditions.

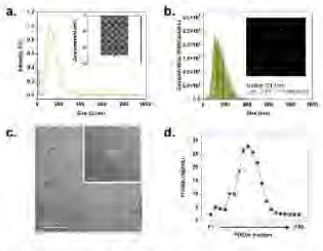

Fig. 1: Properties of PDEVs, (a) hydrodynamic size and zeta-potential, (b) NTA particle distribution and concentration, (c) TEM image, (d) BCA assay-based protein content across SEC fractions.

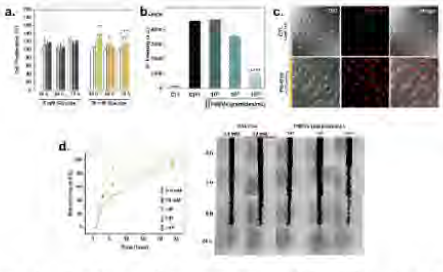

Fig. 2: Biological properties of PDEVs, (a) Cell proliferation in high-glucose HUVECs, (b) DCF-DA assay, (c) cellular uptake of DiI-labeled PDEVs, (d) Wound closure in HG fibroblasts.

DISCUSSION & CONCLUSIONS: We demonstrated the therapeutic potency of a PDEV-based therapeutic platform within a chronic inflammatory wound model. This system offers superior biosafety with substitutes for synthetic nanocarriers and reveals significant potential in mitigating diabetic complications through ROS modulation and enhancement of cellular protection under the HG environment.

REFERENCES: [1]W. J. Jeffcoate et al., (2018) Diabetes Care, **41**, 645–652

ACKNOWLEDGEMENTS: This work was supported by the Sejong Science Fellowship [grant number NRF-RS-2024-00353178] through the National Research Foundation of Korea (NRF), funded by the Ministry of Science and ICT (MSIT).

17th Biometal
25-30 AUGUST, 2025
Grand Hôtel San Michele,
Cetraro, CS, Italy

European Cells and Materials Vol. NN. Suppl. N, 20xx (page htu) ISSN 1473-2262

Machine learning approach for predicting the corrosion behavior of coated magnesium-based materials

Abdelrahman Amin[1], Ibrahim Awad[2], Hamdy Ibrahim[1]

[1]Department of Mechanical Engineering - The University of Tennessee at Chattanooga

[2]Independent Researcher, New York, USA

INTRODUCTION: Magnesium alloys have gained significant interest as new orthopedic implants due to their potential to address issues associated with traditional solutions. However, concerns arise regarding their degradation rate, making it crucial to understand the advantages and challenges of magnesium implementation, as well as strategies to mitigate these issues for optimal outcomes. One effective approach is coating the magnesium substrate with a micro-arc oxidation (MAO) layer, which significantly slows down the degradation process. Although experiments have proven the efficacy of this method in studying corrosion, there remains a need to identify more time- and cost-effective solutions. Finite element analysis offers a potential solution, but the complexity of the factors involved in the MAO process makes machine learning methods a more efficient and time-saving alternative for predicting corrosion behavior. This study aims to expand existing machine learning models from predicting corrosion in uncoated magnesium to innovatively forecasting the degradation of MAO-coated samples, focusing on predicting corrosion current density and corrosion potential based on electrochemical corrosion test data.

METHODS: The key factors involved in the MAO coating process were identified and relevant data was collected from the literature, with more focus on electrochemical corrosion test results, particularly potentiodynamic polarization (PDP) corrosion test. The primary predictive variables were derived from the parameters of the MAO process, while the response variables were the PDP corrosion potential and corrosion current density.

To determine the most accurate predictive model, we evaluated and compared several machine learning algorithms using Python with 80% training and 20% testing data. Once the most effective model was identified, we applied two different predictive approaches for comparison: (i) Exact value prediction, and (ii) Logarithmic value prediction. The model's performance was assessed by comparing the predicted values with the actual test results, using the Mean Absolute Error (MAE) percentage as the primary evaluation metric.

RESULTS: The Random Forest prediction method identifies the stone related to corrosion current prediction due to its wide range. However, the log prediction method addresses the weaknesses observed in the exact prediction method, as demonstrated in Figure 1. Moreover, the Mean Absolute Error (MAE) confirms the model's accuracy. Corrosion Current Density and Corrosion Potential predicted from the log approach were more accurate compared to the obtained values from the exact approach.

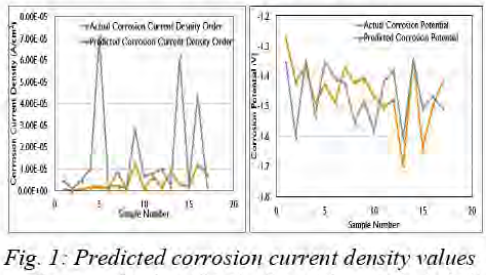

Fig. 1: Predicted corrosion current density values vs the actual values for the logarithm method (left) and exact method (right).

DISCUSSION & CONCLUSIONS: Our study aims to reduce the time required for conducting experimental testing on MAO-coated magnesium-based samples by utilizing a machine learning model that overcomes the limitations of previous models.

The log prediction method demonstrates a significant ability to predict the log of the corrosion current density, as the exact numerical value can vary between individuals. Additionally, the log prediction method effectively predicts corrosion potential with a minimal MAE.

REFERENCES: M. Lu, Zhenxin, Shujing Si, Keying He, Yang Ren, Shuo Li, Shuman Zhang, Yi Fu et al. "Prediction of Mg alloy corrosion based on machine learning models." Advances in Materials Science and Engineering 2022, no. 1 (2022): 9597155.

ACKNOWLEDGEMENTS: The authors acknowledge the support of the National Science Foundation through (NSF) to complete this work.

Metals

Wednesday,
August 27th, 2025

elecell
Hope for Healing

BioActiveMetals
Innovation in Metallic Biomaterials

meo.
Inspiring Materials.

medical magnesium

UNIVERSITÉ LAVAL

CHARITÉ
UNIVERSITÄTSMEDIZIN BERLIN

KeAi
CHINESE ROOTS GLOBAL IMPACT

PEKING UNIVERSITY

European Cells and Materials Vol. NN. Suppl. N, 20xx (page htu) ISSN 1473-2262

Phenomenological studies on powder bed fusion – laser beam processing of biodegradable Mg alloys

F D'Elia

Division of Biomedical Engineering, Department of Materials Science and Engineering, Uppsala University, Uppsala, Sweden.

INTRODUCTION: Powder Bed Fusion – Laser Beam (PBF-LB), as an additive manufacturing (AM) process, enables production of tailored bone implants with complex structures, designed for increased bone ingrowth [1]. As Mg alloys are already used in bone screws, PBF-LB of the same could make personalized, biodegradable implants for the improved healing of large bone defects possible. Nevertheless, there remains numerous challenges regarding printability, primarily due to oxide formation during atomization of powder feedstock and PBF-LB processing itself. Further, while the mechanical properties of AM Mg alloys are, for the most part, up to par with those required for bone implants, challenges in achieving the necessary degradation rates linger, and ultimately impact clinical implementation. In this context, this work provides a detailed overview of printability, microstructure formation, and material properties for a series of Mg alloys produced by PBF-LB, showcasing both opportunities and challenges, on the path towards clinical implementation. Insight into future investigations is also presented.

METHODS: Three Mg alloys (i.e., WE43, MgCaZn, MgLi) were fabricated by PBF-LB using either an EOS M100 (EOS GmbH, Germany) or an Aconity MIDI (Aconity GmbH, Germany). Sample characterisation included microscopy (i.e., optical, SEM, EBSD), mechanical testing (i.e., tension, compression, hardness) and evaluation of corrosion properties (i.e., hydrogen evolution, PDP). For the latter, advanced methods, such as acoustic emission, were also used together with SEM to identify localised corrosion mechanisms in both bulk and porous structures (i.e., lattices, triply periodic minimal surfaces; TPMS). Computational fluid dynamics (CFD) modelling, coupled with in-depth SEM, helped establish the interplay between fluid flow, and thermal history, ultimately determining overall influence on final microstructure.

RESULTS: Variations in printability were observed for the different alloys, with WE43 achieving highest sample densities (e.g., 99.5%). These variations were linked to microstructure, for which the presence of columnar dendrites, and the extent of secondary phase precipitation, were key factors dictating sample quality among the alloys. In WE43, two distinct sub-grain structures (i.e., equiaxed dendrites, and cellular grains) were identified, whose formation during PBF-LB was dependent on melting mode (i.e., conduction, keyhole), and resulting fluid flow patterns (e.g., Marangoni flow), as determined by the CFD model [2]. The significance of such substructures is their impact on material properties, where e.g., dendritic microstructures led to higher mechanical strength but reduced corrosion resistance [3]. Component design also influenced degradation and mechanical properties, as distinct differences were seen for strut-based lattices and TPMS structures (Fig. 1). However, irrespective of alloy composition, degradation rates of AM alloys remain higher than those of conventionally produced counterparts.

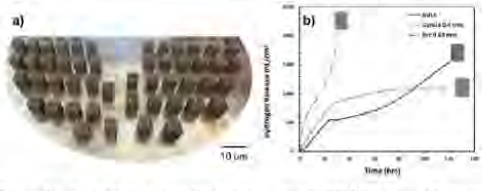

Fig. 1: a) Strut-based lattices and TPMS structures produced by PBF-LB, and b) resulting hydrogen evolution measurements of representative samples.

DISCUSSION & CONCLUSIONS:

Despite the challenge in obtaining the degradation rates of conventionally produced Mg alloys, the results demonstrate opportunities for control of material properties in PBF-LB Mg alloys through design of microstructure and component geometry. Ongoing investigations aim to alleviate issues associated with micro-galvanic corrosion induced by secondary phases, and localised attack in complex structures triggered by stress concentrations. Future studies are geared towards post-processing (e.g., HIPing) as a means to further tailor microstructure and material properties.

REFERENCES: [1] Qin et al. (2019) *Acta Biomater* **98**:3-22. [2] D'Elia et al. (2025) *Mater Des* **253**:113925. [3] Nilsson Åhman et al. (2024) *Mater Today Commun* **39**:108979.

ACKNOWLEDGEMENTS: This work was funded by VINNOVA, SSF and the EU.

European Cells and Materials Vol. NN. Suppl. N, 20xx (page htu) ISSN 1473-2262

Additive manufacturing anatomical magnesium alloy prosthesis for repairing tibial plateau fracture.

Yun Tian[1], Bingchuan Liu[1],Zhengguang Wang[1],Chaoxin Wang[1], Peng Wen[2], Yufeng Zheng[3]

[1] Department of Orthopedics, Peking University Third Hospital, Beijing, China.[2]Department of Mechanical Engineering, Tsinghua University, Beijing. [3]Department of Materials Science and Engineering, Peking University, Beijing

INTRODUCTION: Periarticular fractures with bone defects like tibial plateau fracture are common and complicated diseases. The existing autogenous, artificial, and allogeneic bones are insufficient in anatomical shape matching and overall support capacity. Additive manufacturing of magnesium(Mg) alloy with lattice structures provides the feasibility of realizing bone defect prostheses with personalized and biodegradable functions. This study aimed to systematically evaluate the additive manufacturing mg alloy prostheses in addressing periarticular bone defect repair(tibial plateau fracture).

METHODS: (1) WE43 powder was composed of 3.87 % Y, 2.24 % Nd, 1.16 % Gd, 0.39 % Zr, and balance Mg. A compact L-PBF machine (BLT S210, China) was used to additively manufacture WE43 porous scaffolds.Improving corrosion resistance of additively manufactured WE43 alloy by high-temperature oxidation(HTO)[1]. (2) We conducted a prospective study on patients with periarticular fractures(tibial plateau fracture and bone defects)treated at the Peking University Third Hospital between June 2022 and May 2025. Sixty patients(Thirty patients for each group) with periarticular fractures and bone defects were enrolled in the study, and Mg alloy prostheses were used for internal support combined with steel plate fixation to repair the fracture and bone defects.Hematological examinations were performed in the early postoperative period, X-ray examinations were performed in the long-term postoperative follow-up. Postoperative complications, including infection, failure of internal fixation and malunion, were recorded during the follow-up. The visual analogue scale (VAS) was used to evaluate postoperative pain perceived by the patients, and the the Hospital for Special Surgery Knee Score(HHS) was used to evaluate their postoperative function.

RESULTS: HTO can enhance the corrosion resistance of additive manufacture mg alloy prostheses. In the study of 30 patients with tibial plateau fracture and bone defects, all patients achieved bone healing with an average healing time of 3 months. Hydrogen can be seen in the X ray to precipitate in soft tissues from the 1months, and hydrogen can be absorbed after about 2 months. The Mg alloy prostheses can maintain a support time of over 6 months. All patients achieved good fracture alignment and bone defect repair, and imaging examination showed that the Mg prosthesis degraded gradually with fully bone defect repair in the one year.

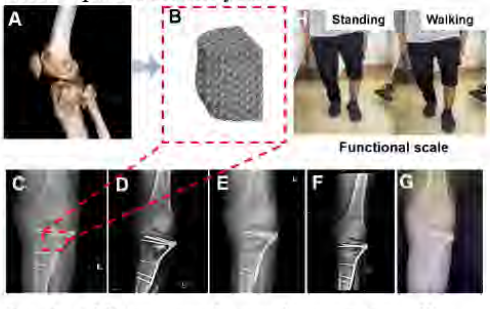

Fig. 1: Additive manufactured magnesium alloy prosthesis for the treatment of tibial plateau fracture.(A)The preoperative 3D CT reconstruction of a 59-year-old male patient with tibial plateau fracture(Schatzker:VI，AO:41C3.1). (B) The fabrication ofAdditive manufacturing Mg alloy (C)Postoperative X-ray scans. (1st day). (D) Postoperative X-ray image (1st month).(E) Postoperative X-ray image (3th month).(F) Postoperative X-ray image (6th month).(G) Postoperative X-ray image (1 years).(H)The lower limbs functional state of the patient.

DISCUSSION & CONCLUSIONS: The use of additive manufacturing Mg alloy anatomical support prostheses can achieve longitudinal conduction at the center of the fracture area, which is more in line with the mechanical conduction characteristics of bone structure. The results showed that biodegradable Mg prosthesis could be effectively used in the clinical treatment of periarticular fractures with bone defects, ensuring safety and satisfactory postoperative functional recovery.

ACKNOWLEDGEMENTS: This work was funded by the National Natural Science Foundation of China (82172065,82372092).This work was funded by the Capital's Funds for Health Improvement and Research (2024-1-4092).

European Cells and Materials Vol. NN. Suppl. N, 20xx (page htu)
ISSN 1473-2262

Additively manufactured biodegradable Zn-Mn-based implants with an unprecedented balance of strength and ductility

C Huang[1], Y Li[1], L Wang[1]

[1] *Beijing Advanced Innovation Center for Materials Genome Engineering, School of Materials Science and Engineering, University of Science and Technology Beijing, 30 Xueyuan Road, Haidian District, Beijing 100083, China.*

INTRODUCTION: Additively manufactured (AM) biodegradable zinc alloys hold huge potential as promising candidates for bone defect and fracture repair, thanks to their suitable biodegradation rates and acceptable biocompatibility. However, the mechanical properties of AM zinc alloys developed so far, ductility in particular, fall short of the requirements for bone repair.

METHODS: Cylindrical (Φ10 × 10 mm) and flat (60 mm × 10 mm × 10 mm) Zn-Mn and Zn-Mn-Mg alloy specimens were fabricated using an LPBF machine (SLM 125 HL, SLM Solution Group AG, Germany) in a closed build chamber with an argon shielding gas atmosphere and a residual oxygen level below 30 ppm.

Electron back-scattered diffraction (EBSD) and transmission electron microscope (TEM) was carried out to investigate the grain structure. Mechanical tests, including hardness, tension, compression, and three-point bending, were performed on Zn-Mn and Zn-Mn-Mg alloy specimens. *In vitro* immersion tests of the specimen were performed in the SBF at 37 °C (pH 7.4) for up to 28 days.

RESULTS: The LPBF Zn-Mn-Mg alloy exhibited an extraordinary balance of strength and ductility, with an ultimate tensile strength of 289 MPa, yield strength of 213.5 MPa, and elongation over 20 %, outperforming all previously reported AM zinc alloys. The simultaneously enhanced strength and ductility of the ternary alloy were attributed to the strong grain-refining effect of the Mg_2Zn_{11} second phase and the synthetic strengthening caused by the dispersion of the $MnZn_{13}$ and Mg_2Zn_{11} second phases inside the grains and at the grain boundaries. In addition, both alloys had similar rates of in vitro biodegradation (~0.15 mm/year), properly aligned with the bone remodeling process, while also demonstrating favorable biocompatibility and upregulating multiple osteogenic markers. The Zn-Mn-Mg alloy showed even better osteogenic potential than the Zn-Mn alloy, owing to the addition of Mg. The combined attributes of the LPBF Zn-Mn-Mg ternary alloy indicated huge potential for its use as a bone repair material, especially for load-bearing bone fixation.

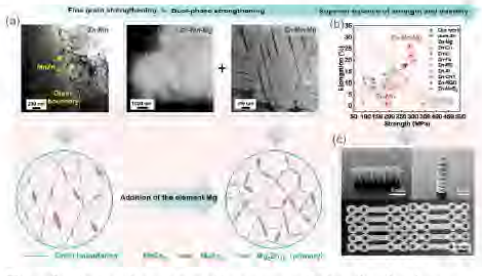

Fig. 1: (a) schematic diagram of the dual-phase synthetic strengthening mechanism, (b) ultimate tensile strength versus elongation – data collected from the current work and other literature, and (c) LPBF Zn-Mn-Mg bone screws and bone plates.

DISCUSSION & CONCLUSIONS: This is the first instance of a directly printed biodegradable alloy meeting the mechanical property requirements for bone fixation devices, such as bone screws or plates, without the need for post-processing. The superior balance of strength and ductility could be attributed to the unique microstructure resulting from the addition of Zn, Mn, and Mg. The distributions of $MnZn_{13}$ and Mg_2Zn_{11} second phases inside the grains and at the grain boundaries contributed to dual-phase synthetic strengthening, resulting in high strength values. The significant refinement of the Zn grains by adding Mg to the Zn-Mn alloy facilitated uniform plastic deformation, resulting in high elongation.

REFERENCES: [1] C. Huang, Y. Wang, F. Yang, et al (2025) *Acta Biomater* **196**:506-522.

ACKNOWLEDGEMENTS: The work was financially supported by the National Key Research & Development Program of China (No. 2023YFB3813000), the National Natural Science Foundation of China (52471260, 52201294).

European Cells and Materials Vol. NN. Suppl. N, 20xx (page htu) ISSN 1473-2262

Electroformed Fe-Zn Binary Alloys for Tiny Medical Devices: Exploring the Effect of Zn on the Microstructure and Electrochemical Properties

CHM Beraldo, C Paternoster, D Mantovani

Laboratory for Biomaterials and Bioengineering, (CRC-Tier I), Dept Min-Met-Materials Eng, & Regenerative Medicine, CHU de Québec, Laval University, Quebec City, Canada.

INTRODUCTION: Iron and its alloys are of great interest in the medical field thanks to their bioresorbability, biocompatibility, and mechanical properties, especially for use as temporary devices. Electroforming emerges as a promising bottom-up technology destinated for the manufacturing of such a kind of tiny devices [1]. Alloying iron is a way to increase this element low degradation rate [2-3], for example with zinc that is more susceptible to the corrosion phenomenon. Nevertheless, Fe-Zn electroforming also faces a challenge called *anomalous codeposition*: zinc preferentially deposits over iron, leading to alloys with low iron content [4]. Overcoming this barrier is crucial to successfully permit the production of the material. The aim of the present of work was to electroform Fe-Zn alloys containing different amounts of zinc and to investigate their effect on the microstructure and electrochemical properties of the alloys.

METHODS: Pure electroformed iron was deposited using a method described elsewhere [2-3]. The Fe-Zn samples were produced in an electrolytic bath composed of a fixed amount of $FeCl_2$, and a variable amount of $ZnCl_2$, in the range 0.68 g L^{-1} (sample Fe-1Zn) and 6.82 g L^{-1} (sample Fe-10Zn). Deposition took place in a three-electrode cell, containing a silver-wire reference electrode, a carbon rod as counter-electrode and a titanium sample as working electrode. Temperature, current density and pH were, respectively, 50 °C, 2.0 A·dm^{-2} and 2.0. The obtained samples were characterized using optical microscopy (OM), scanning electron microscopy (SEM), energy-dispersive X-ray spectroscopy (EDS), contact profilometry and electrochemical impedance spectroscopy (EIS).

RESULTS: Fig. 1 shows the results of OM. The addition of zinc into iron induced the appearance of "rose-like" structures surrounded by a second phase (black areas). Such features were also observed in the SEM analysis. EDS revealed that the zinc amounts were 2.5 wt.% (Fe-1Zn) and 30 wt.% (Fe-10Zn). No significant changes in roughness (R_a) were observed by increasing the amount of zinc, where values of 7.9 µm (Fe-1Zn) to 7.1 µm (Fe-10Zn) were observed. From the EIS, the addition of Zn resulted in the decrease of the impedance modulus (|Z|) from $10^{2.6}$ Ω·cm^2 (pure iron), to $10^{2.1}$ Ω·cm^2 (Fe-10Zn) and to $10^{1.8}$ Ω·cm^2 (Fe-1Zn).

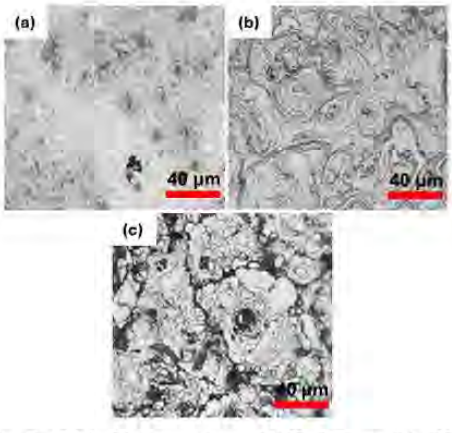

Fig. 1: OM of (a) pure iron, (b) Fe-1Zn and (c) Fe-10Zn.

DISCUSSION & CONCLUSIONS: Results indicated the presence of a second phase, expected to be Γ-phase (based on Fe-Zn phase diagram). The increased amount of zinc leaded to the presence of cracks, since the Γ-phase presents brittle characteristics. Nevertheless, the increase in zinc amount did not cause significant changes in the roughness of the samples, possibly due to the presence of oxides on the surface. From EIS, the addition of zinc decreases the |Z| value of iron, indicating an inferior resistance to corrosion. A superior value of |Z| for sample Fe-10Zn may be related to the formation of corrosion products into the cracks on the surface, slightly improving the resistance to the passage of electrolyte.

REFERENCES: [1] P. Hernández, D. Campos, P. Socorro, et al (2015) *Procedia Eng* **132**:655-62. [2] M. Moravej, F. Prima, M. Fiset, et al (2010) *Acta Biomater* **6**:1726-35. [3] M. Moravej, F. Prima, M. Fiset, et al (2010) *Acta Biomater* **6**:1843-51. [4] W. Wang, J. Wang, and M. Qi (2014) *Adv Mater Res* 1033-1034: 1200-06.

ACKNOWLEDGEMENTS: This project was partially supported by NSERC-Canada, PRIMA-Quebec, and the Quebec University Research Hospital.

European Cells and Materials Vol. NN. Suppl. N, 20xx (page htu)
ISSN 1473-2262

3D-Printed Biodegradable Zn alloy Scaffolds to Suppress Osteosarcoma and Promote Osteogenesis

Dandan Xia[1],Peng Wen[2], Yufeng Zheng[3],

[1]Department of Dental Materials, Peking University School and Hospital of Stomatology, China. [2] Department of Mechanical Engineering, Tsinghua University, China. [3]School of Materials Science and Engineering, Peking University, Beijing, 100871, China

INTRODUCTION: Osteosarcoma is the most common primary bone tumor. After tumor resection, recurrence and postoperative bone defects remain a critical challenge. It is urgent to develop biomaterials which can kill osteosarcoma and promote bone regeneration. In this study, we utilized laser powder bed fusion to fabricate biodegradable Zn-Li pscaffolds that supress tumors and promote osteogenesis.

METHODS: The TPMS method was used to design scaffolds. A Gyroid unit cell with a porosity of 70% was generated. Scaffolds were produced in a laser powder bed fusion printing system with a single-mode ytterbium fiber laser, emitting a 1070 nm laser with a 70 μm-focus spot diameter. The pure Zn and Zn-Li scaffolds surface were observed under Scanning electron microscope (SEM). EBSD analysis was used for the characterization of grain size distribution. Compression tests were conducted via the Shimadzu tester.

RESULTS: The pure Zn and Zn-Li scaffolds were fabricated, (*Fig. 1*). Electron backscattered diffraction (EBSD) analysis revealed the grain size distribution (*Fig. 2*). The average grain size decreased from 10.50 μm in Zn to 8.61 μm in Zn-0.4Li, then increased to 13.96 μm in Zn-0.8Li. The compressive yield strength (CYS) and elastic modulus (E) increased with the Li content (*Fig. 3*). The CYS and E of the Zn-0.8Li scaffolds were 28.87 ± 0.53 and 817.55 ± 59.69 MPa, respectively, higher than that of pure Zn scaffolds (5.50 ± 0.20 and 185.81 ± 9.78 MPa).

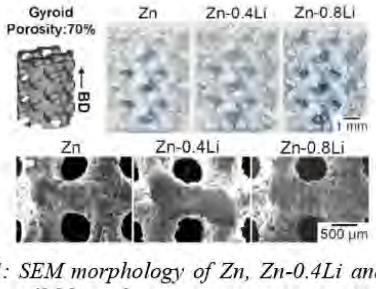

Fig. 1: SEM morphology of Zn, Zn-0.4Li and Zn-0.8Li scaffolds surface.

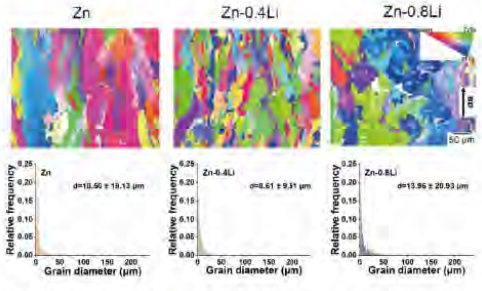

Fig. 2: EBSD inverse pole figure orientation maps.

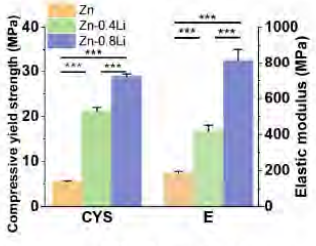

Fig. 3: CYS of Zn and Zn-Li scaffolds.

DISCUSSION & CONCLUSIONS: The mechanical strength, degradation behavior, and biological effects of Zn-Li scaffolds were regulated by structure design and composition optimization[1, 2]. The Zn-0.8Li scaffold showed enhanced strength and moderate corrosion behavior. In addition, the Zn-0.8Li scaffold inhibited osteosarcoma cell proliferation, promoted apoptosis, alleviated migration, and enhanced osteoblasts' osteogenic ability, thereby exhibiting antitumor and osteogenesis properties.

REFERENCES: [1]Dandan Xia, etc. Bioactive Materials, 2023, 19, 12-23. [2] Yu Qin, etc. Acta Biomaterialia, 2022, 145, 403-415.

ACKNOWLEDGEMENTS: This study was supported by the National Key Research and Development Program of China (2023YFC2412600).

European Cells and Materials Vol. NN. Suppl. N, 20xx (page htu) ISSN 1473-2262

Natural ageing and static recrystallisation effects of additively manufactured biodegradable pure Zn and Zn-Mg alloys

H Abenayake[1], L Dieter[1], C Persson[1], F D'Elia[1]

[1] Division of Biomedical Engineering, Department of Materials Science and Engineering, Uppsala University, Sweden

INTRODUCTION: Powder bed fusion–laser beam (PBF-LB) processing of Zn-Mg alloys has gained attention as a promising approach for fabricating biodegradable, patient-specific implants[1]. Although alloying Zn with Mg contents ≤ 1 wt.% enhances tensile performance[2], natural ageing (NA) remains a persistent challenge[3]. This is due to Zn's low melting point, which enables significant atomic diffusion at low temperatures, resulting in an exceptionally low recrystallisation temperature and undesirable changes in mechanical properties over time. Studies on conventionally processed Zn-Mg alloys have reported increased tensile strength over time, accompanied by a significant reduction in ductility, attributed to Mg_2Zn_{11} precipitation[4]. To date, no comprehensive studies have examined the static recrystallisation (SRX) behaviour of pure Zn, or the NA characteristics of Zn-Mg alloys produced via PBF-LB. This work addresses that gap by evaluating the SRX and NA behaviour of PBF-LB processed pure Zn and Zn-1Mg (wt.%) at room temperature (RT) and body temperature (37 °C).

METHODS: Alloys were prepared by mechanical mixing of Zn and Mg powders. Constructs were fabricated using an Aconity Midi PBF-LB system with optimised process parameters (P_L = 60 W, v = 300 mm/s, h = 0.04 - 0.05 mm), achieving > 99.5% relative density. The evolution of mechanical properties of samples aged at RT and 37 °C was assessed by microhardness measurements and compression testing over 90 days. These changes were correlated with microstructural observations obtained via scanning electron microscopy (SEM) and energy dispersive X-ray spectroscopy (EDS). Grain size distribution and precipitation behaviour were examined using EBSD (electron backscattered diffraction) and Rietveld refinement of X-ray diffraction (XRD) patterns. Statistical analysis was performed using SciPy in Python.

RESULTS: The microhardness of pure Zn remained stable at RT but declined at 37 °C after 60 days (Fig. 1). Zn-1Mg showed stable hardness at RT for 30 days yet dropped significantly by 60 days. Similarly, Zn-1Mg exhibited a continuous decline in hardness at 37 °C, with a pronounced drop by 60 days. This trend correlates with the substantial reduction in the $MgZn_2$ phase fraction over time (Table 1).

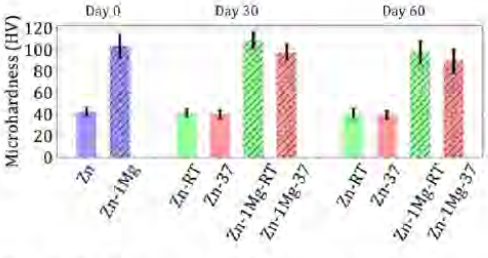

Fig. 1: Evolution of microhardness with time

Table 1. Variation of $MgZn_2$ phase fraction over time in PBF-LB Zn-1Mg alloy

T (°C)	$MgZn_2$ phase fraction (%)		
	0 days	30 days	60 days
RT	1.67 ± 0.06	1.51 ± 0.06	1.49 ± 0.06
37 °C		1.06 ± 0.06	0.98 ± 0.06

DISCUSSION & CONCLUSIONS: At RT, SRX has minimal impact on PBF-LB pure Zn, as indicated by stable microhardness over time. In contrast, the Zn-1Mg shows significant variations, reflecting pronounced natural ageing effect. The temperature-dependent trends in Zn-1Mg further confirm the strong impact of temperature on ageing, primarily driven by the transformation of the hard and brittle $MgZn_2$ intermetallic into more stable phases. In conclusion, PBF-LB Zn-Mg alloys show notable temperature-dependent natural ageing effects. Future works will focus on mitigating this issue through multi-component alloying and optimisation of printing parameters.

REFERENCES: [1]M Voshage et al., Mater Today Commun, 2022, 32, 103805. [2]E. Mostaed et al., Acta Biomater., 2018, 71, 1–23. [3]H. Jin et al., Mater. Sci. Eng., 2018, 84, 67–79. [4]M. S. Ardakani et al, Mater. Sci. Eng., 2020, 770, 138529.

ACKNOWLEDGEMENTS: This work is conducted within the AM4Life Competence Centre with financial support from VINNOVA, Swedish Research Council, and EU.

European Cells and Materials Vol. NN. Suppl. N, 20xx (page htu) ISSN 1473-2262

Optimization of 3D printing parameters to densify the microstructure of FeMnC alloys for biomedical applications

C.A. Cuao-Moreu[1], Carlo Paternoster[1], Simon Gélinas[2], Paolo Mengucci[3], Carl Blais[2] and Diego Mantovani[1]

[1]Laboratory for Biomaterials and Bioengineering, CRC-1, Dept of Min-Met-Materials Engineering and Research Center of CHU de Québec, Division of Regenerative Medicine, Laval University, Quebec City, Canada; [2]Laboratory for Powder Metallurgy, Department of Min-Met-Materials Engineering, Laval University, Quebec City, Canada; [3]Department SIMAU & UdR INSTM, Università Politecnica Delle Marche, Ancona, Italy

INTRODUCTION: The demand for biomedical implants has increased recently, particularly for scaffolds to treat large bone defects or fractures and promote bone regeneration. Recent studies have focused on biodegradable ones (Mg, Zn, and Fe). Fe-based alloys exhibit superior mechanical properties but have a slower corrosion rate than Mg and Zn alloys. To overcome this challenge, different elements like Mn can be incorporated [1,2]. Also, non-conventional fabrication techniques, like 3D printing through Laser Powder Bed Fusion (LPBF) [3], lead to complex microstructural changes affecting the degradation rate, simultaneously allowing the fabrication of complex structures, and creating the wished microstructural features. Typically, LPBF employs pre-alloyed spherical powders ($Ø$ = ~20 ÷ 55 µm), but these are generally produced costly through atomization. Nevertheless, optimizing the 3D-printing parameters for using elementary powder to cut down the powder production cost is an important aspect that is proposed to keep the wished (microstructural, mechanical) properties, reducing the powder fabrication steps. The present work deals with the optimization of the fabrication process of a Fe-12Mn-1.2C alloy, its characterization, and evaluation of the performances through a fabrication process based on quasi-elemental powders.

METHODS: Commercial AISI 1025, Mn and graphite powders were mixed in appropriate amount, pre-sintered in an Ar-feed tubular furnace, and then milled, to improve their flowability. A laser power P in the range 50 – 140 W, and a laser speed in the range 270 – 1030 mm/s were used during the printing, to obtain a volumetric energy E_V in the range 60-200 J/mm^3. Powder morphology and chemical distribution were analyzed through scanning electron microscopy (SEM), and energy dispersive spectroscopy (EDS). Crystallographic structure information was gathered via X-ray diffraction (XRD) while the porosity and microstructure of the sintered samples were examined with optical microscopy.

Fig.1: Printed samples at 140 W (left). Optical micrograph for a (right) 101-W printed sample, (Nital 2 vol%.)

RESULTS & DISCUSSION: A relevant porosity decrease was obtained with increasing laser powers (Fig. 1 - left). After a certain E_V threshold, the particles completely melt, decreasing porosity during solidification: a laser power over 100 W was required to achieve denser samples. An irregular grain shape was obtained, for all the conditions (Fig. 1 – right). Due to the rapid melting process and high cooling rates during LPBF, a random arrangement of irregularly shaped grains was observed, organized in a hierarchal microstructure and with a fine cellular structure. All the investigated condition showed an austenitic microstructure, with traces of other phases (α-, α'-, and ε-Fe). The interdiffusion of elements was already relevant during the powder pre-sintering and milling of the starting powders.

CONCLUSION: The sintering process improved the flowability of the elemental powder, allowing the printing of homogeneous microstructures, whose porosity needs to be optimized. The used printing parameters were similar to those used for printing of prealloyed powders.

REFERENCES: [1]Razavi, M., et al. *Acta Biom.*, 2017. [2]Li, G., et al. *Mat. Sci. and Eng. C*, 2020. [3]Haverkamp, C., et al. *J. of Materials Mat. Res. and Tech.*, 2021.

ACKNOWLEDGEMENTS: This research was partially supported by the Laboratory for Biomaterials and Bioengineering, the Natural Science and Engineering Research Council of Canada, Prima Quebec, and the CHU de Quebec Research Center.

European Cells and Materials Vol. NN. Suppl. N, 20xx (page htu) ISSN 1473-2262

Powder-based precipitation simulation of a MgZnCa alloy

B. Alonso Rancurel[1,2], V. Shtender[1], D. Primetzhofer[3,4] F. D'Elia[1], M Fisk[5], C Persson[1,2]

[1]*Biomaterials System, Department of Material Science and Engineering, Uppsala University,* [2]*Wallenberg Initiative Materials Science for Sustainability, Department of Material Science and Engineering, Uppsala University,* [3]*Department of Physics and Astronomy, Uppsala University,* [4]*Tandem Laboratory, Uppsala University,* [4]*Department of Materials Science and Applied Mathematics, Malmö University*

INTRODUCTION: Developing biodegradable implants is of growing interest to help fight antimicrobial resistance. Magnesium alloys are candidates for orthopaedic applications, but there is a need for improving their corrosion resistance[1]. Alloying reduces corrosion rates, but further improvement could be achieved by microstructural tuning using additive manufacturing (AM). However, process parameter optimization is time and resource consuming, motivating the use of numerical modelling to accelerate alloy development. The aim of this study was to predict the microstructure-temperature relationship for a MgCaZn alloy using the CALPHAD method as input for a classical nucleation and growth theory (CNGT) simulation. To achieve this, raw powder feedstock was characterized, along with a minimal number of printed samples.

METHODS: The powder composition was identified as $Mg_{63.2}Zn_{32}Ca_{4.8}$ by Inductively Coupled Plasma – Optical Emission Spectroscopy (ICP-OES) and compared to the results of ToF-ERDA (Time-of-Flight Elastic Recoil Detection Analysis). The composition of printed samples was also measured to estimate evaporation rates during printing.

X-ray diffraction (XRD) was used for phase identification. Differential Scanning Calorimetry (DSC) was used to characterize phase transitions and generate Time-Temperature-Transformation (TTT) and Continuous-Heating-Transformation (CHT) diagrams.

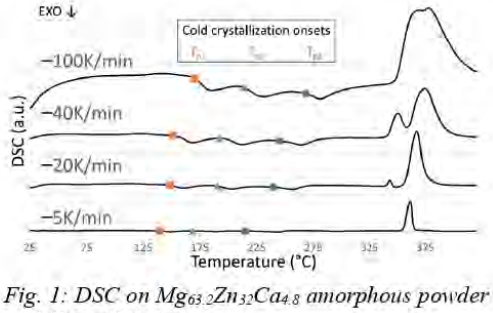

Fig. 1: DSC on $Mg_{63.2}Zn_{32}Ca_{4.8}$ amorphous powder at different heating rates.

RESULTS: Three cold crystallizations were distinguished (see Figure 1) and analysed by XRD. Kissinger analysis[2] was done on four heating rates and the results are shown in Table 1 together with the transformation onset temperatures. Metastable phases were formed at the first (T_{p1}, phase $Mg_{51}Zn_{20}$) and third crystallisation (T_{p3} IM4). Thermodynamic data and unit cell parameters from experimental results and literature[3] were used in a Python code to simulate CHT and TTT diagrams for comparison with the experimental results. The experimental data was used to validate the numerical model.

Table 1. Transformation onsets in function of heating rates, and activation energy (E_a) results.

Heating rate [°C / min]	T_{p1} [°C]	T_{p2} [°C]	T_{p3} [°C]
5	139	168	215
20	149	190	240
40	152	193	245
100	171	214	268
E_a [kJ / mol]	132	111	117

DISCUSSION & CONCLUSIONS: The overall transitions and phases agreed with previous literature, with only significant differences in the obtained energies of activation. The first simulated TTT diagram to our knowledge has been generated for this composition and phases. Synchrotron studies and more compositions should be tested for proper validation of the methodology.

REFERENCES: [1]Radha, R., & Sreekanth, D. (2017), *J. Magnes. Alloy*, **5(3)**, 286–312. [2]Kissinger, H. E. (1957) *Anal. Chem.*, **29(11)**, 1702–1706. [3]Mezbahul-Islam, M. et al. (2014) *Calphad*, **46**, 134–147.

ACKNOWLEDGEMENTS: *This work was supported by the Wallenberg Initiative Materials Science for Sustainability (WISE) funded by the Knut and Alice Wallenberg Foundation and the Swedish Research Council (grant numbers 2019-00191 and 2023-00155) supporting the Ion Technology Center.*

European Cells and Materials Vol. NN. Suppl. N, 20xx (page htu)
ISSN 1473-2262

Enhancing the mechanical performance of biodegradable zinc alloys for vascular stents through trace lithium alloying

Jialin Niu, Xiyuan Zhang, Zilong Wang, Guangyin Yuan
NERC-LAF and State Key Laboratory of Metal Matrix Composite, Shanghai Jiao Tong University, Shanghai, China.

INTRODUCTION: Zinc alloys have emerged as promising candidates for biodegradable vascular stents due to their moderate degradation rate. However, developing zinc-based materials with high strength, ductility, and long-term mechanical stability remains critical for advancing their clinical translation. Based on our previously developed anti-aging Zn-Cu alloys [1-2], this study introduces trace amounts of lithium (Li) to fabricate a novel Zn-Cu-Li ternary alloy. We systematically investigate the influence of Li alloying on the microstructure, mechanical properties, and degradation behavior, and address the processing, and performance evaluation of zinc alloy thin-walled tubes and vascular stents, providing a comprehensive assessment of their potential for clinical applications.

METHODS: The alloy was fabricated via vacuum induction melting. Subsequently, the ingot was extruded into a rod with a diameter of 20 mm. Through a combination of secondary extrusion and multi-pass drawing processes, thin-walled tubes with an outer diameter of 3.0 mm and a wall thickness of 0.16 mm was produced. Vascular stents were then laser cut from the tubes. The microstructure of the alloy was characterized using the following instruments: X-ray diffractometer (XRD, D/MAX 2550, Rigaku Corporation, Japan), optical microscope (OM, Zeiss Axio Observer A1, Germany), scanning electron microscope (SEM, TESCAN MIRA3, Czech Republic), and transmission electron microscope (TEM, TALOS F200X, FEI, USA). Mechanical properties were evaluated through tensile testing using a universal testing machine (Zwick/Roell Z20/Z100, Germany). The radial support force of the stents was assessed using a radial force tester (TTR2, Blockwise, USA). The in vitro degradation behavior was investigated through immersion test.

RESULTS & DISCUSSION:

The microstructure consists of η-Zn matrix with fine equiaxed grains, as well as micron, submicron-sized and coherent nano ε-CuZn4 phases. The introduced trace Li exists as a solute in the η-Zn matrix and ε-CuZn4 phase, and results in the refinement of grains and more uniform distribution of grain sizes for the η-Zn matrix, and the increase of volume fraction for ε-CuZn4 phase. The strengthening mechanisms of Zn-2Cu-0.1Li alloy are grain boundary strengthening, precipitate strengthening of ε-CuZn4 and solid solution strengthening of Li. The alloy also has favorable mechanical property stability, weak tension compression yield asymmetry and strain rate sensitivity. It exhibits uniform degradation. The added trace Li makes the degradation rate slightly increase, which is attributed to the increased ε-CuZn4 volume fraction and improved electrochemical activity of the matrix. The fabricated Zn-2Cu-0.1Li tubes show favorable mechanical properties, with tensile yield strength (TYS) of 304 MPa, UTS of 361 MPa and fracture EL of 30 %.The stents with strut thickness of 119μm exhibit an average radial strength of 118 kPa.

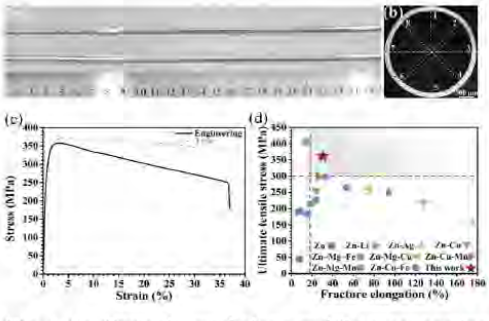

Fig. 1. (a) Optical morphology and (b) cross section of microtubes; (c-d) The mechanical properties of Zn-2Cu-0.1Li alloy tubes.

CONCLUSIONS: Trace Li alloying could significantly enhance the mechanical properties of zinc alloys. The Zn-2Cu-0.1Li alloy thin-walled tubes and stents exhibit excellent mechanical performance, meeting the clinical requirements.

REFERENCES: [1] Niu J, Yuan G, et al (2016). *Materials Science and Engineering C*, 69, 407-413. [2] Tang Z, Niu J, et al (2017). *Journal of the Mechanical Behavior of Biomedical Materials*, 72, 182-191.

European Cells and Materials Vol. NN. Suppl. N, 20xx (page htu) ISSN 1473-2262

Pre-Implantation Property Changes: Monitoring Mechanical Drift in Mg Alloys Over Time

Adam J. Griebel, Phil George, Jeremy E. Schaffer
Fort Wayne Metals, Fort Wayne, IN, USA

INTRODUCTION: Medical devices have expiration dates, before which they are guaranteed by the manufacturer to maintain sterility and functionality[1]. Following production, medical devices often experience prolonged distribution, handling, and storage periods prior to implantation. This process can stretch for months to years. When designing an implant, ensuring functional stability over this time period is critical.

Absorbable metals like Mg and Zn can undergo microstructural changes at relatively low temperatures and hence could be prone to room-temperature aging processes, or "shelf hardening". This risk is amplified when the material is stored in a high-energy, cold worked state. Zn0.08Mg wire, for example, exhibited marked increases in strength and loss of ductility within days[2].

Data on shelf-stability of Mg alloys for medical applications is limited. This paper highlights findings from an in-progress 5-year study, initiated in May 2022, which examines three medical Mg alloys in various sizes and conditions relevant to medical devices.

METHODS: ZXM100, WE22, and LZ21[3] bars and wires were prepared in the sizes and conditions shown in Table 1. Samples were vacuum sealed in 4 mil plastic to prevent surface oxidation. At 0, 4, 8, 12, and 24 months, samples of each were visually inspected, assessed for surface roughness, tensile tested, and measured for open-circuit potentials in PBS. 36-month data will be available at Biometal 17.

Table 1. Materials used in this study.

Alloy	Size	Condition
WE22	0.125 mm	Cold Worked
ZXM100	0.14 mm	Cold Worked
LZ21	0.3 mm	Annealed
WE22	3.0 mm	Annealed
ZXM100	4.75 mm	Cold Worked & Aged

RESULTS: The vacuum seal packaging proved effective at maintaining the starting surface condition, with no notable visual, roughness, or open-circuit potential changes. However, certain samples did exhibit significant changes in tensile properties, as seen in figures 1 and 2. Most pronounced was the cold worked 0.125 mm WE22, increasing in strength from 475 to 521 MPa while elongation decreased from 3.8 to 2.1% over 24 months. Others, particularly the annealed LZ21 wire and WE22 bar, were essentially stable.

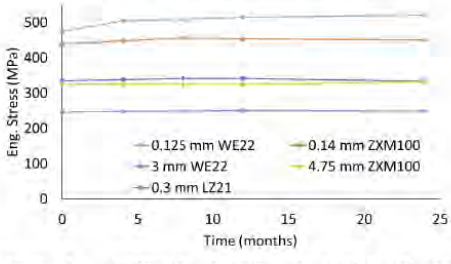

Figure 1. Ultimate tensile strengths of each sample over time.

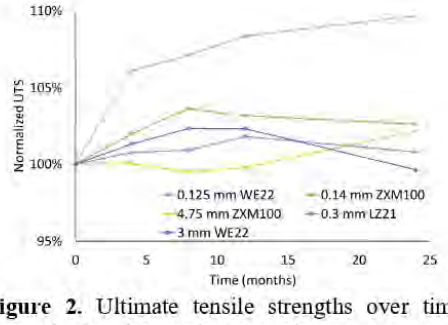

Figure 2. Ultimate tensile strengths over time, normalized to the starting strength.

DISCUSSION: This study shows that certain cold-worked Mg alloys may exhibit moderate shelf-hardening. For high-strength, elastic devices like braided stents, thermal stabilization (e.g., aging or stress relieving) may be warranted. In contrast, ductile annealed Mg used in devices like surgical staples is likely to remain mechanically stable over typical expiration timelines with proper storage.

REFERENCES: [1]A. Downes, D.G. Healy (2024), *The Surgeon* 22:4, 212-214. [2]H. Jin, S. Zhao, R. Guillory, *et al.* (2018), *Mat Sci Eng C* 84, 67-79. [3]A.J. Griebel, J.E. Schaffer US12188108B2.

ACKNOWLEDGEMENTS: The assistance of Dale Herndon, Lane Bailey, the FWM Metlab, Rich Casteñeda and Trevor Dawson is gratefully acknowledged.

European Cells and Materials Vol. NN. Suppl. N, 20xx (page htu) ISSN 1473-2262

Improving the properties of zinc-based alloys: an analysis of the effects of alloying and extrusion on microstructure and mechanical properties.

M. Bieda[1], K. Mycek[1], K. Królewski[1], A. Jarzębska[1], L. Maj[1], L. Rogal[1], M. Kulczyk[2], J. Skiba[2], C. Paternoster[3], D. Mantovani[3]

[1]*Institute of Metallurgy and Materials Science of Polish Academy of Sciences, Krakow, Poland*
[2]*Institute of High Pressure Physics, Polish Academy of Sciences, Warsaw, Poland*
[3] *Laboratory for Biomaterials and Bioengineering, CRC-I, Department of Min-Met-Materials*
14 Engineering, and University Hospital Research Center, Regenerative Medicine, Laval
15 University, Quebec, QC, Canada.

INTRODUCTION: The interest in zinc alloys as bioabsorbable metals gradually increased since it was discovered that pure zinc possesses the optimal corrosion rate for bioabsorbable cardiovascular stents. One of the main disadvantages of pure zinc is its insufficient mechanical properties. A wide range of potential zinc alloy systems were considered, mainly binary and ternary alloys. One of the most examined alloying elements is Mg, e.g. [1]. It forms a eutectic mixture of Zn α and Mg_2Zn_{11} intermetallic phase. The presence of an intermetallic phase prevents the recrystallization process in Zn-Mg alloys. However, the larger content of Mg_2Zn_{11} is not beneficial for the ductility of the material and the uniformity of corrosion properties. Thus, in order to ensure not only high mechanical properties but also optimal corrosion rate and homogenous degradation, some modification of Zn-Mg alloys needs to be applied. For the proposed investigation, the ZnMgMn ternary alloys were chosen.

METHODS: Materials for investigations were prepared by gravity casting in an argon atmosphere from pure zinc with various magnesium and manganese contents (from 0.1 to 0.5% wt. for both) and then deformed using hot extrusion and hydrostatic extrusion. The deformed material was subjected to a microstructure investigation using XRD (X-ray Diffraction), SEM (scanning electron microscope), and TEM (transmission electron microscope). Mechanical properties using static tensile tests and microhardness measurements were analyzed.

RESULTS: The UTS and YS obtained for materials were the highest for ternary alloys with 0.5 % Mg and 0.5 % M, reaching 458 MPa and 449 MPa, respectively. However, the elongation E was below 1%. After hydrostatic extrusion, the same alloy reached E=22 % elongation with slightly decreasing UTS and YS levels down to 437 MPa and 338 MPa, respectively. Detailed microstructure investigation showed significant grain refinement for hot and hydrostatic extrusion for ternary alloys with the highest amount of magnesium and manganese addition (Fig1), especially after hydrostatic extrusion. The average grain size was about 700 nm. Additionally, the grain refinement of intermetallic phases Mg2Zn11 and MnZn13 were noticed after hydrostatic extrusion. There is also a change in the texture of the materials after hydrostatic extrusion.

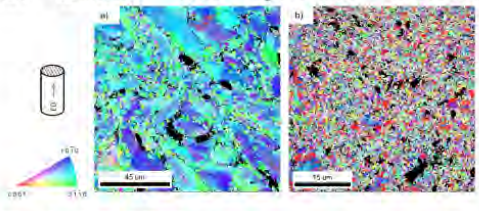

Fig. 1: SEM/EBSD orientation maps of zinc alloy with 0.5 % wt. of Mn and 0.5 % wt. of Mg after hot a) and hydrostatic extrusion b) where black areas are correlated with intermetallic phases (Mg_2Zn_{11}, $MnZn_{13}$).

DISCUSSION & CONCLUSIONS: Alloying with magnesium and manganese is beneficial for improving the mechanical properties of zinc-based alloys. Additionally, applying hydrostatic extrusion is advantageous for the plasticity of those alloys. Modulation of different content of both alloying elements and deformation process parameters influences the final properties and opens the possibility of satisfying demands for particular applications. Further studies will focus on the uniformity of corrosion properties to ensure homogeneous degradation.

REFERENCES: [1] Pachla W et. al, Structural and mechanical aspects of hypoeutectic Zn-Mg alloys for biodegradable vascular stent applications, *Bioactive Materials* 6, 1, 26-44, (2021).

ACKNOWLEDGEMENTS: This work was supported by the National Science Centre Polish UMO-2023/51/B/ST11/02814

European Cells and Materials Vol. NN. Suppl. N, 20xx (page htu) ISSN 1473-2262

Printability, microstructure formation, and material properties for L-PBF of binary Mg-Li alloys

S Kotiadis[1], C Persson[1], T Choma[2], F D'Elia[1]

[1]*Division of Biomedical Engineering, Department of Materials Science and Engineering, Uppsala University, Uppsala, Sweden* [2]*Amazemet Sp. z o.o. [Ltd], Warsaw, Poland*

INTRODUCTION: The biodegradation of magnesium (Mg) implants reduces the need for secondary surgeries, while the similar elastic modulus to bone prevents stress shielding [1]. Indeed, Mg alloys have been used in vascular stents and bone fixation implants. Additive manufacturing (AM) has allowed for advancement in biomedical implant design, primarily due to fabrication of custom components [1]. One disadvantage however, hindering the implementation of AM-fabricated Mg alloys is their limited ductility, given e.g., the propensity of texture formation during such processing. Magnesium-lithium (Mg-Li) alloys can aid in this regard, due to the formation of BCC at Li contents above 11.7wt.%. These alloys are also notable for their ultra lightweight and biocompatibity [2], and in alloys containing BCC Li-phases, improved corrosion resistance is seen through generation of a protective Li_2CO_3 layer. Nevertheless, AM processing of Mg-Li alloys is to the best of our knowledge, yet to be reported. Hence, the aim of this study was to investigate the processability of binary Mg-Li alloys using AM, specifically through laser-powder bed fusion (L-PBF). Both a single- (α-Mg) phase and dual-phase (α-Mg + β-Li) alloy were processed, and evaluated for mechanical properties and corrosion resistance.

METHODS: Laser surface remelting was first carried out on an EOS M100 (EOS GmbH, Germany) to evaluate the effect of rapid solidification on microstructure formation in both Mg-Li alloys. Here, laser tracks were deposited on cast substrates at powers ranging from 15 to 100 W at a speed of 80 mm/s. Melt pool microstructure was characterised by SEM and TEM, setting the stage for fabrication of bulk components by L-PBF.

For bulk printing, ultrasonic atomized powder (Amazemet, Poland) was used as feedstock on an Aconity Midi (Aconity GmbH, Germany) L-PBF printer. Process optimization was performed primarily by varying laser power and scan speed, and sample quality was characterised through density measurements using optical microscopy. Finally, microhardness and hydrogen evolution measurements were performed.

RESULTS: Micrographs in Fig. 1 depict the melt pool microstructure for both alloys at 50 and 65 W. Laser power did not impact the microstructure of the single-phase alloy, where columnar dendrites were predominant throughout. In contrast, a profound effect was seen in the dual-phase alloy, with a transformation from cellular-dendritic substructure at 50W (Fig. 1c) to that of eutectic nano-lamellae at 65W (Fig. 1d). Microhardness and hydrogen evolution were strongly influenced by alloy microstructure, with the dual-phase alloy showing a unique ability to tailor material properties through process-induced microstructural transformations.

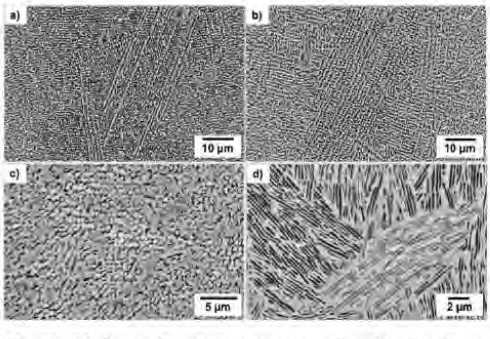

Fig 1. Melt pool microstructure of a single-phase Mg-Li alloy at a) 50W and b) 65W laser powers, and a dual-phase Mg-Li alloy at c) 50W and d) 65W laser powers.

DISCUSSION & CONCLUSIONS: The results demonstrate feasibility in processing Mg-Li alloys by L-PBF, highlighting the potential for the tailored fabrication of Mg-Li components, particularly for dual-phase alloys. Controlled processing of such alloys can enable enhanced versatility by tailoring material properties through unique microstructural transformations. Future work aims to further characterise mechanical and corrosion properties.

REFERENCES: [1] R. Karunakaran, S. Ortgies, A. Tamayol, et al (2020) *Bioact. Mater.* **5**:44-54. [2] W.R. Zhou, Y.F. Zheng, M.A. Leeflang, et al (2013) *Acta Biomater.* **9**:8488-8498.

ACKNOWLEDGEMENTS: This work is funded by the Carl Trygger Foundation (CTS 23-2980), and the EU Horizon 2020 Programme (Marie Curie - 101110609).

European Cells and Materials Vol. NN. Suppl. N, 20xx (page htu) ISSN 1473-2262

Tailoring surface quality and geometrical accuracy in additive manufacturing of biodegradable Mg/Zn alloys via powder quality and laser process control

S Pöstges[1], T Poel[1], F Fischer[2], M Voshage[2], A Kopp[1]

[1] *Meotec GmbH, Aachen, Germany.* [2] *Chair for Digital Additive Production DAP, RWTH Aachen University, Aachen, Germany*

INTRODUCTION: Biodegradable metals, especially zinc (Zn) and magnesium (Mg) alloys, hold considerable promise for biomedical uses, particularly in the development of temporary implants that naturally break down in the body. Recent research has shown that additive manufacturing (AM) can be effectively applied to these materials, enabling the creation of patient-specific implants with intricate and complex geometries[1,2]. This study explores the effect of powder quality and laser process control on the surface quality and geometrical accuracy of AM Mg/Zn parts in as-built state.

METHODS: Gas atomized, pre-alloyed Zn0.5Mg, conventional WE43 as well as medical grade WE43MEO powder is used to carry out the tests. All specimens are manufactured using a modified Laser Powder Bed Fusion system from *Aconity 3D GmbH* adapted to the use of biodegradable, low melting alloys. The effect of the powder quality is studied by comparing thin-walled lattice structures made out of conventional and medical grade powder whereas the influence of the laser parameters is investigated on both, full volume and thin-walled structures. A total of 18 specimens are fabricated with different volume energy density and spot diameter. Additionally, the overhang behaviour is studied by variation of the inclination.

RESULTS: In as-built state, the geometric accuracy is significantly increased when using medical grade WE43MEO powder as shown in Fig. 1. In the top view (Fig. 1 a) and c)), the strut size is decreased from 425,56 ± 17,38 µm for conventional WE43 to 387,11 ± 14,09 µm with WE43MEO. For the perpendicular planes (Fig. 1 b) and d)) this effect is even more visible.

The investigation on Zn0.5Mg demonstrated that a volume energy density of 133,33 J/mm³, when combined with a spot diameter of 80 µm, yields samples with high relative density. However, this parameter combination results in low geometric accuracy, particularly for samples with inclination angles below 45°, which cannot be reproducibly fabricated. By increasing the volume energy density to 170 J/mm³ and the spot diameter to 100 µm, samples with inclination angles of 30° and above are reliably fabricated.

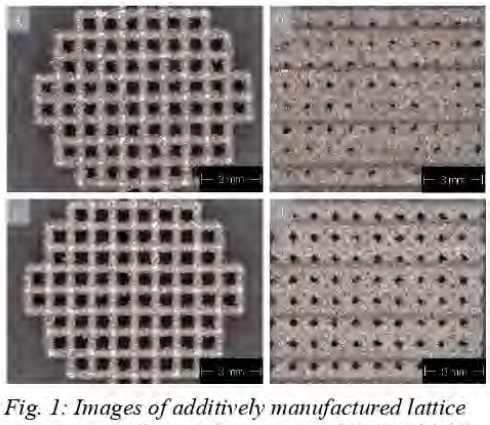

Fig. 1: Images of additively manufactured lattice structures made out of conventional WE43 (a)-b)) vs. WE43MEO (c)-d))

DISCUSSION & CONCLUSIONS: These results highlight the critical role of material selection and parameter tuning in balancing geometric precision and structural integrity for biomedical implants. While for Mg alloys the use of medical grade WE43MEO improves dimensional control, zinc alloys (e.g., Zn0.5Mg) require careful adjustment of energy density and laser intensity to overcome trade-offs between relative density and dimensional accuracy. This underscores the potential for patient-specific biodegradable implants but emphasizes the need for process optimization tailored to material behavior.

REFERENCES: [1]Y. Wu (2022) *Additive manufacturing of Zn-Mg alloy porous scaffolds with enhanced osseointegration: in vitro and in vivo studies*, Materials Science and Engineering: C, 134. [2]M. Voshage et al (2022) *Additive Manufacturing of biodegradable Zn-xMg alloys: Effect of Mg content on manufacturability, microstructure and mechanical properties*, Materials Today Communications 32: 1-9.

ACKNOWLEDGEMENTS: This work has received funding from the Federal Ministry of Education and Research funding indicator 03RU1U173A

European Cells and Materials Vol. NN. Suppl. N, 20xx (page htu) ISSN 1473-2262

Dynamic response of additively manufactured WE43 lattice structures under high-strain compression

Z Alomar[1], B Lukic[2], C Persson[1], P Isaksson[1], F D'Elia[1]

[1] *Department of Materials Science and Engineering, Division of Biomedical Engineering, Uppsala University, Uppsala, Sweden.* [2] *European Synchrotron Radiation Facility (ESRF), Grenoble, France.*

INTRODUCTION: Magnesium ally WE43 is a promising material for bone scaffolds due to its biocompatibility and ability to degrade in a physiological environment. Additive manufacturing (AM) enables the fabrication of patient-specific biodegradable porous lattices that could balance mechanical support and bone ingrowth [1]. While static mechanical properties of such scaffolds are well-studied, their dynamic response under high-strain-rate loading, critical for real-world scenarios like falls or sudden impacts, remains poorly understood [2]. This knowledge gap poses a barrier to designing implants that balance degradation and mechanical integrity during bone healing. This study aims to investigate the dynamic mechanical behavior and failure mechanisms of WE43 lattices under high-strain-rate loading conditions, employing a Split-Hopkinson Pressure Bar (SHPB) combined with synchrotron X-ray phase-contrast imaging to capture real-time microstructural evolution.

METHODS: Two families of lattices, strut-based and Triply Periodic Minimal Surface (TPMS) designs were fabricated from WE43 magnesium alloy, with varying relative densities (11–47%), via laser-powder bed fusion (L-PBF). Dynamic compression testing was conducted on the lattices using a SHPB system, where stress waves were generated by a 250 mm projectile pressurized at 1.2–2.2 bar to achieve high strain rates. Specimens were dynamically imaged in situ at the ESRF ID19 beamline using 60 ps X-ray pulses paired with a Shimadzu-HPVX2 ultra-high-speed camera, covering a 12x8 mm field of view. Post-impact analysis employed image analysis on high-speed radiographs to quantify the strain fields and the energy absorption Additionally, microcomputed tomography analysis was performed on some of the samples to evaluate their printing quality.

RESULTS: The SHPB tests revealed distinct mechanical responses between lattice types. TPMS structures exhibited superior load-bearing capacity, sustaining force outputs at least two times higher than strut-based lattices (e.g., FCC vs Gyroid) under identical impact conditions, see Fig. 1. Synchrotron imaging demonstrated TPMS deformation via progressive pore collapse and plastic densification, while strut-based lattices exhibit brittleness at high pressure, with FCC designs fracturing entirely at the transmission end. The stiffness values of TPMS lattices exceeded those of their strut-based counterparts by 40–60% across the tested relative densities. Moreover, TPMS structures demonstrated greater efficiency in energy absorption. Micro-computed tomography revealed highly dense structures, although a significant amount of semi-melted powder was observed on the surface.

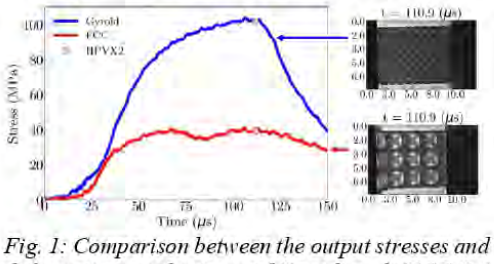

Fig. 1: Comparison between the output stresses and deformation mechanisms of Strut-based (FCC 0.4 mm struts diameter) and TPMS structure (Gyroid 0.4mm wall thickness) under 2.2 bar impact.

DISCUSSION & CONCLUSIONS: The superior dynamic performance of TPMS lattices stems from their continuous, curvature-driven architectures, which mitigate stress concentrations and enable gradual energy dissipation through controlled pore collapse, in contrast to strut-based designs which are prone to sudden fracture. Overall, this work establishes a foundation for optimizing AM-fabricated Mg alloy scaffolds, prioritizing architectures like TPMS to enhance implant durability in dynamic loading scenarios, thereby advancing patient-specific solutions for bone regeneration.

REFERENCES: [1]K. Dachsa, et al. (2024) *Adv in Mat Science and Eng* **2024**:1325004.[2] L. Antoniac, et al. (2022) *Materials* **15**(23):8693.

ACKNOWLEDGEMENTS: This work was supported by the ESRF/ ID19 experiment MA6157 and EU Horizon 2020 (Marie Curie – 101110609).

European Cells and Materials Vol. NN. Suppl. N, 20xx (page htu) ISSN 1473-2262

Development of a novel magnesium alloy with high degradation resistance and osteo/angiogenesis activity through scandium-enhanced growth of passivation film

Zhengguang Wang[1], Shuai Han [1],Bingchuan Liu,Chaoxin Wang[1], **Peng Wen[2], Yufeng Zheng[3], Yun Tian[1]**

[1] Department of Orthopedics, Peking University Third Hospital, Beijing, China.[2]Department of Mechanical Engineering, Tsinghua University, Beijing. [3]Department of Materials Science and Engineering, Peking University, Beijing

INTRODUCTION: Addressing the challenge of balancing rapid degradation and insufficient bio-regenerative capabilities in biodegradable magnesium (Mg) alloys for bone repair is a significant endeavor.

METHODS: In this study, we investigate the influence of Scandium (Sc) content on the microstructure, strength, degradation, cytotoxicity, angiogenesis, and osteogenesis of Mg-4Yttrium(Y)-xSc alloy system, and successfully develop a novel alloy Mg-4Y-2.25Sc (wt.%) that significantly inhibit degradation and promote bone regeneration. This achievement is contributed to the combination of the alloying and high-temperature oxidation (HTO) treatment, guided by a thermodynamic calculation model.

RESULTS: The performance of our alloy notably surpasses that of the widely used biodegradable WE43 alloy. At the microstructural level, a thin and dense protective film of Y2O3/Sc2O3 is introduced to form a passivation effect. The synergetic release of Mg and Sc ions significantly promotes angiogenesis and osteogenesis. In vivo results verifies that Mg-4Y-2.25Sc implants promote osseointegration of implants during the bone healing cycle.

DISCUSSION & CONCLUSIONS: In this study, an Mg-4Y-xSc (0.75, 1.50, 2.25, wt.%) ternary alloy system is proposed to achieve high degradation resistance and osteo/angiogenesis activity simultaneously through the Sc-enhanced growth of the oxidation layer. Under HTO treatment, compared with the protective oxide layers of Y2O3 and MgO, Sc2O3 migrates to the surface of Mg alloy, possessing higher thermodynamic stability. The Mg-4Y-xSc alloy system delivers Mg2+ and Sc3+, shaping the microenvironment for osteogenesis and vascularization, thereby promoting bone repair. Furthermore, the promotion mechanism of cell proliferation and adhesion, osteogenesis, and angiogenesis effects of the HTO combined Sc microalloying on the Mg-4Y-xSc alloy system are systematically evaluated. The novel Mg-4Y-Sc alloy system can be a promising candidate for next-generation high-performance Mg alloys for biodegradable applications.

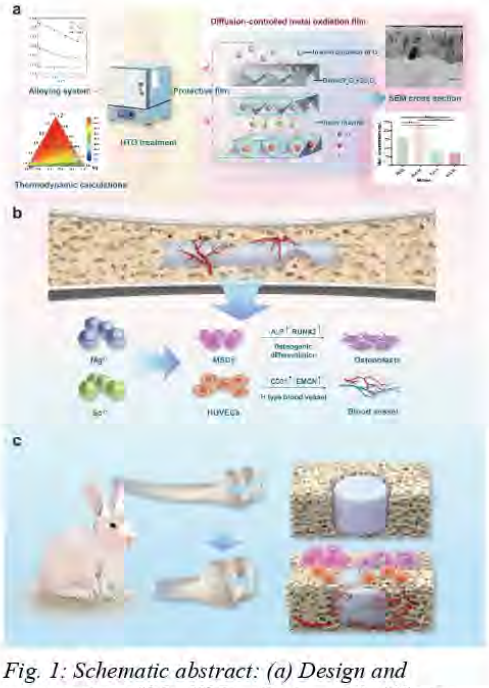

Fig. 1: Schematic abstract: (a) Design and preparation of Mg-4Y-Sc alloying with diffusion controlled metal oxidation film; (b) Regulated release of Mg2+ and Sc3+ ions from the Mg-4Y-2.25Sc alloy facilitates the osteogenic and angiogenic differentiation of bone mesenchymal stem cells (BMSCs) and human umbilical endothelial cells (HUVECs); (c) Implantation of the Mg-4Y-2.25Sc alloy enhances bone regeneration in a bone implant model, synergistically promoting the interfacial osteogenesis and the intra-bone implant integration.

ACKNOWLEDGEMENTS: This work was funded by the National Natural Science Foundation of China (82172065,82372092).This work was funded by the Capital's Funds for Health Improvement and Research (2024-1-4092).

European Cells and Materials Vol. NN. Suppl. N, 20xx (page htu) ISSN 1473-2262

Fe-Mn-C-Zn Coatings via Magnetron Sputtering Co-Deposition: Temperature and Target Power Effects on Microstructure and Electrochemical Properties

X Zhu[1,2], C Paternoster[2], A Gatto[1], D Mantovani[2]

[1] Department of Engineering "Enzo Ferrari" University of Modena and Reggio Emilia, Modena, Italy [2] Lab. for Biomaterials and Bioengineering, CRC-I, Department of Min-Met-Materials Eng., University Hospital Research Center, Regenerative Medicine, Laval University, Québec, Canada

INTRODUCTION: Iron–manganese alloys are emerging as promising candidates for biodegradable metallic implants due to their excellent mechanical properties, which are comparable to those of stainless steel. However, their clinical application is hindered by two key challenges: susceptibility to post-surgical bacterial infections and a slow corrosion rate[1]. *Staphylococcus* species are primarily responsible for implant-associated infections, as they form resilient biofilms that are highly resistant to antibiotics and disinfectants[2]. The aim of this study is to design a Fe–Mn alloy composite with enhanced antibacterial activity. To achieve it, zinc was incorporated into the alloy, taking advantage of its antibacterial mechanisms[3]. This approach aims to enhance also alloys' corrosion resistance due to their differences in electronegativity (-0.89 iron and -1.2 zinc).

METHODS: A silicon wafer and a magnesium alloy (AZ31B) square were used as a substrate for magnetron sputtering deposition. Coating deposition was conducted in a dual magnetron sputtering where commercial zinc and Hadfield steel were used as target. The two target were supplied with different power range to achieve a variation in chemical composition (150-300W for iron and 50-150W for zinc). Depositions were conducted in room temperature and high temperature (150°C). Finally, coatings were characterised using scanning electron microscope (SEM), energy dispersive spectroscopy (EDS), atomic force microscope (AFM), x-ray photo spectroscopy (XPS), x-ray diffraction (XRD), contact angle, antibacterial test, potentiodynamic polarization (PDP) and electrochemical impedance spectroscopy (EIS).

RESULTS: The use of zinc in sputtering leads to the formation of a homogeneous, defect-free coating (Fig. 1). The coatings appear smooth, with an average roughness ranging from 1 to 10 nm, closely matching the one of electropolished metallic samples. Additionally, roughness and porosity are very low, independently from process power. Coating thickness varies from approximately 230 nm for samples obtained at high temperatures to 570 nm for those produced with the highest target powers. EDS shows no significant differences in zinc content as a function of zinc target power, with an average of ~35 wt% under all conditions. However, when the iron-manganese target power is increased to 300 W, the zinc content decreases to ~20 wt%. On the surface, XPS reveals an increase in zinc content with increasing power for both targets.

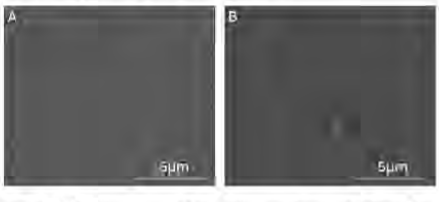

Fig. 1: SEM images of coatings deposited with (A) zinc 75W and (B) zinc 125W. Please note the homogeneity, the absence of defects and of apparent porosity (even at medium-high magnification), independently from process power.

DISCUSSION & CONCLUSIONS: This work presents the development of a composite coating composed of iron-manganese and zinc. Magnetron sputtering enabled the deposition of a high-purity coating consisting of these metals. EDS and XPS analyses highlight differing behaviours of manganese and zinc: manganese is predominantly concentrated in the coating bulk, while a significant portion of zinc is located within the top 5–10 nm of the surface. Temperature is shown to be an influential parameter affecting the microstructure and properties of the coating, further investigation are required.

REFERENCES: [1]Zheng, Y., et al (2023). *J. of Mat. Sci. & Tech., 147*, 132-144.[2]Costerton, J. W et al (2005). *The Int. j. of artificial organs*, *28*(11), 1062-1068. [3]Agarwal, H., et al (2018). *Chem.-biol. Interac., 286*, 60-70.

ACKNOWLEDGEMENTS: This research was partially supported by the LBB, the Natural Science and Engineering Research Council of Canada, Proma Quebec, and the CHU de Quebec Research Centre.

BIODEGRADABLE METALS
17th Biometal
25-30 AUGUST, 2025
Grand Hôtel San Michele,
Cetraro, CS, Italy

There are no molecules in metals and alloys

N. Hort[1,2], D. Tolnai[1], P. Maier[3,4]

[1] Helmholtz-Zentrum Hereon, Geesthacht, Germany; [2] Leuphana University Lüneburg, Lüneburg, Germany; [3] University of Applied Sciences Stralsund, Stralsund, Germany; [4] Lund University, Lund, Sweden

INTRODUCTION: For the development of new metallic biodegradable materials engineers, physicists, chemists, biologists, and physicians need to collaborate and must find their own common language. This also needs a common language to communicate and often enough the wording is the same but the meaning behind it is quite different. In chemistry and related areas, it is very common to talk about atoms and molecules as the smallest units to describe structures. This could be something like H_2, H_2O, CH_4, C_2H_6O or even more complicated molecules. This concept is known by biologists, clinicians but often not same for metal physics regarding crystalline structures and their impact on properties and processing. Metals are crystalline, built from atoms and alloys often contain intermetallic phase (IMP) like Mg_2Si, Mg_2Ca, $Mg_{17}Al_{12}$, Fe_3C. These designations of IMP look like those of molecules but is something completely different often causing misunderstanding!

CRYSTALS: 7 crystal systems, 14 Bravais lattices, 32 crystal classes, and 230 space groups are known. For metals and alloys only hex, fcc and bcc lattices are important (figure 1). Crystal systems are described by their lattice constants a, b, c and the angles α, β, γ between them. The smallest unit in a crystalline structure is called "unit cell" (figure 2).

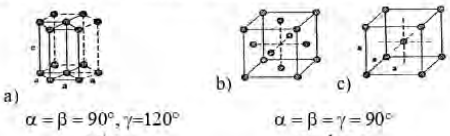

Figure 1: crystal lattices (unit cells), a) hexagonal (hex), b) face centred cubic (fcc), d) body centred cubic (bcc); lattice constants: a, b, c; angles α, β, γ [1]

Figure 2: bcc unit cell (e.g. α-Fe) and atoms involved (2 in total) [2]

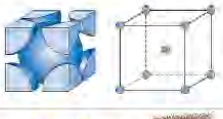

Figure 3: a) unit cell of Mg_2S [3] *and b) its supercell, visualized by Vesta*[4]

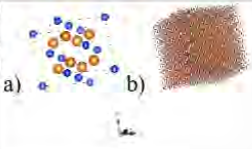

By repetition into all space directions of a crystal lattice it can be used to build the entire structure of different grains, separated by grain boundaries in polycrystalline materials.

PHASES: Phases are defined as areas with a particular chemical composition, constant atomic structure, and its own set of physical properties.

Figure 4:A glass of ice water – an object consisting of multiple phases: glass, liquid water, solid water, gas (approx. 78 % N_2, 21 % O_2, H_2O and other gases) [5]

Hume-Rothery stated that solid solution appears if there would the difference in atomic size by less than 15 %, the same crystal structure, valence, and electronegativity[6]. If these rules are hurt, IMP form. Different phases can exist side by side (figure 4) in each volume besides matrix grains within the grains or on grain boundaries.

The designation of an IMP looks like those of molecules. However, in IMP the designation describes the unit cell and how many atoms are within the unit cell. Different atoms can be part of more than one unit cell (figure 2) while whole atoms are part of a single molecule e.g. like H_2O.

SUMMARY: Metals and alloys are crystalline materials. The smallest unit is the unit cell. The designation of the unit cell e.g. Mg_2Si describes how many atoms are involved. This is not the designation of a molecule as atoms contribute to more than a single unit cell! The unit cells have been developed for metal physics and can be used to describe the behaviour of crystalline structures in ICME.

REFERENCES: [1] HKDH Bhadeshia, *Geometry of crystals, polycrystals, and phase transformations*, CRC Press, 2018. [2] WD Callister, DG Rethwish, *Materials Science and Engineering – An introduction*, 10th Ed., Wiley, 2018. [3] *www.crystallography.net/cod/1011355.html.* [4] K Momma, F Izumi, *VESTA 3 for three-dimensional visualization of crystal, volumetric and morphology data*, J. Appl. Crystallogr. 44 (2011) 1272-1276. [5] *de.123rf.com/ photo_12310503_glas-wasser-mit-eis-isoliert-auf-wei %C3%9F.html.* [6] U Mizutani et al., *The original concepts of the Hume-Rothery rule extended to alloys and compounds whose bonding is metallic, ionic, or covalent, or a changing mixture of these 10.1016/j.pmatsci.2020.100719.*

European Cells and Materials Vol. NN. Suppl. N, 20xx (page htu)
ISSN 1473-2262

Molybdenum Neurovascular Implants: Bridging Biodegradability and Neural Safety for Stroke Management

Yunong Shen[1], Ming Li[2], Xunming Ji[2], Yufeng Zheng[1]

[1] School of Materials Science and Engineering, Peking University; Beijing, China. [2] China-America Institute of Neuroscience, Xuanwu Hospital, Capital Medical University, Beijing, China.

INTRODUCTION: Stroke is the second leading cause of death and the third leading cause of disability worldwide[1]. Current non-degradable implants pose long-term biocompatibility issues. Molybdenum (Mo) shows promise for stroke implants due to its uniform degradation and biocompatibility. Using two pathological animal models, rat tMCAO model and rat aneurysm model, we confirmed its neuro-safety, particularly in compromised blood-brain barrier conditions.

METHODS:

Pure Mo wires (50μm) were braided into stents and wound into coils, then heat-treated for stabilization. In vitro cytocompatibility of pure Mo was tested on large artery cells (HUVECs, HASMCs) and neurovascular unit cells (bEnd.3, C8-D1A, HT22) under normal/OGD-R conditions using CCK-8, LDH, and Live/Dead assays. In vivo mo stent wire/2D coil safety was evaluated in two stroke models: (1) tMCAO rats underwent Mo wire implantation with behavioral tests (Longa score, rotarod, adhesion removal, open field), TTC/Nissl staining, Evans blue assay, and brain water content analysis; (2) Aneurysm rats received Mo coils, assessed via laser speckle imaging, DSA, degradation tracking, and histology.

RESULTS: Study demonstrates molybdenum (Mo) implants exhibit excellent biocompatibility in rat models, showing no significant inflammation or tissue damage, but Mo wires didn't improve neurological outcomes in ischemic stroke models. For the treatment of hemorrhagic stroke 2D Mo coils effectively embolized aneurysms with controlled degradation rates. No harmful Mo accumulation was observed in major organs, confirming its safety for neurovascular applications.

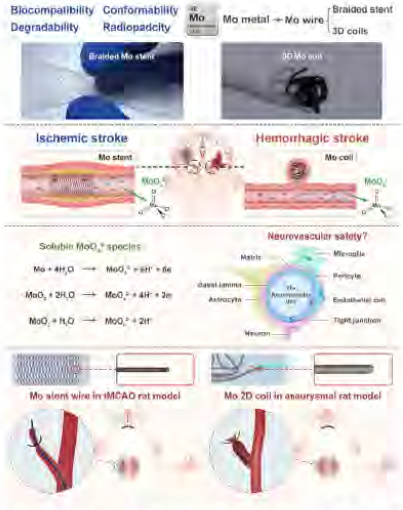

*Fig. 1: **Schematic illustration of the experimental design.** (A)Mo stents treat ischemic stroke; coils treat hemorrhagic stroke. (B)Braided stents and 3D coils shown. (C)Implants degrade safely, interacting with NVU. (D)Safety validated in rat stroke/aneurysm models.*

DISCUSSION & CONCLUSIONS:

Molybdenum (Mo) demonstrates excellent neurobiocompatibility for biodegradable neurovascular implants, showing minimal hemolysis (<5%), no cytotoxicity, and safe degradation (liver/heart accumulation only). In vivo tests confirmed effective aneurysm occlusion with Mo coils and no neurological worsening with Mo stents. Mo's balanced degradation and radiopacity outperform Mg/Fe alloys, making it promising for stroke interventions. Future work requires large-animal trials and device optimization.

REFERENCES: [1] Feigin, Valery L., et al. "Pragmatic solutions to reduce the global burden of stroke: a World Stroke Organization–Lancet Neurology Commission." The Lancet Neurology 22.12 (2023): 1160-1206.

European Cells and Materials Vol. NN. Suppl. N, 20xx (page htu)
ISSN 1473-2262

High-strength, low-degradation Mg microtubes for biodegradable vascular stents

JS Suh[1], CD Yim[1], BC Suh[1], HS Kim[1], SE Lee[1], JS Kim[1], HC Jung[2]

[1] *Korea Institute of Materials Science, Korea.* [2] *CG MedTech Co., Ltd., Korea*

INTRODUCTION: Biodegradable Mg alloys are becoming increasingly popular as potential metallic biomaterials for vascular and orthopedic temporary implants due to their favorable mechanical, electrochemical and biological properties [1,2]. Nevertheless, several challenges persist with Mg scaffolds, including high degradability, inadequate mechanical properties, and intricate manufacturing processes [3]. Alloying and processing are pivotal methods for the improvement of the properties of Mg alloys for use in biomedical applications. The focus of this study is on the process technology for the fabrication of ultra-precise geometries and the achievement of the mechanical and degradation properties for biodegradable vascular stents. To this end, a two-step extrusion process has been developed to fabricate microtubes. The present study investigates the effect of extrusion ratio on the room-temperature tensile properties and vitro degradation behavior of microtubes for two Mg alloys in terms of microstructure and texture.

METHODS: Mg-Zn-Ca (MZ01) alloy was supplied by CG MedTech Co., Ltd. (Korea) in the form of rods with a diameter of 15.9 mm. Mg-Zn-Mn-Sr (ZM115) alloy was also prepared by KIMS (Korea) in the form of rods with a diameter of 15.9 mm. Subsequent machining of the as-extruded rods resulted in the formation of hollow billets with a diameter of 13.9 mm, a height of 30 mm, and a central hole size of 3.1 mm. In conclusion, the MZ01 and ZM115 microtubes were fabricated through a two-step extrusion process at 400°C, employing extrusion ratios of 60, 129, and 242:1, respectively.

RESULTS: Two-step direct extrusion was employed to fabricate microtubes with outer diameters ranging from 3.5 to 1.5 mm and wall thicknesses ranging from 250 to 150 μm, respectively. As the extrusion ratio increased, the dimensional accuracy exhibited an improvement for the outer diameter, whereas a decline was observed for the inner diameter. As the extrusion ratio increased from 60:1 to 242:1, the tensile properties of the microtubes were enhanced by grain refinement, despite a concurrent weakening of the basal texture. Furthermore, an increase in the extrusion ratio led to an accelerated biodegradation rate.

DISCUSSION & CONCLUSIONS: The study involved two-step extrusion process of Mg microtubes with varying extrusion ratios, for applications in biodegradable vascular stents. The findings of the present study demonstrated that an elevated extrusion ratio led to enhanced mechanical properties and accelerated biodegradation. This phenomenon is attributable to alterations in the microstructure and texture. These observations are pivotal in understanding interplay between microstructure, mechanical properties, and biodegradation in the design of Mg-based biodegradable stents.

The present study focused on the realization of the geometry of ultra-precise microtubes. Subsequent research endeavors will investigate the potential for enhancing the precision and strength of microtubes through the proposed two-step extrusion process. Furthermore, additional analysis is required to elucidate the underlying mechanisms responsible for the observed acceleration of biodegradation behavior with increasing extrusion ratio.

REFERENCES: [1] D. Li, D. Zhang, Q. Yuan, et al (2022), *Acta Biomater*, **141**:454-465. [2] G. Song, (2007) *Corros Sci*, **49**: 1696-1701. [3] Y. Xin, T. Hu and P.K. Chu, (2011) *Acta Biomater*, **7**: 1452-9.

ACKNOWLEDGEMENTS: This work was supported by the National Research Foundation of Korea (NRF) grant funded by the Korea government (MSIT) (No. RS-2022-NR068191).

European Cells and Materials Vol. NN. Suppl. N, 20xx (page htu)
ISSN 1473-2262

Development and surface protection of high-purity magnesium materials for medical applications

Zhentao Yu[1], Weihong Jin[1], Qiwei Wang[1], Qingyun Fu[1]

[1] College of Chemistry and Materials Science, Jinan University, Guangzhou, China

INTRODUCTION: Biodegradable metals, such as magnesium (Mg) and its alloys, offer several advantages, including high specific strength, low elastic modulus, and excellent biocompatibility. These properties make them promising candidates for medical applications, particularly in the repair of bone and dental hard tissues, where they could replace conventional devices like bone plates, screws, and oral barrier membranes [1]. However, the use of high-purity Mg (HP Mg, 99.99 wt.%) in biomedical and industrial applications is limited by several challenges: its insufficient strength and toughness due to its hexagonal close-packed (HCP) crystal structure, poor formability at room temperature, and rapid degradation rates. This study focuses on the processing of HP Mg raw materials (99.99 wt.%), the development of high-purity Mg bone screws, and the corresponding surface protective coatings [2]. We have introduced a novel composite strengthening and toughening technique, "warm extrusion–cold rotary forging," for HP Mg. Additionally, we have designed and developed several high-efficiency protective coatings for Mg-based metals. Finally, we explore potential future applications of Mg and its alloys in the bone and dental medical fields.

METHODS: The "warm extrusion-cold forging" composite strengthening and toughening process introduces wide stacking faults (SFs) into high-purity Mg and adjusts its grain size, enhancing both its mechanical properties and corrosion resistance. High-purity Mg was used as the matrix, with dopamine (PDA), which has a strong adsorption capacity, introduced as the intermediate layer. Alginate (ALG) was then spin-coated and grafted onto the surface.

RESULTS: The SFs formed during the annealing process after rotary forging increase the strength of high-purity Mg to over 210 MPa. The sample modified with the PDA/ALG composite coating exhibited a corrosion current density more than 10 times lower than that of the uncoated substrate, along with a charge transfer resistance that increased by a factor of 13.

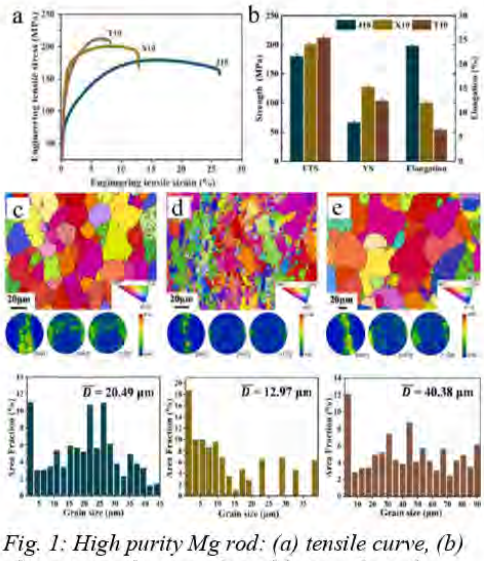

Fig. 1: High purity Mg rod: (a) tensile curve, (b) ultimate tensile strength, yield strength, and elongation; EBSD and grain size analysis: (c) extruded state, (d) swaged state, (e) annealed state.

DISCUSSION & CONCLUSIONS: The SFs not only enhances the mechanical properties but also slows the degradation process. The PDA/ALG composite coating was then applied to further regulate the degradation rate to align with the bone healing rate.

REFERENCES: [1] Q. Fu, C. Wang, Z. Yu, et al (2022) J ALLOY COMPD, **927**:167018. [2] Q. Fu, W. Jin, Z. Yu, et al (2023) J MAGNES ALLOY, **11**:2061-2071.

ACKNOWLEDGEMENTS: This work was financially supported by National Key Research and Development Project of China (No. 2020YFC1107202), Shanxi Provincial Key Research and Development Project (No. 2019ZDLSF03–06), Guangdong Basic and Applied Basic Research Foundation (No. 2020B1515120078), and Science and Technology Planning Project of Guangdong Province (No. 2021A0505030042).

European Cells and Materials Vol. NN. Suppl. N, 20xx (page htu) ISSN 1473-2262

Power source device considerations for Micro Arc Oxidation to coat Mg1.2Zn0.5Ca0.5Mn alloy coupons with large surface area

LH Olivas-Alanis[1,2], S Dutta[1], J Vazquez-Armendariz[1,2] G Krieger[1], A Luo[1], D Dean[1,3]

[1] *Material Science and Engineering, The Ohio State University, Columbus, OH, US.* [2] *School of Engineering and Sciences, Tecnologico de Monterrey, Monterrey, MX.* [3] *Plastic and Reconstructive Surgery, The Ohio State University, Columbus, OH, US.*

INTRODUCTION: The use of resorbable Mg alloy components for orthopaedic fixation and joint replacement devices are promising due to their ability to resorb and the fact that their stiffness is similar to bone, The latter property helps avoid stress shielding-induced bone loss and stress concentration-induced device failures. In previous work, we have employed Micro-Arc Oxidation (MAO) surface treatment to ensure tight binding of a sol gel-deposited calcium phosphate coating [1]. In the cited study, we showed that 15 layers provide modest protection. However, we have only recently begun testing our expectation that at least a 30 μm, and possibly over 100 μm, thick CaP coating would protect the underlying Mg alloy from degradation for at least 2 months. However, that study worked with coupons that were relatively small compared to the size of human skeletal fixation and joint replacement devices. In the current study, we encountered several issues in coating larger coupons.

METHODS: Mg samples were Electric Discharge Machine (EDM) cut and polished with a graded series of sandpaper up to 1200 grit size. Samples were then surface treated with MAO in a phosphate electrolyte under 50mA/cm^2 for 15 min. Three different power sources where evaluated: AMJ-0.5B80 (Matsusada Precision, Shiga, Japan), PowerPac Universal Power Supply (Bio-Rad, Hercules, CA US), and 62024P-600-8 (Chroma Systems Solutions, Guishan District, Taiwan). Technical specifications are shown in Table 1.

Table 1. Technical specifications of the power sources evaluated for micro-arc oxidation.

Model	Current, I, [A]	Voltage, V, [V]
AMJ-0.5B80 (Matsusada)	0.08	500
PowerPac (BioRad)	5.00	500
62024P-600-8 (Chroma)	8.00	600

Finally, the samples received 15 or 25 sol-gel layers. We employed an automated set-up for that dip coating process. Two linear guides are used to move the samples in the x (left – right) and z (up and down) directions. The process is depicted in Figure 1.

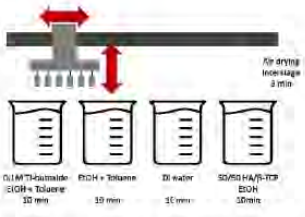

Figure 1. Sol-gel dip coating process.

RESULTS: When applying a 50mA/cm^2 current profile, the Matsusada power supply was able to produce a coating in samples with a surface area of 1.6 cm^2, while the BioRad and the Chroma devices are technically capable of processing samples with surface areas up to 100 cm^2 and 160 cm^2, respectively. However, the current control system in the BioRad device was not capable of withstanding the microarc effects. Thus, it is not capable of delivering a constant current, failing the construction of a coating layer. Thus, we chose to employ the Chroma Systems due its larger current capacity and control system.

DISCUSSION & CONCLUSIONS: We found that the quality and relevance of a professional grade power supply for MAO coating did not correspond to price. We also found that when inquiring, vendors were not sensitive to our needs for well-modulated (i.e. stable, not fluctuating) and invariant high voltage and low amperage current to be maintained with invariance for an hour or more. The next challenge we face is to combine our MAO and Sol Gel coating systems into a professional, stand-alone unit that is easy to use and can hold up in relevant OR settings.

REFERENCES: [1]H. Ibrahim, et al. (2019) *Ceramic coating for delayed degradation of Mg-1.2Zn-0.5Ca-0.5Mn bone fixation and instrumentation.* Thin Solid Films. 687:137456.

ACKNOWLEDGEMENTS: This research was, in part, funded by the Advanced Research Projects Agency for Health (ARPA-H). The views and conclusions contained in this document are those of the authors and should not be interpreted as representing the official policies, either expressed or implied, of the United States Government.

European Cells and Materials Vol. NN. Suppl. N, 20xx (page hru)
ISSN 1473-2262

Degradation behavior of as-cast and extruded Mg-Dy-Zn alloys under physiological conditions

Genzhi Jiang[1, *], Yuanding Huang[1, **], Heike Helmholz[2], Yue Zhang[1], Zijian Yu[3], Domonkos Tolnai[1], Norbert Hort[1, 4]

[1] Institute of Metallic Biomaterials, Helmholtz-Zentrum Hereon, Geesthacht 21502, Germany. [2] Institute of Surface Science, Helmholtz-Zentrum Hereon, Geesthacht 21502, Germany. [3] College of Materials Science and Engineering, Beijing University of Technology, Beijing 100124, China. [4] Institute of Product Technology and Systems, Leuphana University Lüneburg, Lüneburg 21335, Germany

INTRODUCTION: Previous work indicated that long-period stacking ordered (LPSO) phase and/or γ′ in rare earth containing Mg alloys had contradictory mechanisms responsible for their degradation in less complex or standard salt media, such as 0.9% NaCl solution [1,2]. They needed to be further investigated in a more realistic simulated body fluid (SBF).

METHODS: Mg-xDy-1.5Zn (x = 5, 10, 15 wt. %) were prepared using direct chill casting process in a permanent mould [3]. After 48 hours heat treatment at 500 °C, the ingot was extruded from the 50 mm billet to a final diameter of 10 mm at 360 °C at a speed of 0.6 mm/s.

Weight loss tests were performed in DMEM+Glutamax ((+) 4.5 g/L D-Glucose, (+) Pyruvate, Life Technologies) together with 10% FBS (PAA Laboratories) and 1% Penicillin Streptomycin (PenStrep) under cell culture conditions (37°C, 20% O_2, 5% CO_2, 95% relative humidity) in the incubator.

RESULTS: In as-cast alloys, the degradation rate of Mg-5Dy-1.5Zn alloy consistently increased. In contrast, though the volume fraction of intermetallics in Mg-10Dy-1.5Zn and Mg-15Dy-1.5Zn alloys are larger than Mg-5Dy-1.5Zn alloys, their degradation rates are lower than Mg-5Dy-1.5Zn alloy.

In extruded with a 48h preheating treatment alloys, the volume fraction of intermetallics increased with the addition of Dy content. However, Mg-5Dy-1.5Zn alloy showed the highest degradation rate among three extruded alloys. Meanwhile, the W phase in Mg-10Dy-1.5Zn alloy did not trigger severe local corrosion. In addition, the Mg-10Dy-1.5Zn alloy contained the dense γ′ phase which act as cathode that accelerates the degradation of Mg matrix, therefore exhibited a higher degradation rate than Mg-15Dy-1.5Zn alloy. The degradation rate results were shown in Fig. 1.

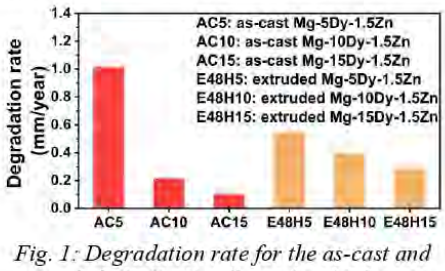

Fig. 1: Degradation rate for the as-cast and extruded Mg-Dy-Zn alloys after 14 days of immersion in DMEM+10%FBS medium

DISCUSSION & CONCLUSIONS: The distribution, type and amounts of intermetallics significantly influenced the degradation behavior of Mg-Dy-Zn alloys. In the as-cast alloys, the continuous network structure of intermetallics (γ′ and 18R LPSO) and a compact degradation layer provided protection from further degradation for AC10 and AC15 alloys, contributing to their lower degradation rate. In the extruded alloys, the denser compact degradation layer on the surface of γ′ phase, which retard the corrosive ions for further penetration to Mg matrix, thus effectively inhibit the further galvanic corrosion triggered by W phase in E48H10 alloy, resulting the lower degradation rate compared to E48H5 alloy.

REFERENCES: [1]J. Xie, Z. Zhang, H. Dong, et al (2025) *Corrosion Science* **243**:112592. [2]C. Dai, J. Wang, Y. Pan, et al (2024) *Journal of Materials Science & Technology* **168**:88-102. [3]F. R. Elsayed, N. Hort, M. A. Salgado-Ordorica, et al (2011) *Mater. Sci. Forum* **690**:65-68.

ACKNOWLEDGEMENTS: Mr. Genzhi Jiang and Dr. Yue Zhang would like to thank the China Scholarship Council for the award of fellowship and funding (Nos. 202106890013 and 202206095009).

European Cells and Materials Vol. NN. Suppl. N, 20xx (page htu) ISSN 1473-2262

In vitro degradation behavior of composite MAO/sol gel coated Mg-1.6Zn-0.5Ca-0.5Mn alloy

S Dutta[1], LH Olivas-Alanis[1,2], G Krieger[1], A Luo[1], D Dean[1,3]

[1] Materials Science and Engineering, The Ohio State University, Columbus, OH, US. [2] School of Engineering and Sciences, Tecnologico de Monterrey, Monterrey, MX. [3] Plastic and Reconstructive Surgery, The Ohio State University, Columbus, OH, US.

INTRODUCTION: Several magnesium (Mg)-based alloys are promising degradable bone implant materials due to their biocompatibility, strength, and low Young's modulus.[1] Resorbable implants have the benefit of facilitating healing and then, unlike permanent implants, removing all risk of interrupting normal function of the healed tissue. However, unless well-timed, Mg alloys may degrade before the healing process is complete. Degradable surface coatings may delay the underlying Mg alloy from degrading until it is no longer needed. Thus, key design criteria for coatings include controlled degradation rates providing a "time-certain" start to the Mg alloy component's degradation. Among the inorganic, organic, and hybrid coatings that have been studied, calcium phosphate (CaP) coatings have been studied because of their chemical similarity to natural bone. CaP coating may also enhance implant integration with surrounding tissue. We evaluated the *in vitro* degradation behavior of Ca-P coatings on heat-treated Mg-1.6Zn-0.5Ca-0.5Mn (OSU Mg alloy) in simulated body fluid (SBF).

METHODS: Rectangular cuboid samples (6 mm x 4.5 mm x 4 mm) were machined from a heat-treated OSU Mg alloy plate using an Electric discharge machine (EDM). The samples were polished with a graded series of sandpaper up to a 1200 grit and then cleaned with ethanol. Next, Micro Arc Oxidation (MAO) was performed in a phosphate electrolyte at 50 mA/cm² for 15 minutes. Subsequently, the samples were coated with a sol gel sealing layer of TiO_2 and entrapped HAP/β-TCP nanoparticles. Three different coating thicknesses were applied: 15, 25, and 50 layers. In vitro degradation was evaluated in SBF at 37°C for 7 and 14 days via hydrogen evolution. Hydrogen evolution was observed using a funnel burette. Sample weight was recorded before and after immersion. The corrosion rate in Millimeters Per Year (MMPY), based on hydrogen evolution data, was calculated via: $2.279*V_h$ (V_h = ml/cm²/d).[2]

RESULTS: Fig. 1(a) shows the corrosion rate of OSU Mg alloy with various coating layers. During the initial immersion period (up to 16 hours), no hydrogen evolution was observed, regardless of the coating type. However, after 24 hours, hydrogen evolution became evident and increased over time. The lowest corrosion rate (0.80 ± 0.09 MMPY) was observed for the 50-layer coating after 14 days of immersion. Additionally, the mass loss measurements correlated well with the corrosion rate determined from the hydrogen evolution test, as shown in Figure 1(b).

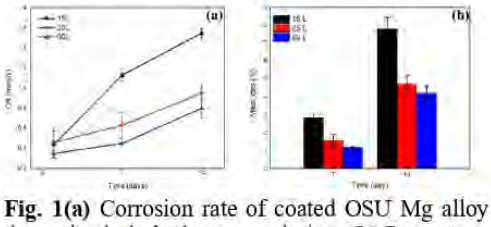

Fig. 1(a) Corrosion rate of coated OSU Mg alloy determined via hydrogen evolution. **(b)** Percentage of mass loss evaluated from weight loss method.

DISCUSSION & CONCLUSIONS:
CAP coating thickness significantly influences the degradation behavior of Mg alloys. Increasing the CaP coating delays the degradation of the underlying OSU Mg alloy device. Determining the optimal coating thickness is essential to preventing the underlying OSU Mg alloy device from the loss of mechanical strength during the healing period. It would be useful to explore whether coatings greater than 50 layers will ensure adequate protection (e.g., 2 months). A time-certain, sufficiently delayed start to degradation of the OSU Mg alloy component may facilitate successful clinical application of this technology.

REFERENCES:

[1] M. P. Staiger, A. M. Pietak, J. Huadmai, G. Dias, *Biomaterials* 2006, *27*, 1728.
[2] W. Zhao, J. Wang, J. Weiyang, B. Qiao, Y. Wang, Y. Li, D. Jiang, *Journal of Magnesium and Alloys* 2020, *8*, 374.

ACKNOWLEDGEMENTS: This research was, in part, funded by the Advanced Research Projects Agency for Health (ARPA-H). The views and conclusions contained in this document are those of the authors and should not be interpreted as representing the official policies, either expressed or implied, of the United States Government.

European Cells and Materials Vol. NN. Suppl. N, 20xx (page htu) ISSN 1473-2262

Stronger Absorbable Wire for Small Anatomies

Jeremy E. Schaffer, Adam J. Griebel
Fort Wayne Metals, Fort Wayne, IN, USA

INTRODUCTION: Stronger absorbable wire materials with good degradation profiles can enable valuable new interventions, especially in small vascular anatomies where relative device downsizing is important. Strength levels beyond 2 GPa are a critical ingredient to success in many medical interventions requiring thin gage wire elements. The strongest material used in medical intervention today is tungsten. This cold drawn microwire breaks at greater than 5 GPa with a modulus of elasticity of 400 GPa and is braided into devices such as neurovascular catheters to provide taut handling, elastic kink resistance, and x-ray visibility. Stainless steel with strengths exceeding 2.9 GPa are routinely used in guidewire cores and provide elastic tip navigation power in delivery of Co-Ni-Cr alloy self-expanding braids with strengths exceeding 2 GPa.

Among absorbable device candidates, magnesium alloys can be processed to achieve strength levels of up to 0.6 GPa with good elasticity on account of low stiffness. Monolithic iron alloys, such as FeMnN, can achieve strengths of more than 2 GPa and about 4x Mg-stiffness with a major drawback of localized breakup[1,2]. New strength levels with useful degradation profiles may be possible with alloy and composite strategies.

This paper highlights findings from work on FeMn with N and C additions as well as via composites of FeMn with molybdenum to prospect high strength solutions for eventual downsized device service, such as in neurovascular flow diverters.

METHODS: Molybdenum (Mo), Fe-30Mn-0.10N-0.08C (FeMnNC), FeMnN-DFT-30%Mo (N30Mo), Fe-35Mn-0.10N (FeMnN), and WE22 magnesium alloy were drawn and processed to near maximum strength through grain refinement and cold-working to a diameter of nominally 0.025 mm and then evaluated by tensile testing for strength comparison.

RESULTS: The highly drawn pure molybdenum wire withstood a stress of greater than 3.2 GPa before fracture. Strengths of other materials fell to FeMnNC, N30Mo, FeMnN, and WE22 respectively as 2.5, 2.4, 2.1, and 0.52 GPa. The elastic range of all wires was tested at greater than 1% strain to yield with wide variation in elastic moduli and good plastic yielding in all materials before rupture, indicating some ability to be formed.

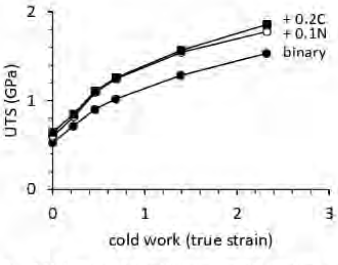

Figure 1. Ultimate tensile strength gains with cold work in Fe-Mn binary and with + 0.10 N or + 0.20 C (both wt.%) wire.

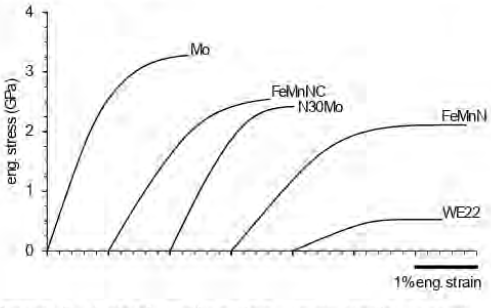

Figure 2. Actual engineering stress-strain curves for a variety of absorbable metal candidates processed to near maximum strength performance.

DISCUSSION: This study shows that certain cold-worked absorbable alloys can exhibit strengths on par with conventional high strength medical wire used in interventional service. Even greater strength and stiffness combinations should be possible with increasing molybdenum composite content while maintaining galvanic deterrent of fragmentation, with potential utility in future low-profile applications.

REFERENCES: [1]J.E. Schaffer, E.A. Nauman, and L. A. Stanciu, *Metal Mater Trans* B 43 (2012): 984-994. [2]A.J. Griebel, et al., *Bioactive Materials* 40 (2024): 74-87.

ACKNOWLEDGEMENTS: The assistance of Dale Herndon, Lane Bailey, Mario Gomez, and the FWM Metlab, is gratefully acknowledged.

European Cells and Materials Vol. NN. Suppl. N, 20xx (page htu) ISSN 1473-2262

Engineering solvent-free resorbable polymer-metal hybrid structures for next generation bone implants

C. Ingelmo[1], S. Sánchez [1], M.D. López[1], P. Rodrigo[1], J. Rams[1], J.P. Fernández-Hernán [1], **S.C. Cifuentes[1*]**

[1] *Dpto. de Matemática Aplicada, Ciencia e Ingeniería de Materiales y Tecnología Electrónica, ESCET, Universidad Rey Juan Carlos, Móstoles, Madrid, 28933, Spain.*

INTRODUCTION: For bone regeneration applications, researchers have developed resorbable metal–polymer composites by incorporating magnesium (Mg) particles into a polylactic acid (PLA) matrix or by applying polymeric coatings onto resorbable metallic scaffolds[1,2]. Other studies have explored reinforcing PLA with Mg wires[3]. These composites offer mutual benefits: Mg enhances the mechanical strength and bioactivity of PLA, while the polymer matrix moderates the corrosion rate of Mg. However, current approaches have yet to achieve the required balance between mechanical strength and biodegradability for clinical applications in bone regeneration. Key limitations include restricted design flexibility, time-consuming and labor-intensive fabrication methods, and the use of toxic organic solvents (e.g., chloroform, dichloromethane), which compromise biocompatibility. Therefore, advancing solvent-free fabrication techniques capable of producing complex geometries is essential to enable clinical translation.

In this study, we developed a novel solvent-free, multi-material manufacturing approach for fabricating resorbable polymer–metal hybrid structures. This method combines metal additive manufacturing (Laser Powder Bed Fusion, LPBF) with polymer processing via compression moulding.

METHODS: Hybrid polymer–metal structures were fabricated using a PLA matrix and AZ91 magnesium alloy. PLA preforms were produced by hot plate pressing, varying temperature and pressure to ensure compatibility with the metallic component. LPBF parameters (laser power and scan speed) were adjusted to fabricate metallic slabs with different surface roughness. Integration of the metal into the polymer matrix was performed via compression moulding, varying preform geometry, moulding temperature, and pressure. A two-month hydrogen release test was conducted to evaluate the degradation behavior of the hybrid structures.

RESULTS: Figure 1 displays the hybrid structures fabricated by combining LPBF and compression moulding. The interfacial bonding strength was modulated by altering LPBF parameters, which influenced the surface morphology of the metallic slabs. Three sample types were immersed in simulated physiological fluid, yielding different degradation behaviors. Sample 1 exhibited structural failure; in Sample 2, hydrogen release caused delamination of the polymer from the metal, forming a gas bubble. In contrast, Sample 3 maintained its structural integrity throughout the two-month period.

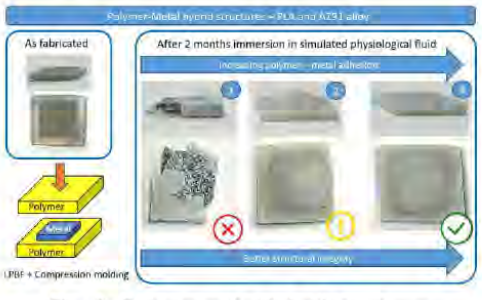

Fig. 1: Polymer-metal hybrid structures.

DISCUSSION & CONCLUSIONS: The integration of LPBF and compression moulding enables the fabrication of solvent-free, resorbable polymer–metal hybrid structures. Surface morphology of the metallic component plays a critical role in interfacial bonding and degradation behavior. Optimized combinations can maintain structural integrity over extended periods, highlighting the potential of this method for developing clinically viable bone regeneration implants.

REFERENCES: [1] R. García-Sobrino et al (2023) *Polymers* **15** https://doi.org/10.3390/polym15244667

[2] S.C. Cifuentes et al (2022) *Metals* **12**:566 https://doi.org/10.3390/met12040566

[3] W. Ali et al (2024) *Advanced Engineering Materials* **26(13)**:2400617 https://doi.org/10.1002/adem.202400617

ACKNOWLEDGEMENTS: The authors would like to thank the funding provided for this research by Universidad Rey Juan Carlos through the project 2024/SOLCON-137037.

BIODEGRADABLE METALS
17th Biometal
25-30 AUGUST, 2025
Grand Hôtel San Michele,
Cetraro, CS, Italy

European Cells and Materials Vol. NN. Suppl. N, 20xx (page htu) ISSN 1473-2262

Microstructural and degradation evaluation of Fe-based biodegradable scaffolds fabricated using polyurethane templates

M Grodzicka[1], G Gąsior[1], A Radtke[1]

[1] *Nicolaus Copericus Univerity in Torun, Faculty of Chemistry, Poland*

INTRODUCTION: Biodegradable materials in biomedical engineering, such as iron alloys, represent a promising solution in orthopaedic implantology. Their advantage is that they can be degraded in a physiological environment, eliminating the need for surgical removal of the implant once it has fulfilled its function. Iron and its alloys have good biocompatibility and adequate mechanical properties, but their corrosion rate is relatively low, which may limit their use in implantology. The addition of elements such as manganese and copper allows the rate of degradation to be accelerated and regenerative processes to be actively promoted. Manganese stimulates angiogenesis by regulating growth factors (e.g. VEGF), stabilises the HIF-1α pathway and reduces oxidative stress in endothelial cells[1]. In addition, it promotes macrophage polarisation towards the M2 phenotype, promoting tissue healing and remodelling[2]. Copper exhibits anti-inflammatory and anticoagulant effects and promotes collagen synthesis and vascular regeneration[3]. Its presence in biomaterials benefits endothelial function, strengthens the structure of regenerating tissues and protects cells from oxidative stress. Fe-Mn and Fe-Cu alloys, due to their modified microstructure and electrochemical properties, degrade much faster than pure iron and represent a promising group of materials for temporary bone implants.

METHODS: The materials studied were: Fe, Fe35Mn, Fe1Cu and Fe35Mn1Cu (designations: Fe, FeMn, FeCu, FeMnCu). Alloys were produced from Fe, Mn and Cu powders using polyurethane (PU) foam as a template. The foams were moulded and dipped in a mixture of metal powders with a 5% polyvinyl alcohol solution (1:2 by weight), dried (95°C, 35 min) and then sintered in a tube furnace (Czylok). Morphology was analysed by SEM (Quanta 3D FEG), elemental composition by EDS (Bruker) and crystalline phases by XRD (Philips X'Pert, CuKα, incident angle 2°). Degradation was studied by potentiodynamic polarisation (BioLogic SP-200) in HBSS (37 ± 2 °C, range ±250 mV vs OCP, 0.5 mV/s). Three-electrode system: working electrode, counter electrode (Pt), reference electrode (Ag/AgCl). The corrosion current density was determined using the Tafel extrapolation method.

RESULTS: FeCu, FeMn and FeMnCu scaffolds were obtained using a polyurethane template, perfectly reproducing it. However, differences in alloy morphology can be seen. In the FeMn sample, the pore walls are thinner and smoother than in the FeMnCu sample. The FeMnCu foam shows the least homogeneous pore wall structure of all the samples analysed. The pore walls in the FeCu alloy are the smoothest. In the FeMn-PU samples, the manganese content was significantly higher than the assumed 35wt%. Local fluctuations in chemical composition were recorded, related to the tendency to form larger metal element clusters.

DISCUSSION & CONCLUSIONS: All analysed iron alloys obtained with the PU template showed a porous structure that reproduced the foam geometry well. FeCu stood out for having the thinnest, smooth walls. In the FeMn and FeMnCu samples, more variability in microstructure was observed, especially in the case of FeMnCu, where the structure was the least homogeneous. EDS analysis revealed an excess of the assumed manganese content (35 wt%) in the FeMn sample, indicating its local accumulation and uneven distribution in the material. This may affect the control of the degradation process and the mechanical properties of the implants. In conclusion, the PU template allows regular porous structures to be obtained. The inhomogeneous distribution of Mn in the scaffold requires further optimisation.

REFERENCES: [1]Wu Jinfu, Qin C *et al.* An immunomodulatory bioink with hollow manganese silicate nanospheres for angiogenesis. *Applied Materials Today*. 2021; 23: 101015.

[2] Wang J, Wang Y et *al.* A Bioinspired Manganese-Organic Framework Amelioratez Ischemic Stroke through its Intrinsic Nanozyme Activity and Upregulating Endogenous Antioxidant Enzymes. *Advanced Science*. 2023; 10: 2206854.

[3] Yue F *et al.* Dealloyed nano-porous TiCu coatings with controlled copper release for cardiovascular devices. *Biomaterials Advances*. 2024; 157: 213728.

Corrosion

Thursday,
August 28th, 2025

elecell
Hope for Healing

BioActiveMetals
Innovation in Metallic Biomaterials

meo.
Inspiring Materials.

medical magnesium

UNIVERSITÉ LAVAL

CHARITÉ
UNIVERSITÄTSMEDIZIN BERLIN

KeAi
CHINESE ROOTS GLOBAL IMPACT

PEKING UNIVERSITY

European Cells and Materials Vol. NN. Suppl. N, 20xx (page htu) ISSN 1473-2262

High-throughput robotic and machine learning-driven discovery of dissolution modulators for post-PEO functionalization of Mg surfaces

B. Vaghefinazari, T. Würger, C. Blawert, M. L. Zheludkevich, C. Feiler, S.V. Lamaka

Institute of Surface Science, Helmholtz-Zentrum Hereon, Geesthacht, Germany.

INTRODUCTION: Plasma electrolytic oxidation (PEO), also known as Microarc Oxidation (MAO), offers well adhering, porous, biocompatible, ceramic-like coatings, providing corrosion resistance, especially when combined with incorporated corrosion inhibitors and sealed by organic or inorganic coatings [1, 2]. Porous PEO coatings with the thickness varying between 1 µm ("flash PEO") to 30 µm also possess high loading capacity and can incorporate corrosion inhibitors, among other functional molecules. The field of potential corrosion inhibitors is close to infinite, as any, of organic molecules reported up to date (ca. 160 million according to CAS) or potentially synthesizable according to the organic chemistry rules (ca. 10^{63}), may possess corrosion modulating ability, slowing down or accelerating degradation of Mg (and any other metallic material) [3].

METHODS: We will demonstrate the experimental setup for high-throughput robotic testing of metallic materials, including those coated by PEO, in complex aqueous environments. The custom-designed robotic platform is capable of precise powder dispensing by analytical balance, multi-channel electrolyte dosing, mixing and aspiration, pH adjustment, batch-removal of corrosion products (e.g. by chromic acid), QR code labeling/reading, measuring weight loss, collecting electrochemical data and image acquisition, among other tasks.

RESULTS: Custom workflows were designed and implemented for batch-testing, including uniform preparation of magnesium surface. Over a hundred organic compounds, including those possessing biological functions, have been tested towards measuring their Mg dissolution modulation efficiency, as one of the target property. Collected datasets are used for training quantitative structure-property relationship (QSPR) machine learning models. For that, the molecular descriptors derived from geometry and DFT calculations encode the molecular information of each compound. Recursive feature elimination is used to select the features most relevant to the target property. The performance of the supervised learning approaches is compared and the prediction accuracy of the data-driven models is assessed by experimental blind testing. This enables virtual, *in silico* screening, potentially outperforming by its throughput even the robotic testing. Active design of experiments includes several testing-prediction-validation rounds, each enlarging the experimental dataset and improving model prediction accuracy.

Fig. 1: Robotic testing platform at Institute of Surface Science, Helmholtz-Zentrum Hereon for high-throughput testing of metallic materials in complex aqueous electrolytes.

DISCUSSION & CONCLUSIONS:

This complex approach enables machine-learning-assisted identification of new, highly efficient dissolution modulators for bare or PEO-coated Mg alloys. Combining dissolution modulation with other target properties enables smart surface functionalization of PEO treated alloys.

REFERENCES: [1] S.V. Lamaka, G. Knörnschild, D.V. Snihirova, M.G. Taryba, M.L. Zheludkevich, M.G.S. Ferreira, (2009) *Electrochimica Acta*, **55**:131-141. [2] B. Vaghefinazari, E. Wierzbicka, P. Visser, R. Posner, R. Arrabal, E. Matykina, M. Mohedano, C. Blawert, M.L. Zheludkevich, S.V. Lamaka, (2022) *Materials*, **15**:8489. [3] D.A. Winkler, A.E. Hughes, C. Özkan, A. Mol, T. Würger, C. Feiler, D. Zhang, S. Lamaka, (2025) *Progress in Materials Science*, **149**:101392.

ACKNOWLEDGEMENTS: DFG, German Research Foundation – project number 535656357, OPTIMA (Identification of optimal corrosion inhibitors for bare and PEO coated magnesium alloy by combining machine learning and robotic testing).

17th Biometal
25-30 AUGUST, 2025
Grand Hôtel San Michele, Cetraro, CS, Italy

European Cells and Materials Vol. NN. Suppl. N, 20xx (page htu) ISSN 1473-2262

Specification setting for RESOLOY®: Influence of dysprosium on property evolution across manufacturing stages in biodegradable cardiovascular stents

HC Trinh[1], N Ihmann[2], R Menze[1], C Podolsky[2]

[1] *MeKo Manufacturing e.K., Sarstedt, Germany.* [2] *Faculty of Engineering and Health, HAWK Göttingen, Göttingen, Germany*

INTRODUCTION: RESOLOY® is a rare-earth based magnesium alloy developed for use in biodegradable cardiovascular implants [1]. Previous studies identified a Dysprosium (Dy) content of around 10 wt.% as delivering a suitable combination of mechanical and corrosion properties [2]. This study aims to define a practical Dy specification range based on experimental evidence and production feasibility, and explore potential alloy development opportunities. To this end, we performed a systematic analysis of microstructure, mechanical properties, and degradation behavior across a series of RESOLOY® variants containing 8–14 wt.% Dy. Testing was conducted on semi-finished materials, as well as on laser-cut cardiovascular stents, to assess application-relevant performance and track property evolution throughout manufacturing.

METHODS: RESOLOY® alloys with Dy concentrations of 8%, 10%, 11%, 12%, and 14% were fabricated by MeKo Manufacturing e.K. (Sarstedt, Germany) while maintaining constant secondary element levels [3]. Microstructural characterization was performed via light and scanning electron microscopy (SEM). Mechanical properties were assessed through Vickers hardness and uniaxial tensile testing. In vitro degradation behavior was evaluated in a semi-static incubator setup (37°C, CO2 buffering) by mass loss and photometric analysis in phosphate-buffered saline (PBS) [1,3]. Testing was conducted on semi-finished materials (cast, bar, tube) and final stent devices.

RESULTS: Hardness and tensile strength increased with rising Dy content, accompanied by a slight reduction in ductility. This is linked to the increased presence of long-period stacking ordered phases [4] which also have a strong impact on degradation homogeneity (Fig. 1). Degradation rates showed a mild increase at higher Dy levels (12–14%). The grain size remained largely stable across Dy variations. Critically, stent testing confirmed that mechanical integrity and controlled degradation behavior were maintained at the device level, demonstrating material performance for potential clinical applications.

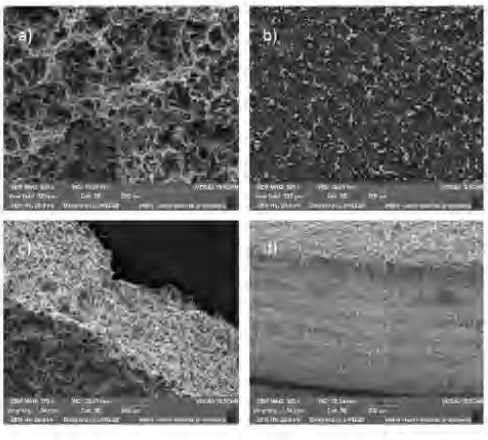

Fig. 1: SEM images of cast (a/c) and bar (b/d) degradation samples, showing cast samples exhibit more inhomogeneous degradation.

DISCUSSION & CONCLUSIONS: The findings suggest that a Dy-specification ranging from 9–11 wt.% for RESOLOY® is an appropriate balance of manufacturing practicality and robustness of material properties. Moderate trends in hardness, strength, and degradation behaviour were observed with Dy variation, but no critical deterioration occurred beyond this range. Hence, future improvements may be more effectively achieved by refining processing parameters to enhance performance. Several Dy-sensitive properties were identified that are well suited for early-stage quality monitoring strategies. Together, these results offer a data-driven foundation for specification setting and demonstrate how material understanding can be translated into an efficient, regulatory-ready production for medical-grade alloy systems.

REFERENCES:

[1] R. Menze, E. Wittchow. J. Biomed. Mater. Res. Vol. 109, 9 (2021). 1292-1302
[2] L. Yang, Y. Huang et al. Mat. Sci. Eng.: B. Vol. 176, 20 (2011). 1827-1834
[3] J. Gonzalez, R.Q. Hou, E. Nidadavolu et al. Bio. Mat. Vol. 3, 2 (2018). 174-185
[4] P. Maier et al. JOM. Vol 72 (2020). 1870-1879

European Cells and Materials Vol. NN. Suppl. N, 20xx (page htu) ISSN 1473-2262

Toward a mechanistic understanding of trace-element influence on corrosion at the magnesium-biology interface

M.Hannard[1,2], M.Cihova[1], D.Bleiner[2,3], P.Schmutz[1]

[1] *Laboratory for Joining Technologies and Corrosion, Empa - Swiss Federal Laboratories for Materials Science and Technology, Dübendorf, CH* [2] *Graduate School of Chemical and Molecular Sciences Zurich, University of Zürich, Zurich, CH.* [3]*Laboratory for Advanced Analytical Technologies Empa - Swiss Federal Laboratories for Materials Science and Technology, Dübendorf, Switzerland.*

INTRODUCTION: Biodegradable magnesium (Mg) implants are promising alternatives to permanent metallic implants in biomedical applications. Yet, their clinical use is hampered by its complex and still not precisely predicted corrosion mechanisms in the physiological environment [1]. A key parameter influencing the reaction kinetic is the presence/reactivity of trace elements (Fe, Zn, Cu), noble to Mg, present in the peri-implant microenvironment and as impurities in Mg. These elements are known to impact Mg dissolution by creating active cathodic sites in simple salt containing electrolyte, though their reactivity in complex physiological conditions is still unknown.

METHODS: In this study, the complex interplay of Fe (the most catalytic impurity) ions with complex electrolytes and its reduction is studied by electrochemical quartz microbalance (eQCM) at potentials establishing on corroding Mg surfaces.

The results obtained are then correlated with an analysis of trace elements present on the Mg surfaces and in corrosion products after exposure to iron containing solution using Laser Ablation coupled with Inductively Coupled Plasma Mass Spectrometry (LA-ICP-MS) [2]. Additionally, an analysis of the electrolyte in contact with Mg was conducted using classical ICP-MS to determine ionic concentration changes in the liquid phase.

RESULTS: eQCM measurements revealed insight into Fe-redeposition kinetics, particularly in the electrochemical potential range (-1.6$V_{vs\ Ag/AgCl}$) where strong hydrogen reduction dominates the current signal and prevent any analysis of minor reduction reactions. Additionally, LA-ICP-MS trace-element analysis, calibrated on Mg model systems with varying trace-element purity, demonstrated the ppm sensitivity of the method. With this method, Fe presence (orange signal) within the corrosion layer after immersion in Fe-containing buffered solutions could clearly be identified (Fig. 1A). The Fe content of the immersion solution was also monitored over time and showed a decreasing trend (Figure 1B), which correlated well with LA-ICP-MS results.

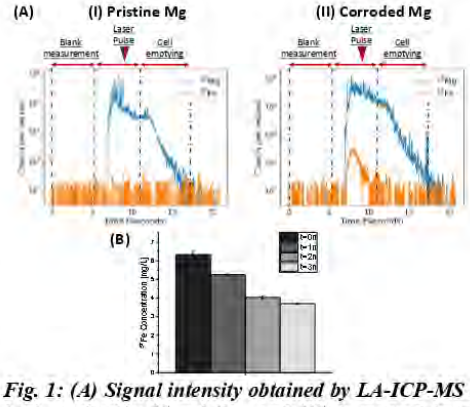

Fig. 1: (A) Signal intensity obtained by LA-ICP-MS of high purity-Mg (I) pristine and (II) immersed in Fe-containing solution. The laser firing started after 5 s of measurement. (B) Histogram showing the evolution of ^{56}Fe over time, following the immersion of High Purity-Mg in Fe-containing solution.

DISCUSSION & CONCLUSIONS: LA-ICP-MS has been able to assess trace element presence in Mg samples and eQCM allowed us to follow and quantify deposition of metallic Iron as trace element in a domain of electrochemical potential (-1.6$V_{vs\ Ag/AgCl}$) where electrochemical signal cannot be interpreted. This comprehensive approach aims to improve knowledge about the key factors impacting Mg In-vivo biocorrosion, offering valuable insights for the larger user of more reliable biodegradable implant in biomedical applications.

REFERENCES: [1]*Amukarimi, S., & Mozafari, M. (2021). MedComm, 2(2), 123–144* [2]*M. Stafe* et al., *Pulsed Laser Ablation of Solids, Springer Series in Surface science, Vol. 53, 2014, pp. 241.*

ACKNOWLEDGEMENTS: This research is financially supported by the MAGnostic project, funded by the Swiss National Science Foundation (SNSF, grant No: 310030E_205609).

European Cells and Materials Vol. NN. Suppl. N, 20xx (page htu) ISSN 1473-2262

Antibacterial Biodegradable Fe-Mn-C-Cu Sintered Alloys: Mechanical Properties, Degradation Behavior, and Biological Performances

Abdelhakim Cherqaoui[1], Carlos Henrique Michelin Beraldo[1], Carlo Paternoster[1], Simon Gélinas[2], Carl Blais[2], Diego Mantovani[1]

[1]: Laboratory for Biomaterials and Bioengineering, Research Center of CHU de Quebec, Quebec City, G1L 3L5, Canada;
[2]: Department of Min-Met-Materials Engineering, Laval University, Quebec City, G1V 0A6, Canada.

INTRODUCTION: Fe-Mn-C alloys have recently garnered significant attention for use in temporary biodegradable implants due to their excellent mechanical properties and good biocompatibility [1]. However, tailoring their degradation rate remains essential to expand their clinical applicability [2]. In this context, the present study explores the effect of Cu addition on the mechanical, degradation, and biological performances of Fe-Mn-C-based alloys fabricated via pressing and sintering process. The influence of Cu on microstructural evolution, mechanical strength, corrosion behavior, and antibacterial properties of the sintered alloys is systematically evaluated.

METHODS: Powder mixtures were prepared by blending for 1 h a gas-atomized Fe-16Mn-0.6C powder (75 wt.%) with a mechanically mixed powder of identical composition (25 wt.%) and varying additions of pure Cu at 0, 1, and 5 wt. %. The particle size distribution, powder morphology, and chemical composition were analyzed using a laser particle size analyzer, SEM/EDS, and microwave plasma atomic emission spectroscopy (MP-AES), respectively. Compacts were uniaxially pressed at 600 MPa and sintered at 1200 °C for 180 min under Ar-10 vol.% H_2, with a 10 °C/min heating rate and rapid cooling (26 °C/min). Microstructural and mechanical characterizations were carried out via SEM, X-ray diffraction (XRD), and three points bending testing. Degradation behavior was assessed using electrochemical testing in Hanks' solution (pH 7.4) at 37 °C. Biological performances were evaluated through in vitro cell viability assays and colony-forming unit (CFU) tests to assess cytocompatibility and antibacterial activity, respectively.

RESULTS: The prealloyed gas-atomized Fe-Mn-C powder used in this study contains approximately 16 wt.% Mn and 0.6 wt.% C, with a low O content of ~ 0.05 wt.%. The powder particles exhibited a highly spherical morphology, as shown in Fig. 1a (SEM image at 200 µm scale), which enhanced the overall flowability of the starting powder, with an average measured flow rate of 24 s/50 g. SEM micrographs of the A0 condition, presented in Fig. 1b, confirmed the predominance of an austenitic microstructure, as predicted by the Schumann's diagram of Fe-Mn-C system [3]. As illustrated in Fig. 1b, the microstructure was fine but somewhat heterogeneous, with the presence of both large and small pores, the latter located within the grains. Cu was observed to form aggregates and islands, whose size depends on its overall amount.

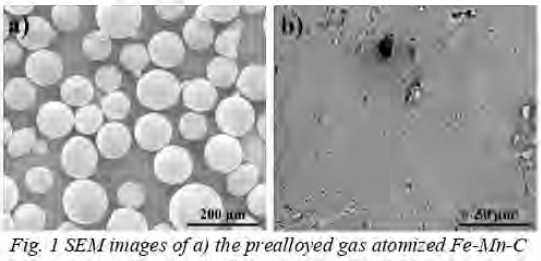

Fig. 1 SEM images of a) the prealloyed gas atomized Fe-Mn-C powder; b) A0 after etching with Nital 2%.

DISCUSSION & CONCLUSION: Fe-Mn-C-Cu samples were successfully produced via pressing and sintering using prealloyed gas-atomized powder. All the sintered alloys exhibited a high fraction of austenitic phase due to the high Mn and C content, which is particularly advantageous for MRI imaging, given the non-magnetic nature of austenite [3]. The addition of Cu is expected to influence both corrosion and biological behavior. Specifically, Cu promotes localized galvanic interactions that can accelerate the degradation process, especially in the A5 condition. Additionally, Cu's well-known antimicrobial properties are anticipated to enhance the antibacterial performance of the alloys, making them promising candidates for temporary implants with reduced infection risk. Ongoing work will address in-depth the degradation mechanism, the mechanical properties, and the biological responses of the sintered alloys to validate their clinical potential.

REFERENCES: *[1] Gambaro S. et al., Mat Tod Comm 27 (2021) 102250; [2] Schinhammer M. et al., Acta Bio 6 (2010) 1705; [3] Cherqaoui A. et al, Bioact. Mater. 41 (2024) 96-107.*

ACKNOWLEDGEMENTS: This work was funded by NSERC-Canada under the Alliance program.

European Cells and Materials Vol. NN. Suppl. N, 20xx (page htu)
ISSN 1473-2262

Localized accelerated degradation of magnesium: A new insight into the mechanism of its biomedical degradation

Y Zhang[1, 2], YD Huang[1], J Bai[2, 3], N Hort[1]

[1] *Institute of Metallic Biomaterials, Helmholtz-Zentrum Hereon, Geesthacht, DE.* [2] *School of Materials Science and Engineering, Southeast University, Nanjing, CHN.* [3] *Institute of Biomedical devices, Southeast University, Suzhou, CHN.*

INTRODUCTION: A distinctive phenomenon involving the localized accelerated degradation of magnesium (Mg) can be traced numerous times on bone fixation devices *in vivo*, as well as on Mg tubes and porous Mg *in vitro*. It caused Mg to degrade several times to even a dozen times faster. The present investigation reproduced this phenomenon using the Mg tubes in artificial blood plasma (ABP) and explored its occurrence mechanism. We proposed a new insight into the mechanism of Mg degradation and emphasized the importance of considering the relevant factors leading to such a phenomenon in future Mg applications.

METHODS: Mg-4Zn (96 wt.% Mg, 4 wt.% Zn) tubes with a wall thickness of 0.15 mm and a length of 10 mm were used in this study. The sheets and half tubes were fabricated from a tube by mechanically flattening and cutting the intact tube in half longitudinally, respectively. Their degradation behaviors in ABP solution at (37.5 ± 0.5) °C were investigated through a combination of the hydrodynamic platform, real-time electrochemical detection, COMSOL simulation, and morphological observations. The chemical composition of the degradation products on the surface was determined by EDX, XRD, XPS and FTIR. The release of Mg^{2+} was detected by ICP. Hydra-Medusa software was used to calculate the possible formation of precipitations in the chemical system of ABP.

RESULTS: The degradation rate of the Mg-4Zn tube is nearly four times higher than that of the same material in sheet form after static immersion in ABP for 14 h (Fig. 1). Further investigations show that the hydrodynamic condition leads to a decrease in the degradation rate of intact tubes compared to the static condition, while its effect on half tubes is adverse. The solution pH value inside the intact tube is significantly higher than that outside the tube. Moreover, when the pH value of ABP exceeds 8.6, the corrosion resistance of Mg-4Zn declines sharply, coinciding with a reduction in the concentration of Ca^{2+} and PO_4^{3+} and the appearance of insoluble precipitates.

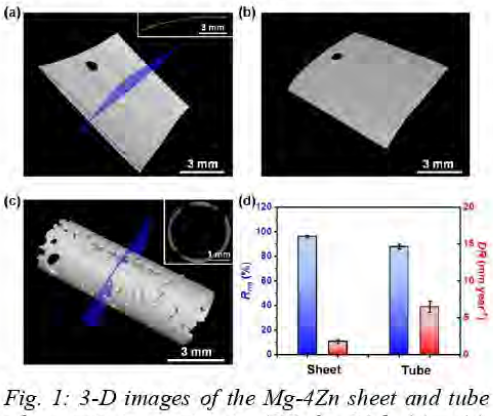

Fig. 1: 3-D images of the Mg-4Zn sheet and tube after static immersion in ABP for 14 h (a) - (c), and the corresponding mass loss data (d).

DISCUSSION & CONCLUSIONS: The degradation rate of Mg-4Zn tubes decreases with the increase of FISS values initially, followed by an increase when the FISS value is greater than 0.96 Pa. In contrast, the degradation rate of Mg-4Zn half tubes increase as the FISS value increases. The deficiency of Ca^{2+} and PO_4^{3+} in the static solution with a relatively enclosed environment, which is induced by the excessively high pH value, results in an inhomogeneous distribution of the Ca-P-rich precipitates on the surface. These resultant degradation products hardly provide effective protection for the magnesium matrix. This is the fundamental reason for such a localized accelerated degradation.

REFERENCES: [1]Y. Zhang, K. Yan, W. Xu, et al (2024) *Corros Sci* **237**:112335.

ACKNOWLEDGEMENTS: This work was supported by the Sino-German program for the award of fellowship and funding (202206095009, 91870848), the Science and Technology Project of Jiangsu Province (BE2023719).

17th Biometal
25-30 AUGUST, 2025
Grand Hôtel San Michele,
Cetraro, CS, Italy

European Cells and Materials Vol. NN. Suppl. N, 20xx (page htu) ISSN 1473-2262

Impact of heat treatment on the degradation behaviour of electropolished WE43

J Kloiber[1,2], S Rieger[1], H Hornberger[1,2]

[1] Biomaterials Laboratory, Faculty of Mechanical Engineering, Ostbayerische Technische Hochschule (OTH) Regensburg, Regensburg, Germany. [2] Regensburg Center of Biomedical Engineering (RCBE), Ostbayerische Technische Hochschule (OTH) Regensburg and University of Regensburg, Regensburg, Germany.

INTRODUCTION: By using specific selected rare earths metals, the Mg-alloy WE43 is of great interest for biodegradable implants. However, Mg-based material carry the risk of inhomogeneous degradation [1]. Electropolishing has developed into a promising surface treatment for Mg materials [2], but local property changes in the microstructure limit the quality level of electropolished surfaces which can be decisive for subsequent corrosion processes. The aim of the study was to investigate the degradation of electropolished WE43 with (1) coarse, (2) dissolved and (3) finely dispersed precipitates to obtain a correlation of bulk heat treatment and corrosion behaviour after electropolishing for this bioresorbable metal.

METHODS: WE43 discs (Y 4.8 wt.%, Nd 2.1 wt.% and Zr 0.1 wt.%) with a surface area of 1 cm² were used as working material. The samples were first solution annealed (T4) at 540°C for 4h. Half of them were then immediately aged (T6) at 300°C for 1h (Fig. 1a). Electropolishing was carried out at 21°C in a mixture of phosphoric acid, ethanol and deionized water in a ratio of 40:56:4 at a voltage of 2 V up to 18C [3] (Fig. 1b). The degradation behaviour was investigated by potentiodynamic polarization using the electrolyte Dulbecco's Modified Eagle's Medium (DMEM). The corroded surface areas were observed using a confocal laser scanning microscope (CLSM) and a scanning electron microscope (SEM).

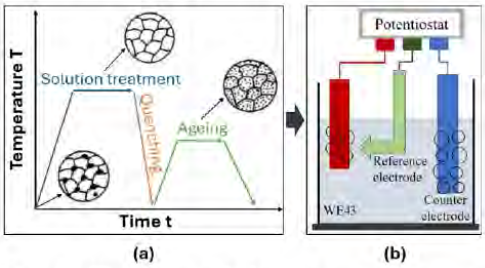

Fig. 1: Illustration of the processing steps on WE43 which consists of a combination of (a) heat treatment processes and (b) an electropolishing process for Mg materials.

RESULTS: The electrochemical surface treatment led to a significant reduction in the corrosion rate (< 0.1 mm/year). The lowest degradation rates of electropolished WE43 were found in the initial and T6 condition. However, the solution annealed and aged alloy showed a less attacked surface in DMEM and the most homogeneous corrosion morphology (Fig. 2). The needle-shaped precipitates after T6 led to uniform material removal during electropolishing and thus contributed corrosion resistance, while the coarse secondary phases in the initial state caused irregularities on the electropolished surface.

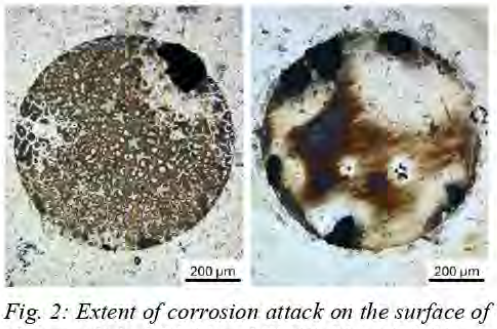

Fig. 2: Extent of corrosion attack on the surface of electropolished WE43 and WE43-T4 in DMEM.

DISCUSSION & CONCLUSIONS: The best relation of moderate corrosion rate and regular corrosion morphology was found with finely precipitated, electropolished WE43. The electrochemical results confirmed that the microstructure plays an important role for subsequent electropolishing, suggesting that the corrosion behaviour of electropolished surfaces can be modified via heat treatment by changing the amount and size of precipitates.

REFERENCES: [1] A.H. Martinez Sanchez (2015) *Acta. Biomater.* **13**:16-31. [2] J. Kloiber et al. (2024) *Mater. Today Commun.* **38**:107983. [3] J. Kloiber et al. (2025) *Electrochim. Acta* **513**:145547.

ACKNOWLEDGEMENTS: We gratefully thank Regensburg Center of Biomedical Engineering (RCBE) for the support of laboratory consumables.

European Cells and Materials Vol. NN. Suppl. N, 20xx (page htu) ISSN 1473-2262

Controlling the corrosion rate of a WE43 biodegradable alloy by surface engineering

S Galea[1], L Fanton[1], J Buhagiar[1], DA Vella[1], B Mallia[1]

[1] *Department of Metallurgy & Materials Engineering, Faculty of Engineering University of Malta, Msida MSD 2080, Malta*

INTRODUCTION: Bone is the second most transplanted tissue worldwide, underscoring the clinical demand for effective solutions to repair skeletal defects [1]. Magnesium-based alloys offer a compelling alternative to permanent implants due to their mechanical compatibility with bone, biodegradability, and inherent biocompatibility [2]. However, their rapid corrosion in physiological environments hinders clinical use. This study investigates calcium phosphate chemical conversion treatments (CaP) and dual CaP–polylactic acid (PLA) coating system on WE43, with the aim of reducing the corrosion rate and ensuring sustained mechanical support during the tissue healing process in orthopaedic applications.

METHODS: The surface of extruded T5 WE43 coupons were subjected to chemical conversion by 1h immersion in a 40 mL bath containing 0.2mol/L phosphoric acid (H_3PO_4) 0.2mol/L calcium nitrate ($Ca(NO_3)_2$) and maintained at a set temperature of 70°C. Bath pH was adjusted to 3 using 3 molar sodium hydroxide (NaOH) solution. Biodegradable PLA having a molecular weight of 55k g/mol was solvent casted from a 5 wt.% solution in tetrahydrofuran. An ACEdip-coater was used to deposit a uniform film of PLA on the CaP layer.

Surface morphology was examined using a Zeiss optical microscope and a field emission scanning electron microscope (SEM), with elemental composition assessed via energy-dispersive X-ray spectroscopy (EDS). Crystalline phases were identified using a Rigaku Ultima IV X-ray diffractometer (XRD). Corrosion behavior was assessed in Hank's Balanced Salt Solution (HBSS) + Ca^{2+} at 37 ± 1°C using a potentiostat. Hydrogen evolution tests in HBSS + Ca^{2+} further investigate long-term degradation mechanisms.

RESULTS: The untreated WE43 surface exhibited a smooth, featureless morphology typical of mechanically polished magnesium alloys. Following the applied surface treatment, distinct microstructural differences were observed (Fig. 1). The CaP conversion layer revealed a densely packed, plate-like crystalline morphology. EDS analysis indicated that the crystalline features were composed of 51.5 at.% O, 25.2 at.% Ca, and 24.5 at.% Ca. XRD analysis confirmed the presence of brushite, calcium hydrogen phosphite, and monetite as the major crystalline phases. The CaP-PLA coating maintained the plate-like morphology, exhibiting a smoother, more homogenised appearance, with localised PLA accumulation causing partial surface levelling. EDS showed a composition of 49.8 at.% C, 24.1 at.% O, 14.5 at.% P, and 11.6 at.% Ca. This modified topography, suggests enhanced wettability and potential for improved interfacial integration with tissue.
Potentiodynamic polarisation tests showed that CaP and CaP-PLA reduced the initial corrosion rate. The CaP layer offered short-term protection, while PLA further delayed corrosion. Degradation increased over time as the coatings dissolved, with the rate influenced by the thickness of the layers.

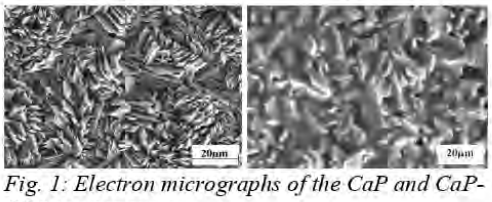

Fig. 1: Electron micrographs of the CaP and CaP-PLA coating system.

DISCUSSION & CONCLUSIONS: The porous, plate-like CaP layer created a high-surface-area layer conducive to anchoring, while the PLA coating exhibited good wettability and strong adhesion. The corrosion data showed a reduction in corrosion current density and an extended induction period prior to corrosion onset of the WE43 alloy. These findings support CaP–PLA coating system as an effective way to delay corrosion and preserve mechanical integrity for bone-contact applications.

REFERENCES: [1] H. Shegarfi and O. Reikeras (2019) *Review article: Bone transplantation and immune response*, Journal of Orthopaedic Surgery, vol. 17, no. 2. [2] J. Wang et al (2022) *Research progress of biodegradable magnesium-based biomedical materials*, Journal of Alloys and Compounds, vol. 923.

ACKNOWLEDGEMENTS: This template was modified with kind permission from eCM Journal. This work was supported through the ENDEAVOUR II Scholarship.

17th Biometal
25-30 AUGUST, 2025
Grand Hôtel San Michele,
Cetraro, CS, Italy

Liquid Ag, Zn, and Zn-based Alloys on Biodegradable Hadfield Steel for Biomedical Applications: Wettability and Interfacial Reactivity

S Gambaro[1,2], C Paternoster[2], A Bigos[3], M Janusz-Skuza[3], M Rancan[1], L Armelao[4], J Wojewoda-Budka[3], D Mantovani[2], F Valenza[1]

[1] *National Research Council, Institute of Condensed Matter Chemistry and Technologies for Energy, ICMATE, Italy*
[2] *Laboratory for Biomaterials and Bioengineering, Laval University, Quebec City, Canada*
[3] *PAS-IMMS – Polish Academy of Sciences - Institute of Metallurgy and Materials Science, Poland*
[4] *Department of Chemical Sciences, University of Padova, Italy*

INTRODUCTION: Fe-Mn steel is an interesting candidate for load-bearing biodegradable implants [1]. This kind of steel can be used together with other elements, added for specific purposes (e.g. Zn and Ag for antibacterial properties). Zn and Ag, known for antimicrobial and osteogenic properties, can be used as coatings to improve performance[2]. These alloys, which can be produced in many ways, has a strong tendence to oxidation, because of the high Mn amount; the presence of oxygen have strong effect on the formed phases when Zn and Ag are in contact. Understanding the wetting and interfacial behavior of a Fe-12Mn-1.2C with different surface chemistries (mechanically polished - MP, or oxidized under control with a plasma treatment-PO) is the key to optimize a series of processes and procedure in the fabrication of the multielement alloy.

METHODS: Fe12Mn1.2C coupons, after MP and PO, were used as two different substrates. Ag, Zn, Zn–Ag alloys were arc-melted into spherical buttons under Ar. Starting materials were characterized by SEM-EDS, XPS and 3D-profilometry before high-T tests. Wettability was assessed by sessile-drop tests in a custom alumina-tube furnace at selected temperature for each system. Microstructure and interfacial phases of cross-sectioned samples were assessed by SEM-EDS/TEM analysis.

RESULTS: XPS analysis, used to characterize the surface oxide, showed O a Fe layer. Unlike the native oxide on MP samples, which contains mixed oxides and metallic traces, the PO surface shows no metallic Mn or Fe. Depth profiling confirms a uniform oxide film ~ 100 nm thick. Zn and its alloys showed a reactive wetting on MP-Hadfield, with contact angles steadily decreasing and stabilizing after 200 s (Fig.1a). All exhibited similar slopes and symmetric drop profiles after 300 s, with final contact angles, $\theta < 20°$. In contrast, the liquids on PO-Hadfield failed to wet, maintaining $\theta > 140°$ (Fig.1b). Ag, however, behaved differently: on both substrates, θ quickly stabilized at ~ 65° after melting and remained constant to 300 s. The analyses of cross-sectioned samples showed that continuous interfacial layers of Fe-Zn and Fe-Zn-Ag intermetallic compounds formed at Zn-based liquid and MP-substrate. No metal diffusion nor interfacial layers were instead found for pure Ag/Hadfield system.

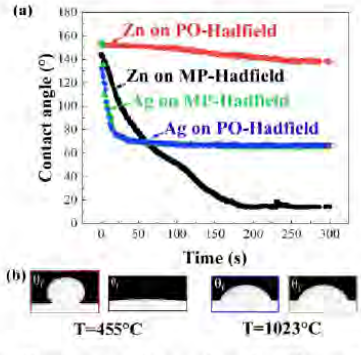

Fig. 1: Contact angle vs *time for Zn and Ag on MP- and PO-Hadfield (a); drop profiles after 300 s at the selected temperature (b).*

DISCUSSION & CONCLUSIONS: Zn and Zn–Ag alloys showed ideal wetting on MP-Hadfield, making them suitable for industrial use, but failed to wet the PO surface. In contrast, Ag wetted both substrates without forming a reactive layer, likely due to its ability to dissolve O in the liquid state. Due to the low contact angle and distribution of the intermetallic phases, Zn7Ag/MP-Hadfield interface seemed to be the most promising and its corrosion and biocompatibility need to be assessed.

REFERENCES: [1] S Gambaro et al (2021) Mater Today Commun 7. [2] M Hussain et al (2022) J Funct Biomater 14.

ACKNOWLEDGEMENTS: Memorandum of Understanding between CNR-ICMATE (Genoa, IT) and Laval University-LBB (Quebec, CA).

European Cells and Materials Vol. NN. Suppl. N, 20xx (page htu) ISSN 1473-2262

Effect of Tensile and Compression Loading on the Degradation Behaviour and Subsequent Cyclic Testing Response of Coated and Uncoated WE43 Mg Alloy

R Correa Schragen[1], M Behbahani[2], A Kopp[1], JM Seitz[1]

[1] *Medical Magnesium GmbH, Medical Magnesium GmbH, Aachen, Germany*

[2] *Aachen University of Applied Sciences, Jülich Campus, Med. Eng.and Technomath., Aachen, Germany*

INTRODUCTION: Degradable polymer-based biomaterials were introduced into clinical practice several decades ago, with their material-specific limitations being carefully considered.[1] The advent of biodegradable metal-based devices aimed at overcoming these limitations has significantly heightened the importance of investigating corrosion-related material behavior under physiological load conditions.[2] Particularly, orthopedic implants experience a wide range of loading conditions while implanted, influencing their degradation process in vivo. Both tensile and compressive forces, may affect the corrosion resistance of these implants and, consequently, their ability to effectively support the surrounding tissue.[3] This study examines the effects of high physiological static tensile and compressive loads on the in vitro degradation of the magnesium alloy WE43 and its subsequent cyclic performance and offers potential protection strategies.

METHODS: Round tensile test alike samples with a cannulated shaft, fabricated from the magnesium alloy WE43MEO in coated and non-coated state, were subjected to in vitro degradation in phosphate-buffered saline (PBS) at 37°C for up to 10 days, maintaining a pH between 7.4 ± 0.2 in accordance with ASTM F3268. The samples in non-coated state and those that featured PEO and MgF_2 surface modifications, were exposed to static tensile or compressive loads of 230 N, corresponding to 50 MPa based on the cross-sectional area of the shaft segment. The static loads were applied via a mounting rig incorporating either tension or compression springs. To prevent galvanic corrosion between the rig and the samples, the rig was partially coated with wax, leaving only the samples' shaft exposed to the PBS. Subsequent sinusoidal cyclic testing (with a tension/compression stress ratio of R = -1) was performed at a frequency of 25 Hz, applying a stress amplitude of 656 N (~136 MPa), which approximately corresponded to the previously determined fatigue strength in the non-degraded state (Fig. 1). The pH evolution, gas release, and mass loss of the samples were measured as a function of the applied load conditions, surface treatment, and degradation duration. Using cyclic testing the remaining cycles to failure were determined in identical dependence.

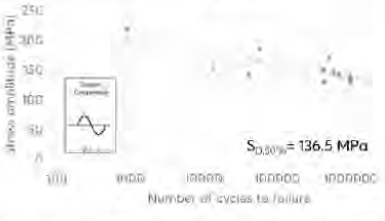

Fig. 1: S-N curve of non-coated WE43MEO

RESULTS: In non-coated condition, gas release measurements showed no statistically significant differences in release rates considering loads. A trend toward reduced gas release was observed in samples subjected to constant compressive loading, with an average decrease of 31 % after 72 hours. Conversely, samples under constant tensile loading exhibited a tendency toward increased gas release, with an average increase of 11 % after 72 hours. This trend persisted throughout the 10-day corrosion period. Subsequent cyclic testing resulted in 13,314 ± 3,484 load cycles for non-coated but 72 h degraded samples. Cycles until failure (8,661 ± 2,053) were reduced for samples that previously degraded under tensile loads after 72 h of corrosion. Constant compressive loads increased the cycles until failure by approx. 46.7 % after 240 h of corrosion. Both coatings PEO and MgF_2 reduced degradation and had an increasing positive impact on cycles until failure.

DISCUSSION & CONCLUSIONS: This study demonstrates the critical influence of mechanical loading on the degradation behavior of magnesium implants. Compressive loading may extend implant lifetime, whereas tensile loading can accelerate degradation. The presented coatings show potential to reduce load-induced corrosion effects and improve performance. Results of this study have to be carefully considered when designing new implants.

REFERENCES: [1] C. Li, C. Guo, V. Fitzpatrick, et al. (2020) *Nat Rev Mater* **5**:61-81. [2] Q. Tian, J.A. Mendeza, l. Rivera-Castaneda, et al. (2018) *Mater. Let.* **217**:27-32. [3] Y. Koo, H.-B. Lee Z. Dong,et al. (2017) *Nature Sci. Rep.* **7**:14710.

Residual mechanical properties of corroded WE43, ZX10 and Mg10Gd under varying degree of pitting corrosion

A Dimakopoulou[1], J Bohlen[2], P Maier[1,3]
[1]*University of Applied Sciences Stralsund, Stralsund, Germany,* [2]*Helmholtz-Zentrum Hereon, Geesthacht, Germany,* [3]*Lund University, Lund, Sweden*

INTRODUCTION: In addition to the corrosion rate, corrosion morphology also plays a crucial role in the development of Mg alloys with the application of bioresorbable implants[1,2]. This study investigates the influence of corrosion behaviour on the residual mechanical properties during corrosion of extruded Mg alloys for WE43, ZX10 and Mg10Gd. In particular, pitting corrosion is considered, as it can lead to premature failure[3]. The project focuses on how critical pitting is exactly and whether the failure mechanism changes over the corrosion period to "small area failure".

METHODS: The corrosion rate of cylindrical samples was evaluated by weight loss during immersion in HBSS solution at 37 °C. Different corrosion times were applied. Also, the gauge length of tensile specimens (diameter of 4 mm and length of 9 mm) was corroded to investigate the residual tensile strength. The specimens undergo µCT scans after corrosion - before tensile testing, and after tensile testing. With that, the fractured area can be correlated with the corrosion morphology to determine the influence of pits.

RESULTS and DISCUSSION: The grain size of the Mg-RE alloys is in a similar range: 6.61 µm ± 9.00 µm for WE43 and 9.63 µm ± 1.81 µm for Mg10Gd, ZX10 has grains of 13.0 µm ± 0.40 µm. Aligned precipitates in the extrusion direction were found in WE43 and Mg10Gd, but all materials are homogeneously recrystallised. The tensile strength is with 238 MPa the highest for Mg10Gd. WE43, at 218 MPa, has a similar strength compared to ZX10 with 213 MPa. Figure 1a shows the residual tensile strength of extruded WE43, ZX10 and Mg10Gd as a function of corrosion exposure time. Even as the data points scatter, it becomes clear that WE43 and Mg10Gd lose their strength stronger over corrosion time than ZX10. The strength loss over the smallest remaining cross-section (Figure 1b) shows in agreement that WE43 loses the strength the most, already by small corrosion attack. ZX10 retains its initial sample size and load up to 10 days with a slight decrease at 12 days, but no more than 89 %. Whereas the corrosion rate of Mg10Gd and WE43 is increasing over time, it is decreasing for ZX10. By µCT-2D and 3D data evaluation of each single tensile specimen according to the location of the fractured

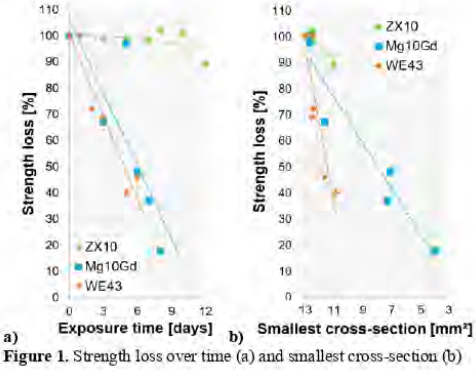

Figure 1. Strength loss over time (a) and smallest cross-section (b)

area, or better according to the crack initiation site, the "weakest region" can be identified. The evaluation of the gauge length of Mg10Gd after 3 days in HBSS is shown in Figure 2. It was determined that the specimen failed neither at the smallest remaining cross-section after corrosion nor at the deepest pit, which was here in agreement with the smallest cross-section. The smallest cross-section shows overlapped pit accumulation on opposite sides. However, the specimen failed at a deep corrosion pit, which was only located on one side of the gauge length. Other samples show fracture at the smallest cross-section, others at the deepest pit. These facts raise the need for in-depth

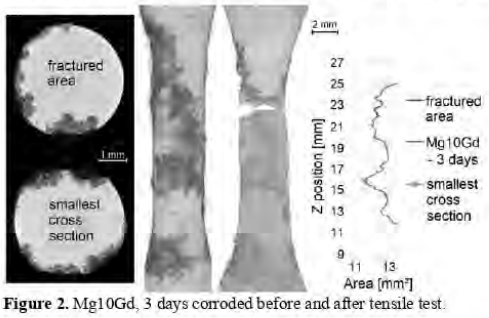

Figure 2. Mg10Gd, 3 days corroded before and after tensile test.

investigations as it seems that the deepest pit is not always most critical within failure. More statistics are needed for all alloys. It will make it possible to reconsider the dependence of strength loss on the deepest pit / smallest area - in the future it will be possible to determine the critical pitting corrosion.

References: [1]Maier, P. (2024) Magnesium Technology 2024, 3-5, [2]Van Gaalen, K. et al. (2022) Bioact. Mater., 8, 545-558, [3]Kovacevic, S. et al. (2023) Acta Biomater. 164,1, 641-658.

European Cells and Materials Vol. NN. Suppl. N, 20xx (page htu) ISSN 1473-2262

Assessment of degradation and cytotoxicity of Fe-Mg and Fe-Zn-Mg alloys

R Estrada[1,2], N Fagali[3], R M Lozano[4], M Lieblich[1], M Multigner[2]

[1]National Centre for Metallurgical Research, CENIM-CSIC, Madrid, Spain. [2]Dep. of Science and Engineering of Materials, ESCET, URJC, Móstoles (Madrid) Spain, [3]INIFTA/ CONICET/UNLP, Argentina. [4]CIB-CSIC, Madrid, Spain

INTRODUCTION: Absorbable Fe-Mg alloys are potential candidates for biomedical applications [1]. Addition of Mg to Fe may provide enhanced degradation rate. This work presents results on degradation behavior of Fe-Mg and Fe-Zn-Mg alloys in three simulated body fluids (SBF): PBS, Hanks' (HBSS) and modified Hanks' solutions (mHBSS). The alloys were obtained by attrition milling of the individual powders and consolidated by spark plasma sintering (SPS). SPS offers rapid heating and densification at low temperatures, which minimizes solute segregation and magnesium's oxidation. The microstructure of as-processed and degraded materials was thoroughly investigated, including type and percentage of degradation products as function of SBF type and time, pH evolution and type and concentration of ion released. Possible routes for the evolution of degradation are proposed. Cytotoxicity is also evaluated and compared with elemental Fe.

METHODS: The following materials were produced (wt.%): Fe, milled Fe, Fe-2.5 Mg, Fe-5 Mg, Fe-10 Mg, Fe-20 Zn, (Fe-20 Zn)-5 Mg, and (Fe-20 Zn)-10 wt.% Mg. The SPS process was conducted at 500 °C and 80 MPa for 5 minutes, resulting in discs of 8 mm in diameter and 2 mm high. The as-processed and degraded discs were characterized by SEM, XRD with a cobalt X-ray tube, and TEM. Degradation in PBS, HBSS and HBSSm was evaluated for 3, 14 and 28 days at 37 °C with volume-to-sample surface area ratio of 20 cm^3/cm^2. pH evolution and type and concentration of ion released was monitored. A lactate dehydrogenase (LDH) activity assay and a Calcein-AM/Hoechst assay were performed using two cell lines: MC3T3-E1 pre-osteoblasts to evaluate the initial interaction with bone cells, and L929 fibroblasts as a model for connective tissue interaction.

RESULTS: The analysis of the results revealed that, following sintering, zinc and magnesium were partially expelled from the iron matrix, forming regions of periclase and zincite, thereby reducing the solid solution of these elements in the Fe matrix. Degradation products appear as oxides, oxyhydroxides, phosphates and carbonates. Fig. 1 (left) is an example of phosphates on Fe-5Mg with different composition and two structures: ribbon-like with higher oxygen and lower phosphorous (point 1) than the pyramid-like (point 2). Fig. 1 (right) shows a discontinuous phosphate layer potentially creating different growth pathways. The presence of zinc significantly modified Fe and Fe-Mg degradation behavior by enlarging Fe lattice parameter and increasing solid solubility of Mg.

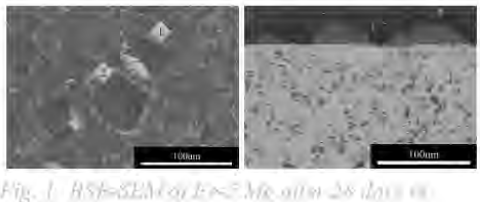

Fig. 1. BSE-SEM of Fe-5Mg after 28 days in HBSS. Left: surface, right: cross-section.

DISCUSSION & CONCLUSIONS: These studies shows that corrosion rates and the formation of degradation products on Fe-Mg and Fe-Mg-Zn alloys was generally higher in HBSS, while the buffered solutions HBSSm and PBS tended to stabilize pH and reduce corrosion. The formation of phosphate layers, such as vivianite and phosphophyllite, and carbonate layers influenced the corrosion rates. Chemical analysis of the degradation solutions highlighted notable differences in ion release among materials and solutions, with HBSS releasing the highest amount of Mg ions. Direct contact cytotoxicity assays with fibroblasts and pre-osteoblasts revealed significant toxicity. The observed toxicity was correlated with the formation of insoluble rust products, particularly in materials with higher corrosion rates.

REFERENCES: [1] R.G. Estrada, N. Fagali, M. Multigner, M. Lieblich (2025) *JOM* 10.1007/s11837-025-07216-2.

ACKNOWLEDGEMENTS: Grant PID2022-139323NB-I00, PID2021-123891OB-I00 and PRE2020-092118 (R.E.) funded by MCIN/AEI/ 10.13039/501100011033. CONICET [PIP 2021 11220200100315CO].

European Cells and Materials Vol. NN. Suppl. N, 20xx (page htu)
ISSN 1473-2262

Degradation behaviors of Mg-5Sn-xZn alloys in Hank's balanced salt solution

CD Yim[1,2], YJ Won[1], SK Woo[3]

[1] *Lightweight Materials Research Division, Korea Institute of Materials Science, Korea.*

[2] *Advanced Materials Engineering, University of Science and Technology, Korea*

[3] *Production Technology Research Center, Samsung Heavy Industries, Korea*

INTRODUCTION: In order to expand the application of biodegradable magnesium alloys in medical devices, it is necessary to suppress the generation of hydrogen during the degradation process and control the degradation. Sn and Zn are the effective elements which can suppress a hydrogen evolution and improve protectiveness of surface film. In this study, we aim to systematically investigate the influence of microstructural factors on the degradation behavior of Mg-5Sn-xZn (TZ5x) alloys.

METHODS: The plates of TZ5x alloys with the cross-sectional dimension with a thickness of 2 mm and width of 28 mm were fabricated by direct extrusion at 573 K. The extrusion ratio and speed were 90:1 and 1.0 m/min, respectively.

The potentiodynamic polarization behavior in HBSS was evaluated at 310 ± 0.5 K. The external voltage was changed form -0.25 V to 0.5 V with respect to OCP at the rate of 1.0 mV/s. The corrosion rate was measured by immersion test. The specimen was immersed into HBSS at 310 K for 10~30 days. The weight loss after immersion test was converted to the corrosion rate. The average corrosion rate was determined as the average value of three test results.

RESULTS: The microstructures of as-extruded TZ5x alloys showed a typical equiaxed grain structure by dynamic recrystallization during hot extrusion. The major constituent phases of as-extruded TZ5x alloys were α-Mg and Mg_2Sn. Figure 1 shows the potentiodynamic polarization curves of as-extruded TZ5x alloys. The hydrogen evolution rate at cathodic region and the passive current density at anodic region in TZ51, TZ52 and TZ53 alloys were similar. TZ54 alloys showed relatively high hydrogen evolution rate and low passive current density. The fraction of ZnO in the surface film might increase with increasing Zn content, which would enhance the protectiveness of surface film[1]. The passive current density decreased with increasing Zn content. Simultaneously, the hydrogen evolution rate increased with increasing Zn content due to high conductivity of ZnO. The corrosion rates of as-extruded TZ5x alloys decreased by addition of Zn except TZ54 alloy. The corrosion behavior of as-extruded TZ5x alloys would change according to relative contributions of following factors; acceleration by formation of micro-galvanic cell between α-Mg and Mg_2Sn particles and increase of the protectiveness of surface film by higher fraction of ZnO in the surface film.

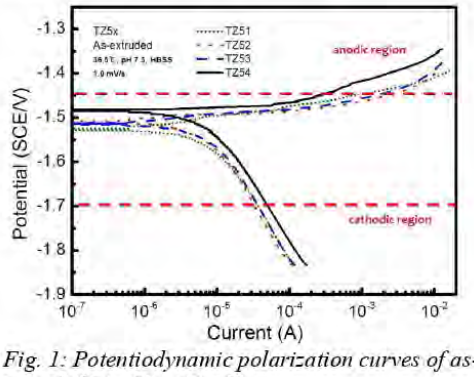

Fig. 1: Potentiodynamic polarization curves of as-extruded Mg-5Sn-xZn alloys.

DISCUSSION & CONCLUSIONS: The change of corrosion behaviors of as-extruded TZ5x alloys according to Zn content was strongly related to the changes of microstructures and composition of surface film. The increase of ZnO content in the surface film improved the protectiveness of the surface film. The increase of fraction of Mg_2Sn particles accelerated the corrosion by formation of micro-galvanic cell with the matrix.

REFERENCES: [1]H.Y. Ha et al (2013) *Corrosion Science* **75**:426-433.

ACKNOWLEDGEMENTS: This research was supported by the National Research Foundation of Korea (NRF) grant funded by the Korea government (MSIT) (RS-2022-NR068191).

17th Biometal
25-30 AUGUST, 2025
Grand Hôtel San Michele,
Cetraro, CS, Italy

In-situ study of degradation controlled smart 4D actuator designs and their load-bearing capabilities for biomedical applications

Muzi Li[1], Guillermo Domínguez[1], William Solórzano-Requejo[2], Simon Pöstges[3], Alex Kopp[3], Conall Quinn[4], Jennifer Patterson[1] and Jon Molina-Aldareguía[1,2]

[1]*IMDEA Materials Institute, Getafe, Madrid 28906, Spain*

[2]*Department of Materials Science, Polytechnic University of Madrid, 28040 Madrid, Spain*

[3]*Meotec GmbH, 52068 Aachen, Germany*

[4]*National University of Ireland Galway, Galway, H91 TK33, Ireland*

The emerging field of 4D printing, which introduces time-dependent shape transformation into additively manufactured structures, offers unprecedented opportunities for dynamic biomedical applications. In this study, we explore the integration of biodegradable magnesium (Mg) and zinc (Zn) alloys—noted for their biocompatibility, mechanical properties, and controlled degradation profiles—into 4D-printed actuators designed for biomedical applications. Specifically, we focus on the application of these materials in addressing craniosynostosis, a congenital condition characterized by the premature fusion of cranial sutures, which impairs normal brain and skull growth. Traditional surgical interventions for craniosynostosis are invasive and often require repeated procedures. We propose a novel solution: 4D-printed, bioresorbable actuators composed of Mg/Zn alloys that can be implanted to apply gradual, controlled mechanical forces to promote cranial expansion over time, reducing the need for repeat surgeries.

In this work, the selected smart 4D actuator designs for the shape-morphing structures were evaluated and how the degradation of the different biodegradable metallic elements control the rate and extent of expansion of the 4D actuators were studied *in situ*, as well as the temporal evolution of their load-bearing capability. Three different actuator designs are evaluated: a serpentine spring actuator, a conical spring actuator, and an auxetic spring actuator. They are made of two different metallic alloys: nitinol, for the shape-morphing part of the actuator, and the Mg based WE43MEO alloy, for the biodegradable anchoring elements that hold the spring in its initial state. The degradation of the anchoring elements triggers the shape morphing over a period of time in multiple steps depending on their configuration and corrosion rates. The initial result of the serpentine actuator is shown in Figure 1. A Zn alloy (Zn1Mg) will replace nitinol in the next step, to make the actuator fully biodegradable.

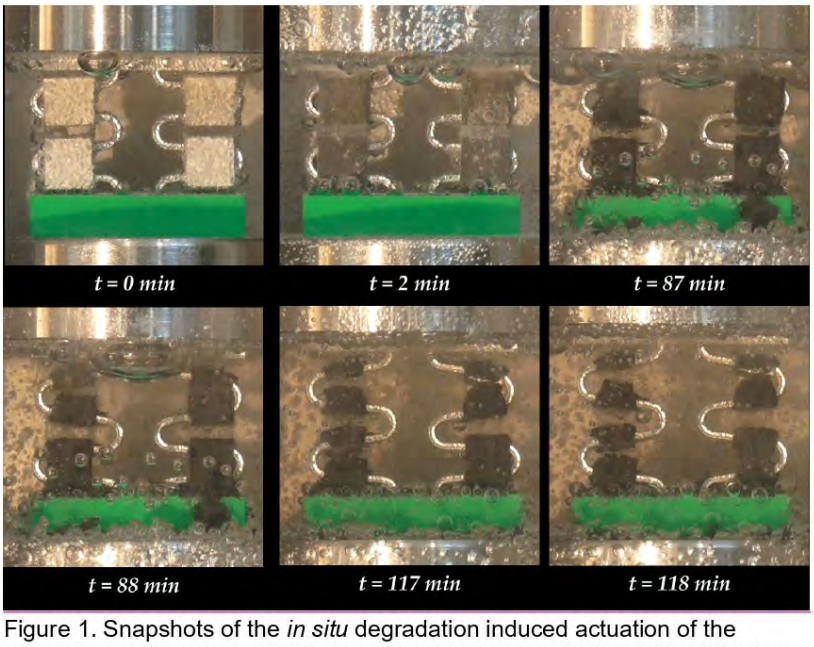

Figure 1. Snapshots of the *in situ* degradation induced actuation of the serpentine spring at specific time points. The top two WE43MEO anchoring brackets were 0.6 mm in thickness, while the bottom two were 0.8 mm thick.

European Cells and Materials Vol. NN. Suppl. N, 20xx (page htu) ISSN 1473-2262

Oxygen Plasma Immersion Ion Implantation on AZ31B for Clinical Applications

Malvestiti L[1,2], Paternoster C[1], Beraldo C[1], Ceré S[2], Mantovani D[1]

[1]Lab. for Biomaterials and Bioengineering, CRC-I, Department of Min-Met-Materials Eng., University Hospital Research Center, Regenerative Medicine, Laval University, Québec, Canada; and [2]INTEMA-CONICET, Mar del Plata National University, Argentina

INTRODUCTION: Mg-based alloys have been extensively studied for temporary implants due to their biodegradability, biocompatibility, mechanical properties, and biological functions of Mg^{+2} [1]. However, their main limitation is its high corrosion rate in physiological environment triggering an immune response. To reduce the degradation rate and improve biological response, an oxygen plasma-immersion ion implantation (O-PIII) treatment has been proposed [2]. Through O-PIII, a relatively homogeneous magnesium oxide is generated on the alloy surface. Moreover, Mg topography, wettability and electrochemical behavior were also modified, enhancing the interface between Mg based alloy- physiological environment.

METHODS: A commercial AZ31B alloy (Al 3 wt.%, Zn 1 wt.%, Mg bal.) was treated. After chemical polishing, an O-PIII was performed in a PBII-300 system (Plasmionique, Varennes, CA) varying different working parameters, such as working pressure (P_W – 5 to 50 mTorr), plasma exposition time (t_d – 60 to 300 min.) and pulse repetition rate (f – 200 to 1000 Hz). The morphological, chemical and electrochemical characterization were carried out by scanning electron microscopy (SEM), X-ray photoelectron spectroscopy (XPS), static drop contact angle, X-ray diffraction (XRD), and potentiodynamic polarization curves in Hanks' solution.

RESULTS: The alloy was chemically polished before O-PIII (as-received condition, AR). The plasma treatment introduced different surface features depending on the used parameter values (Fig. 1), which affected the morphology, roughness, chemical composition, and corrosion resistance. In particular, after O-PIII, XPS revealed a general increase in surface oxygen content with increasing pressure, reaching values in the range of ~35–40 at. %; O was bound to the metallic substrate mainly in the form of metal oxides and hydroxides [3]. The hydrophilicity of the treated surfaces decreased, from ~40° for AR to a minimum value for lower P_W and shorter t_d (~100°). After O-PIII, the corrosion rate (CR), proportional to the corrosion current was reduced by half, modifying also the corrosion pattern of the material. XRD showed the presence of a modified alloy texture, after the implantation process, especially at high implant pressure, likely due to the heath exchange related to the process.

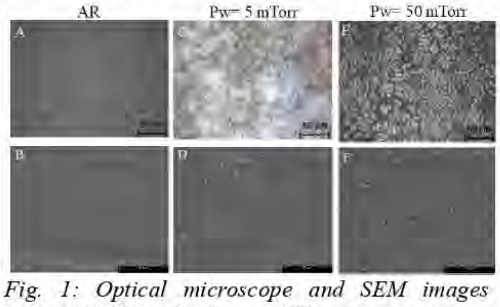

Fig. 1: Optical microscope and SEM images before (A-B) and after O-PIII varying working pressure (C-F).

DISCUSSION & CONCLUSIONS: The final surface morphology after implantation was modified in terms of surface chemical composition (O amount, presence of Mg oxide and hydroxide-related species), the roughness, and the physical properties (such as surface energy), being influenced by the alloy features (grain boundaries, precipitates, second phases, surface texture, etc.). The presence of a surface O-rich layer can also affect the formation of corrosion products. These results support the use of O-PIII technique and selected parameters as a potential surface modification, constituting a valid approach for clinical application. Biological tests related to cell viability (osteoblasts and neuronal cells) and hemocompatibility are carried out.

REFERENCES: [1]X. Zhang et al., J. Biomater. Appl. 35 (2021) 1275-1283. [2]M. Benčina et al., Molecules. 26 (2021). [3]S. Feliu et al., Appl. Surf. Sci. 347 (2015) 736-746.

ACKNOWLEDGEMENTS: LBB, NSERC-Canada, Prima Quebec, and the CHU de Quebec Research Centre. LM was awarded PhD scholarship from CONICET, Argentina.

European Cells and Materials Vol. NN. Suppl. N, 20xx (page htu) ISSN 1473-2262

On the possibility of additive manufacturing of Mg-Zn-Ca biodegradable alloys

A.Dobkowska [1], J. Ciftci [2], Ł. Żrodowski [2], W. Święszkowski [1]

[1] Faculty of Materials Science and Engineering, Warsaw University of Technology, Warsaw, Poland [2] Amazemet Ltd., Warsaw, Poland

INTRODUCTION: The use of additive manufacturing for the production of biomedical Mg alloys addresses challenges associated with fabricating implants of complex shape and geometry using conventional methods such as extrusion or turning[1]. This approach can significantly reduce manufacturing costs, increase process efficiency, and potentially enhance the properties of Mg implants. Nevertheless, the additive manufacturing of Mg alloys requires a comprehensive understanding of both the process and the material, particularly the optimization of parameters that determine the alloy's final properties[2]. In this study, we attempted to fabricate Mg-Zn-Ca alloys using laser powder bed fusion (LPBF) with custom-made powder materials atomized via an induction method.

METHODS: The cast rods of ZX00, ZX50, and ZX50+Ag were atomized via ultrasonic atomization using a rePowder device (AMAZEMET, Poland). The alloy was melted in a graphite crucible. The molten alloy was poured using pressure differential pressure through nozzle on a plate-type sonotrode. The bulk materials in a cubic form 10×10×10 mm^3 were printed using AconityMIDI+ printer (Aconity3D, Germany). The particle size distribution was analyzed using Horiba LA-950 laser scattering particle size distribution analyzer. The printed materials were scanned using a microfocused X-ray tomographic system (MicroXCT- 400, Xradia - Zeiss), at 40 kV and 200 µA. The microstructure of the materials was characterized using scanning electron microscope (SEM, Hitachi SU70, Japan) equipped with Bruker EBSD detector. Afterwards, corrosion properties of the alloys were investigated using electrochemical methods and immersion tests. The antibacterial properties were tested.

RESULTS: As a result of the atomization process, powders with high sphericity were produced (Fig. 1). The average particle size varied depending on the chemical composition of the alloys, measuring 201 µm for ZX00, 107 µm for ZX50, and 118 µm for ZX50+Ag. Chemical composition analysis confirmed that no Zn evaporation occurred, and Ag was still present in the powder particles. The printed alloys exhibited a density of approximately 95%. Depending on their chemical composition, the resulting microstructures varied. As shown in Fig. 2, the addition of Ag to ZX50 affected microstructural recrystallization, leading to the formation of the equiaxed grains.

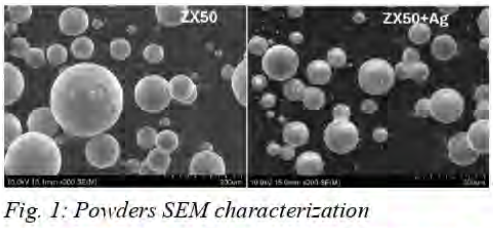

Fig. 1: Powders SEM characterization

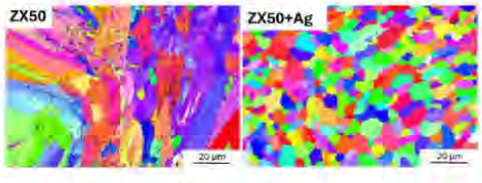

Fig. 2: Inverse pole figures maps

The electrochemical measurements and immersion tests demonstrated that corrosion behavior is highly dependent on the microstructure, with porosity playing a predominant role in the degradation performance.

DISCUSSION & CONCLUSIONS:

Modern powder production methods enable a broad research perspective on critically important biodegradable alloys for biomedical applications. The chemical composition of alloys can be tailored to impart desired properties, such as antibacterial activity. By mitigating porosity in additively manufactured magnesium alloys, their corrosion resistance can be significantly enhanced.

REFERENCES: [1]D. C. Martinez et al., Bioact. Mater., vol. 28, no. April, pp. 132–154, 2023, doi: 10.1016/j.bioactmat.2023.05.004. [2]A. Dobkowska et al., J. Magnes. Alloy., vol. 10, no. 12, pp. 3553–3564, 2022, doi: 10.1016/j.jma.2022.06.003.

ACKNOWLEDGEMENTS: The research founded by the Warsaw University of Technology within the Excellence Initiative: Research University (IDUB) programme.

European Cells and Materials Vol. NN. Suppl. N, 20xx (page htu) ISSN 1473-2262

Effect of laser shock peening on the microstructure of coarse-grained Zn-based biodegradable alloy

J Capek[1], J Pinc[1], J Kaufman[1]

[1] *FZU– Institute of Physics of the Czech Academy of Sciences, Na Slovance 1999/2, 182 00 Prague 8, Czech Republic*

INTRODUCTION: Selected Zn-based materials are considered as candidates for the fabrication of temporary, biodegradable implants. The main advantage of Zn-based biodegradable materials is their corrosion rate, which lies between Mg- and Fe-based materials, which are investigated for the same purposes [1]. One of the weaknesses of the Zn-based biomaterials is their low wear resistance. This property is closely connected to surface hardness, i.e., higher surface hardness usually results in higher wear resistance. One of the approaches to increase the resistance of the material to wear damage [2], but also to enhance the resistance to stress corrosion cracking and fatigue, is the refinement of the microstructure and implementation of residual compressive stresses into the surface/sub-surface layer. This can be very effectively reached by laser shock peening (LSP) – a method using the interaction between the material and short, high-energy laser pulses [3].
In the presented study, we treated a Zn-Mg0.8-Sr0.2 alloy by LSP and investigated the changes in surface and sub-surface microstructure and microhardness.

METHODS: A Zn-Mg0.8-Sr0.2 (wt.%) alloy was prepared by melting and gravity casting into an ingot with a diameter of 75 mm and a length of approximately 120 mm. The ingot was annealed at 350 °C for 24 h following water quenching and forged at low deformation speeds at a temperature ranging between 175 and 225 °C to obtain a rod of a square cross-section with a side length of 25 mm. The implemented true strain was approximately 2.4. The rod was cut into pieces 15 mm in length and ground using SiC sandpapers P400 – P1200. The surface of the samples was covered with a vinyl tape and treated by the LSP process under a water flow. For the treatment, a diode-pumped laser with a wavelength of 1064 nm, pulse energy of 3 J, pulse length 17 ns, repetition frequency of 10 Hz, and spot size of 2 mm was used. The overlap of individual spots was 75%.

The microstructure evolution was examined by means of X-ray diffraction, electron backscattered diffraction, and the hole drilling method.

RESULTS: The initial material – hot-worked Zn-Mg0.8-Sr0.2 alloy – consisted of Zn matrix (containing only negligible amounts of dissolved alloying elements) and a mixture of intermetallic particles based on Mg_2Zn_{11} and $SrZn_{13}$ phases. The intermetallic particles formed a continuous network surrounding the areas of original grains in the annealed material (the consequence of the solidification process). As clearly visible in Fig. 1a, those areas were approximately 50 – 100 μm in diameter. In this paper, we will focus on the microstructure evolution of the Zn-based matrix, whose grain size ranged mainly between 10 and 50 μm, suggesting that recrystallization took place during the hot working. As shown in Fig. 1, the material was textured with basal planes oriented close to the bar axis and both types of prismatic planes perpendicular to that (Figs. 1a and b). After LSP, twinning, whose intensity decreased with the distance from the surface, was observed.

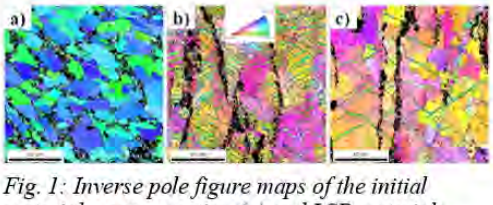

Fig. 1: Inverse pole figure maps of the initial material – cross-section (a) and LSP materials – longitudinal section – 50 μm (b) and 650 μm from the surface.

DISCUSSION & CONCLUSIONS: The coarse-grain size and so-called hard texture resulted in twinning during the LSP process, rather than extensive slip initiating recrystallization and subsequent grain refinement. The Schmid factor for basal slip in twins was significantly higher than that in the matrix, resulting in a negligible increase in microhardness. Fine-grained and differently textured materials are of interest because more significant microstructural changes are expectable.

REFERENCES: [1] E. Wolker, et al (2015) *J Biotech & Biomat* **05**: article no.1000178, [2] D.H. Jeong, D.H., et al (2003) *Scripta Materialia* **48**(8): pp 1067-1072, [3] W. Wang, et al (2023) *Wear* **524-525**: article no. 204866.

ACKNOWLEDGEMENTS: This research was funded by the Czech Science Foundation, grant number 23–05592S, and Ferroic Multifunctionalities project, supported by the Ministry of Education, Youth, and Sports of the Czech Republic. Project No CZ.02.01.01/00/22_008/0004591, co-funded by the European Union.

In Vitro

Friday,
August 29th, 2025

elecell
Hope for Healing

BioActiveMetals
Innovation in Metallic Biomaterials

meo.
Inspiring Materials.

medical magnesium

UNIVERSITÉ LAVAL

CHARITÉ
UNIVERSITÄTSMEDIZIN BERLIN

KeAi
CHINESE ROOTS GLOBAL IMPACT

PEKING UNIVERSITY

European Cells and Materials Vol. NN. Suppl. N, 20xx (page nnn) ISSN 1473-2262

In vivo monitoring of oxygen concentration at Mg interface in porcine bladder

S.V.Lamaka[1], M.Pacheco[2], C.Oliveira[2], Z.Jafari[1], M.Nienaber[3], J.Bohlen[3], M.Zheludkevich[1], E.Lima[4], A.Barros[2]

[1] *Institute of Surface Science, Helmholtz-Zentrum Hereon, Geesthacht, Germany*
[2] *ICVS/3B's-PT Government Associate Laboratory, Braga/Guimarães, Portugal Portugal*
[3] *Institute of Materials and Process Design, Helmholtz-Zentrum Hereon, Geesthacht, Germany*
[4] *Life and Health Sciences Research Institute (ICVS), University of Minho, Braga, Portugal*

INTRODUCTION: We report an unexpected pathway of cathodic process measured *in vivo*, highlighting largely unexplored complexity of reduction reactions at the interface of Mg alloys.

METHODS: Female sus scrofa domesticus was used. No irrigation with saline or other solutions was applied, to preserve the native composition of the urine within the animal's bladder. With the animal positioned in dorsal recumbency, an access cannula was advanced through the abdominal region to puncture the bladder and to fit the micro-optode holder system. Two retractable optic-fiber oxygen micro-sensors (OXR50-UHS, hereafter micro-optode), and a temperature probe (TSUB21), were controlled by FireSting-Pro (all from PyroScience, Germany). The micro-optodes were installed into custom-designed polymeric holders, of which one was fitted with coiled Mg-0.79Y extruded wire, of 0.6 mm diameter[1].Comparative readings were recorded reflecting dissolved oxygen (DO) concentration in bulk urine and urine microenvironment 140 µm from Mg-0.79Y ureteral stent degrading in porcine bladder. The temperature sensor was placed deep in the pig's mouth. Prior to the measurements, the micro-optodes were calibrated using air-saturated 30 mM saline solution and deionized water with 30 g/L Na_2SO_3 (O_2 scavenger) at ca. 37°C with auto-compensation for the real-time temperature.

RESULTS: DO concentration in bulk urine varied in the range 4.3-4.8 ppm. In contrast, DO concentration in the microenvironment surrounding degrading Mg-0.79Y wire varied in a much wider range. First minutes of stent and micro-optode contact with bladder's urine were characterized by low DO values down to 3.2 ppm, followed by gradual increase to 4.6 ppm after 20 min of immersion, and kept increasing from that point on. The highest DO value of 10.55 ppm was recorded at the last moments of the *in vivo* test, lasting for ca. 2 h. Such high DO readings were unexpected, especially that this greatly exceeded DO concentration in the bulk urine. Thus, the control measurements in calibration solutions were performed minutes after the micro-optodes were removed from porcine bladder. Both micro-optodes and the temperature sensor were placed in 30 g/L Na_2SO_3 at ca. 37°C. The micro-optode measuring the DO of the bulk urine immediately returned to 0.0 ppm, but the micro-optode placed 140 µm above the Mg-0.79Y wire has not returned to 0, showing 2.6 ppm DO as the lowest. However, as soon as the micro-optode was lifted 3.10 mm above the Mg-0.79Y wire, it quickly returned to 0.0 ppm DO in the same calibration solution. This has strongly validated the DO measurements in porcine urine and indicated strong O_2 generation, locally overruling O_2 scavenger at Mg interface.

DISCUSSION & CONCLUSIONS: Active yet short O_2 consumption phase followed by prolonged and intense phase of O_2 generation has been recorded during *in vivo* degradation of Mg-0.79Y wire in porcine bladder. While O_2 consumption observed in saline solution at RT has been previously reported and the mechanism explained[2], O_2 generation has not been previously published. One of the obvious pathways, water splitting, thermodynamically can only occur at much higher potential of ca. +0.8V at pH 7.4, which is ca. 3V higher than that of Mg alloys. The mechanism involving H_2O_2 formation and its decomposition with O_2 evolution accelerated at 37 °C appears most plausible. It is remarkable, that the first experimental evidence of ROS formation on Mg (including H_2O_2), has been recently observed *in vivo*[3]. We propose the following mechanism of enhanced O_2 generation at Mg-0.79Y interface *in vivo:* atomic hydrogen generated and adsorbed on Mg surface according to Volmer-Heyrovský HER pathway[4] is a strong reducing agent, inducing intermediate hydroxyl radical formation (·OH), that recombine into H_2O_2 species. Formation of adsorbed ·OHad species that can recombine into H_2O_2 has also been shown recently[5]. H_2O_2 decomposition to O_2 and H_2O and is catalysed by Y_2O_3, especially efficient at 37°C.

REFERENCES: [1] M. Pacheco, I.M. Aroso, J.M. Silva, S.V. Lamaka, J. Bohlen, M. Nienaber, D. Letzig, E. Lima, A.A.Barros, R.L.Reis, (2023) *J.Magnesium&Alloys*. [2] C. Wang, K. Qian, Y. Wu, D. Mei, C. Chu, F. Xue, J. Bai, M.L. Zheludkevich, S.V. Lamaka, (2024) *Corrosion Science*. [3] J. Kim, J.L. Gilbert, W.W. Lv, P. Du, H. Pan, (2025) *Bioactive Materials*.[4] D.Hoche, C.Blawert, S.V.Lamaka, N.Scharnagl, C.Mendis, M.L.Zheludkevich, (2016) *Phys.Chem.Chem. Phys.* [5]A.Zeradjanin, P.Narangoda, J.Masa,(2024) *ChemCatChem*.

ACKNOWLEDGEMENTS: *In vivo* authorization DGAV 013778; bilateral DAAD-FCT project ID: 57665092; MSCA-DN DurAMat GA no. 101119767.

European Cells and Materials Vol. NN. Suppl. N, 20xx (page htu) ISSN 1473-2262

Influence of sterilisation methods and selected test conditions on cell viability assays with Zn-based materials

FM Seabra[1,2,3], MM de Castro[2], M Balog[1,2], P Krížik[1], M Takáčová[4], J Lapinová[4], E Švastová[2,4], V Hybášek[5], J Kubásek[5]

[1] *Institute of Materials and Machine Mechanics, SAS, Slovakia.* [2] *Centre of Excellence for Advanced Materials Application, SAS, Slovakia.* [3] *Faculty of Materials Science and Technology in Trnava, STU, Slovakia.* [4] *Biomedical Research Center, Institute of Virology, SAS, Slovakia.* [5] *Department of Metals and Corrosion Engineering, UCT, Czech Republic.*

INTRODUCTION: Zn is a bioresorbable metal with a corrosion rate that has been shown to be close to ideal for temporary implant applications. *In-vivo* experiments with pure Zn have been conducted in the past, showing that long-term implantation does not lead to an adverse cellular response. However, when *in-vitro* cytotoxicity assays such as the ones defined by ISO 10993-5 are performed for Zn-based materials, inconsistent results have been reported across the literature, with a cytotoxic response being common [1-2]. Thus, there is a need to understand what is causing this inconsistency and propose a protocol that will lead to replicable and meaningful results. In this work, three types of Zn-based materials were tested: cast Zn, extruded Zn and Zn-based composites, with an ultrafine-grained Zn matrix stabilised by nanometric ZnO dispersoids [2-3]. The materials were submitted to different sterilisation methods and extracted under different ratios and media composition, and their biological response was assessed and compared, in order to better understand how the parameters selection may be influencing the results obtained.

METHODS: Cylindrical samples from the different Zn materials were disinfected with isopropanol and then sterilised with either autoclave or UV irradiation. Extraction was conducted following ISO 10993-12, in a DMEM medium at 37 ºC for 24 h. Two variables were compared for extraction: FBS medium content (5% and 10%) and extraction ratio (0.2 $g.mL^{-1}$ and 1.25 $cm^2.mL^{-1}$). The biological response was assessed with two assays: an MTT cell viability assay according to ISO 10993-5 and an impedance-based cell proliferation assay using the xCELLingence system. Extract dilutions (25% and 10%) were also tested. Additionally, the Zn ion content of the extracts was assessed with ICP-OES.

RESULTS: Regarding the sterilisation methods, when samples were autoclaved, a strong cytotoxic response was observed, accompanied by the highest Zn ion concentration in the extracts. When UV irradiation was used, the biological response depended on the other factors. With the surface area-based extraction ratio, a consistent cytotoxic response was observed, while with the weight-based extraction ratio, cell viability varied. With the weight-based extraction ratio, the Zn ion concentration was lower than with the surface area-based one. For the dilutions, cell viability was consistently achieved.

DISCUSSION & CONCLUSIONS: The biological response is dependent on the Zn ion concentration present in the extract. With lower Zn ion concentrations, cell viability is consistently achieved and with higher Zn ion concentrations, a cytotoxic behaviour is consistently observed. Yet, when the Zn ion concentration is close to the cell viability threshold, inconsistencies can be observed between tests. While ISO 10993-5 defines protocols to test *in-vitro* cytotoxicity, several parameters are left for the researchers to choose. These choices will result in very different Zn ion concentrations in the extracts and, therefore, different cell responses. For instance, while autoclaving is a standard practice, it was been shown that it induces surface modifications that lead to higher corrosion rates [4]. Hence, it is important not only to accurately describe the protocol implemented but also to discuss how this protocol is leading to meaningful and replicable results, which can be translated to *in vivo* and real-life applications.

REFERENCES: [1] Q Liu et al (2023) *J Funct Biomater* **14**:206. [2] M Balog et al (2023) *J Mater Res Technol* **25**:4510-4527. [3] M Balog et al (2024) *J Mater Res Technol* **33**:7458-7468. [4] LP Zhang et al (2021) *Mater Sci Eng C* **130**:112430.

ACKNOWLEDGEMENTS: This work was supported by the VAIA 09I03-03-V04-00718, APVV-20-0417, ITMS 313021T081, and VEGA 2/0157/24 projects.

European Cells and Materials Vol. NN. Suppl. N, 20xx (page htu) ISSN 1473-2262

Characterization of thin zinc-alloy wires for biodegradable cardiovascular stent applications

DEJ Anderson[1], Morath L[2], CA Baker[1], J Johnson[1], Rahim SA[2], J Drelich[2], J Goldman[2], MT Hinds[1]

[1] *Department of Biomedical Engineering, Oregon Health & Science University, Portland, OR, USA.*
[2] *Department of Biomedical Engineering, Michigan Technological University, Houghton, MI, USA.*

INTRODUCTION: Biodegradable cardiovascular stents offer a promising solution for treating vascular occlusion with a temporary device, allowing for potential reintervention and reducing the need for long-term antithrombotic therapies. However, zinc-based implants often trigger a chronic inflammatory response, albeit typically mild. Developing zinc-based stents with thinner struts could reduce toxicity and improve delivery of the stents. This study evaluates the in vitro, ex vivo, and in vivo responses to novel Zn alloys with reduced dimensions.

METHODS: Zn alloys with a stainless steel (SS) control were tested *in vitro* using human blood plasma to examine coagulation FXII activation and fibrin generation. Zn alloy (AMZ, ACMZ, CMM) and SS coils were also tested in an ex vivo non-human primate model using whole, flowing blood without anticlotting medication for 1hr.[1] Blood metrics for inflammation, platelet activation, and thrombosis were measured downstream of the alloy wires. Separately, the zinc-alloy wires were implanted into rat arteries to investigate the biological responses over a period of 3mths by histological staining.

RESULTS: Quantitative FXII activation and fibrin generation results showed no significant results from the human plasma. Similarly, the flowing ex vivo blood tests showed similar platelet and fibrin accumulation on the metals. Qualitatively, all the wires showed thrombus with fibrin, red blood cells, platelets, and immune cells from scanning electron microscope visualization (Fig. 1). Implants in rat arteries experienced healthy tissue growth with mild to moderate levels of chronic inflammation (Fig. 2), consistent with prior reports of zinc implants into arterial tissue. The area of neointimal tissue (NA) formed around arterial implants was significantly reduced in 120 vs. 250 μm diameter wires.

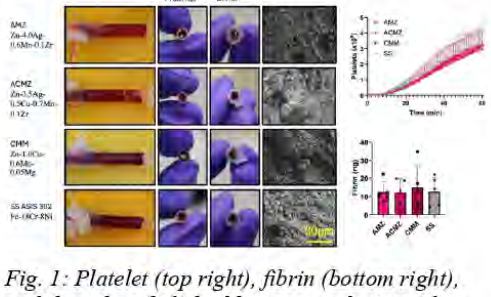

*Fig. 1: Platelet (top right), fibrin (bottom right), and thrombus (left) buildup on metal wires after 1hr of blood flow. Cross-section images show proximal (left) and distal (right) ends. Platelet data were analyzed with 1-way repeated measures ANOVA, and fibrin data with 1-way ANOVA (** p<0.01, ***p<0.001).*

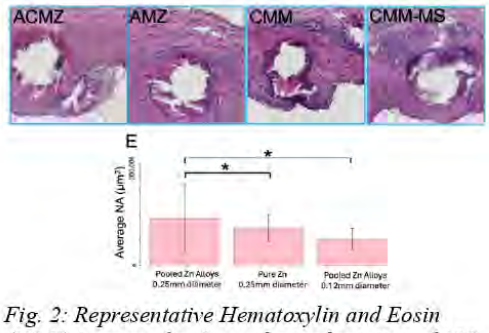

*Fig. 2: Representative Hematoxylin and Eosin (H&E) images after 3 months implantation of 120 um diameter wires for the alloys pooled. (*p-value<0.05) for neointimal area (NA) via Kruskal Wallis.*

DISCUSSION & CONCLUSIONS: The lack of significant differences between SS and Zn alloys when tested for thrombogenicity suggests that the experimental alloys will perform similarly to current clinical devices when used for cardiovascular applications. The reduction in NA in the thin wire implants suggest that reduced dimensions favor the biocompatibility of zinc-alloys.

REFERENCES: [1] N.M. Keeling, et al. (2024) *J Throm Haemo* **7**: 1433-46.

ACKNOWLEDGEMENTS: Fort Wayne metals drew the metal wires. This project was supported by NIH grants, R01HL144113, R01HL167442, and R01HL168696. We gratefully acknowledge the veterinary staff at the Oregon National Primate Research Center, supported by P51OD011092.

17th Biometal
25-30 AUGUST, 2025
Grand Hôtel San Michele,
Cetraro, CS, Italy

The biocompatibility of molybdenum – a 10-year-roundup of findings at Fraunhofer IFAM and TU Dresden

C. Redlich[1], T. A. Schroeder[2], M.-E. Prieto Jarabo[3], A. Schauer[4], G. Poehle[1], T. Weissgaerber[1,5], L. M. Kroschwald[2], P. Quadbeck[6], V. Adams[4] M. Wagner[3], G. Lauer[2]

[1] Fraunhofer Institute for Manufacturing Technology and Advanced Materials IFAM, Dresden Branch
[2] Department of Oral and Maxillofacial Surgery, University Hospital Carl Gustav Carus, Technical University Dresden
[3] Clinic for Internal Medicine and Cardiology, Heart Center Dresden, Technical University Dresden
[4] Laboratory of Experimental and Molecular Cardiology, Heart Center Dresden, Technical University Dresden
[5] Chair of Powder Metallurgy, Institute of Materials Science, Technical University Dresden
[6] Department of Electrical Engineering, Medical Engineering and Computer Science, Offenburg University of Applied Sciences

INTRODUCTION: The refractory metal molybdenum could be a game changer for high load-bearing biodegradable implants such as stents or fracture screws. Its strength and elastic modulus are comparable to those of CoCr alloys while exhibiting highly uniform degradation at moderate rates. But is it also biocompatible? The presentation will discuss current findings of the authors' and state-of-the art literature data on the in vitro and in vivo biocompatibility of biodegradable molybdenum for various applications.

METHODS: Our own data on cell compatibility as well as systemic and organ accumulation of dissolved molybdate species from research projects spanning more than 10 years was compared to collected literature data on systemic, local and cell toxicity of molybdenum. The physiological role and metabolism of the trace element molybdenum was investigated and brought in context to our data. Finally, biocompatibility profiles of potential future Mo implants are assessed based on the degradation mechanism and degradation rates of molybdenum.

RESULTS: Soluble molybdate ions (MoO_4^{2-}) are both the product of Mo implant degradation and the metabolizable form of molybdenum. Mo levels in the body are homeostatically regulated by renal excretion. Thus, systemic and cell toxicity of Mo towards diverse human cell lines is low according to the current level of knowledge. This is underscored by our own findings for human cardiovascular [1], cardiac [2], gingival, fibroblast and osteoblast cells, which all tolerate molybdenum levels close to the solubility limit in aqueous media. Furthermore, in vivo data point towards actual renal excretion and no significant accumulation of Mo [3]. There are, however, open questions concerning further cell lines, e.g. nerve cells, and the biological mechanism of Mo excretion pathways from the implant. Furthermore, Mo implant size and design are limited by the degradation rate and thus the release rate of molybdate ions. The design must thus be balanced between adequate degradation and respecting the local tolerance towards dissolved Mo species.

DISCUSSION & CONCLUSIONS: So far, none of the available data on the biocompatibility of degradable Mo raises concerns. On the contrary, dissolved Mo species appear to be well tolerated by human cells. However, particularly more in vivo and clinical data must be collected before a first Mo implant becomes reality.

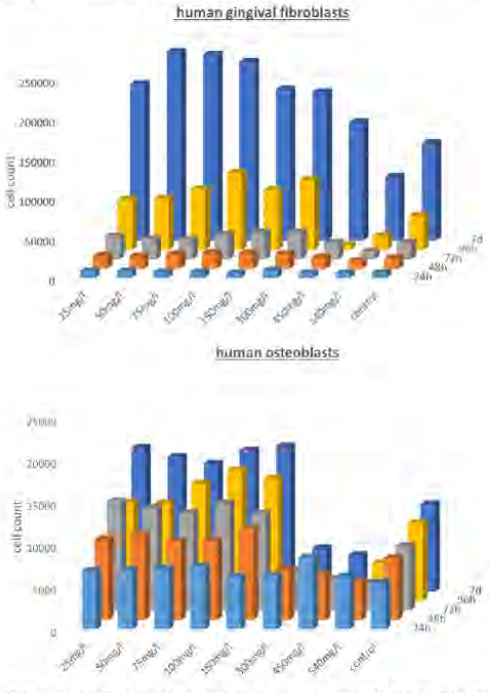

Fig. 1: Cell viability of human gingival fibroblasts (a) and osteoblasts (b) in dependence on molybdenum concentration in the medium and incubation time.

REFERENCES:

[1] C. Redlich et al., *Metals* **2021**, 11, 761
[2] M.-E. Prieto Jarabo et al., *Acta Biomat* **2024**, 1, 178.
[3] A. Schauer et al., *Materials* **2021**, 14, 7776.

ACKNOWLEGDEMENT: The presented results were collected in projects that received funding from SMWK/SAB, BMBF and Else Kröner Fresenius Zentrum (EKFZ) for Digital Health.

European Cells and Materials Vol. NN. Suppl. N, 20xx (page htu) ISSN 1473-2262

A Finite Element Model for crimping and free deployment in the design of bioabsorbable metallic coronary stents

Diego Blunda[1], Ted J. Vaughan[1]

[1] *Biomedical Engineering, School of Engineering, College of Science and Engineering, University of Galway*

INTRODUCTION: Cardiovascular diseases (CVDs) are the leading global cause of death[1], with myocardial infarction, due to coronary artery occlusion, being a common manifestation[1]. Percutaneous Transluminal Coronary Angioplasty (PTCA) with drug-eluting stents (DES) is the current standard treatment to prevent infarction. While effective, DESs pose risks such as chronic inflammation, late thrombosis and restenosis due to their permanent presence in the body[2,3]. Bioresorbable stents, which degrade over time, offer a promising alternative by providing temporary support until the vessel heals and re-endothelializes[3]. Magnesium is a promising material for bioabsorbable stents, but its lower mechanical strength compared to DESs and manufacturing challenges necessitate innovative design solutions. This study focuses on the design and optimization of a thin-strut Mg/Zn bioresorbable coronary stent, with the first phase developing a crimping and free deployment finite element model (FEM) of an older Bare Metal Stent provided by B.Braun, Melsungen, to analyze the impact of geometric parameters on stent performance. Next steps include the optimization of novel stent concepts, and the usage of a corrosion model and its calibration on experimental data of magnesium components.

METHODS: To develop the crimping and free deployment FEM, the Abaqus finite element solver was used. Figure 1 illustrates the process, involving several components: an internal rigid shaft, a folded balloon, the stent (CoroFlex Blue, B.Braun), and crimping tools. The balloon's geometry, obtained by previous simulations similar to the one described by Geith et al.[4] was modelled using a hyperelastic (1st order Ogden) material, with parameters fitted from nylon testing.

The stent geometry, derived from data provided by B.Braun, featured a hybrid-cell design and was assigned an elasto-plastic material model to simulate the CoCr L605 alloy (E = 240.74 GPa, ν = 0.3). The crimping tools (n = 12) were modelled as rectangular rigid bodies.

The simulation consisted of five steps: in the first step, the crimping tools crimp the stent onto the folded balloon; in the second step, the crimping tools were removed; in the third step, the stent was deployed by inflating the balloon, in the fourth step, the balloon was deflated, allowing for the observation of stent recoil and, in the fifth, the stent was radially crimped. The simulation was performed using the SIMULIA Abaqus FEA explicit solver.

Experimental deployment and crimping studies were conducted to validate the model.

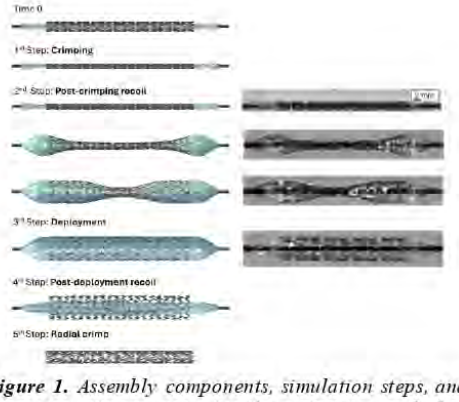

Figure 1. *Assembly components, simulation steps, and important time points in the crimping and free deployment simulation, compared to a study from literature*[5].

RESULTS: The simulation results (Figure 1) showed that the stent was effectively crimped onto the balloon, undergoing plastic deformation. In the second step, the stent recovered its elastic deformation. The stent was expanded to a maximum internal diameter of approximately 4 mm, which resulted in a peak von Mises stress of ~1750 MPa. Then, during the fourth step, the overall stent recoil was approximately 4.79%, which closely resembles the one obtained by B.Braun experimental test data (4.7%). Finally, the stent was radially tested to obtain the radial force-diameter curve. A qualitative comparison with a study from literature reveals an almost perfect agreement. The quantitative comparison against experimental data validates the model.

DISCUSSION & CONCLUSIONS: This study demonstrated an efficient and rigorous validated FEM for crimping and deployment, which will be utilized to design and optimize biodegradable coronary stent designs. As observed, the stent recoil value of 4.79% is almost identical to the 4.7% indicated by B.Braun experimental deployment test data. Also, the pressure-diameter curve during expansion and the radial force-diameter curve during the radial test validate the model.

REFERENCES: [1] WHO, Cardiovascular diseases (CVDs) Fact Sheet, 2021. [2] Kapoor *et al.*, Materials and Design, 2023. [3] Udriste *et al.*, Materials, 2021. [4] Geith *et al.*, International Journal for Numerical Methods in Biomedical Engineering, 2019. [5] Wiesent et al., PLOS ONE., 2019.

European Cells and Materials Vol. NN. Suppl. N, 20xx (page htu)
ISSN 1473-2262

hydrogen-gel for selective ROS modulation strategy to eliminate bacteria and promote wound healing

Tairan Quan[1,2], Xiao Hou[3], Yu Yin[3], Guangyin Yuan[1], Daijie Chen[3], Wenjiang Ding[1], Jia Pei[1]

[1] School of Materials and Engineering, Shanghai Jiao Tong University, China. [2] School of Chemical Engineering, University of New South Wales, Australia. [3] School of Pharmacy, Shanghai Jiao Tong University, China

INTRODUCTION: Wound infections remain a major challenge in clinical settings due to the emergence of antibiotic-resistant bacteria and the limitations of conventional antimicrobial strategies [1]. Recent studies have highlighted the potential of hydrogen-based therapies as a novel approach for antimicrobial intervention. In this context, we developed a magnesium hydride-based temperature phase change hydrogel to serve as an effective wound healing adjuvant.

This composite hydrogel enables sustained release of hydrogen, significantly enhancing its bactericidal efficacy. MgH_2 exerts its antimicrobial activity by disrupting oxidative phosphorylation on the bacterial membrane, leading to elevated intracellular reactive oxygen species (ROS) levels and reduced ATP production, ultimately causing bacterial death. In parallel, the released hydrogen alleviated oxidative stress in host cells, thereby attenuating inflammation and promoting wound tissue regeneration. These findings underscore the therapeutic promise of MgH_2 in combating infection and facilitating wound repair.

METHODS: Bacteria were mixed with different concentrations of MgH_2 hydrogel containing LB medium. After incubation, colonies growing on each LB agar medium plate were counted.

The expression of genes encoding cytochrome C oxidase and ATP synthase was verified by RT-qPCR.

The healing activity and inflammatory response of the wound tissue were assessed by H&E and Masson staining histological images.

RESULTS: The MgH_2 hydrogel group exhibited an irregular morphology with broken and crumpled cell membranes and exposed cell contents (Fig. 1).

The treated wounds showed significant epidermal and dermal structure with improved inflammatory response and more collagen deposition (Fig. 2).

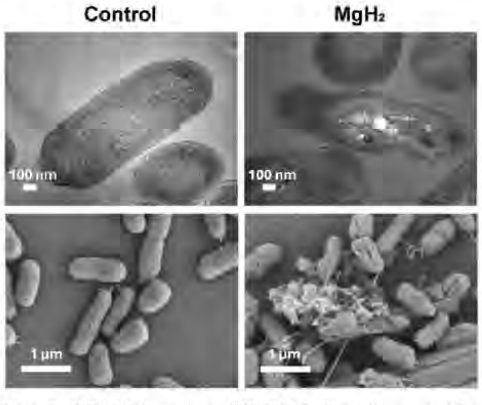

Fig. 1: TEM (above) and SEM (below) images of Pseudomonas aeruginosa before and after MgH_2 treatment.

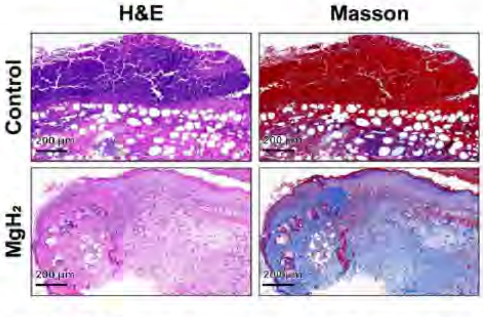

Fig. 2: H&E and Masson staining of mice infected skin before and after MgH_2 treatment.

DISCUSSION & CONCLUSIONS: MgH_2 hydrogel achieves efficient killing of pathogens in vitro and in vivo by slowing down the release of hydrogen. MgH_2 induced oxidative stress and energy deficiency in the bacteria, leading to their death. Hydrogel also has wound healing activity and alleviates oxidative stress in wound tissue.

REFERENCES: [1] C. Tu, H. Lu, T. Zhou, et al (2022) *Biomaterials* **286**:121597.

European Cells and Materials Vol. NN. Suppl. N, 20xx (page htu) ISSN 1473-2262

The role of metal degradation in *in vitro* biological evaluation

EB Montufar

Central European Institute of Technology, Brno University of Technology, Brno, Czech Republic

INTRODUCTION: Traditionally, metal degradation and in vitro biological evaluation have been conducted independently. However, cell responses in vitro are influenced by the degradation process (Figure 1), and as a result, biological assessment methods should be adapted accordingly [1]. This contribution highlights key considerations and proposes alternatives to integrate them into future experimental designs.

METHODS: A literature review was conducted to identify current practices in the biological evaluation of biodegradable metals. These practices were then benchmarked against known degradation mechanisms and kinetics, enabling the identification of best practices and opportunities for improvement.

RESULTS: The in vitro biological characterization of biodegradable metals involves evaluating cytotoxicity, osteoconductive potential, and inflammatory response, using methods aligned with ISO 10993 series of standards. Among the exposure methods outlined in the standard, material extracts are most used to assess the cytotoxicity of magnesium- and zinc-based biodegradable alloys. Indirect cell culture models are also employed to evaluate bone-forming and inflammatory responses. When direct contact studies are used with magnesium-based materials, cells typically adhere to degradation products or corrosion protection coatings. Cell attachment to degrading metallic surfaces has been reported in iron-based biodegradable metals, which typically exhibit low degradation rates.

Cell cultures are typically performed on as-processed metallic samples, often without accounting for degradation mechanism. Extracts are frequently diluted arbitrarily to compare the cytotoxicity of different alloys, but the dilution factors are not justified in terms of degradation kinetics or the body's physiological homeostatic capacity.

A key challenge in achieving more accurate in vitro biological evaluations is replicating the body's ability to buffer soluble degradation products and pH fluctuations. Additionally, there is limited understanding of cell-mediated degradation of corrosion products and protective coatings.

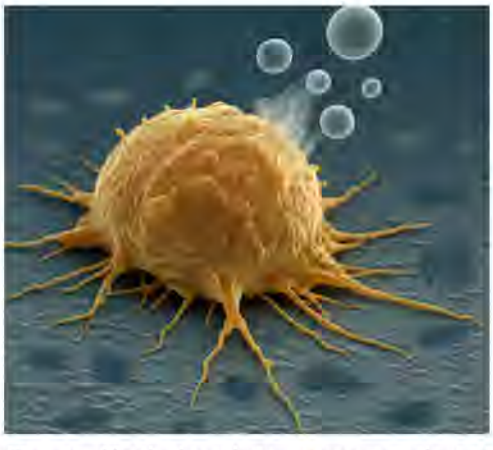

Fig. 1: Metal degradation generates physical (surface instability, gas release) and biochemical (ion release, pH shifts) factors that stress cells in vitro, especially without homeostatic mechanisms.

DISCUSSION & CONCLUSIONS: A straightforward approach to incorporating the degradation process into in vitro biological evaluations of biodegradable metals is to initiate cell cultures at different stages of material degradation, using both direct and indirect methods. This strategy could enable the assessment of inflammatory responses to rapid initial degradation, the transition to a less stressful phase due to passivation, cellular behaviour under steady-state degradation conditions, and the role of cells in mediating the degradation of solid corrosion products.

In conclusion, in vitro biological evaluation of biodegradable metals has advanced significantly, offering valuable insights into their biological safety and performance. The next steps in the field involve modifying standard methods for studying in vitro cell responses incorporating the effects of the degradation process.

REFERENCES: [1]EB Montufar (2025) *Bone Response to Biodegradable Metals and In Vitro Evaluation of the Cytocompatibility*, *JOM*, https://doi.org/10.1007/s11837-025-07353-8.

ACKNOWLEDGEMENTS: This work was supported by the Czech Ministry of Health (NW24-10-00195) and the Horizon Europe European Innovation Council (101186758).

European Cells and Materials Vol. NN. Suppl. N, 20xx (page htu) ISSN 1473-2262

Manufacturing matters: cytotoxicity and degradation of Mg-5Gd produced by extrusion and 3D printing

K Pérez Zapata[1], E Nidadavolu[1], T Ebel[1], B Wiese[1], H Helmholz[1], B Zeller-Plumhoff[1], R Willumeit-Römer[1]

[1]*Institute of Metallic Biomaterials, Helmholtz-Zentrum Hereon GmbH, Germany.*

INTRODUCTION: Mg-Gd alloys have been extensively studied for their potential as implant materials, but only a few focused on their process-property correlations [1]. To meet the stringent requirements for implant applications, their degradation and cell biocompatibility should be understood at the material microstructure level, which in turn depends on the manufacturing process. Hence, Mg-5Gd materials produced by extrusion and binder-based 3D printing were evaluated for their degradation rate and their direct and indirect cell response with Saos-2 cells.

METHODS: Cylinders of Mg-5Gd specimens (2 mm height x 10 mm diameter) were fabricated by extrusion (400 °C, 2.2 mm/s extrusion rate) [2] and binder based 3D printing followed argon gas sintering at 642 °C for 32 h. The materials are surface finished using 1000 SiC paper. *In vitro* degradation was carried out under physiological cell culture conditions (37 °C, 5% CO_2, 20% O_2, 95% RH) using DMEM + Glutamax (+10% FBS) medium. Two types of cytotoxicity assays were performed with Saos-2 cells: (1) direct contact with 1×10^4 cells per specimen for 5 days and cell viability staining analysis via fluorescence microscopy (Calcein-AM, Ethidium Homodimer-1, Höchst 33342); (2) cell exposure to material extracts between the Mg concentrations of 2 and 20 mM for 3 days; CCK-8 kit for quantification by absorbance spectroscopy. Additional material characterizations involved scanning electron microscopy (SEM), X-ray diffraction (XRD) and inductively coupled plasma optical emission spectroscopy (ICP-OES).

RESULTS: Both Mg-5Gd materials showed similar degradation rates; 0.35 mm/year for extruded material and 0.40 mm/year for 3D printed. However, differences were observed in the morphology of the degradation products, with the printed material showing rough and protruding degradation products compared to the extruded (Fig. 1). In the direct assays (Fig.2), both the glass (control) and the extruded material showed high cell viability, while the printed material showed low cell activity and signs of a certain cell death associated possibly with hydrogen evolution.

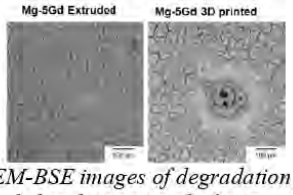

Fig. 1: SEM-BSE images of degradation products on extruded and 3D printed after in vitro test.

The indirect assays showed good biocompatibility at extract concentrations below 15 mM but evidenced cytotoxicity at higher concentrations for both materials, indicating the non-toxic nature of extracts.

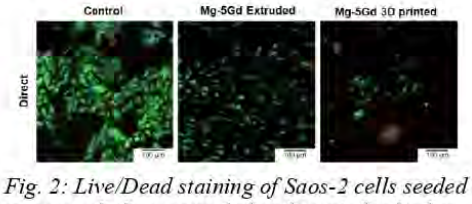

Fig. 2: Live/Dead staining of Saos-2 cells seeded on control glass, extruded and printed cylinders.

DISCUSSION & CONCLUSIONS: The presence of numerous oxides and hydrides in the 3D printed Mg-5Gd microstructure seem to physically inhibit the direct cell adhesion due to *in vitro* progressive H_2 evolution and degradation products morphology compared to the extruded material. However, the results confirm the non-toxicity nature of 3D printed Mg-5Gd in the indirect assay. The localized microstructure effects on product formation and cell interaction are the subject of further investigations.

REFERENCES: [1] D. Krüger (2021) *Assessing the microstructure and in vitro degradation behavior of Mg-xGd screw implants using µCT*, JMA. [2] J. Harmuth (2019) *Wide range mechanical customization of Mg-Gd alloys with low degradation rates by extrusion*, Front. Mater.

ACKNOWLEDGEMENTS: This research was carried out in the framework of VIP+ project BioMag3D (code Nr. 03VP09852) financed by the BMBF. The authors acknowledge H Lüneburg, A Borkam-Schuster, M Schenke for their expertise in methodology and technical assistance.

European Cells and Materials Vol. NN. Suppl. N, 20xx (page htu) ISSN 1473-2262

Corrosion extracts of different Zn alloys with and without Mg addition led to different cell viability in dependence of cell line and alloy composition

N Angrisani[1], J Reifenrath[1], M Bieda[2]

[1] Department of Orthopaedic Surgery, Hannover Medical School, Hannover, D, [2] Institute of Metallurgy and Materials Science, Polish Academy of Sciences, Krakow, PL

INTRODUCTION: In the light of difficult mechanical properties of Mg based absorbable implants, alloys based on other biodegradable metals as Zn have moved to the focus of research. As trace element, it plays an important role e.g. in the function of enzymes, syntheses of DNA and proteins or as supporter of immune functions [1]. Numerous papers have been published on the *in vitro* cell biocompatibility of Zn based alloys involving a broad range of cell types. However, comparison of results is complicated and limited due to different experimental set ups including media used, time periods, preparation and dilution of extracts and evaluation tests. Aim of this study was to examine systematically the *in vitro* biocompatibility of different Zn-based alloys with and without Mg addition on cells lines L929 and U2OS using identical set ups.

METHODS: Zn disks (Zn, Zn-0.6Mg, ZnMgCaSr and ZnCaSr, n=5 each) were prepared by gravity casting in an argon atmosphere and then deformed using hydrostatic extrusion (HE)method [2] (5x1mm each). Cleaning consisted of stepwise immersion in aceton and ethanol. Then, disks were immersed in ROTI®Cell Eagle´s MEM/Earle´s (Art.No. 9047, Roth) supplemented with FCS, Glutamax®, penicillin/streptomycin and non-essential-aminoacids, for 24 h. Extracts were diluted to concentrations of 100%, 50%, 37.5%, 25%, 10%, 5%, 3.75% and 2.5%. L929 and U2OS cells were seeded into 96 well plates with a density of 10.000 cells/well. After 24 h, media was replaced by the different extract dilutions and incubated for 24 h. Afterwards, samples were collected separately, and cell viability assay was performed according (Cell Counting Kit 8, ab228554, abcam). Zn concentration of extracts and pH-value, Glucose and Lactate content of incubated samples were determined.

RESULTS: Overall, extract dilutions of Zn and ZnMg from 25% downwards can be classified as non-cytotoxic for both cell types, while L929 still reached only 52.8% cell viability in contact to the 37.5%-pure Zn extract. (Fig.1) For all concentrations, U2OS cells showed better compatibility. While the addition of Mg to pure Zn led to lower cytotoxicity for both cell types, this effect was reversed in the alloys with additional Ca and Sr content. Lactate and glucose values reflected viability results well, while no differences in pH-values were present.

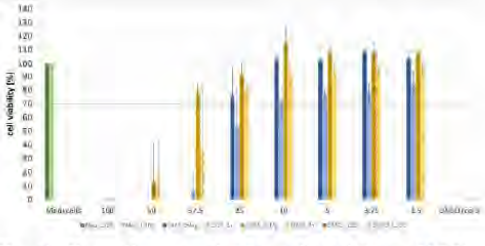

Fig. 1: Exemplary results for cell viability of L929 and U2OS cells lines (24 h in corrosion extracts of Zn and Zn-0.6Mg).

DISCUSSION & CONCLUSIONS: Cell-dependant compatibility has been reported by different papers and was seen also here. L929 fibroblasts are more sensitive to corrosion extracts of Zn alloys than U2OS osteosarcoma cells. Mg seems to enhance biocompatibility in alloys with few alloying components in contrast to alloys with three or four components. The current examination used a Mg-containing media so different Mg contents released during corrosion are most probably not the reason for these results. Instead, different corrosion rates might have led to different Zn concentration in the different extracts. The current study shows the importance of consistent experimental set ups and exact reporting of methods and results for best comparability.

REFERENCES: [1] J. Kubasek et al. (2016) Mat Sc Eng C **58** 24-35; [2] W. Pachla W et. al, (2021) *Bioact. Mater.* 6, 1, 26-44,

ACKNOWLEDGEMENTS: The authors thank Prof. Gebauer´s working group (Inst. For Anorganic Chemistry, Leibniz University Hannover) and Karol Krolewski for technical support. This work was supported by the Institute of Metallurgy and Materials Science, Polish Academy of Sciences, within a statutory work.

European Cells and Materials Vol. NN. Suppl. N, 20xx (page htu)
ISSN 1473-2262

Tracing immunological interaction of zinc-based membrane microenvironment during guided bone regeneration: Single-cell transcriptome analysis

Huibin Liang[1], Jingtao Dai[2], Ping Li[1]

[1] School and Hospital of Stomatology, Guangzhou Medical University, Guangzhou, China. [2] Stomatological Hospital, School of Stomatology, Southern Medical University, Guangzhou, China

INTRODUCTION: Zinc (Zn)-based biodegradable metals are promising candidates for guided bone regeneration (GBR) membranes due to their tunable degradation, biocompatibility, and osteogenic capacity [1]. However, the immunological mechanisms underlying Zn-induced bone repair remain poorly characterized. Single-cell RNA sequencing (scRNA-seq) now permits high-resolution profiling of complex biological processes. This study employs scRNA-seq to dissect the immunological profiles and regulatory networks associated with Zn-based GBR membranes.

METHODS: Pure Zn (99.9 wt%) membranes were implanted in a femoral defect model using 6–8-week-old Sprague–Dawley rats. Cylindrical defects (3 mm × 4 mm) were created in both femoral epiphyses, with Zn implants placed unilaterally (experimental group) and titanium implants as contralateral controls. On postoperative day 3, granulation tissue from defect sites was harvested for histological assessment. Hematoxylin-eosin (HE) and Masson's trichrome staining were performed to evaluate cellular infiltration and neovascularization. Meanwhile, the scRNA-seq was conducted to characterize immune cell dynamics during material degradation and early bone repair. On day 28, femoral samples were stained with Masson's trichrome and methylene blue to quantify new bone formation in the defects.

RESULTS: The HE staining revealed elevated immune cell infiltration and collagen deposition in the Zn group on day 3 (Fig. 1A). On postoperative day 3, compared to the Ti group, Zn implants induced a higher proportion of immune cells on day 3, especially for T cells (Fig. 1B). On day 28, Masson's trichrome and methylene blue staining indicated similar new bone formation between groups. The results of scRNA-seq identified enriched Gene Ontology terms associated with T-cell biology in the Zn group. Notably, T cell subsets in the Zn group exhibited stronger potential interactions with osteogenic progenitor cells than those in the Ti group (Fig. 1C-D).

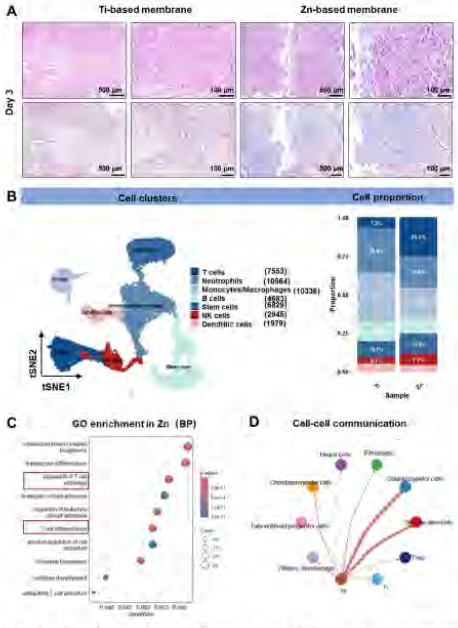

Fig. 1: Zn-based membrane modulates immune microenvironment and cellular dynamics. (A) H&E staining at day 3. (B) t-SNE plot of seven cell clusters (scRNA-seq, n = 4) and stacked bar plot of lineage abundance in Zn vs. Ti groups. (C) GO enrichment of Zn-associated genes reveals T cell activation and osteoimmunomodulation pathways. (D) Enhanced T cell-osteogenic progenitor cell interactions in the Zn group.

DISCUSSION & CONCLUSIONS: This study demonstrates that Zn implants elicit a heightened immune response, characterized by increased T cell recruitment and enhanced cross-talk with osteogenic cells. Despite comparable new bone formation on day 28, the early immune cell infiltration and T cell-specific gene enrichment in the Zn group suggest an immunomodulatory mechanism underlying Zn-induced osteogenesis.

REFERENCES: [1]W. Zhang, P. Li, et al (2021), *Bioactive Materials* 6(4) 975-989.

ACKNOWLEDGEMENTS: This research was supported by NSFC (Grant No. 82301134).

European Cells and Materials Vol. NN. Suppl. N, 20xx (page htu) ISSN 1473-2262

Shelf-life and stability of simulated body fluids used for in vitro tests biodegradable alloys

C. D. dos Reis Barros[1], J. A. C. Ponciano Gomes[1]

[1] *Labcorr, COPPE/UFRJ, Federal University of Rio de Janeiro, Rio de Janeiro, Brazil*

INTRODUCTION: In vitro biomaterials testing recommends the use of several simulate body fluids solutions. The literature reports a wide variety of formulations, from variable salinity inorganic to organic based complex solutions. The assessment of the same material in different media can yield varying results, as dissolution rates and formation of different corrosion products layers. The instability of these solutions, particularly when considering pH fluctuations and degradation in over extended test periods, may result in unreliable values of dissolution rates and surface morphologies [1-3]. This study aimed to characterize the physicochemical stability of the commonly used solutions for in vitro tests of biodegradable alloys, focusing both on their shelf-life stability, and their stability under long term experimental conditions.

METHODS: The solutions selected for this study were: Hanks Balanced Salt Solution (HBSS), Simulated Body Fluid (SBF), and Dulbecco's Modified Eagle Medium (DMEM). HBSS was evaluated in both commercial and prepared in laboratory. DMEM solution was evaluated with no supplementation, and with FBS and penicillin supplementation. The study period of 90 days was established, with analysis made at intervals of every 15 days. The shelf-life stability was conducted through pH, conductivity, and visual inspections. For shelf-life stability, aliquots obtained from storage conditions, 8±2°C, were analysed at 37±1 °C. The stability under testing conditions, was conducted in double-walled cells maintained at 37±1 °C during all study period, in setups like those used in immersion tests, also evaluated regarding pH, conductivity, and visual inspection at all proposed time points. In compliance with pH criteria, a range of 7.4 ± 0.2 was considered, as recommended by standards for in vitro evaluations aiming at simulating the human body environment.

RESULTS: SBF, commercial HBSS, and both DMEM solutions showed the ability to maintain pH values in accordance with the criteria, when stored under recommended conditions. Lab-prepared HBSS demonstrated shelf-life stability in pH for up to 60 days, when storage in similar recommended conditions to the commercial one. Under experimental conditions, such as immersion tests, with a continuous maintenance at 37 ±1°C, in the visual inspection only SBF remained without visual changes, HBSS solutions changed from reddish-orange colour to red, remained in this tone. DMEM solutions after 7 days, achieved a pinkish red tone shifted to purple, and increased turbidity, up to 30 days. This modification suggests the degradation of the environment. Only SBF showed the capacity to maintain pH for a long period within the required range. The commercial HBSS, as well as both DMEM exhibited an overall increase in pH over time, up to 15 days. The lab-prepared HBSS remained below the range in the period of 15 to 30 days, returning to the range in 60 days, thereafter, following at lower values than that, as disposal in Figure 1.

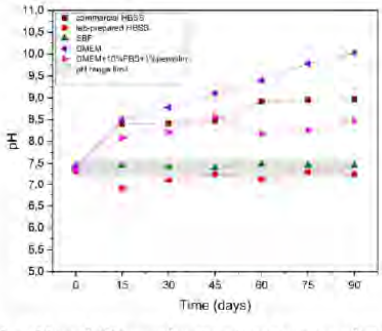

Fig. 1: pH stability under in vitro test conditions.

CONCLUSIONS: A shelf-life storage up to 90 days can be considered adequate for SBF, commercial HBSS and DMEM. Laboratory prepared HBSS exhibit lower shelf-life stability, 60 days. Under experimental conditions, the SBF solution showed better physical and chemical stability and was the best choice to perform long term in vitro tests.

REFERENCES: [1] J. Gonzalez et al. (2018) *Bioactive materials* **3**(2):174-185. [2] K. Törne, A. Örnberg and J. Weissenrieder (2017) *J Biomed Mater Res Part B* **105B**:1490–1502. [3] D. Mei et al. (2020) *Corrosion Science* **101**:182-192.

ACKNOWLEDGEMENTS: The financial support from the FAPERJ Brazilian research funding (E-26/204.450/2021).

17th Biometal
25-30 AUGUST, 2025
Grand Hôtel San Michele,
Cetraro, CS, Italy

European Cells and Materials Vol. NN. Suppl. N, 20xx (page htu) ISSN 1473-2262

Enhanced corrosion resistance and bioactivity of metallic alloys via non-toxic nitrogen-doped carbon film transfer and laser-deposited bioactive glass

S Bajda[1], A Rai[1], K Cholewa-Kowalska[1], B Wiese[2], Y Liu[3], M Krzyzanowski[1,4]

[1] Faculty of Metals Engineering and Industrial Computer Science, AGH University of Krakow, Poland. [2] Helmholtz-Zentrum Hereon, Institute of Metallic Biomaterials, Functional Magnesium Materials, Germany. [3] Manufacturing Technology Centre, Coventry UK. [4] CEBE, Birmingham City University, Birmingham, UK.

INTRODUCTION: The application of ultrathin, ultrasmooth and corrosion resistant nitrogen-doped amorphous carbon (a-C:N) thin film on a magnesium alloy (Mg-0.5Zn-0.2Ca) and S520 bioactive glass on an ultrafine-grained Ti-6Al-7Nb titanium alloy by a laser-directed energy deposition (LDED) process is studied. Carbon is a potentially suitable choice to improve the biocompatibility and corrosion resistance of Mg-based implants, while Ti-based material without potentially toxic vanadium coated with S520 may be a choice for its use in biomedical load bearing implants.

METHODS: The Mg alloy was fabricated using direct chill casting, melted at 720°C in an Ar-SF6 atmosphere, cast into preheated molds at 680°C, water-quenched, and solution annealed at 450°C for 16 hours to achieve a homogeneous microstructure. The a-C:N film was synthesized by mixing β-PEI and glucose in a 1:1 vol ratio, optimizing nitrogen concentration and transfer. AFM, SEM, and EDS were used to examine the film's topology, thickness, morphology, and structure. Electrochemical corrosion and cytotoxicity tests with the MG-63 cell line were also conducted.

S520 bioactive glass powder was produced using a quenching technique to achieve the desired wetting angle for LDED. The Ti-6Al-7Nb alloy was ultrafine-grained through Equal Channel Angular Pressing (ECAP). A 5-axis Mikron 450u machine was used for the hybrid LDED system, combined with a modified laser deposition and multi-material powder delivery system. The laser operated at 1064 nm with a 1200 W output. Samples were analyzed using light microscopy, SEM with EBSD, and EDS for chemical analysis.

RESULTS:

The a-C:N film's amorphous nature was confirmed by HRTEM, XRD, XPS, and Raman spectroscopy, showing sp^2 clusters [1]. Nitrogen's electron-donating ability improves interaction with Mg^{2+} ions, enhancing film-substrate adhesion. No delamination was observed after seven days in dilute HCl. Electrochemical tests showed a lower I_{corr} for the coating and higher R_{pc}, R_{ct} values, indicating improved corrosion resistance. After long-term immersion in PBS and HCl, the coated surface showed less degradation than the bare magnesium alloy.

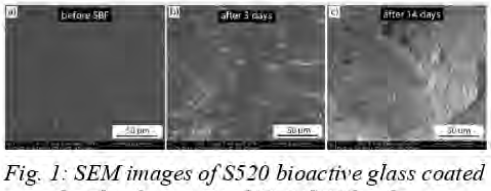

Fig. 1: SEM images of S520 bioactive glass coated onto the ultrafine-grained Ti-6Al-7Nb substrate before (a), after 3 (b) and after 14 (c) days of immersion in simulated body fluid (SBF).

The application of bioactive glass S520 on ultrafine-grained Ti-6Al-7Nb via LDED creates a biocompatible material for biomedical implants without toxic vanadium [2]. The laser cladding process melts the titanium surface and infuses it with bioactive glass, leading to crystallization and the formation of large grains. Laser-induced heat causes a martensitic transformation, forming α′ acicular martensite, while the heat-affected zone (HAZ) shows refined grains. Concerns about Al toxicity in the glass arise as it dissolves in the body. After 14 days in SBF, the samples formed hydroxyapatite (HCA) with significant P reduction, demonstrating high bioactivity.

DISCUSSION & CONCLUSIONS: Cytotoxicity tests confirmed the studied materials are non-toxic, making it a promising candidate for orthopaedic implants, though further biocompatibility studies are needed.

REFERENCES: [1] A. Rai, M. Szczerba, J. Karbowniczek, et al (2025) *Applied Surface Science* **695**: 162847. [2] S. Bajda, K. Cholewa-Kowalska, M. Krzyzanowski, et al. (2024) *Surface & Coatings Technology* **485**: 130904.

ACKNOWLEDGEMENTS: The support from the National Science Centre, Poland (grant no. 2024/53/B/ST11/00799) is greatly appreciated.

European Cells and Materials Vol. NN. Suppl. N, 20xx (page htu) ISSN 1473-2262

Influence of texture on the mechanical performance of a wire-form bioabsorbable vascular scaffold

K MacLeod[1], D Nash[1], C MacLeod[2], M Steckel[2]

[1]University of Strathclyde, Glasgow [2]Lumenology Ltd., Glasgow

INTRODUCTION: Bioabsorbable vascular scaffolds (BVS) seek to improve the clinical outcomes for arterial disease relative to current drug eluting stents (DES) by elimination of the permanent foreign body implant. However, the relatively poor mechanical properties of available bioabsorbable materials, compared to the those applied in DES, has limited the success of BVS technology to date. To overcome the limitations of past BVS devices, a novel wire-form BVS device, manufactured from a Mg-Li-Y alloy is proposed. The influence that altering the material processing of the wire has on the microstructure and mechanical performance of the device is investigated herein.

METHODS: Mg-4Li-1Y alloy wire cold drawn to a diameter of 125µm was used in the manufacture of the wire-form BVS device (Figure 1a). The wire is formed through a sequential bending process into the shape of the BVS device and subsequently annealed. The device processing has then been modified to alter the dominant recrystallisation mechanisms during the required annealing step to tailor the texture for optimal mechanical performance

The microstructure of the device was characterised using SEM and EBSD analysis. Benchtop expansion and radial force testing were employed to assess its mechanical performance.

RESULTS: In the device manufactured using the original process, a split in texture is developed (Figure 1b). In contrast, the device manufactured using the modified process develops a more uniform texture distribution at the same location following the required annealing step (Figure 1c). During benchtop expansion testing, the modified device exhibits >20% increase in mechanical performance compared to the original process, whilst maintaining the same over-expansion limits.

DISCUSSION & CONCLUSIONS: The wire used to manufacture the device exhibits a typical basal texture, with the grains aligned with their c-axis perpendicular to the drawing direction. During device manufacture, tensile and compressive loading along the drawing direction of the wire results in compressive and tensile loading of the c-axis of the grains respectively. This promotes the activation of tensile twinning through regions of the wire deformed through compressive loading. Following annealing, the original device has a recrystallised microstructure dominated by grains nucleated from these tensile twins (Figure 1b+d). In contrast, using the modified process, a number of alternative nucleation sites were present in the device prior to annealing. Consequently, a range of nucleation sites are available, and a more uniform texture is developed following recrystallisation in the modified device (Figure 1c+e).

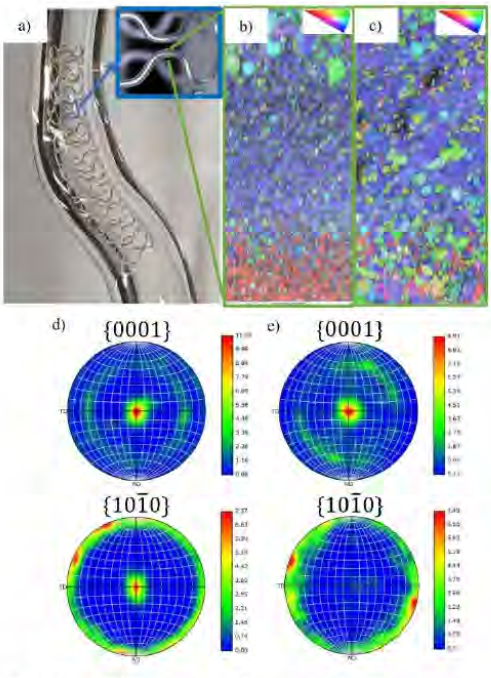

Fig. 1: a) BVS device b) Inverse pole figure map of device manufactured using original process c) Inverse pole figure map of device manufactured using modified process d) Pole figures for original process e) Pole figures for modified process

The texture developed in the modified device is more favourable for the activation of prismatic slip during device deployment. Consequently, it exhibits a >20% increase in mechanical performance compared to the original device.

ACKNOWLEDGEMENTS: This research was funded by the Medical Research Council

European Cells and Materials Vol. NN. Suppl. N, 20xx (page htu)
ISSN 1473-2262

Magnesium-microbiome interactions in the human oral cavity—an *in-situ* study

Lian Huang[1], Janak L Pathak[1], Zhentao Yu[2], Jingtao Dai[3], Ping Li[1]

[1] *School and Hospital of Stomatology, Guangzhou Medical University, Guangzhou, China.* [2] *Institute of Advanced Wear & Corrosion Resistant and Functional Materials, Jinan University, Guangzhou 510632, China.* [3] *Stomatological Hospital, School of Stomatology, Southern Medical University, Guangzhou, China*

INTRODUCTION: High-purity magnesium (Mg), commercially available for guided bone regeneration (GBR) membranes, faces oral application challenges due to interactions with salivary enzymes and biofilms [1]. While Mg degradation's ecological effects on oral microbiota—including community shifts and virulence factor expression—remain poorly understood, its corrosion behavior in oral environments varies with physiological conditions and inter-individual differences. This study examines Mg-microbe interactions at the bacterial-material interface to elucidate mechanisms underlying material performance and microbial responses in clinical settings.

METHODS: Certified medical-grade Mg and Ti6Al4V alloy (Ti) were used. Biofilm dynamics on Mg and Ti surfaces, alongside Mg corrosion patterns, were monitored *in vivo* using a custom-designed oral splint worn by systemically healthy volunteers (Fig. 1). The study protocol was approved by the local Ethics Committee (ID: JCYJ 2023006). Each participant wore the splint for 8-hour intervals, after which specimens were immediately transported to the laboratory for multimodal characterization. Scanning electron microscopy (SEM) and confocal laser scanning microscopy (CLSM) were employed for morphological/topographical analysis, while bacterial DNA collected via sterile swab sampling underwent 16S rRNA gene sequencing and metagenomic profiling to resolve microbial community structures.

Fig. 1: Image of the in-situ device.

RESULTS: Live bacteria displayed a diffuse, punctate distribution pattern within Mg biofilms but formed dense aggregates on Ti surfaces (Fig. 2A). SEM revealed enhanced Mg corrosion with increased byproduct formation in vitro, whereas minimal in situ corrosion was detected (Fig. 2B). Metabolic pathway analysis showed Ti-associated upregulation of translation, replication/repair, amino acid metabolism, and membrane transport processes. Conversely, Mg exposure correlated with downregulated energy metabolism, signal transduction, and nucleotide metabolism (Fig. 2C). Notably, inter-individual variability significantly modulated microbial metabolic responses to Mg degradation products, with linear mixed-effects models indicating donor-specific effects on carbon metabolism and quorum sensing pathways.

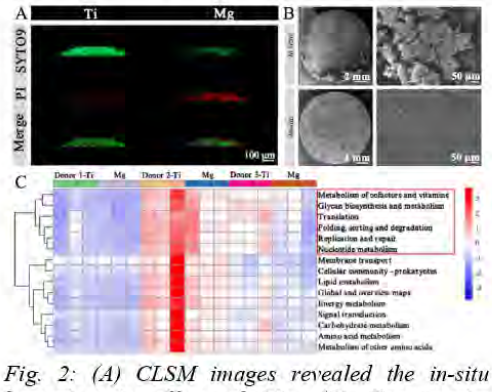

Fig. 2: (A) CLSM images revealed the in-situ bacteriostatic effect of Mg. (B) Comparative corrosion morphology under in vitro and in-situ conditions. (C) KEGG pathway enrichment analysis of metabolic alterations.

DISCUSSION & CONCLUSIONS: High-purity Mg showed bacteriostatic effect *in-situ*. The results revealed distinct metabolic shifts between Ti and Mg groups, with Mg exhibiting a suppressive effect on microbial metabolism, consistent with its known antimicrobial properties. However, the impact varies between individuals.

REFERENCES: [1]W. Zhang, P. Li, et al (2021), *Bioactive Materials* 6(4) 975-989.

ACKNOWLEDGEMENTS: This research was supported by NSFC (Grant No. 82301134).

European Cells and Materials Vol. NN. Suppl. N, 20xx (page htu) ISSN 1473-2262

Bioresorbable magnesium implants promote osteogenesis in the medullary cavity and glycogenolysis in the liver

B Okutan[1], DCF Wieland[2], UY Schwarze[1], H Habisch[3], T Madl[3], NG Sommer[1], AM Weinberg[1]

[1] Department of Orthopaedics and Traumatology, Medical University of Graz, Graz, Austria. [2]Institute of Metallic Biomaterials, Helmholtz-Zentrum Hereon, Geesthacht, Germany. [3]Otto Loewi Research Center, Medical University of Graz, Graz, Austria.

INTRODUCTION: In the last decades, magnesium (Mg)-based implants have become alternative candidates in orthopedic applications due to their biodegradability, suitable mechanical, and osteoconductive properties[1]. However, it is still lack in literature if and how released Mg^{2+} ions from Mg-based implants influence bone remodeling in the medullary cavity and systemic regulation of other organs. Hence, the aim of this study is to evaluate the early and mid-term local and systemic tissue responses of degrading ZX00 (Mg-Zn-Ca alloy) and extra high-purity Mg (XHP-Mg) pins in juvenile healthy rats.

METHODS: In this study, five SD rats per group underwent bilateral, transcortical implantation of cylindrical ZX00, XHP-Mg, and Titanium (Ti) pins into the diaphysis of both femurs. Moreover, sham-operated and control groups (non-intervention) were used. Animals were euthanized after 3, 14, 42, 168 days, post-surgery. Early and mid-term local responses were investigated via gene expression, histological, and SAXS analyses, whereas biochemical analyses and NMR spectroscopy were performed to investigate potential systemic responses to Mg-based implants.

RESULTS: Both ZX00 and XHP-Mg pins support new bone formation via stimulating osteogenic lineage commitment of bone marrow stromal cells within the first 14 days, post-surgery. Qualitative histological analysis revealed good osseointegration and new bone tissue formation around both ZX00 and XHP-Mg pins (Figure 1).

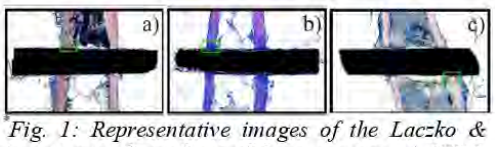

Fig. 1: Representative images of the Laczko & Levai stained rat femoral bone sections a) ZX00, b) XHP-Mg, and c) Ti [2].

Moreover, we found a more parallel hydroxyapatite/collagen orientation along ZX00 and XHP-Mg pins in the perimeter region compared to Ti pins. Decreased glycogen levels in both Mg-based implanted groups demonstrated that degradation products can promote glycogenolysis in the liver (Figure 2).

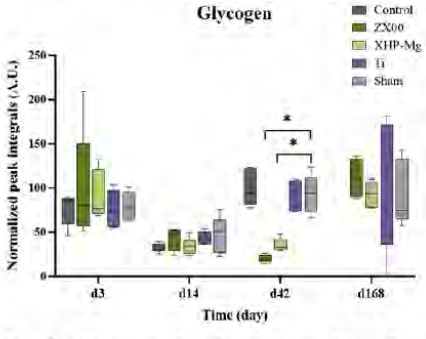

Fig 2. Glycogen levels in liver throughout 168 days (24 weeks) of study period [2].

DISCUSSION & CONCLUSIONS: Here, our findings suggest that ZX00 and XHP-Mg pins stimulate osteogenesis mainly via *Bmp2* and *Opg* in the medullary cavity and promote glycogenolysis in the liver, while the higher degradation rate of XHP-Mg pins resulted in upregulation of different genes and metabolites.

REFERENCES: [1]F. Xing, *et al.*, Recent progress in Mg-based alloys as a novel bioabsorbable biomaterials for orthopedic applications, *J. Magnes. Alloys* 10 (2022) 1428–1456. [2]B. Okutan, *et al.*, Biodegradable ultrahigh-purity magnesium and its alloy ZX00 promote osteogenesis in the medullary cavity and glycogenolysis in the liver. *Acta Biomater (2025) 195:599-613.*

ACKNOWLEDGEMENTS: This study has received funding from the European Union's Horizon 2020 research and innovation program under the Marie Sklodowska-Curie grant, agreement No 811226 and the PhD program "Molecular Medicine" at Medical University of Graz.

In Vivo

Friday,
August 29th, 2025

elecell
Hope for Healing

BioActiveMetals
Innovation in Metallic Biomaterials

meo.
Inspiring Materials.

medical magnesium

UNIVERSITÉ LAVAL

CHARITÉ
UNIVERSITÄTSMEDIZIN BERLIN

KeAi
CHINESE ROOTS GLOBAL IMPACT

PEKING UNIVERSITY

European Cells and Materials Vol. NN. Suppl. N, 20xx (page htu)
ISSN 1473-2262

Multiscale hard-soft structured Zn-based alloy with ultrahigh strength and deformability used for biodegradable anastomosis staples

Xiyuan Zhang, Jialin Niu, Guangyin Yuan*

School of Materials Science and Engineering, Shanghai Jiao Tong University, Shanghai, China

*E-mail: gyyuan@sjtu.edu.cn

INTRODUCTION: Zn-based alloys have great potential to be employed in biodegradable implants due to their satisfying degradation rate and acceptable biocompatibility. However, their strength is insufficient to meet broader application requirements. In this study, a new type of Zn-Cu-Li alloy with a unique multiscale hard-soft structure is designed and developed by the author's group, which exhibits ultrahigh strength and elongation (YS: 550 MPa, UTS: 600 MPa, and EL:55%) and can be fabricated anastomosis staples.

METHODS: The microstructure of the alloy was characterized by OM, SEM (equipped with TOF-SIMS), high-resolution TEM, and APT techniques from the micron and sub-micron to the nano and atomic scale. The deformation behavior during the tensile test was analyzed through SEM accompanied by EBSD and TEM.

RESULTS: The alloy consists of hard micron beta-$LiZn_4$ intermetallic (solid solution with Cu) (~1.64 μm), soft submicron eta-Zn phase (~0.60 μm) and hard nano epsilon-$CuZn_4$ precipitates (length ~42.38 nm and diameter ~6.76 nm). The rod-shaped nano precipitates exhibit a coherent interface with the matrix and grow along the direction with minimum lattice misfit. During the deformation, the CDRX related to dislocation absorption and <c+a> dislocations can be activated for the alloy. The strengthening effects can mainly be attributed to the hard beta matrix with fine grains, the solid solution strengthening from Cu and the precipitate strengthening of nano epsilon precipitates, while the ductilizing effects can mainly be attributed to the deformable disordered electron compound matrix, activated CDRX, <c+a> dislocations and soft eta-Zn phase, as shown in Fig.1. The newly patented alloy with excellent strength and ductility has been successfully drawn into fine wire with diameter of 0.22mm and fabricated into the anastomosis staples.

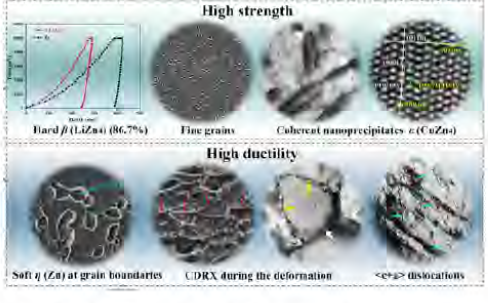

Fig. 1: Microstructure of as-extruded Zn-2Cu-0.8Li alloy

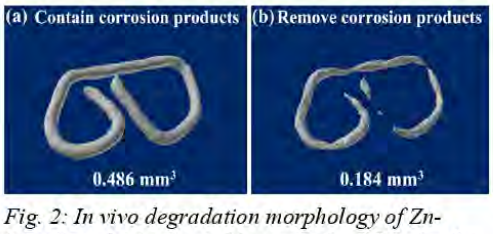

Fig. 2: In vivo degradation morphology of Zn-based staples implanted in stomach of Beagles for 12 months.

DISCUSSION & CONCLUSIONS: The biodegradable Zn-Cu-Li anastomosis staples has been implanted into the beagles model successfully for 12 months (Fig.2) and exhibited great prospects of clinical applications, which are promising to replace the traditional non-degradable Ti-based anastomosis staples.

REFERENCES: [1] X Zhang, G. Liu, G. Yuan, et al (2023) *Int. J. Plast.* **169**: 103731. [2] Z. Gao, X. Zhang, G. Yuan, et al (2022) *Materials Characterization* **185**: 111722.

ACKNOWLEDGEMENTS: This work was funded by Natural Science Foundation of China (No.51971134).

European Cells and Materials Vol. NN. Suppl. N, 20xx (page htu) ISSN 1473-2262

Local sustained magnesium delivery to harness Mg biological activity: examples of applicable clinical applications

Charles Sfeir, Nursima Lacin, Jin Gao, Yejin Cho, Julie Kobyra, Flavy Roseren, Lu Li, Patricia Diaz
[1] *University of Pittsburgh, Pittsburgh, PA USA*

INTRODUCTION: Resorbable magnesium (Mg) metal has made significant strides over the past two decades, evolving into a clinically viable material for biomedical applications, particularly in orthopedics and cardiovascular medicine. These advancements were due to alloy development, surface modification technologies, our biological understanding and safety, and clinical validation. But the area of sustained delivery of magnesium, considering it as a drug, has been understudied. In this presentation, we will discuss our efforts to deliver magnesium to harness its biological activities and avoid some of the hydrogen gas evolution and localized alkalization. We will present new data on the role of Mg's immunomodulation properties to treat periodontal disease, and also integrate the canine socket preservation data.

METHODS: Mg-loaded controlled-release biodegradable poly(lactic-co-glycolic acid) (PLGA) were manufactured in microparticles form, sheet form as an electrospun PLGA and Mg particles. The microparticles were administered locally following the initiation of ligature-induced periodontitis in mice. Alveolar bone loss was assessed using micro-computed tomography (μCT). Flow cytometry was performed to evaluate macrophage polarization. Microbiome composition was analyzed via 16S rRNA sequencing. Single-cell RNA sequencing was used to characterize transcriptomic effect of Mg on the immune response. We will also incorporate some of our published work where Mg/PLGA were used to treat socket preservation.

RESULTS: Our data demonstrate that local sustained Mg delivery inhibited inflammatory bone loss and promoted M2 macrophage polarization in the surrounding tissues. Intriguingly, 16S rRNA sequencing revealed persistent microbial dysbiosis despite improved disease outcomes, suggesting an uncoupling of host-microbiome interactions. Single-cell RNA sequencing further showed that local Mg delivery reversed disease-associated inflammatory pathways by downregulating the STAT3 signaling pathway in macrophages and T cells.

DISCUSSION & CONCLUSIONS: Our findings suggest that locally sustained Mg delivery promotes M2-like anti-inflammatory macrophage polarization and mitigates alveolar bone loss, even in the presence of a dysbiotic microbiome, supporting its potential as a feasible immunomodulatory therapy for periodontitis.

ACKNOWLEDGEMENTS: Funding from the Center for Craniofacial Regeneration.

European Cells and Materials Vol. NN. Suppl. N, 20xx (page htu)
ISSN 1473-2262

In vivo compatibility and anti-bacterial activity of semi-solid rheo-formed Mg-Sr-Ag alloy in urinary system

Di Tie[1,*], Xia Wu[1], Guangyin Yuan[2], Xiaoli Cui[1], Dongsong Yin[1], Magdalena Bieda-Niemiec[3], Anastassios Papageorgiou[1]

[1] *School of Materials Science and Engineering, Guangdong Ocean University , China.* [2] *School of Materials Science and Engineering, Shanghai Jiao Tong University, China.* [3] *Institute of Metallurgy and Materials Science of Polish Academy of Sciences, Poland.*

INTRODUCTION: Biodegradable magnesium ureteral implant materials are gaining increasing research interest duo to their constantly degrading surface, which are immune to biofilm formation. Here, we develop a new Mg-Sr-Ag alloy (JQ alloy) and intensively study its biocompatibility and the antibacterial effect in urinary system.

METHODS: Mg-1.0Sr-0.5Ag (wt.%) alloy stent was fabricated by semi-solid rheo-extrusion, and Bama Minipigs were used as the animal implantation model. Bladder urodynamics were evaluated using an automatic urodynamics analyzer, and bacteriuria was examined via agar diffusion methods. Histological evaluation was performed at 12w post-implantation..

RESULTS: Semi-solid rheo-solidification led to evident grain refinement strengthening effect. The JQ alloy obtained ca. 111% increase in ultimate tensile strength (223.7 MPa). The CCK-8 results showed no significant difference between the LO2 cell proliferation rate in JQ and Mg groups.

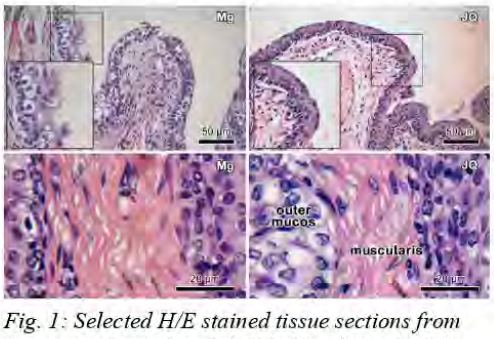

Fig. 1: Selected H/E stained tissue sections from the ureter (upper) and the bladder (lower) of the test animals at 12w post-operation.

Absence of necrotic tissue and similar cellular structures were observed in both magnesium and JQ groups. The bladder wall structure appeared normal after 12 weeks implantation, and there were no inflammatory infiltrates in the outer mucosa and the muscularis. Cystometric results revealed less negative influence on bladder functions of JQ groups than Mg groups. Higher bladder capacity and starting filling pressure (15.8 ± 6.2 cm H_2O) were observed in Mg group after operation.

The cells in JQ group showed more compact nucleus with uniformly distributed loose chromatin. Narrow bands of condensed chromatin were observed on the inner nuclear membrane. The smooth endoplasmic reticulum was better developed in JQ group, and a decreased lamina propria widening was also observed in JQ group.

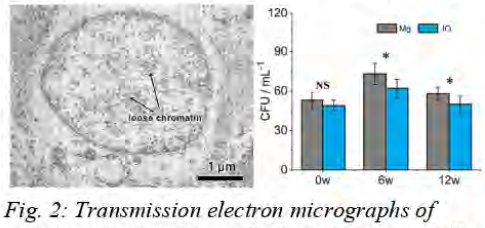

Fig. 2: Transmission electron micrographs of transitional epithelium cells from the ureter wall (left) and bacteria numbers in urine (right) of the experimental animals in JQ group .

DISCUSSION & CONCLUSIONS: JQ alloy shows satisfactory compatibility and improves the post-operative bladder functions. We also observed significantly less CFUs in urine, which further led to an absence of nucleus fragmentation and recovered lamina propria. These discoveries make antibacterial biodegradable metallic materials represented by JQ alloy particularly noteworthy candidates as ureteral implant materials.

REFERENCES: [1] D. Tie, N. Hort, M. Chen, *et al* (2022) *Bioact Mater* **7**:254-262. [2] D. Tie, H. Liu, *et al* (2020) *ACTA Biomater* **116**:415-425.

ACKNOWLEDGEMENTS: The authors appreciate the financial support from National Natural Science Foundation of China (52171235, W2521039), Dalian Science and Technology Bureau (2023RJ008), Yangjiang Science and Technology Bureau (RCZX2023004), and Guangdong Ocean University (YJR24003).

European Cells and Materials Vol. NN. Suppl. N, 20xx (page htu) ISSN 1473-2262

Multiscale investigation of bone quality at the interface formed by biodegradable magnesium implants using 2D qBEI imaging and 3D micro-CT

S Schimek[1], AM Batouche[2], I Fiedler[2], K Jähn-Rickert[2], B Busse[2], DCF Wieland[1]

[1] *Institute of Metallic Biomaterials, Helmholtz-Zentrum Hereon, Germany* [2] *Department of Osteology and Biomechanics, University Medical Center Hamburg-Eppendorf, Germany*

INTRODUCTION: The majority of implants used for fracture treatment are made from non-degradable materials like titanium alloys, which remain in the body unless surgically removed. Magnesium (Mg) alloys offer an innovative alternative due to their biodegradability, biocompatibility, and mechanical properties resembling those of cortical bone, making them promising for osteoimplants [1,2]. However, understanding the mutual interaction of the degradation process of Mg implants with tissue remodeling remains challenging. This study investigates the influence of Mg-based implants on bone mechanical properties and ossification processes. It aims to analyze the multiscale impact of Mg alloys on bone quality, focusing on early-stage healing using both 2D and 3D methods on the same samples.

METHODS: To study the multiscale impact, a comprehensive range of analysis is planned along with a correlative analysis for a scale bridging understanding. The employed methods including micro-computed tomography (µCT), in situ diffraction nanoindentation, histology, EDX analysis, and quantitative backscattered electron microscopy (qBEI). Therefore, Tibiae of rats were implanted with Mg alloy WE43 and titanium alloys, which served as control. The rats were sacrificed after 3, 7, 14, 28, and 90 days. 2D-qBEI was employed to examine bone-implant interfaces, focusing on bone area fraction, mineral density distribution, and the density of osteocyte lacunae near the implantSynchrotron micro-CT measurements were utilized to provide detailed assessments of bone volume fraction (BV/TV), degradation and the spatial organization of lacunae (Fig. 1). Additionally, a comprehensive overview of the applied methods and workflow is being demonstrated, showcasing the multiscale analysis approach.

RESULTS: The results show that Mg implants stimulated bone turnover, resulting in lower mineralization and calcium heterogeneity, likely due to insufficient time for bone maturation. The 2D and 3D analyses revealed decreased lacuna density and BV/TV for Mg implants compared to titanium. Furthermore, the interaction between bone formation and lacunae network development for early stage healing will be shown on a local and global scale. As the Mg implants revealed a volume loss of approx. 20 % after 90 days, an interaction between the degradation processes, bone formation and lacunae network will be presented, indicating a significant influence of the degradation processes of WE43 on the bone formation and morphology.

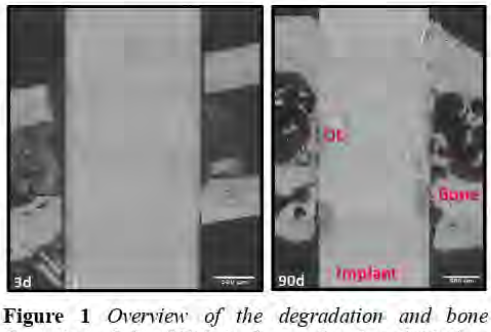

Figure 1 *Overview of the degradation and bone formation of the WE43 implants after 3 and 90 days using synchrotron radiation micro-CT.*

DISCUSSION & CONCLUSION:
The advanced multiscale approach demonstrates efficacy, revealing significant differences in bone quality parameters between titanium and magnesium implants during the early stage of healing. The results on the lacunae network and the mineralization better allow understanding the differences in the bone remodelling at degradable and non-degradable implants by correlating the degradation and bone formation parameters.

REFERENCES: [1]J. Hofstetter, M. Becker, E. Martinelli, et al., High-strength low-alloy (HSLA) Mg-Zn-Ga alloys with excellent biodegradation performance, JOM 66, 566-572 (2014) [2]N.G. Grün, P. Howleg, S. Tangl, et al., Comparison of a resorbable magnesium implant in small and large growing-animal model, Acta. Biomater 78, 379-386 (2018)

European Cells and Materials Vol. NN. Suppl. N, 20xx (page htu) ISSN 1473-2262

Investigating the effect of surface treatments on Mg-based implant behavior in male, juvenile, growing rats

N Zechmann[1], B Okutan[1], UY Schwarze[1,2], AM Weinberg[1], NG Sommer[1]

[1] *Department of Orthopaedics and Traumatology, Medical University of Graz, Graz, Austria*

[2] *Department of Dental Medicine and Oral Health, Medical University of Graz, Graz, Austria*

INTRODUCTION: Magnesium (Mg)-based implants are gaining attention as innovative solutions for fracture fixation, owing to their biocompatibility, biodegradability, and favorable mechanical characteristics. Unlike traditional permanent implants, Mg-based implants naturally resorb, avoiding the need for surgical removal [1, 2]. Nevertheless, Mg's accelerated degradation *in vivo* presents a significant challenge [3]. Surface treatments such as autoclaving and Atomic Layer Deposition (ALD) have emerged as promising strategies to tailor degradation rates, and therefore, do not interfere with bone healing [4]. Autoclaving generates a protective oxide layer, whereas ALD enables the application of uniform, ultrathin coatings [5].

METHODS: Bioresorbable Mg-based ZX00 pins (<0.5 wt% Zn, <0.5 wt% Ca; diameter = 1.6 mm, length = 8 mm) were transcortically implanted into the femoral diaphysis of 6-week-old male Sprague Dawley rats (n = 6 per group). Five experimental groups were studied: untreated controls, autoclaved once (1xa) or three times (3xa), and two ALD-coated groups (ALD1 and ALD2). Implant degradation was assessed using *in vivo* micro-computed tomography (µCT), with imaging conducted immediately after implantation and at 2, 6, 12, 18, and 26 weeks. *Ex vivo* µCT imaging was carried out at 26 weeks post-surgery (Fig. 1). Additionally, histological analyses were performed at the end of the study period.

RESULTS: Initial implant volumes and surface areas were larger in the treated groups than in the controls. Throughout the 26-week period, degradation rates were higher in treated samples, particularly those autoclaved three times. ALD-coated implants (ALD1, ALD2) exhibited reduced degradation during the critical early healing phase (weeks 6–12), suggesting a protective influence. Surface area changes between groups were less prominent. Gas formation remained low across all groups, except at isolated time points, with no significant differences. Histological evaluations are ongoing to verify that there is no negative impact on new bone formation.

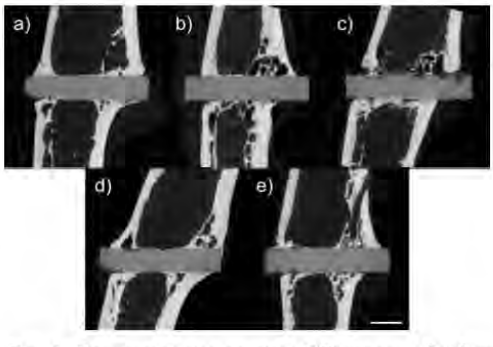

Fig. 1: Representative ex vivoµCT images of either a) untreated, b) 1xa, c) 3xa, d) ALD1-coated, or e) ALD2-coated ZX00 pins 26 weeks after implantation. Scale bar = 2 mm.

DISCUSSION & CONCLUSIONS: The bioresorbable ZX00 implants, whether untreated or surface-modified, are not anticipated to impair bone regeneration. Our findings show the complexity of optimizing surface treatments to control Mg implant degradation. In this study, ALD coatings showed the greatest potential to moderate degradation during the essential early healing period, highlighting their promise for future clinical application.

REFERENCES: [1] F. Witte (2010) *Acta Biomater.* **6**:1680-92. [2] F. Xing, S. Li, D. Ying, et al (2022) *J. Magnes. Alloy,* **10**:1428-56. [3] T. Kraus, S. F. Fischerauer, A. C. Hänzi, et al (2012) *Acta Biomater,* **8**:1230-38. [4] Z. Xi, Y. Wu, S. Xiang, et al (2020) *ACS Omega,* **5**:4548-57. [5] P.-C. Lin, K. Lin, Y.-H. Lin, et al (2022) *Coatings*, **12**:212.

ACKNOWLEDGEMENTS: This work was funded by Bioretec Ltd.

17th Biometal
25-30 AUGUST, 2025
Grand Hôtel San Michele,
Cetraro, CS, Italy

European Cells and Materials Vol. NN. Suppl. N, 20xx (page htu) ISSN 1473-2262

Ultrasonic atomization of medical grade Mg alloys for additive manufacturing

J Cruz[1], F Wisotzki[1], A Mainguy[1,2], H Mescheder[3], S Pöstges[1], A Kopp[1]

[1]*Meotec GmbH, Aachen, Germany.* [2]*IMDEA Materials Institute, Getafe, Spain.*

[3]*Fraunhofer Institute for Production Technology IPT, Aachen, Germany*

INTRODUCTION: Additive manufacturing (AM) of magnesium alloys has gained significant attention in medical applications due to the ability to create complex, patient-specific structures[1]. Powder production plays a critical role in the outcomes of AM, as the properties of the powder directly impact the quality and precision of the manufactured parts[1,2]. Ultrasonic atomization (UA) enables the production of powders with a narrow size distribution, spherical particles, and minimal impurities. However, given their limited commercial availability, thorough characterization of the powders produced by UA-based systems is essential to ensure they meet the requirements of AM applications[2]. This study investigates the UA of WE43MEO and ZX00MEO powders using two different feedstock configurations (rod feeder and crucible) and evaluates their morphological and size distribution characteristics.

METHODS: The input materials used were 6.0 mm diameter rods of WE43MEO and ZX00MEO (Meotec GmbH, Aachen, Germany). Powder production was carried out using the ATO Lab Plus system with the Induction Melting System (IMS) module (3D Lab, Warsaw, Poland). The ZX00MEO powder was processed using the rod directly in the rod feeder setup, while the WE43MEO rod was cut to fit into the crucible. The reverse feedstock configurations will be tested to complete the study. The powders were sieved to below 90 µm prior to characterization. Morphology was characterized by using a 3D laser scanning microscope (Keyence VK-X100). The particle size distribution (PSD) was determined from Laser Scanning Microscopy (LSM) images using ImageJ (NIH, Bethesda, MD, USA), with D10, D50, D90, and span calculated, and the mean particle size and circularity also reported. Further characterization via Scanning Electron Microscopy (SEM) combined with Energy Dispersive Spectroscopy (EDS) is planned to provide a more detailed analysis of the particle size, morphology, and chemical composition of the powders.

RESULTS: WE43MEO powder showed D10 of 26.2 µm, D50 of 72.5 µm, and D90 of 91.4 µm, while ZX00MEO showed D10 of 20.7 µm, D50 of 65.6 µm, and D90 of 87.9 µm. The calculated span was 0.90 for WE43MEO and 1.02 for ZX00MEO. Mean particle sizes were 66.4 ± 22.7 µm (WE43MEO) and 62.4 ± 22.9 µm (ZX00MEO). Circularity analysis indicates high sphericity for both powders: 0.94 ± 0.04 (WE43MEO) and 0.95 ± 0.06 (ZX00MEO). LSM imaging (Fig. 1) confirmed generally spherical morphology, with some irregular particles observed.

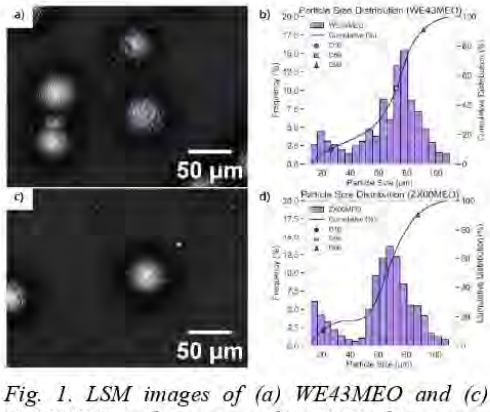

Fig. 1. LSM images of (a) WE43MEO and (c) ZX00MEO and corresponding PSD histograms with cumulative distribution plotted for (b) WE43MEO and (d) ZX00MEO.

DISCUSSION & CONCLUSIONS: The preliminary results demonstrate that UA via induction melting can produce fine, spherical Mg alloy powders suitable for AM applications. Both alloys exhibited high sphericity and acceptable PSDs. Completion of the full experimental matrix will allow further assessment of the influence of atomization setup and alloy type on powder properties. Planned SEM and EDS analyses will provide deeper insights into microstructure and compositional uniformity. Future work will also focus on process optimization.

REFERENCES: [1]Zeng, Z. et al. *J. of Magnes. Alloys* **10**, 1511–1541 (2022). [2]Khan, S. A. et al. *Powder Technol.* **455**, 120725 (2025).

ACKNOWLEDGEMENTS: This project has received funding from the European Union's Horizon 2020 research and innovation programme under Marie-Sklodowska Curie grant agreement ID no. 101120006.

European Cells and Materials Vol. NN. Suppl. N, 20xx (page htu) ISSN 1473-2262

On the trail of Mg - Incorporation and diffusion of Mg into the bone structure during the biodegradation of a MgGd screw

S Torkornoo[1], DC Florian Wieland[2], B Zeller-Plumhoff[2], B Gault[1,3], **TM Schwarz[1]**

[1] Max-Planck-Institute for Sustainable Materials GmbH, Düsseldorf, Germany [2] Institute of Metallic Biomaterials, Helmholtz-Zentrum Hereon, Geesthacht, Germany [3] Department of Materials, Imperial College London, London, United Kingdom

INTRODUCTION: Research into magnesium (Mg) based alloys has progressed in recent years, with studies focusing on the modulation of their degradation behaviour and their potential application as bioresorbable implants in orthopaedics. High concentrations of Mg ions from the degraded Mg implants have been shown to have a local influence on the structure and formation of the bone mineral, i.e hydroxyapatite (HAP), as revealed by small-angle X-ray scattering (SAXS) and X-ray diffraction (XRD)[1]. However, these techniques do not reveal the diffusion pathway and precise spatial distribution of the Mg enrichment within the complex interconnected network of bone at the desired length scale to understand the biomineralization mechanism. In addition, it is analytically difficult to quantify elements with low Z numbers using spectroscopic techniques, which hinders rationalising the Mg distribution at the nanoscale[2,3]. Recent studies using laser ablation time-of-flight mass spectrometry indicate an increase in Mg in the bone adjacent to the implant interface. Bone is the largest reservoir of Mg in the organism and is one of the major cofactors for the enzymes involved in bone matrix synthesis. This raises the question of how Mg from implant degradation gets integrated into the bone. It can be incorporated either directly into the HAP crystals, as Mg^{2+} cations can replace Ca^{2+} in HAP; or into the collagen matrix between the HAP crystals. To answer this question, it is necessary to simultaneously characterise the three-dimensional (3D) composition of bone at the nanometre scale, which can in principle be achieved using atom probe tomography (APT).

METHODS: We used electron microscopy (SEM) and APT to analyze the degradation products of a Mg-10 wt.% Gd (Mg-10Gd) screw implanted in the tibia of a rat over a period of 18 weeks[2,3]. APT analysis were performed at increasing distance from the interface to the old bone to quantify the incorporation and diffusion of Mg into the bone.

RESULTS: Our observations showed a significant accumulation of Mg between the hydroxyapatite crystals, with a clear gradient towards the implant site.

DISCUSSION & CONCLUSIONS: APT is able to provide information on the arrangement of collagen fibrils and the segregation of trace elements at the interface between the collagen fibrils and the HAP crystals[4]. These results provide new insights into possible diffusion pathways of Mg ions from the degraded Mg implant and the adaptation of HAP in the presence of Mg during bone remodelling and give information about the possible organic incorporation into the corrosion products. In correlation with other techniques, APT can provide insights into the local chemistry of bones, including the elusive Mg nanoscale distribution.

REFERENCES: [1] T. A. Grünewald *et al. (2016)* Magnesium from bioresorbable implants: Distribution and impact on the nano- and mineral structure of bone, *Biomaterials*. [2] B. Zeller-Plumhoff *et al. (2020)* Analysis of the bone ultrastructure around biodegradable Mg–*x*Gd implants using small angle X-ray scattering and X-ray diffraction, *Acta Biomater.* [3] K. Iskhakova *et al. (2024)*, Multi-modal investigation of the bone micro- and ultrastructure, and elemental distribution in the presence of Mg-xGd screws at mid-term healing stages, *Bioact. Mater.* [4] *T.M. Schwarz et al. (2025),* Advancing atom probe tomography capabilities to understand bone microstructures at the near-atomic scale, Acta Biomater.

ACKNOWLEDGEMENTS: T.M.S gratefully acknowledges the financial support of the Walter Benjamin Program of the German Research Foundation (DFG) (Project No. 551061178). S.T., T.M.S. and B.G. grateful for funding of the DFG through the Leibniz Award of B.G..

European Cells and Materials Vol. NN. Suppl. N, 20xx (page htu) ISSN 1473-2262

Fracture healing with Mg alloy -based implants in a big animal model:

I Szyszko Mertelseder[1], C Stahle[2], UY Schwarze[1,3], B Okutan[1], NG Sommer[1], AM Weinberg[1]

[1] *Department of Orthopedics and Traumatology, Medical University of Graz, Graz, Austria*
[2] *Bioretec OY, Tampere, Finland*
[3] *Department of Dental Medicine and Oral Health, Medical University of Graz, Graz, Austria*

INTRODUCTION: Today fractures are primarily treated with titanium and stainless-steel implants. However, their high Young's modulus can cause stress shielding[1]. Often, they also require implant extraction surgeries. Bioabsorbable alternatives, such as magnesium (Mg) alloys, combine mechanical support with gradual absorption behavior. WE43 (MgYREZr) and ZX00, are already in clinical use, valued for their biocompatibility and mechanical properties. The physiologically relevant elements in ZX00[2] further support biocompatibility and osteogenic potential.
In this study, we investigate fracture healing in an osteotomy model in adult sheep fixated with either WE43 or ZX00 headless cannulated screws. By evaluating the fracture healing and osseointegration associated with both alloys, we aim to determine how both alloying systems perform and assess their potential as alternatives for fracture fixation.

METHODS: Twenty-four adult sheep underwent proximal tibial osteotomies, stabilized using either WE43 (d: 3.2 mm, l: 40mm) or ZX00 (d: 3.5 mm, l: 40 mm) screws (n = 2 per animal). The sheep were sacrificed at either 6 or 12 weeks (n = 6 animals per screw material and time point). For all animals, *ex vivo* µCT of excised tibiae was performed. For the 12-week group, healing was monitored via X-ray and clinical CT (cCT) at 3, 6, and 12 weeks (n = 4 animals per material). Additionally, histology was performed on all animals in which slides were prepared in two cut types: cross-sectional for evaluating fracture healing and longitudinal for overview of screw integration. For each cut, three slides were prepared.

RESULTS: *In vivo* cCT revealed comparable fracture healing progression in both groups (Figure 1). *Ex vivo* µCT images were qualitatively analyzed using a fracture healing score[3] (Figure 2). The fracture gap started to fill with woven bone by week 6. At 12 weeks, all animals achieved a grade of 3, except one WE43 animal scoring 2, showing prolonged healing. Histology demonstrated good implant integration for both alloys, with new bone in direct contact with implant surfaces or degradation layer. Fracture gaps were filled with woven bone, showing early bone remodeling processes toward the lamellar bone.

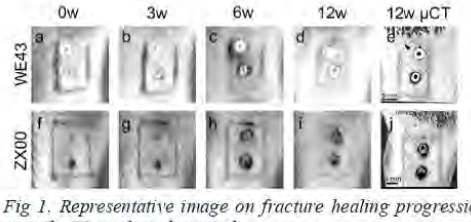

Fig 1. Representative image on fracture healing progression over the 12-week study period.

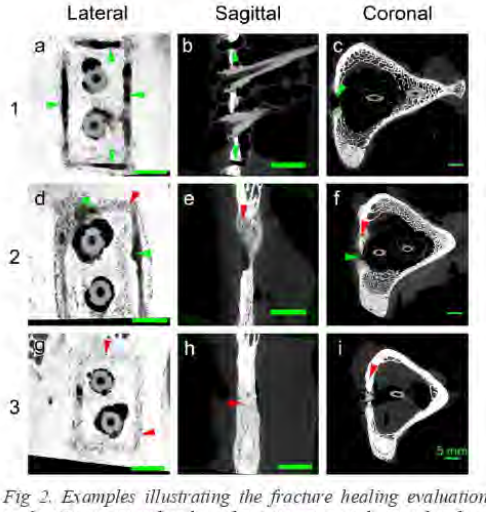

Fig 2. Examples illustrating the fracture healing evaluation scale. Green arrowheads = fracture gaps, red arrowheads = fully consolidated bone. 1 = no consolidation, 2 = incipient consolidation, and 3 = consolidation in all 3 planes.

DISCUSSION & CONCLUSIONS: Both WE43 and ZX00 supported effective fracture healing, as seen in cCT, µCT, and histology. Fracture gaps filled over time with woven bone, and lamellar remodeling was visible. The findings support the clinical viability of ZX00 and WE43 as bioabsorbable alternatives.

LIMITATIONS: Small sample sizes, different screw dimensions, qualitative analysis.

REFERENCES: [1]H. Weinans *et al.*, J. Biomech. 33(7):809–817, 2000. [2]B. Okutan *et al.*, Biomaterials Adv. 146:213287, 2023. [3]P. Holweg et al., Acta Biomater. 113:646–659, 2020.

ACKNOWLEDGEMENTS: This study was supported by Bioretec Ltd.

Posters

Wednesday,
August 27th, 2025

elecell
Hope for Healing

BioActiveMetals
Innovation in Metallic Biomaterials

meo.
Inspiring Materials.

medical magnesium

UNIVERSITÉ LAVAL

CHARITÉ
UNIVERSITÄTSMEDIZIN BERLIN

KeAi
CHINESE ROOTS GLOBAL IMPACT

PEKING UNIVERSITY

European Cells and Materials Vol. NN. Suppl. N, 20xx (page htu) ISSN 1473-2262

Comparison of silk fibroin and PEO coating on WE43 specimen

Marius Thiel[2], Ted Vaughan[1], Alexander Kopp[2], Benedetta Isella[2]

[1]University of Galway, Dept. of Biomedical Engineering Galway, Ireland, [2]Fibrothelium GmbH, Aachen, Germany

INTRODUCTION: Silk fibroin has emerged as a promising biopolymer for corrosion-inhibiting surface coatings, particularly relevant for biodegradable magnesium-based implants.[1] However, traditional aqueous silk fibroin solutions are not ideal for magnesium substrates like WE43 due to their inherent reactivity with water. The present study investigates the use of alternative solvents[2] and compares different deposition methods for applying silk fibroin coatings onto WE43 specimen. The silk fibroin coatings are compared against PEO surface modification.

METHODS: Silk fibroin was dissolved in three different solvent systems: firstly, an aqueous solution, secondly, 1-ethyl-3-methylimidazolium acetate (EMIMAc), and thirdly, a deep eutectic solvent (DES) composed of choline chloride and urea. The WE43 specimen were coated using two techniques: dip coating and electrodeposition (EPD). For the dip coating of EMIMAc and DES, specimens were immersed for 30 seconds, rinsed with ethanol, and this cycle was repeated three times. Electrodeposition in EMIMAc and DES was performed at 30 V, 0.05 A for 30 seconds, followed by ethanol rinsing. Electrodeposition in aqueous solution was conducted under the same electrical conditions and immersion duration. The surface of the specimen were modified via plasma electrolytic oxidation (PEO), which was used as a reference surface modification for the silk fibroin, to assess its performance in terms of corrosion inhibition. Following the coating/modification process, the specimens were analysed using a laser scanning microscope to assess surface roughness and a scanning electron microscope (SEM) to evaluate morphology. Additionally, the resistance of the coating under deformation of the samples was assessed qualitatively.

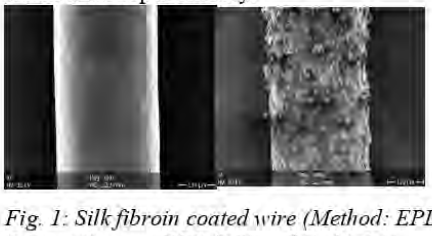

Fig. 1: Silk fibroin coated wire (Method: EPD; Solvent System: DES (left) and IL (right)).

Furthermore, a 3-day corrosion test in Simulated Body Fluid (SBF) was conducted to preliminarily assess coating stability and performance.

RESULTS: Silk fibroin coatings were successfully deposited using the here investigated methods. The application of coatings from DES and EMIMAc system resulted in an absence of uniform surface coverage. The most uniform layer was yielded by aqueous dip coating, while aqueous electrodeposition resulted in encapsulated bubble structures within the coating. The PEO modified specimen display a uniform porous layer.

DISCUSSION & CONCLUSIONS: The uniformity of coatings, particularly in EMIMAc and DES-based systems, is challenged by high solution viscosity, leading to accumulation and drip marks during retraction. Further analysis is required to quantify corrosion protection. Furthermore, tensile strength testing should be conducted in order to evaluate the influence of the coating method on the mechanical properties of the wires. Notwithstanding, the general methodology has been shown to be feasible for the application of silk fibroin coatings to WE43 specimen.

REFERENCES: [1] J. Hu, Z. Jiang, J. Zhang, und G. Yang, „Application of silk fibroin coatings for biomaterial surface modification: a silk road for biomedicine“, *J. Zhejiang Univ.-Sci. B*, Bd. 24, Nr. 11, S. 943–956, Nov. 2023, doi: 10.1631/jzus.B2300003.

[2] H.-Y. Wang, Zhang ,Yu-Qing, und Z.-G. and Wei, „Dissolution and processing of silk fibroin for materials science“, *Crit. Rev. Biotechnol.*, Bd. 41, Nr. 3, S. 406–424, Apr. 2021, doi: 10.1080/07388551.2020.1853030.

ACKNOWLEDGEMENTS: This project has received funding from the European Union's EU Framework Programme for Research and Innovation Europe Horizon
(Grant Agreement No 101120006).

This template was modified with kind permission from eCM Journal.

European Cells and Materials Vol. NN. Suppl. N, 20xx (page htu) ISSN 1473-2262

Controlling the corrosion rate of a WE43 biodegradable alloy by surface engineering

S Galea[1], L Fanton[1], J Buhagiar[1], DA Vella[1], B Mallia[1]

[1] *Department of Metallurgy & Materials Engineering, Faculty of Engineering University of Malta, Msida MSD 2080, Malta*

INTRODUCTION: Bone is the second most transplanted tissue worldwide, underscoring the clinical demand for effective solutions to repair skeletal defects [1]. Magnesium-based alloys offer a compelling alternative to permanent implants due to their mechanical compatibility with bone, biodegradability, and inherent biocompatibility [2]. However, their rapid corrosion in physiological environments hinders clinical use. This study investigates calcium phosphate chemical conversion treatments (CaP) and dual CaP–polylactic acid (PLA) coating system on WE43, with the aim of reducing the corrosion rate and ensuring sustained mechanical support during the tissue healing process in orthopaedic applications.

METHODS: The surface of extruded T5 WE43 coupons were subjected to chemical conversion by 1h immersion in a 40 mL bath containing 0.2mol/L phosphoric acid (H_3PO_4) 0.2mol/L calcium nitrate ($Ca(NO_3)_2$) and maintained at a set temperature of 70°C. Bath pH was adjusted to 3 using 3 molar sodium hydroxide (NaOH) solution. Biodegradable PLA having a molecular weight of 55k g/mol was solvent casted from a 5 wt.% solution in tetrahydrofuran. An ACEdip-coater was used to deposit a uniform film of PLA on the CaP layer.

Surface morphology was examined using a Zeiss optical microscope and a field emission scanning electron microscope (SEM), with elemental composition assessed via energy-dispersive X-ray spectroscopy (EDS). Crystalline phases were identified using a Rigaku Ultima IV X-ray diffractometer (XRD). Corrosion behavior was assessed in Hank's Balanced Salt Solution (HBSS) + Ca^{2+} at 37 ± 1°C using a potentiostat. Hydrogen evolution tests in HBSS + Ca^{2+} further investigate long-term degradation mechanisms.

RESULTS: The untreated WE43 surface exhibited a smooth, featureless morphology typical of mechanically polished magnesium alloys. Following the applied surface treatment, distinct microstructural differences were observed (Fig. 1). The CaP conversion layer revealed a densely packed, plate-like crystalline morphology. EDS analysis indicated that the crystalline features were composed of 51.5 at.% O, 25.2 at.% Ca, and 24.5 at.% Ca. XRD analysis confirmed the presence of brushite, calcium hydrogen phosphite, and monetite as the major crystalline phases. The CaP-PLA coating maintained the plate-like morphology, exhibiting a smoother, more homogenised appearance, with localised PLA accumulation causing partial surface levelling. EDS showed a composition of 49.8 at.% C, 24.1 at.% O, 14.5 at.% P, and 11.6 at.% Ca. This modified topography, suggests enhanced wettability and potential for improved interfacial integration with tissue.
Potentiodynamic polarisation tests showed that CaP and CaP-PLA reduced the initial corrosion rate. The CaP layer offered short-term protection, while PLA further delayed corrosion. Degradation increased over time as the coatings dissolved, with the rate influenced by the thickness of the layers.

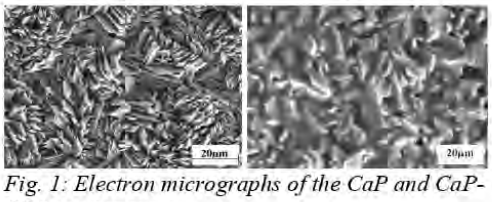

Fig. 1: Electron micrographs of the CaP and CaP-PLA coating system.

DISCUSSION & CONCLUSIONS: The porous, plate-like CaP layer created a high-surface-area layer conducive to anchoring, while the PLA coating exhibited good wettability and strong adhesion. The corrosion data showed a reduction in corrosion current density and an extended induction period prior to corrosion onset of the WE43 alloy. These findings support CaP–PLA coating system as an effective way to delay corrosion and preserve mechanical integrity for bone-contact applications.

REFERENCES: [1] H. Shegarfi and O. Reikeras (2019) *Review article: Bone transplantation and immune response*, Journal of Orthopaedic Surgery, vol. 17, no. 2. [2] J. Wang et al (2022) *Research progress of biodegradable magnesium-based biomedical materials*, Journal of Alloys and Compounds, vol. 923.

ACKNOWLEDGEMENTS: This template was modified with kind permission from eCM Journal. This work was supported through the ENDEAVOUR II Scholarship.

17th Biometal
25-30 AUGUST, 2025
Grand Hôtel San Michele,
Cetraro, CS, Italy

European Cells and Materials Vol. NN. Suppl. N, 20xx (page htu) ISSN 1473-2262

Impact of heat treatment on the degradation behaviour of electropolished WE43

J Kloiber[1,2], S Rieger[1], H Hornberger[1,2]

[1] Biomaterials Laboratory, Faculty of Mechanical Engineering, Ostbayerische Technische Hochschule (OTH) Regensburg, Regensburg, Germany. [2] Regensburg Center of Biomedical Engineering (RCBE), Ostbayerische Technische Hochschule (OTH) Regensburg and University of Regensburg, Regensburg, Germany.

INTRODUCTION: By using specific selected rare earths metals, the Mg-alloy WE43 is of great interest for biodegradable implants. However, Mg-based material carry the risk of inhomogeneous degradation [1]. Electropolishing has developed into a promising surface treatment for Mg materials [2], but local property changes in the microstructure limit the quality level of electropolished surfaces which can be decisive for subsequent corrosion processes. The aim of the study was to investigate the degradation of electropolished WE43 with (1) coarse, (2) dissolved and (3) finely dispersed precipitates to obtain a correlation of bulk heat treatment and corrosion behaviour after electropolishing for this bioresorbable metal.

METHODS: WE43 discs (Y 4.8 wt.%, Nd 2.1 wt.% and Zr 0.1 wt.%) with a surface area of 1 cm² were used as working material. The samples were first solution annealed (T4) at 540°C for 4h. Half of them were then immediately aged (T6) at 300°C for 1h (Fig. 1a). Electropolishing was carried out at 21°C in a mixture of phosphoric acid, ethanol and deionized water in a ratio of 40:56:4 at a voltage of 2 V up to 18C [3] (Fig. 1b). The degradation behaviour was investigated by potentiodynamic polarization using the electrolyte Dulbecco's Modified Eagle's Medium (DMEM). The corroded surface areas were observed using a confocal laser scanning microscope (CLSM) and a scanning electron microscope (SEM).

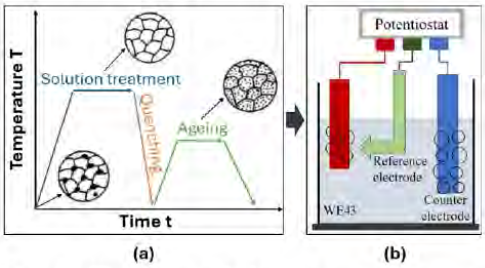

Fig. 1: Illustration of the processing steps on WE43 which consists of a combination of (a) heat treatment processes and (b) an electropolishing process for Mg materials.

RESULTS: The electrochemical surface treatment led to a significant reduction in the corrosion rate (< 0.1 mm/year). The lowest degradation rates of electropolished WE43 were found in the initial and T6 condition. However, the solution annealed and aged alloy showed a less attacked surface in DMEM and the most homogeneous corrosion morphology (Fig. 2). The needle-shaped precipitates after T6 led to uniform material removal during electropolishing and thus contributed corrosion resistance, while the coarse secondary phases in the initial state caused irregularities on the electropolished surface.

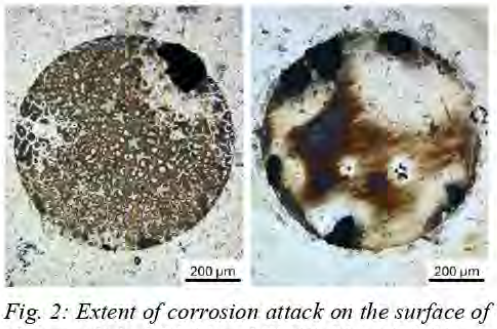

Fig. 2: Extent of corrosion attack on the surface of electropolished WE43 and WE43-T4 in DMEM.

DISCUSSION & CONCLUSIONS: The best relation of moderate corrosion rate and regular corrosion morphology was found with finely precipitated, electropolished WE43. The electrochemical results confirmed that the microstructure plays an important role for subsequent electropolishing, suggesting that the corrosion behaviour of electropolished surfaces can be modified via heat treatment by changing the amount and size of precipitates.

REFERENCES: [1] A.H. Martinez Sanchez (2015) *Acta. Biomater.* **13**:16-31. [2] J. Kloiber et al. (2024) *Mater. Today Commun.* **38**:107983. [3] J. Kloiber et al. (2025) *Electrochim. Acta* **513**:145547.

ACKNOWLEDGEMENTS: We gratefully thank Regensburg Center of Biomedical Engineering (RCBE) for the support of laboratory consumables.

European Cells and Materials Vol. NN. Suppl. N, 20xx (page htu) ISSN 1473-2262

Improving the functionality of polyelectrolyte oxide coatings by incorporation of nanoparticles

Katharina Lammers[1], Heike Helmholz[1], Carsten Blawert[2], Maria Serdechnova[2], Regine Willumeit-Römer[1], Berit Zeler-Plumhoff[1,2], DCF Wieland[1]

[1] *Institute of Metallic Biomaterials, Helmholtz-Zentrum Hereon, Germany,* [2] *Institute of Surface Science, Helmholtz-Zentrum Hereon, Germany,*[3] Data-driven Analysis and Design of Materials, Fakultät für Maschinenbau und Schiffstechnik, Universität Rostock

INTRODUCTION: Different coatings have proven their versatility in reducing the degradation of magnesium, along with high biocompatibility. One important class are plasma electrolytic oxidation coatings, which yield remarkable resistance against wear and reduced degradation.[1] These coatings can be further modified by incorporating nanoparticles, opening a further route for surface modification by providing an active component. We have explored the possibility of incorporating three different nanoparticles: calcium phosphate, silver, and gadolinium oxide, as these nanoparticles could either promote bone formation or introduce antibacterial properties. The degradation properties of those layers' and their cell compatibility were investigated.

METHODS: Magnesium samples in the shape of discs were prepared and subjected to the PEO coating process. The electrolyte solution contained 10 g/L Na_3PO_4 (trisodium phosphate), 2 g/L KOH (potassium hydroxide), and 5 g/L of the chosen nanoparticles. Four different electrolytes were used, each containing one of the three different nanoparticles and one electrolyte solution without nanoparticles as a reference. The samples were subjected to degradation experiments in DMEM for two weeks, and cell compatibility was tested by cultivating human umbilical cord perivascular (HUCPV) cells on the surface and investigating cell viability. During the degradation and cell tests, the pH value and ion concentrations were determined. Furthermore, SEM investigations to examine the microstructure along with EDX mapping were performed to analyze the element distribution along with the PEO structure.

RESULTS: The distribution of the nanoparticles was not homogeneous, and some clustering could be observed. Figure 1 shows this exemplary for the Gd distribution. The coating properties, such as pore size and PEO layer thickness, were comparable, yielding the same values for both nanoparticle samples and the reference, as well as the degradation properties.

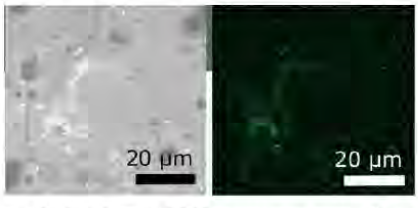

Figure 2 *SEM and EDX measurements of a PEO coating with Gd NP. Left: SEM. Right: Gd distribution*

The cell compatibility experiments showed a viability rate of over 97% on all four coatings, indicating that these modified PEO coatings exhibit no cytotoxic effect on HUCPV cells.

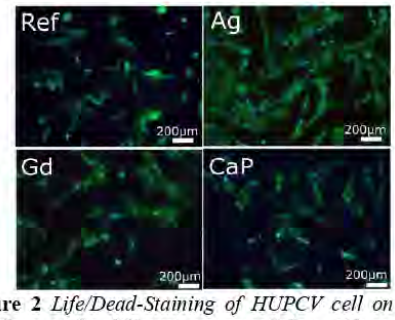

Figure 2 *Life/Dead-Staining of HUPCV cell on PEO interface with different nanoparticles: Silver (Ag), Gadolinium (Gd), Calciumphosphate (CaP) and without additives (Ref) (green Calcein-AM vital, blue - DAPI nucleus)*

DISCUSSION & CONCLUSION: In summary, we demonstrated that the PEO-nanoparticles coating did not influence the PEO formation process. Furthermore, the coating with NP showed the degradation behaviour and cell compatibility as the reference and, thus, no negative impact.

REFERENCES: [1] Blawert et al., Anodizing Treatments for Magnesium Alloys and Their Effect on Corrosion Resistance, ADVANCED ENGINEERING MATERIALS 2006, 8, No. 6, [2] Francesca Cecchinato et al., *Influence of Magnesium Alloy Degradation on Undifferentiated Human Cell*, 23rd November 2015, PLOS ONE

In situ monitoring of corrosion in Resoloy with isothermal calorimetry

P Maier[1,2], B Clausius[1], L Wadsö[2], D Orlov[2]
[1]*University of Applied Sciences Stralsund, School of Mechanical Engineering, Stralsund, Germany,*
[2]*Lund University, Faculty of Engineering, Lund, Sweden*

INTRODUCTION: The effects of Dy content in Resoloy, a Mg-Dy based alloy being developed for bio-resorbable vascular implants[1], is the focus of this study. Isothermal calorimetry is used for *in situ* monitoring of corrosion rate (CR) by heat production and enthalpy during corrosion in correlation with pressure changes, and offers an attractive way to study the kinetics of Mg degradation[2]. Former studies showed nicely that isothermal calorimetry reveals new insights in the time-dependent kinetics during Mg corrosion under the influence of alloying elements and corrosion environment[3-5].

METHODS: The CR of cylindrical samples of extruded Resoloy (5 mm in diameter and 10 mm in height, with 5 and 10 wt. % Dy) is evaluated by performing isothermal calorimetry and collecting hydrogen gas for up to 24 h during immersion in 17 ml Ringer solution at 37°C. This CR was compared with immersion (gravimetric method) in 330 ml for an exposure time of up to 168 h.

RESULTS and DISCUSSION: Fig. 1 shows micrographs of Resoloy with 5 and 10 wt.% Dy. The grain sizes have similar values, 8.7 ± 4.5 µm for 5 wt. % Dy and 11.3 ± 6.3 µm for 10 wt. % Dy. The higher Dy content leads to a higher volume fraction of block LPSO phases aligned in extrusion direction, see here Fig. 1b. The CR determined by immersion over 7 days shows, in agreement with [6], that 5 wt. % of Dy leads to a higher CR than 10 wt.% (2.86 ± 0.39 mm/a and 1.51 ± 0.03 mm/a).

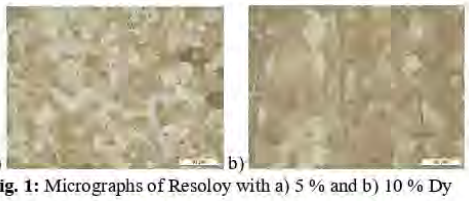

a) b)

Fig. 1: Micrographs of Resoloy with a) 5 % and b) 10 % Dy

Fig. 2a shows that the CR from isothermal calorimetry at 5 wt.% Dy (4.64 ± 0.61 mm/a) also is higher than for 10 wt.% Dy (2.24 ± 0.27 mm/a). The absolute values of CR are somewhat overestimated compared to the other reports due to the lower amount of electrolyte and the method used, but a ratio of 1:2 is preserved. Lower CR leads to a decrease in thermal power, Fig. 2b, so less heat is released during dissolution. The enthalpy values at 24 h, see Fig. 2c, are higher for 10 wt. % Dy. However, there is no clear trend compared to 5 wt. %. Since the corrosion of pure Mg results in ~ 350 kJ/mol in 0.9% NaCl[2], higher enthalpy in Mg-Dy alloys is possibly caused by the corrosion of rare-earth element and more complex electrolyte. Interesting for 10 wt.% Dy are the time intervals in which the enthalpy increases with a similar slope. Dy is beside uniformly distributed and enriched in the corrosion layer, concentrated in the block LPSO phases[7,8]. The resulting micro-galvanic coupling regions, where the LPSO phases are acting as a cathode, pushing the corrosion layer formation gradually, reducing CR and increasing enthalpy. Corrosion products, forming a rather uniform layer[9], consist mainly of Ca, P, O and Dy. Further research will focus on the reaction kinetics of individual oxide and hydroxide formation.

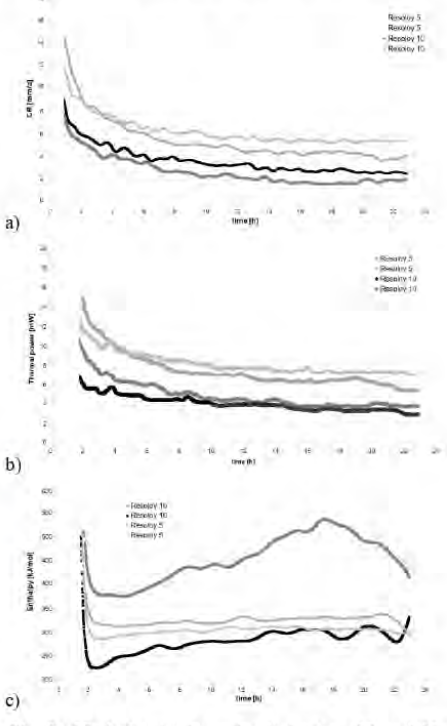

a) b) c)

Fig. 2: *CR during isothermal calorimetry of 5 and 10 wt. % Dy alloying, b) the thermal power curves and c) the enthalpy.*

REFERENCES: [1]Menze and Wittchow (2021) *J Biomed. Mater. Research*, 109, 9, 1292-1302. [2]Wadsö and Orlov (2018) *Magnesium Technology 2018*. 31-36. [3]Singh et al. (2021) *J Alloys and Compounds*, 882, 160659 [4]P. Maier et al. (2024) *Magnesium Technology 2024*. 35-39. [5]D. Orlov et al. (2022) *Magnesium Technology 2022*, 253-54. [6]Yang et al (2011) *Mater. Sci. Eng. B*, 690, 417-421. [7]Xue et al. (2021) *Adv. Eng. Mater.*, 23, 4, 2001278. [8]Maier et al. (2020) *JOM*, 72, 1870-1879. [9]Menze et al. (2024) *Bioactive Materials*, 32, 1-11.

European Cells and Materials Vol. NN. Suppl. N, 20xx (page htu) ISSN 1473-2262

In vitro degradation behavior of composite MAO/sol gel coated Mg-1.6Zn-0.5Ca-0.5Mn alloy

S Dutta[1], LH Olivas-Alanis[1,2], G Krieger[1], A Luo[1], D Dean[1,3]

[1] Materials Science and Engineering, The Ohio State University, Columbus, OH, US. [2] School of Engineering and Sciences, Tecnologico de Monterrey, Monterrey, MX. [3] Plastic and Reconstructive Surgery, The Ohio State University, Columbus, OH, US.

INTRODUCTION: Several magnesium (Mg)-based alloys are promising degradable bone implant materials due to their biocompatibility, strength, and low Young's modulus.[1] Resorbable implants have the benefit of facilitating healing and then, unlike permanent implants, removing all risk of interrupting normal function of the healed tissue. However, unless well-timed, Mg alloys may degrade before the healing process is complete. Degradable surface coatings may delay the underlying Mg alloy from degrading until it is no longer needed. Thus, key design criteria for coatings include controlled degradation rates providing a "time-certain" start to the Mg alloy component's degradation. Among the inorganic, organic, and hybrid coatings that have been studied, calcium phosphate (CaP) coatings have been studied because of their chemical similarity to natural bone. CaP coating may also enhance implant integration with surrounding tissue. We evaluated the *in vitro* degradation behavior of Ca-P coatings on heat-treated Mg-1.6Zn-0.5Ca-0.5Mn (OSU Mg alloy) in simulated body fluid (SBF).

METHODS: Rectangular cuboid samples (6 mm x 4.5 mm x 4 mm) were machined from a heat-treated OSU Mg alloy plate using an Electric discharge machine (EDM). The samples were polished with a graded series of sandpaper up to a 1200 grit and then cleaned with ethanol. Next, Micro Arc Oxidation (MAO) was performed in a phosphate electrolyte at 50 mA/cm² for 15 minutes. Subsequently, the samples were coated with a sol gel sealing layer of TiO_2 and entrapped HAP/β-TCP nanoparticles. Three different coating thicknesses were applied: 15, 25, and 50 layers. In vitro degradation was evaluated in SBF at 37°C for 7 and 14 days via hydrogen evolution. Hydrogen evolution was observed using a funnel burette. Sample weight was recorded before and after immersion. The corrosion rate in Millimeters Per Year (MMPY), based on hydrogen evolution data, was calculated via: $2.279*V_h$ (V_h = ml/cm²/d).[2]

RESULTS: Fig. 1(a) shows the corrosion rate of OSU Mg alloy with various coating layers. During the initial immersion period (up to 16 hours), no hydrogen evolution was observed, regardless of the coating type. However, after 24 hours, hydrogen evolution became evident and increased over time. The lowest corrosion rate (0.80 ± 0.09 MMPY) was observed for the 50-layer coating after 14 days of immersion. Additionally, the mass loss measurements correlated well with the corrosion rate determined from the hydrogen evolution test, as shown in Figure 1(b).

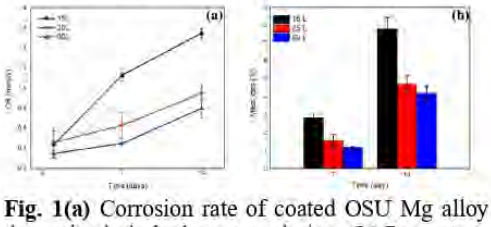

Fig. 1(a) Corrosion rate of coated OSU Mg alloy determined via hydrogen evolution. **(b)** Percentage of mass loss evaluated from weight loss method.

DISCUSSION & CONCLUSIONS:
CAP coating thickness significantly influences the degradation behavior of Mg alloys. Increasing the CaP coating delays the degradation of the underlying OSU Mg alloy device. Determining the optimal coating thickness is essential to preventing the underlying OSU Mg alloy device from the loss of mechanical strength during the healing period. It would be useful to explore whether coatings greater than 50 layers will ensure adequate protection (e.g., 2 months). A time-certain, sufficiently delayed start to degradation of the OSU Mg alloy component may facilitate successful clinical application of this technology.

REFERENCES:

[1] M. P. Staiger, A. M. Pietak, J. Huadmai, G. Dias, *Biomaterials* 2006, *27*, 1728.
[2] W. Zhao, J. Wang, J. Weiyang, B. Qiao, Y. Wang, Y. Li, D. Jiang, *Journal of Magnesium and Alloys* 2020, *8*, 374.

ACKNOWLEDGEMENTS: This research was, in part, funded by the Advanced Research Projects Agency for Health (ARPA-H). The views and conclusions contained in this document are those of the authors and should not be interpreted as representing the official policies, either expressed or implied, of the United States Government.

Magnetically assisted corrosion of a novel LPBF-manufactured Fe20Mn0.5C alloy in simulated physiological conditions

I. Limón[1], D. Valdés[1,2], M. Multigner[1], M. Lieblich[3], C. Paternoster[4], D. Mantovani[4], B. Torres[1,2], J. Rams[1,2]

[1] *Dpto Ciencia e Ingeniería de Materiales, ESCET, Universidad Rey Juan Carlos, c/Tulipán s/n, Móstoles, Madrid 28933, Spain;* [2] *Inst. de Inv. en Tecnologías para la Sostenibilidad, ITPS, Universidad Rey Juan Carlos, Madrid 28933, Spain;* [3] *CENIM-CSIC, Avda. Gregorio del Amo 8, 28040 Madrid, Spain;* [4] *Laboratory for Biomaterials and Bioengineering, CRC-I, Dept Min-Met-Materials Eng. & CHU de Quebec Research Center, Regenerative Medicine, Laval University, Canada*

INTRODUCTION: Iron-based alloys are promising for temporary biomedical applications due to their biocompatibility and mechanical properties, but their degradation rate is often too slow. Strategies such as alloying, surface treatments, and external stimuli have been explored to enhance corrosion [1]. This study evaluates the degradation of a novel Fe20Mn0.5C alloy, produced by Laser Powder Bed Fusion (LPBF), and the potential of magnetic stimulation. The effect of low-intensity continuous (H_{DC}) and alternate (H_{AC}) magnetic fields, on alloy degradation was studied in modified Hanks' solution at 37 °C.

METHODS: Austenitic Fe20Mn0.5C samples with paramagnetic behavior were obtained by LPBF using optimized parameters (60 µm layer thickness, 200 W power, 540 mm/s scan speed), achieving ~98% relative density. Rectangular specimens (14×7×3 mm) were polished subjected to static corrosion tests for up to 14 days at 37 °C in modified Hanks' solution (pH 7.4). Three conditions were evaluated: exposure to H_{DC} and H_{AC} magnetic fields (14 mT), and with no field (control), each in triplicate. Corrosion was assessed via thickness loss, and surfaces and corrosion products were characterized using profilometry, SEM, FTIR, XRD, and ICP analysis.

RESULTS: The Fe-20Mn-0.5C alloy exhibited increased degradation under magnetic stimulation, with corrosion rates rising by ~30% under H_{AC} and ~50% under H_{DC} fields compared to the control (Fig. 1a) and with the majority presence of Mn ions in the dissolution (Fig. 1b). The corrosion products formed in the presence of magnetic fields formed thicker layers, but did not provide effective protection against further degradation. Dimensional metrology measurements offered more reliable insight into the corrosion rate than gravimetric analysis alone, due to the influence of adherent corrosion layers on mass-loss measurements.

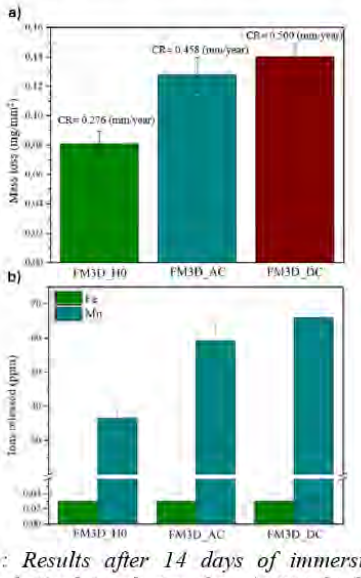

Fig. 1: Results after 14 days of immersion in modified Hanks' solution for a) Weight loss of Fe20Mn0.5C and b) Fe and Mn ions released.

DISCUSSION & CONCLUSIONS: Even without magnetic stimulation, Fe-20Mn-0.5C corroded more than twice as fast as LPBF pure Fe. The application of low-intensity H_{DC} and H_{AC} magnetic fields further increased its degradation rate. Although magnetic exposure promoted the formation of thicker corrosion layers, these did not offer effective protection. These results suggest that magnetic fields enhance electrochemical activity at the alloy–solution interface, accelerating degradation. This highlights their potential to modulate the corrosion behavior of bioresorbable iron-based alloys, even in paramagnetic systems.

REFERENCES:[1] *I. Limón, M. Multigner, C. Paternoster, et al (2024), Bioact Mater 40:524–540.*

ACKNOWLEDGEMENTS:

Grant PID2021-123891OB-I00 funded by MCIN/AEI/https://doi.org/10.13039/501100011033 and grant PEJ-2023-AI/TEC28287 funded by Comunidad deMadrid.

European Cells and Materials Vol. NN. Suppl. N, 20xx (page htu) ISSN 1473-2262

Modulating ZnO thin film structure, stoichiometry, and corrosion resistance through oxygen-to-argon ratio in reactive sputtering

CG Hynes[1], CHM Beraldo[1], C Paternoster[1], A Sarkissian[2], D Mantovani[1]

[1] *Laboratory for Biomaterials and Bioengineering (CRC-Tier 1), Dept. Min-Met Materials Eng, & Regenerative Medicine, CHU de Quebec, Laval University, & Plasmionique, Varennes, Canada*

INTRODUCTION: Zinc (Zn) and its oxides' (ZnO) inherent biodegradability and overall properties make them a promising material for biomedical applications. Reactive magnetron sputtering (RMS) is a versatile deposition technique that enables precise control over film composition and microstructure.[2] RMS allows for modulation of the plasma gas composition, which can significantly influence the resulting film properties.[3] It is hypothesised that controlled modulation of the reactive gas ratio can influence film structure, degradation behaviour, and Zn ion release. Understanding these relationships will provide a foundation for optimising Zn-based coatings for biomedical surfaces and future multi-component thin film systems.

METHODS: ZnO thin films were deposited via RMS on Si wafers, under varying argon-to-oxygen ($Ar:O_2$) ratios. Three sample groups were produced: (1) ZnO from a ZnO target, (2) ZnO from a Zn target with alternating $Ar:O_2$ flow (2s:32s), and (3) ZnO from a Zn target with alternating $Ar:O_2$ flow (2s:8s). Deposition was conducted at 100 W and a chamber pressure of 10 and 15 mTorr for Ar and O_2 respectively. Thickness was controlled by deposition time to 80–120 nm. X-ray photoelectron spectroscopy (XPS) and atomic force microscopy (AFM) were employed to assess stoichiometry and surface morphology. Corrosion of the films was assessed via electrochemical tests.

RESULTS: Electrochemical analysis revealed a stepwise increase in corrosion current density (I_{corr}) from condition 1 to 2 to 3 (Fig. 1), this was consistent with the observed increase in surface roughness (Table 1), which elevates the electrochemically active area. From XPS analysis (Table 1), surface oxygen vacancies (Vo) and hydroxide species (-OH) are relevant features influencing corrosion mechanisms by acting as reactive sites and modifying surface wettability, respectively. However, a lack of direct correlation between the proportions of these and the I_{corr} values suggests a more intricate relationship between surface chemistry and electrochemical degradation.

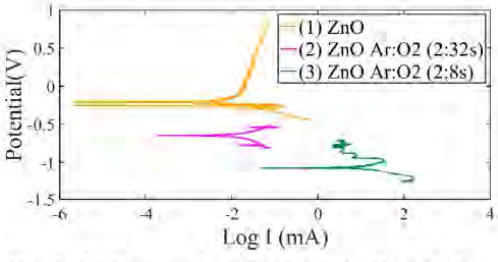

Fig. 1: PDP curves for conditions (1), (2) and (3).

Table 1. Corrosion potential, surface roughness and stoichiometry ratios of ZnO films

ZnO Film	Icorr (mA)	Roughness (Ra) (nm)	XPS normalised at% of O1S curve		
			ZnO	Vo	-OH
(1)	$5.76x10^{-8}$	1.67	50.1	13.9	7.09
(2)	$1.42x10^{-5}$	4.46	43.3	8.4	18.2
(3)	$1.97x10^{-2}$	5.11	66.2	10.6	2.6

DISCUSSION & CONCLUSIONS: This preliminary analysis compares the properties of conventional RF sputtering- and RMS-deposited ZnO. RMS significantly altered the corrosion rate compared to the ZnO target condition, with lower O_2 ratios increasing I_{corr}. Film roughness was also influenced by the O_2 pulse ratio, where the ZnO target yielded a smoother morphology. T. Angkuratipakorn et al.[3] reported the introduction of O_2 pulsed timing forced the growth along differing crystallographic planes as indicated by x-ray diffraction (XRD) data; further analysis of these film structures may offer insight into the observed corrosion behaviour. Through optimisation of the deposition process to control inherent film characteristics produced via reactive sputtering, these ZnO coatings hold promise for tailored performance in various biomedical applications.

REFERENCES: **1.** Wang et al. J Nanobiotech. (2021) 19:353 **2.** Y. Deng, et al. Ceram. Int. 46 (2020) 18373–18390 **3.** T. Angkuratipakorn et al. Ceram. Int. 49 (2023) 19102–19108

AKNOWLEDGEMENTS: This research was partially supported by the Fonds de Recherche du Québec (Strategia), the Natural Science and Engineering Research Council of Canada, Prima Quebec, and the CHU de Quebec Research Centre.

European Cells and Materials Vol. NN. Suppl. N, 20xx (page htu) ISSN 1473-2262

Uneven corrosion analysis via X-ray microtomography

I Ročňáková, M Horynová, T Zikmund, L Klakurková, L Čelko, J Kaiser, EB Montufar

Central European Institute of Technology, Brno University of Technology, Brno, Czech Republic

INTRODUCTION: Biodegradable magnesium (Mg) alloys are promising materials for temporary orthopaedic implants due to their biocompatibility and bone-like mechanical properties. However, heterogeneities in microstructural features induce uneven corrosion that pose significant challenges. Traditional methods like mass loss, gas evolution, or electrochemical tests lack precision in evaluating localized corrosion. X-ray computed micro-tomography (µCT) offers high-resolution 3D imaging that can non-destructively quantify spatial corrosion patterns [1-3]. The aim of this study was to evaluate µCT's capacity to assess uneven corrosion in Mg under simulated physiological conditions and compare it to traditional methods.

METHODS: Commercially pure (99.9%) extruded Mg discs with unpolished edge surface were immersed in either 0.9% NaCl or Hank's solution at 37 °C for up to eight weeks. µCT was used to evaluate volume loss, surface area, and spatial corrosion patterns. Regions of interest (ROIs) were defined for top/bottom surfaces and edges to assess independently the corrosion behavior. Complementary techniques included gravimetric analysis, SEM, XRD, ICP-OES, and potentiodynamic polarization.

RESULTS: The Mg discs exhibited an equiaxial grain microstructure with variable twin densities. Twinning was most concentrated at the edges (Fig. 1), which contributed to microstructural inhomogeneity. The µCT results showed more severe and localized corrosion at the edge surfaces of Mg discs compared to the top/bottom surfaces (Fig. 1), particularly in NaCl. SEM revealed plate-like microporous solid corrosion products, with XRD identifying $Mg(OH)_2$ in both media, and carbonates forming only in Hank's solution. These carbonates contributed to reduced corrosion in Hank's solution. µCT and gravimetric results were in good agreement, though polarization tests yielded higher average corrosion rates.

DISCUSSION & CONCLUSIONS: The results demonstrate that µCT is a robust, quantitative, and non-destructive technique for assessing uneven corrosion of Mg. It outperforms conventional methods in detecting spatial degradation heterogeneity, especially at edge surfaces with high twin density. Traditional gravimetric and electrochemical methods provide average degradation rates but overlook the spatial distribution of corrosion. µCT enables visualization of degradation and quantification of surface-to-volume ratio changes, distinguishing between surface zones with different corrosion mechanisms, thus identifying high-risk degradation zones influenced by microstructure, and capturing morphological differences, such as deeper pits and irregular corrosion product thicknesses.

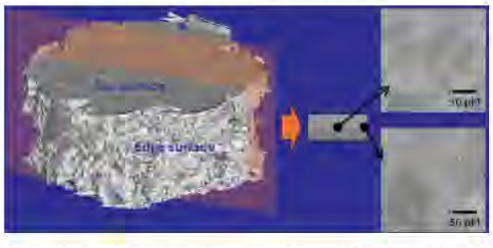

Fig. 1: µCT reconstruction of a Mg disc after 4 weeks of degradation in Hank's solution, with corrosion products virtually removed. Insets show the microstructure at the disc center and near the edge surface.

Uneven corrosion correlated strongly with higher twin density and unpolished surface conditions. The formation of carbonates in Hank's solution had a protective effect, while $MgCl_2$ formation in NaCl accelerated corrosion. The findings underscore the significance of microstructure and medium composition in determining corrosion behaviour.

Despite its strengths, µCT cannot resolve submicron features or provide mechanistic insights into electrochemical processes. Thus, it should be combined with SEM, XRD, and electrochemical tests for a comprehensive understanding.

REFERENCES: [1] I. Ročňáková, et al (2016) *Corrosion Science* **104**: 187-96. [2] G. Tian, et al (2024) *Corrosion Science* **229**: 111848. [3] W. Fu, et al (2023) *Journal of Magnesium and Alloys* **11**: 3214-3230.

ACKNOWLEDGEMENTS: This work was supported by the Horizon Europe European Innovation Council (101186758) and the Czech Science Foundation (GA23-07879S).

European Cells and Materials Vol. NN. Suppl. N, 20xx (page htu)
ISSN 1473-2262

Localized accelerated degradation of magnesium: A new insight into the mechanism of its biomedical degradation

Y Zhang[1, 2], YD Huang[1], J Bai[2, 3], N Hort[1]

[1] *Institute of Metallic Biomaterials, Helmholtz-Zentrum Hereon, Geesthacht, DE.* [2] *School of Materials Science and Engineering, Southeast University, Nanjing, CHN.* [3] *Institute of Biomedical devices, Southeast University, Suzhou, CHN.*

INTRODUCTION: A distinctive phenomenon involving the localized accelerated degradation of magnesium (Mg) can be traced numerous times on bone fixation devices *in vivo*, as well as on Mg tubes and porous Mg *in vitro*. It caused Mg to degrade several times to even a dozen times faster. The present investigation reproduced this phenomenon using the Mg tubes in artificial blood plasma (ABP) and explored its occurrence mechanism. We proposed a new insight into the mechanism of Mg degradation and emphasized the importance of considering the relevant factors leading to such a phenomenon in future Mg applications.

METHODS: Mg-4Zn (96 wt.% Mg, 4 wt.% Zn) tubes with a wall thickness of 0.15 mm and a length of 10 mm were used in this study. The sheets and half tubes were fabricated from a tube by mechanically flattening and cutting the intact tube in half longitudinally, respectively. Their degradation behaviors in ABP solution at (37.5 ± 0.5) °C were investigated through a combination of the hydrodynamic platform, real-time electrochemical detection, COMSOL simulation, and morphological observations. The chemical composition of the degradation products on the surface was determined by EDX, XRD, XPS and FTIR. The release of Mg^{2+} was detected by ICP. Hydra-Medusa software was used to calculate the possible formation of precipitations in the chemical system of ABP.

RESULTS: The degradation rate of the Mg-4Zn tube is nearly four times higher than that of the same material in sheet form after static immersion in ABP for 14 h (Fig. 1). Further investigations show that the hydrodynamic condition leads to a decrease in the degradation rate of intact tubes compared to the static condition, while its effect on half tubes is adverse. The solution pH value inside the intact tube is significantly higher than that outside the tube. Moreover, when the pH value of ABP exceeds 8.6, the corrosion resistance of Mg-4Zn declines sharply, coinciding with a reduction in the concentration of Ca^{2+} and PO_4^{3+} and the appearance of insoluble precipitates.

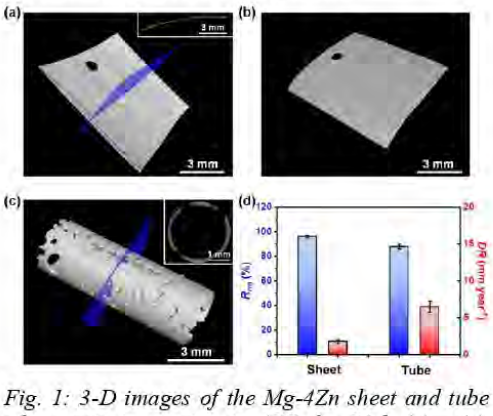

Fig. 1: 3-D images of the Mg-4Zn sheet and tube after static immersion in ABP for 14 h (a) - (c), and the corresponding mass loss data (d).

DISCUSSION & CONCLUSIONS: The degradation rate of Mg-4Zn tubes decreases with the increase of FISS values initially, followed by an increase when the FISS value is greater than 0.96 Pa. In contrast, the degradation rate of Mg-4Zn half tubes increase as the FISS value increases. The deficiency of Ca^{2+} and PO_4^{3+} in the static solution with a relatively enclosed environment, which is induced by the excessively high pH value, results in an inhomogeneous distribution of the Ca-P-rich precipitates on the surface. These resultant degradation products hardly provide effective protection for the magnesium matrix. This is the fundamental reason for such a localized accelerated degradation.

REFERENCES: [1]Y. Zhang, K. Yan, W. Xu, et al (2024) *Corros Sci* **237**:112335.

ACKNOWLEDGEMENTS: This work was supported by the Sino-German program for the award of fellowship and funding (202206095009, 91870848), the Science and Technology Project of Jiangsu Province (BE2023719).

European Cells and Materials Vol. NN. Suppl. N, 20xx (page htu) ISSN 1473-2262

Surface stabilization of partially bioresorbable Ti-Mg dental implant.

M Balog[1], A M H Ibrahim[1], M Takacova[2], F M Seabra[1], J Lapinova[2], M M de Castro[3], J Skiba[4]
[1]Institute of Materials and Machine Mechanics, SAS, Slovakia. [2]Biomedical Research Center, Institute of Virology, SAS, Slovakia. [3]Centre for advanced materials application, SAS, Slovakia. [4]Institute of High Pressure Physics, PAS, Poland.

INTRODUCTION: Although Ti-based dental implants (DI) show good clinical performance, there are two issues that have not been fully addressed yet: i) the insufficient bioactivity of DI with surrounding bone in as-processed condition and ii) the stress-shielding effect of implant over underlying bone structure [1]. We introduced a novel Ti-17vol%Mg composite tailored for CNC fabrication of DI [2-4], which reduces the drawbacks of the established Ti-based DI. The metal-metal composite selectively exploits the advantages of both biometals. While a permanent Ti serves as the matrix material providing the implant with requested mechanical properties, a bioresorbable Mg component acts as a beneficiary modulator for generating an osseoconductive surface via spontaneous dilution in the body environment, as well as a bone formation stimulant. In addition to its very good biodegradation potential, Mg has a Young's modulus (E) much lower than that of Ti and it gives rise to a reduction of the stress-shielding effect upon loading. Owing to the porosity, which forms with time as a result of the selective Mg dilution from the surface and the volume of the implant, the E of Ti-Mg is further decreased and the osseointegration and bonding strength at the bone–implant's interface improves further. The Ti-17vol%Mg maintains the mechanical performance and fatigue endurance, which complies with the minimum values specified for the Type 4 biomedical material (ISO 22674) with the advantage of the reduced E. The mechanical performance of the corroded DI CNC machined from the 17vol%Mg composite complied with ISO14801 for the fatigue testing of endosseous DI.

METHODS: Raw Ti17vol%Mg material rods were produced from a plasma atomized TiGR1 and a gas atomized Mg99.8wt.% powders by a powder metallurgy hydro-extrusion. DI with an integrated design was CNC machined from the raw material. The corrosion rate (CR) of Mg from the surface of the DI was evaluated by H_2 evolution volumetric method (ASTM G31–72). The biocompatibility of the as-machined and pre-washed (in HBSS) DI was evaluated via an indirect contact cytotoxicity colorimetric MTT assay (ISO10993-5). Additionally, cell proliferation and adhesion were studied by the cell impedance-based xCELLigence system and cell stress was accessed with a Proteome Profiler antibody array kit. The L929 cell line was used for the MTT and xCELLigence assays. For the cell stress assay, the Saos-2 cell line was chosen. The reference TiGR4 DI with the sand blasted and HNO_3+HF-soaked surface were used for a comparison.

RESULTS&DISCUSSION&CONCLUSIONS:

The question arising from the *in-vitro* testing results is whether the impractical pre-washing procedure in HBSS, applied to reduce initial intense initial H_2 evolution during the immersion corrosion tests, is really necessary for the following *in-vivo* step and, ultimately, for a final product. The MTT assay showed a clear toxic behaviour for the as-machined DI, indicating the pre-washing procedure was necessary. Yet, the toxic effect of the as-machined DI was reduced as the incubation time increased. In contrast, the cell impedance and cell stress assays showed a non-toxic response and little difference between the as-machined and prewashed DI. The contradictory results may be explained by the different principles of the assays. This way, it is possible for the early-stage pronounced CR to have noticeable effects on cell metabolic activity, while allowing the cells to proliferate normally and without inducing a stress response. However, from these *in-vitro* data, it is definitely possible to conclude that, with a prewashing treatment no undesirable behaviour should be expected from the DI implantation. Though, assuming the site of implantation of DI and the variations of the actual and simulated physiological conditions, an acceptable biological response *in-vivo* of the as-machined DI is likely.

REFERENCES: [1] C Sotova et al. (2023) *Materials* **16**: 7383. [2] M Balog et al. (2019) *J. Mech. Behav. Biomed. Mater.* **90**: 45. [3] A M H Ibrahim et al. (2020) *J. All. Compd.* **839**: 155663. [4] A M H Ibrahim et al. (2021) *Mater. Sci. Eng., C.* **127**: 112259.

ACKNOWLEDGEMENTS: Supported by the APVV-20-0417, VAIA 09I03-03-V04-00718, VEGA-2-0157-24 and ITMS 313021T081 projects and the Stefan Schwarz Fund.

European Cells and Materials Vol. NN. Suppl. N, 20xx (page htu) ISSN 1473-2262

The role of metal degradation in *in vitro* biological evaluation

EB Montufar

Central European Institute of Technology, Brno University of Technology, Brno, Czech Republic

INTRODUCTION: Traditionally, metal degradation and in vitro biological evaluation have been conducted independently. However, cell responses in vitro are influenced by the degradation process (Figure 1), and as a result, biological assessment methods should be adapted accordingly [1]. This contribution highlights key considerations and proposes alternatives to integrate them into future experimental designs.

METHODS: A literature review was conducted to identify current practices in the biological evaluation of biodegradable metals. These practices were then benchmarked against known degradation mechanisms and kinetics, enabling the identification of best practices and opportunities for improvement.

RESULTS: The in vitro biological characterization of biodegradable metals involves evaluating cytotoxicity, osteoconductive potential, and inflammatory response, using methods aligned with ISO 10993 series of standards. Among the exposure methods outlined in the standard, material extracts are most used to assess the cytotoxicity of magnesium- and zinc-based biodegradable alloys. Indirect cell culture models are also employed to evaluate bone-forming and inflammatory responses. When direct contact studies are used with magnesium-based materials, cells typically adhere to degradation products or corrosion protection coatings. Cell attachment to degrading metallic surfaces has been reported in iron-based biodegradable metals, which typically exhibit low degradation rates.

Cell cultures are typically performed on as-processed metallic samples, often without accounting for degradation mechanism. Extracts are frequently diluted arbitrarily to compare the cytotoxicity of different alloys, but the dilution factors are not justified in terms of degradation kinetics or the body's physiological homeostatic capacity.

A key challenge in achieving more accurate in vitro biological evaluations is replicating the body's ability to buffer soluble degradation products and pH fluctuations. Additionally, there is limited understanding of cell-mediated degradation of corrosion products and protective coatings.

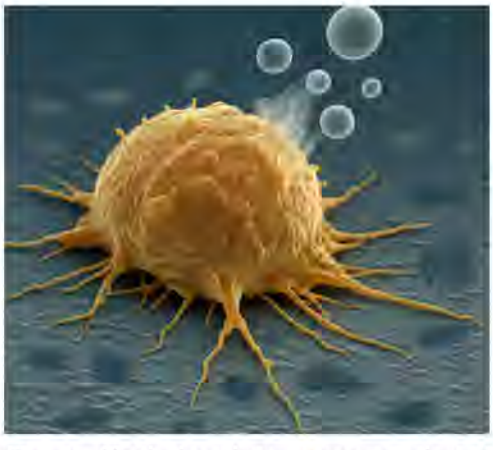

Fig. 1: Metal degradation generates physical (surface instability, gas release) and biochemical (ion release, pH shifts) factors that stress cells in vitro, especially without homeostatic mechanisms.

DISCUSSION & CONCLUSIONS: A straightforward approach to incorporating the degradation process into in vitro biological evaluations of biodegradable metals is to initiate cell cultures at different stages of material degradation, using both direct and indirect methods. This strategy could enable the assessment of inflammatory responses to rapid initial degradation, the transition to a less stressful phase due to passivation, cellular behaviour under steady-state degradation conditions, and the role of cells in mediating the degradation of solid corrosion products.

In conclusion, in vitro biological evaluation of biodegradable metals has advanced significantly, offering valuable insights into their biological safety and performance. The next steps in the field involve modifying standard methods for studying in vitro cell responses incorporating the effects of the degradation process.

REFERENCES: [1]EB Montufar (2025) *Bone Response to Biodegradable Metals and In Vitro Evaluation of the Cytocompatibility*, *JOM*, https://doi.org/10.1007/s11837-025-07353-8.

ACKNOWLEDGEMENTS: This work was supported by the Czech Ministry of Health (NW24-10-00195) and the Horizon Europe European Innovation Council (101186758).

European Cells and Materials Vol. NN. Suppl. N, 20xx (page htu) ISSN 1473-2262

Development of a Composite Filler for Oral Tissue Regeneration Using Magnesium-Substituted Apatite

Kang-sik Lee[1],Minseong Chae[1], Yoon-Ji Kim[2],Jin-Yong Jeong[3] ,Yu-Chan Kim [4], Hojeong Jeon[4], Chris Hyung-Seop Han[4], Kyungwoo Lee [5], Hyunwoo Han[5], Jinkyung Son[5]

[1] *Biomedical Engineering Research* Center, *Asan Medical Center, College of Medicine, University of Ulsan,*

[2] *Department of Orthodontics, Asan Medical Center, University of Ulsan College of Medicine, Seoul,*

[3] *Department of Convergence Medicine and Asan Institute for Life Sciences, Asan Medical Center, University of Ulsan College of Medicine,*

[4] *Biomaterial Research Center , Korea Institute of Science and Technology (KIST)*

[5] *Research and development team BM Port*

INTRODUCTION: Open gingival embrasure (OGE), also known as the 'black triangle,' refers to interdental soft tissue recession and loss due to aging and periodontal disease, causing aesthetic and functional discomfort. Traditional hyaluronic acid (HA) fillers have limitations due to rapid absorption in vivo. In this study, we developed a composite Mg-apatite-hyaluronic acid (MgAp-HA) filler incorporating magnesium-substituted apatite (MgAp) as a matrix to decrease diffusion-driven absorption and enhance filler retention

METHODS: To establish an OGE recession model, a 5-mm spring U-shaped wire, matching the length of interdental papillae, was inserted interdentally in rats for 7 days to intentionally induce papilla recession. Papilla distance (PD), measured from root to papilla tip, was assessed to evaluate the recession rate. After recession induction, Mg·HA, HA and Phosphate-Buffered Saline (PBS), fillers were injected into the interdental papillae. PD changes were recorded at 1, 7, and 28 days post-injection. Extracted tissues underwent Hematoxylin & Eosin and Masson's Trichrome staining to evaluate residual filler volume and collagen formation.

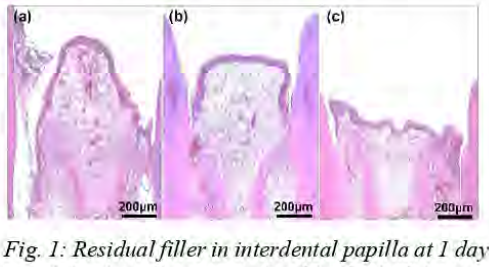

Fig. 1: Residual filler in interdental papilla at 1 day post-injection. Representative histological images after 0.2 mL filler injection following 7-day OGE model formation: (a) Mg·HA, (b) HA, (c) PBS.

RESULTS: The interdental papillae in the OGE model receded 0.86 ± 0.15 mm after 7 days. In the PBS group, recession continued post-injection. Mg·HA maintained consistently higher retention rates (65.3%, 56.4%, 47.0%) compared to HA (66.6%, 44.4%, 33.3%). Residual filler volume of Mg·HA was 1.89 times higher at day 1, 2.72 times higher at day 7, and 3.97 times higher at day 28 compared to HA. Collagen formation was also higher in Mg·HA at ratios of 1.03, 1.07, and 1.17 times at days 1, 7, and 28, respectively.

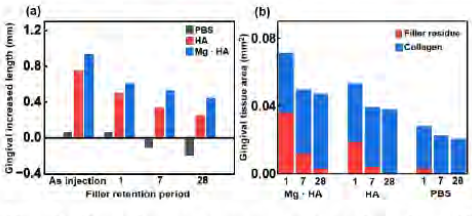

Fig. 2: Quantitative changes in interdental papilla post-injection. : (a) Papilla volume retention and (b) residual filler with collagen regeneration area

DISCUSSION & CONCLUSIONS: These findings suggest that the matrix effect of MgAp plays a significant role in sustaining filler volume and enhancing collagen production.

REFERENCES: [1] S.-B. Kim, J. Cho, S.-S. Jue, J.H. Park, and J.-Y. Kim (2020) Effect of Hyaluronic Acid Filler Injection on the Interdental Papilla in a Mouse Model of Open Gingival Embrasure, Int J Environ Res Public Health 17:4956.

ACKNOWLEDGEMENTS: This research was supported by the Seoul Bio-Medical Technology Commercialization Support Project (BT230213).

European Cells and Materials Vol. NN. Suppl. N, 20xx (page htu)
ISSN 1473-2262

hydrogen-gel for selective ROS modulation strategy to eliminate bacteria and promote wound healing

Tairan Quan[1,2], Xiao Hou[3], Yu Yin[3], Guangyin Yuan[1], Daijie Chen[3], Wenjiang Ding[1], Jia Pei[1]

[1] School of Materials and Engineering, Shanghai Jiao Tong University, China. [2] School of Chemical Engineering, University of New South Wales, Australia. [3] School of Pharmacy, Shanghai Jiao Tong University, China

INTRODUCTION: Wound infections remain a major challenge in clinical settings due to the emergence of antibiotic-resistant bacteria and the limitations of conventional antimicrobial strategies [1]. Recent studies have highlighted the potential of hydrogen-based therapies as a novel approach for antimicrobial intervention. In this context, we developed a magnesium hydride-based temperature phase change hydrogel to serve as an effective wound healing adjuvant.

This composite hydrogel enables sustained release of hydrogen, significantly enhancing its bactericidal efficacy. MgH_2 exerts its antimicrobial activity by disrupting oxidative phosphorylation on the bacterial membrane, leading to elevated intracellular reactive oxygen species (ROS) levels and reduced ATP production, ultimately causing bacterial death. In parallel, the released hydrogen alleviated oxidative stress in host cells, thereby attenuating inflammation and promoting wound tissue regeneration. These findings underscore the therapeutic promise of MgH_2 in combating infection and facilitating wound repair.

METHODS: Bacteria were mixed with different concentrations of MgH_2 hydrogel containing LB medium. After incubation, colonies growing on each LB agar medium plate were counted.

The expression of genes encoding cytochrome C oxidase and ATP synthase was verified by RT-qPCR.

The healing activity and inflammatory response of the wound tissue were assessed by H&E and Masson staining histological images.

RESULTS: The MgH_2 hydrogel group exhibited an irregular morphology with broken and crumpled cell membranes and exposed cell contents (Fig. 1).

The treated wounds showed significant epidermal and dermal structure with improved inflammatory response and more collagen deposition (Fig. 2).

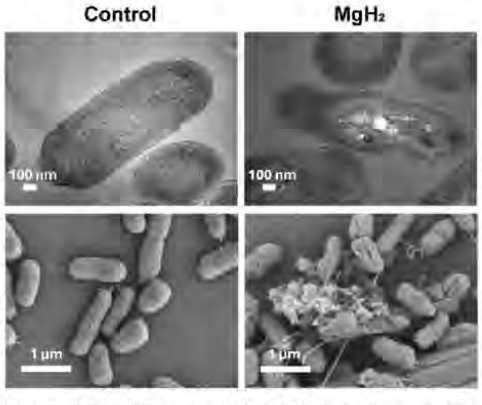

Fig. 1: TEM (above) and SEM (below) images of Pseudomonas aeruginosa before and after MgH_2 treatment.

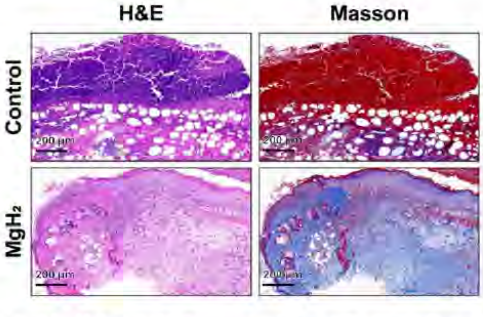

Fig. 2: H&E and Masson staining of mice infected skin before and after MgH_2 treatment.

DISCUSSION & CONCLUSIONS: MgH_2 hydrogel achieves efficient killing of pathogens in vitro and in vivo by slowing down the release of hydrogen. MgH_2 induced oxidative stress and energy deficiency in the bacteria, leading to their death. Hydrogel also has wound healing activity and alleviates oxidative stress in wound tissue.

REFERENCES: [1] C. Tu, H. Lu, T. Zhou, et al (2022) *Biomaterials* **286**:121597.

European Cells and Materials Vol. NN. Suppl. N, 20xx (page htu) ISSN 1473-2262

Investigating the effect of surface treatments on Mg-based implant behavior in male, juvenile, growing rats

N Zechmann[1], B Okutan[1], UY Schwarze[1,2], AM Weinberg[1], NG Sommer[1]

[1] *Department of Orthopaedics and Traumatology, Medical University of Graz, Graz, Austria*

[2] *Department of Dental Medicine and Oral Health, Medical University of Graz, Graz, Austria*

INTRODUCTION: Magnesium (Mg)-based implants are gaining attention as innovative solutions for fracture fixation, owing to their biocompatibility, biodegradability, and favorable mechanical characteristics. Unlike traditional permanent implants, Mg-based implants naturally resorb, avoiding the need for surgical removal [1, 2]. Nevertheless, Mg's accelerated degradation *in vivo* presents a significant challenge [3]. Surface treatments such as autoclaving and Atomic Layer Deposition (ALD) have emerged as promising strategies to tailor degradation rates, and therefore, do not interfere with bone healing [4]. Autoclaving generates a protective oxide layer, whereas ALD enables the application of uniform, ultrathin coatings [5].

METHODS: Bioresorbable Mg-based ZX00 pins (<0.5 wt% Zn, <0.5 wt% Ca; diameter = 1.6 mm, length = 8 mm) were transcortically implanted into the femoral diaphysis of 6-week-old male Sprague Dawley rats (n = 6 per group). Five experimental groups were studied: untreated controls, autoclaved once (1xa) or three times (3xa), and two ALD-coated groups (ALD1 and ALD2). Implant degradation was assessed using *in vivo* micro-computed tomography (µCT), with imaging conducted immediately after implantation and at 2, 6, 12, 18, and 26 weeks. *Ex vivo* µCT imaging was carried out at 26 weeks post-surgery (Fig. 1). Additionally, histological analyses were performed at the end of the study period.

RESULTS: Initial implant volumes and surface areas were larger in the treated groups than in the controls. Throughout the 26-week period, degradation rates were higher in treated samples, particularly those autoclaved three times. ALD-coated implants (ALD1, ALD2) exhibited reduced degradation during the critical early healing phase (weeks 6–12), suggesting a protective influence. Surface area changes between groups were less prominent. Gas formation remained low across all groups, except at isolated time points, with no significant differences. Histological evaluations are ongoing to verify that there is no negative impact on new bone formation.

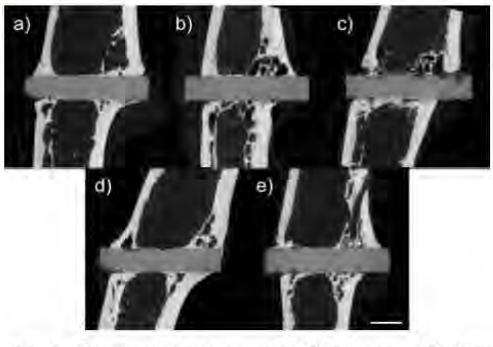

Fig. 1: Representative ex vivo µCT images of either a) untreated, b) 1xa, c) 3xa, d) ALD1-coated, or e) ALD2-coated ZX00 pins 26 weeks after implantation. Scale bar = 2 mm.

DISCUSSION & CONCLUSIONS: The bioresorbable ZX00 implants, whether untreated or surface-modified, are not anticipated to impair bone regeneration. Our findings show the complexity of optimizing surface treatments to control Mg implant degradation. In this study, ALD coatings showed the greatest potential to moderate degradation during the essential early healing period, highlighting their promise for future clinical application.

REFERENCES: [1] F. Witte (2010) *Acta Biomater.* **6**:1680-92. [2] F. Xing, S. Li, D. Ying, et al (2022) *J. Magnes. Alloy,* **10**:1428-56. [3] T. Kraus, S. F. Fischerauer, A. C. Hänzi, et al (2012) *Acta Biomater,* **8**:1230-38. [4] Z. Xi, Y. Wu, S. Xiang, et al (2020) *ACS Omega,* **5**:4548-57. [5] P.-C. Lin, K. Lin, Y.-H. Lin, et al (2022) *Coatings*, **12**:212.

ACKNOWLEDGEMENTS: This work was funded by Bioretec Ltd.

17th Biometal
25-30 AUGUST, 2025
Grand Hôtel San Michele, Cetraro, CS, Italy

European Cells and Materials Vol. NN. Suppl. N, 20xx (page htu) ISSN 1473-2262

Multiscale investigation of bone quality at the interface formed by biodegradable magnesium implants using 2D qBEI imaging and 3D micro-CT

S Schimek[1], AM Batouche[2], I Fiedler[2], K Jähn-Rickert[2], B Busse[2], DCF Wieland[1]

[1] *Institute of Metallic Biomaterials, Helmholtz-Zentrum Hereon, Germany* [2] *Department of Osteology and Biomechanics, University Medical Center Hamburg-Eppendorf, Germany*

INTRODUCTION: The majority of implants used for fracture treatment are made from non-degradable materials like titanium alloys, which remain in the body unless surgically removed. Magnesium (Mg) alloys offer an innovative alternative due to their biodegradability, biocompatibility, and mechanical properties resembling those of cortical bone, making them promising for osteoimplants [1,2]. However, understanding the mutual interaction of the degradation process of Mg implants with tissue remodeling remains challenging. This study investigates the influence of Mg-based implants on bone mechanical properties and ossification processes. It aims to analyze the multiscale impact of Mg alloys on bone quality, focusing on early-stage healing using both 2D and 3D methods on the same samples.

METHODS: To study the multiscale impact, a comprehensive range of analysis is planned along with a correlative analysis for a scale bridging understanding. The employed methods including micro-computed tomography (µCT), in situ diffraction nanoindentation, histology, EDX analysis, and quantitative backscattered electron microscopy (qBEI). Therefore, Tibiae of rats were implanted with Mg alloy WE43 and titanium alloys, which served as control. The rats were sacrificed after 3, 7, 14, 28, and 90 days. 2D-qBEI was employed to examine bone-implant interfaces, focusing on bone area fraction, mineral density distribution, and the density of osteocyte lacunae near the implantSynchrotron micro-CT measurements were utilized to provide detailed assessments of bone volume fraction (BV/TV), degradation and the spatial organization of lacunae (Fig. 1). Additionally, a comprehensive overview of the applied methods and workflow is being demonstrated, showcasing the multiscale analysis approach.

RESULTS: The results show that Mg implants stimulated bone turnover, resulting in lower mineralization and calcium heterogeneity, likely due to insufficient time for bone maturation. The 2D and 3D analyses revealed decreased lacuna density and BV/TV for Mg implants compared to titanium. Furthermore, the interaction between bone formation and lacunae network development for early stage healing will be shown on a local and global scale. As the Mg implants revealed a volume loss of approx. 20 % after 90 days, an interaction between the degradation processes, bone formation and lacunae network will be presented, indicating a significant influence of the degradation processes of WE43 on the bone formation and morphology.

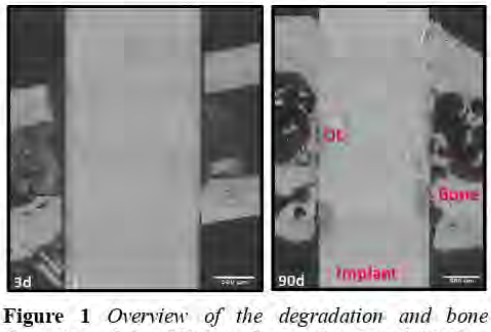

Figure 1 *Overview of the degradation and bone formation of the WE43 implants after 3 and 90 days using synchrotron radiation micro-CT.*

DISCUSSION & CONCLUSION:
The advanced multiscale approach demonstrates efficacy, revealing significant differences in bone quality parameters between titanium and magnesium implants during the early stage of healing. The results on the lacunae network and the mineralization better allow understanding the differences in the bone remodelling at degradable and non-degradable implants by correlating the degradation and bone formation parameters.

REFERENCES: [1]J. Hofstetter, M. Becker, E. Martinelli, et al., High-strength low-alloy (HSLA) Mg-Zn-Ga alloys with excellent biodegradation performance, JOM 66, 566-572 (2014) [2]N.G. Grün, P. Howleg, S. Tangl, et al., Comparison of a resorbable magnesium implant in small and large growing-animal model, Acta. Biomater 78, 379-386 (2018)

European Cells and Materials Vol. NN. Suppl. N, 20xx (page htu)
ISSN 1473-2262

3D-Printed Biodegradable Zn alloy Scaffolds to Suppress Osteosarcoma and Promote Osteogenesis

Dandan Xia[1],Peng Wen[2], Yufeng Zheng[3],

[1]Department of Dental Materials, Peking University School and Hospital of Stomatology, China. [2] Department of Mechanical Engineering, Tsinghua University, China. [3]School of Materials Science and Engineering, Peking University, Beijing, 100871, China

INTRODUCTION: Osteosarcoma is the most common primary bone tumor. After tumor resection, recurrence and postoperative bone defects remain a critical challenge. It is urgent to develop biomaterials which can kill osteosarcoma and promote bone regeneration. In this study, we utilized laser powder bed fusion to fabricate biodegradable Zn-Li pscaffolds that supress tumors and promote osteogenesis.

METHODS: The TPMS method was used to design scaffolds. A Gyroid unit cell with a porosity of 70% was generated. Scaffolds were produced in a laser powder bed fusion printing system with a single-mode ytterbium fiber laser, emitting a 1070 nm laser with a 70 μm-focus spot diameter. The pure Zn and Zn-Li scaffolds surface were observed under Scanning electron microscope (SEM). EBSD analysis was used for the characterization of grain size distribution. Compression tests were conducted via the Shimadzu tester.

RESULTS: The pure Zn and Zn-Li scaffolds were fabricated, (*Fig. 1*). Electron backscattered diffraction (EBSD) analysis revealed the grain size distribution (*Fig. 2*). The average grain size decreased from 10.50 μm in Zn to 8.61 μm in Zn-0.4Li, then increased to 13.96 μm in Zn-0.8Li. The compressive yield strength (CYS) and elastic modulus (E) increased with the Li content (*Fig. 3*). The CYS and E of the Zn-0.8Li scaffolds were 28.87 ± 0.53 and 817.55 ± 59.69 MPa, respectively, higher than that of pure Zn scaffolds (5.50 ± 0.20 and 185.81 ± 9.78 MPa).

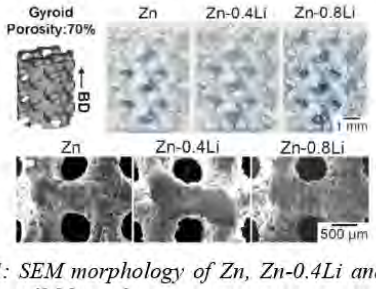

Fig. 1: SEM morphology of Zn, Zn-0.4Li and Zn-0.8Li scaffolds surface.

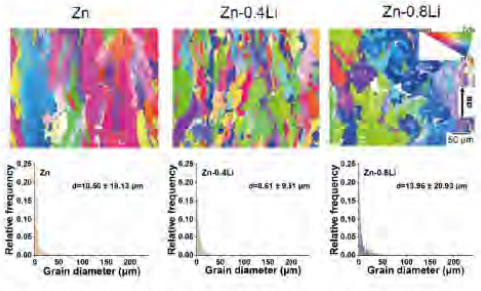

Fig. 2: EBSD inverse pole figure orientation maps.

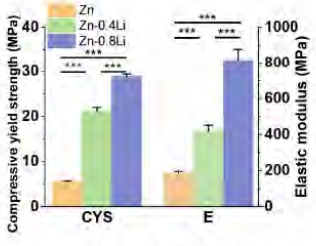

Fig. 3: CYS of Zn and Zn-Li scaffolds.

DISCUSSION & CONCLUSIONS: The mechanical strength, degradation behavior, and biological effects of Zn-Li scaffolds were regulated by structure design and composition optimization[1, 2]. The Zn-0.8Li scaffold showed enhanced strength and moderate corrosion behavior. In addition, the Zn-0.8Li scaffold inhibited osteosarcoma cell proliferation, promoted apoptosis, alleviated migration, and enhanced osteoblasts' osteogenic ability, thereby exhibiting antitumor and osteogenesis properties.

REFERENCES: [1]Dandan Xia, etc. Bioactive Materials, 2023, 19, 12-23. [2] Yu Qin, etc. Acta Biomaterialia, 2022, 145, 403-415.

ACKNOWLEDGEMENTS: This study was supported by the National Key Research and Development Program of China (2023YFC2412600).

European Cells and Materials Vol. NN. Suppl. N, 20xx (page hru) ISSN 1473-2262

Creep properties of bioabsorbable ultrafine-grained Zn+ZnO composites

YJ Zhao[1,2], M Balog[1,3], P Krizik[1], P Krajnakova[1,3], F Seabra[1,2,3]

[1] *Institute of materials & machine mechanics, SAS, Bratislava, Slovakia*
[2] *Faculty of materials science and technology in Trnava, STU, Trnava, Slovakia*
[3] *Centre of excellence for advanced materials application, SAS, Bratislava, Slovakia*

INTRODUCTION: Zn is a promising material candidate for bioresorbable implants. Nevertheless, owing to its low melting point Zn-based materials suffer from rather poor creep resistance at temperature of human body (THB). For their potential use in biomedical applications such as endovascular stents and orthopedic internal fixators, it is essential to understand material response to creep loading and their susceptibility to creep deformation, and fracture at THB. In the present work we utilized a small punch test (SPT) to determine the creep properties and behavior. SPT is a novel testing method, which utilizes small volume disk samples. While SPT can provide practical and sensitive insight into time-dependent deformation, there is no clear standard, so it is necessary to establish robust correlations between force-deflection data and tensile creep behavior. For this reason, the SPT results were compared with conventional tensile creep analysis to get predictive correlations. We pursued the creep testing for the novel stable ultrafine-grained (UFG) pure Zn composite, with ZnO nanoparticles stabilizing Zn high-angle grain boundaries (HAGB) [1, 2]. The results were compared to the ingot fine grained pure Zn material [1]

METHODS: The extruded powder metallurgy Zn+4.75vol.%ZnO and ingot metallurgy Zn99.99wt.% materials with the grain size of 0.75 and 18.4 μm, respectively, were used. For both materials extrusion was realized at the room temperature and reduction ratio of 11:1. The discs with a diameter of 8 mm and thickness of 0.5 mm were creep tested at 23, 37, and 51 °C under varying loads using a custom SPT setup in accordance with ASTM E3205–20. Conventional tensile creep tests using the samples with 4 mm gauge diameter and 20 mm gauge length were conducted at 23 °C under varying loads following ASTM E8/E8M-24. Fracture surfaces of discs were analyzed by SEM.

RESULTS: Results showed that at all testing temperatures, distinct regions corresponding to elastic, elastic-plastic, geometric softening, crack nucleation, and crack growth were identified. Strain hardening was limited. At all testing temperatures, an increase in applied force (F) led to an exponential decrease in time to fracture (t_f). A relationship between time to fracture and minimum deflection rate (δ_{min}) was established (1), the Norton and Monkman-Grant relationship confirmed that the GBS was the dominant mechanism with the creep behavior in both SPT and tensile creep modes. The correlation between stress (σ) and F was also derived (2). The relationship between creep rate (ε) and deflection rate ($\dot{\delta}$) was investigated, so that we could directly translate SPT data to conventional creep strain metrics (3).

$$t_f = 3.31E{-}4/(\delta_{min})^{0.9556} \quad (1)$$

$$F/\sigma = 1.3258 \quad (2)$$

$$\varepsilon = 0.2454\dot{\delta}^2 + 0.3732\dot{\delta} \quad (3)$$

DISCUSSION & CONCLUSIONS: SPT at lower loading forces were stopped early once steady-state creep was reached. At low forces (50.1–59.8 N), the Zn+ZnO showed a slower deflection rate than pure Zn, up to five times lower at 50.1 N, demonstrating better creep resistance. However, at higher forces (69.7–108.9 N), the trend reversed: Zn+ZnO deformed faster and failed sooner than pure Zn. Importantly, higher yield force of Zn+ZnO means it could resist the start of deformation better under different temperatures and loading forces. This makes it suitable for biomedical applications where materials undergo long-term, low-stress conditions. Higher δ_{min} of the Zn+ZnO at higher stress was attributed to its UFG structure, which promoted grain boundary sliding mechanism (GBS). The activation energies for creep confirmed temperature-driven deformation mechanisms as the rate-limiting process. The study confirmed that, in principle, UFG Zn with stabilized HAGB exhibited reasonable creep resistance, particularly under low loads, which challenges conventional expectations.

REFERENCES: [1] M. Balog et al (2023) *J Mater Res Technol* **25**:4510-4527. [2] M. Balog et al (2024) *J Mater Res Technol* **33**:7458-7468.

ACKNOWLEDGEMENTS: This work was supported by the VAIA 09I03-03-V04-00718, APVV-20-0417, ITMS 313021T081, and VEGA 2/0157/24 projects.

European Cells and Materials Vol. NN. Suppl. N, 20xx (page hru)
ISSN 1473-2262

Degradation behavior of as-cast and extruded Mg-Dy-Zn alloys under physiological conditions

Genzhi Jiang[1, *], Yuanding Huang[1, **], Heike Helmholz[2], Yue Zhang[1], Zijian Yu[3], Domonkos Tolnai[1], Norbert Hort[1, 4]

[1] Institute of Metallic Biomaterials, Helmholtz-Zentrum Hereon, Geesthacht 21502, Germany. [2] Institute of Surface Science, Helmholtz-Zentrum Hereon, Geesthacht 21502, Germany. [3] College of Materials Science and Engineering, Beijing University of Technology, Beijing 100124, China. [4] Institute of Product Technology and Systems, Leuphana University Lüneburg, Lüneburg 21335, Germany

INTRODUCTION: Previous work indicated that long-period stacking ordered (LPSO) phase and/or γ′ in rare earth containing Mg alloys had contradictory mechanisms responsible for their degradation in less complex or standard salt media, such as 0.9% NaCl solution [1,2]. They needed to be further investigated in a more realistic simulated body fluid (SBF).

METHODS: Mg-xDy-1.5Zn (x = 5, 10, 15 wt. %) were prepared using direct chill casting process in a permanent mould [3]. After 48 hours heat treatment at 500 °C, the ingot was extruded from the 50 mm billet to a final diameter of 10 mm at 360 °C at a speed of 0.6 mm/s.

Weight loss tests were performed in DMEM+Glutamax ((+) 4.5 g/L D-Glucose, (+) Pyruvate, Life Technologies) together with 10% FBS (PAA Laboratories) and 1% Penicillin Streptomycin (PenStrep) under cell culture conditions (37°C, 20% O_2, 5% CO_2, 95% relative humidity) in the incubator.

RESULTS: In as-cast alloys, the degradation rate of Mg-5Dy-1.5Zn alloy consistently increased. In contrast, though the volume fraction of intermetallics in Mg-10Dy-1.5Zn and Mg-15Dy-1.5Zn alloys are larger than Mg-5Dy-1.5Zn alloys, their degradation rates are lower than Mg-5Dy-1.5Zn alloy.

In extruded with a 48h preheating treatment alloys, the volume fraction of intermetallics increased with the addition of Dy content. However, Mg-5Dy-1.5Zn alloy showed the highest degradation rate among three extruded alloys. Meanwhile, the W phase in Mg-10Dy-1.5Zn alloy did not trigger severe local corrosion. In addition, the Mg-10Dy-1.5Zn alloy contained the dense γ′ phase which act as cathode that accelerates the degradation of Mg matrix, therefore exhibited a higher degradation rate than Mg-15Dy-1.5Zn alloy. The degradation rate results were shown in Fig. 1.

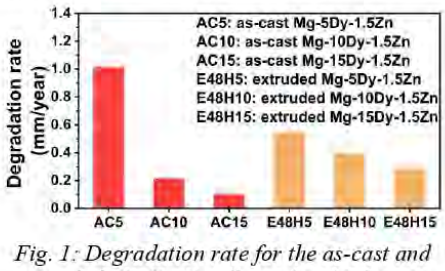

Fig. 1: Degradation rate for the as-cast and extruded Mg-Dy-Zn alloys after 14 days of immersion in DMEM+10%FBS medium

DISCUSSION & CONCLUSIONS: The distribution, type and amounts of intermetallics significantly influenced the degradation behavior of Mg-Dy-Zn alloys. In the as-cast alloys, the continuous network structure of intermetallics (γ′ and 18R LPSO) and a compact degradation layer provided protection from further degradation for AC10 and AC15 alloys, contributing to their lower degradation rate. In the extruded alloys, the denser compact degradation layer on the surface of γ′ phase, which retard the corrosive ions for further penetration to Mg matrix, thus effectively inhibit the further galvanic corrosion triggered by W phase in E48H10 alloy, resulting the lower degradation rate compared to E48H5 alloy.

REFERENCES: [1]J. Xie, Z. Zhang, H. Dong, et al (2025) *Corrosion Science* **243**:112592. [2]C. Dai, J. Wang, Y. Pan, et al (2024) *Journal of Materials Science & Technology* **168**:88-102. [3]F. R. Elsayed, N. Hort, M. A. Salgado-Ordorica, et al (2011) *Mater. Sci. Forum* **690**:65-68.

ACKNOWLEDGEMENTS: Mr. Genzhi Jiang and Dr. Yue Zhang would like to thank the China Scholarship Council for the award of fellowship and funding (Nos. 202106890013 and 202206095009).

European Cells and Materials Vol. NN. Suppl. N, 20xx (page htu)
ISSN 1473-2262

Degradation behaviors of Mg-5Sn-xZn alloys in Hank's balanced salt solution

CD Yim[1,2], YJ Won[1], SK Woo[3]

[1] *Lightweight Materials Research Division, Korea Institute of Materials Science, Korea.*

[2] *Advanced Materials Engineering, University of Science and Technology, Korea*

[3] *Production Technology Research Center, Samsung Heavy Industries, Korea*

INTRODUCTION: In order to expand the application of biodegradable magnesium alloys in medical devices, it is necessary to suppress the generation of hydrogen during the degradation process and control the degradation. Sn and Zn are the effective elements which can suppress a hydrogen evolution and improve protectiveness of surface film. In this study, we aim to systematically investigate the influence of microstructural factors on the degradation behavior of Mg-5Sn-xZn (TZ5x) alloys.

METHODS: The plates of TZ5x alloys with the cross-sectional dimension with a thickness of 2 mm and width of 28 mm were fabricated by direct extrusion at 573 K. The extrusion ratio and speed were 90:1 and 1.0 m/min, respectively.

The potentiodynamic polarization behavior in HBSS was evaluated at 310 ± 0.5 K. The external voltage was changed form -0.25 V to 0.5 V with respect to OCP at the rate of 1.0 mV/s. The corrosion rate was measured by immersion test. The specimen was immersed into HBSS at 310 K for 10~30 days. The weight loss after immersion test was converted to the corrosion rate. The average corrosion rate was determined as the average value of three test results.

RESULTS: The microstructures of as-extruded TZ5x alloys showed a typical equiaxed grain structure by dynamic recrystallization during hot extrusion. The major constituent phases of as-extruded TZ5x alloys were α-Mg and Mg_2Sn. Figure 1 shows the potentiodynamic polarization curves of as-extruded TZ5x alloys. The hydrogen evolution rate at cathodic region and the passive current density at anodic region in TZ51, TZ52 and TZ53 alloys were similar. TZ54 alloys showed relatively high hydrogen evolution rate and low passive current density. The fraction of ZnO in the surface film might increase with increasing Zn content, which would enhance the protectiveness of surface film[1]. The passive current density decreased with increasing Zn content. Simultaneously, the hydrogen evolution rate increased with increasing Zn content due to high conductivity of ZnO. The corrosion rates of as-extruded TZ5x alloys decreased by addition of Zn except TZ54 alloy. The corrosion behavior of as-extruded TZ5x alloys would change according to relative contributions of following factors; acceleration by formation of micro-galvanic cell between α-Mg and Mg_2Sn particles and increase of the protectiveness of surface film by higher fraction of ZnO in the surface film.

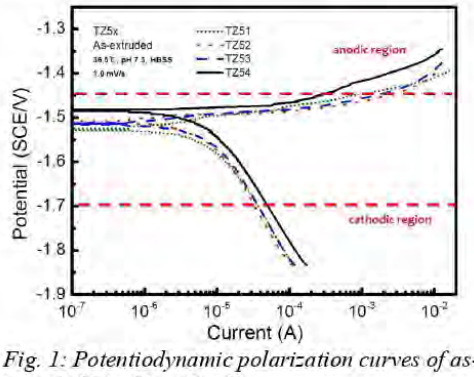

Fig. 1: Potentiodynamic polarization curves of as-extruded Mg-5Sn-xZn alloys.

DISCUSSION & CONCLUSIONS: The change of corrosion behaviors of as-extruded TZ5x alloys according to Zn content was strongly related to the changes of microstructures and composition of surface film. The increase of ZnO content in the surface film improved the protectiveness of the surface film. The increase of fraction of Mg_2Sn particles accelerated the corrosion by formation of micro-galvanic cell with the matrix.

REFERENCES: [1]H.Y. Ha et al (2013) *Corrosion Science* **75**:426-433.

ACKNOWLEDGEMENTS: This research was supported by the National Research Foundation of Korea (NRF) grant funded by the Korea government (MSIT) (RS-2022-NR068191).

European Cells and Materials Vol. NN. Suppl. N, 20xx (page htu) ISSN 1473-2262

Dynamic response of additively manufactured WE43 lattice structures under high-strain compression

Z Alomar[1], B Lukic[2], C Persson[1], P Isaksson[1], F D'Elia[1]

[1] *Department of Materials Science and Engineering, Division of Biomedical Engineering, Uppsala University, Uppsala, Sweden.* [2] *European Synchrotron Radiation Facility (ESRF), Grenoble, France.*

INTRODUCTION: Magnesium ally WE43 is a promising material for bone scaffolds due to its biocompatibility and ability to degrade in a physiological environment. Additive manufacturing (AM) enables the fabrication of patient-specific biodegradable porous lattices that could balance mechanical support and bone ingrowth [1]. While static mechanical properties of such scaffolds are well-studied, their dynamic response under high-strain-rate loading, critical for real-world scenarios like falls or sudden impacts, remains poorly understood [2]. This knowledge gap poses a barrier to designing implants that balance degradation and mechanical integrity during bone healing. This study aims to investigate the dynamic mechanical behavior and failure mechanisms of WE43 lattices under high-strain-rate loading conditions, employing a Split-Hopkinson Pressure Bar (SHPB) combined with synchrotron X-ray phase-contrast imaging to capture real-time microstructural evolution.

METHODS: Two families of lattices, strut-based and Triply Periodic Minimal Surface (TPMS) designs were fabricated from WE43 magnesium alloy, with varying relative densities (11–47%), via laser-powder bed fusion (L-PBF). Dynamic compression testing was conducted on the lattices using a SHPB system, where stress waves were generated by a 250 mm projectile pressurized at 1.2–2.2 bar to achieve high strain rates. Specimens were dynamically imaged in situ at the ESRF ID19 beamline using 60 ps X-ray pulses paired with a Shimadzu-HPVX2 ultra-high-speed camera, covering a 12x8 mm field of view. Post-impact analysis employed image analysis on high-speed radiographs to quantify the strain fields and the energy absorption Additionally, microcomputed tomography analysis was performed on some of the samples to evaluate their printing quality.

RESULTS: The SHPB tests revealed distinct mechanical responses between lattice types. TPMS structures exhibited superior load-bearing capacity, sustaining force outputs at least two times higher than strut-based lattices (e.g., FCC vs Gyroid) under identical impact conditions, see Fig. 1. Synchrotron imaging demonstrated TPMS deformation via progressive pore collapse and plastic densification, while strut-based lattices exhibit brittleness at high pressure, with FCC designs fracturing entirely at the transmission end. The stiffness values of TPMS lattices exceeded those of their strut-based counterparts by 40–60% across the tested relative densities. Moreover, TPMS structures demonstrated greater efficiency in energy absorption. Micro-computed tomography revealed highly dense structures, although a significant amount of semi-melted powder was observed on the surface.

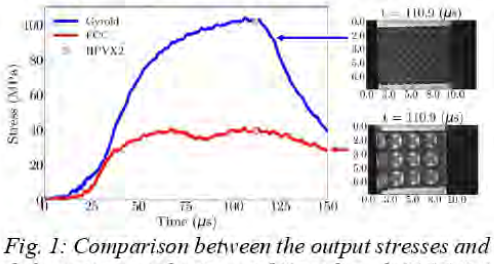

Fig. 1: Comparison between the output stresses and deformation mechanisms of Strut-based (FCC 0.4 mm struts diameter) and TPMS structure (Gyroid 0.4mm wall thickness) under 2.2 bar impact.

DISCUSSION & CONCLUSIONS: The superior dynamic performance of TPMS lattices stems from their continuous, curvature-driven architectures, which mitigate stress concentrations and enable gradual energy dissipation through controlled pore collapse, in contrast to strut-based designs which are prone to sudden fracture. Overall, this work establishes a foundation for optimizing AM-fabricated Mg alloy scaffolds, prioritizing architectures like TPMS to enhance implant durability in dynamic loading scenarios, thereby advancing patient-specific solutions for bone regeneration.

REFERENCES: [1]K. Dachsa, et al. (2024) *Adv in Mat Science and Eng* **2024**:1325004.[2] L. Antoniac, et al. (2022) *Materials* **15**(23):8693.

ACKNOWLEDGEMENTS: This work was supported by the ESRF/ ID19 experiment MA6157 and EU Horizon 2020 (Marie Curie – 101110609).

17th Biometal
25-30 AUGUST, 2025
Grand Hôtel San Michele,
Cetraro, CS, Italy

European Cells and Materials Vol. NN. Suppl. N, 20xx (page htu) ISSN 1473-2262

Engineering solvent-free resorbable polymer-metal hybrid structures for next generation bone implants

C. Ingelmo[1], S. Sánchez [1], M.D. López[1], P. Rodrigo[1], J. Rams[1], J.P. Fernández-Hernán [1], **S.C. Cifuentes[1*]**

[1] *Dpto. de Matemática Aplicada, Ciencia e Ingeniería de Materiales y Tecnología Electrónica, ESCET, Universidad Rey Juan Carlos, Móstoles, Madrid, 28933, Spain.*

INTRODUCTION: For bone regeneration applications, researchers have developed resorbable metal–polymer composites by incorporating magnesium (Mg) particles into a polylactic acid (PLA) matrix or by applying polymeric coatings onto resorbable metallic scaffolds[1,2]. Other studies have explored reinforcing PLA with Mg wires[3]. These composites offer mutual benefits: Mg enhances the mechanical strength and bioactivity of PLA, while the polymer matrix moderates the corrosion rate of Mg. However, current approaches have yet to achieve the required balance between mechanical strength and biodegradability for clinical applications in bone regeneration. Key limitations include restricted design flexibility, time-consuming and labor-intensive fabrication methods, and the use of toxic organic solvents (e.g., chloroform, dichloromethane), which compromise biocompatibility. Therefore, advancing solvent-free fabrication techniques capable of producing complex geometries is essential to enable clinical translation.

In this study, we developed a novel solvent-free, multi-material manufacturing approach for fabricating resorbable polymer–metal hybrid structures. This method combines metal additive manufacturing (Laser Powder Bed Fusion, LPBF) with polymer processing via compression moulding.

METHODS: Hybrid polymer–metal structures were fabricated using a PLA matrix and AZ91 magnesium alloy. PLA preforms were produced by hot plate pressing, varying temperature and pressure to ensure compatibility with the metallic component. LPBF parameters (laser power and scan speed) were adjusted to fabricate metallic slabs with different surface roughness. Integration of the metal into the polymer matrix was performed via compression moulding, varying preform geometry, moulding temperature, and pressure. A two-month hydrogen release test was conducted to evaluate the degradation behavior of the hybrid structures.

RESULTS: Figure 1 displays the hybrid structures fabricated by combining LPBF and compression moulding. The interfacial bonding strength was modulated by altering LPBF parameters, which influenced the surface morphology of the metallic slabs. Three sample types were immersed in simulated physiological fluid, yielding different degradation behaviors. Sample 1 exhibited structural failure; in Sample 2, hydrogen release caused delamination of the polymer from the metal, forming a gas bubble. In contrast, Sample 3 maintained its structural integrity throughout the two-month period.

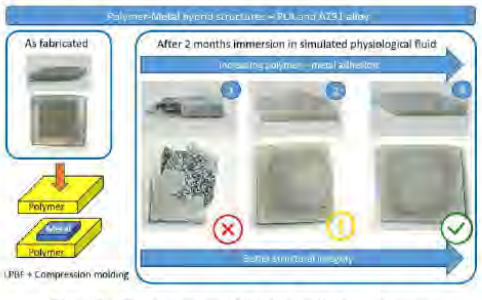

Fig. 1: Polymer-metal hybrid structures.

DISCUSSION & CONCLUSIONS: The integration of LPBF and compression moulding enables the fabrication of solvent-free, resorbable polymer–metal hybrid structures. Surface morphology of the metallic component plays a critical role in interfacial bonding and degradation behavior. Optimized combinations can maintain structural integrity over extended periods, highlighting the potential of this method for developing clinically viable bone regeneration implants.

REFERENCES: [1] R. García-Sobrino et al (2023) *Polymers* **15** https://doi.org/10.3390/polym15244667

[2] S.C. Cifuentes et al (2022) *Metals* **12**:566 https://doi.org/10.3390/met12040566

[3] W. Ali et al (2024) *Advanced Engineering Materials* **26(13)**:2400617 https://doi.org/10.1002/adem.202400617

ACKNOWLEDGEMENTS: The authors would like to thank the funding provided for this research by Universidad Rey Juan Carlos through the project 2024/SOLCON-137037.

European Cells and Materials Vol. NN. Suppl. N, 20xx (page htu) ISSN 1473-2262

Enhanced corrosion resistance and bioactivity of metallic alloys via non-toxic nitrogen-doped carbon film transfer and laser-deposited bioactive glass

S Bajda[1], A Rai[1], K Cholewa-Kowalska[1], B Wiese[2], Y Liu[3], M Krzyzanowski[1,4]

[1] Faculty of Metals Engineering and Industrial Computer Science, AGH University of Krakow, Poland. [2] Helmholtz-Zentrum Hereon, Institute of Metallic Biomaterials, Functional Magnesium Materials, Germany. [3] Manufacturing Technology Centre, Coventry UK. [4] CEBE, Birmingham City University, Birmingham, UK.

INTRODUCTION: The application of ultrathin, ultrasmooth and corrosion resistant nitrogen-doped amorphous carbon (a-C:N) thin film on a magnesium alloy (Mg-0.5Zn-0.2Ca) and S520 bioactive glass on an ultrafine-grained Ti-6Al-7Nb titanium alloy by a laser-directed energy deposition (LDED) process is studied. Carbon is a potentially suitable choice to improve the biocompatibility and corrosion resistance of Mg-based implants, while Ti-based material without potentially toxic vanadium coated with S520 may be a choice for its use in biomedical load bearing implants.

METHODS: The Mg alloy was fabricated using direct chill casting, melted at 720°C in an Ar-SF6 atmosphere, cast into preheated molds at 680°C, water-quenched, and solution annealed at 450°C for 16 hours to achieve a homogeneous microstructure. The a-C:N film was synthesized by mixing β-PEI and glucose in a 1:1 vol ratio, optimizing nitrogen concentration and transfer. AFM, SEM, and EDS were used to examine the film's topology, thickness, morphology, and structure. Electrochemical corrosion and cytotoxicity tests with the MG-63 cell line were also conducted.

S520 bioactive glass powder was produced using a quenching technique to achieve the desired wetting angle for LDED. The Ti-6Al-7Nb alloy was ultrafine-grained through Equal Channel Angular Pressing (ECAP). A 5-axis Mikron 450u machine was used for the hybrid LDED system, combined with a modified laser deposition and multi-material powder delivery system. The laser operated at 1064 nm with a 1200 W output. Samples were analyzed using light microscopy, SEM with EBSD, and EDS for chemical analysis.

RESULTS:

The a-C:N film's amorphous nature was confirmed by HRTEM, XRD, XPS, and Raman spectroscopy, showing sp^2 clusters [1]. Nitrogen's electron-donating ability improves interaction with Mg^{2+} ions, enhancing film-substrate adhesion. No delamination was observed after seven days in dilute HCl. Electrochemical tests showed a lower I_{corr} for the coating and higher R_{pc}, R_{ct} values, indicating improved corrosion resistance. After long-term immersion in PBS and HCl, the coated surface showed less degradation than the bare magnesium alloy.

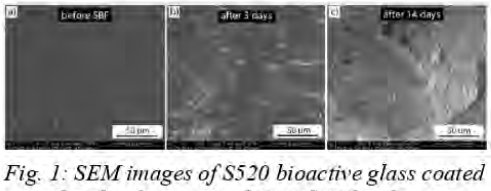

Fig. 1: SEM images of S520 bioactive glass coated onto the ultrafine-grained Ti-6Al-7Nb substrate before (a), after 3 (b) and after 14 (c) days of immersion in simulated body fluid (SBF).

The application of bioactive glass S520 on ultrafine-grained Ti-6Al-7Nb via LDED creates a biocompatible material for biomedical implants without toxic vanadium [2]. The laser cladding process melts the titanium surface and infuses it with bioactive glass, leading to crystallization and the formation of large grains. Laser-induced heat causes a martensitic transformation, forming α′ acicular martensite, while the heat-affected zone (HAZ) shows refined grains. Concerns about Al toxicity in the glass arise as it dissolves in the body. After 14 days in SBF, the samples formed hydroxyapatite (HCA) with significant P reduction, demonstrating high bioactivity.

DISCUSSION & CONCLUSIONS: Cytotoxicity tests confirmed the studied materials are non-toxic, making it a promising candidate for orthopaedic implants, though further biocompatibility studies are needed.

REFERENCES: [1] A. Rai, M. Szczerba, J. Karbowniczek, et al (2025) *Applied Surface Science* **695**: 162847. [2] S. Bajda, K. Cholewa-Kowalska, M. Krzyzanowski, et al. (2024) *Surface & Coatings Technology* **485**: 130904.

ACKNOWLEDGEMENTS: The support from the National Science Centre, Poland (grant no. 2024/53/B/ST11/00799) is greatly appreciated.

European Cells and Materials Vol. NN. Suppl. N, 20xx (page htu) ISSN 1473-2262

Evaluation of *in situ* resistivity measurement for the development of Mg-based implant materials

Björn Wiese[1], Norbert Hort[1,2]

[1] *Functional Magnesium Materials, Institute of Metallic Biomaterials, Geesthacht, Germany.*
[2] *Production Technology and Systems (IPTS), Leuphana University Lüneburg, Lüneburg, Germany.*

INTRODUCTION: Material development aimed to meeting specific requirements, whereby the composition or processing must be optimised. There are numerous possible combinations to determine the optimum process parameters, for example for heat treatments such as ageing or recrystallisation. Conventional methods are time-consuming. Resistivity measurements in a furnace offer the possibility of an *in situ* measurement, which provides insight into the process and reduces the number of trials to select a reasonable parameter combination.

METHODS: The influence of process parameters - temperature and time - during different heat treatments, as well as the effect of material on resistivity, will be investigated. The 4-point probe method, described in [1, 2], was used to measure the resistivity. This setup was extended with a ThermConcept ROK 150/500/11 furnace (Fig. 1a) to allow measurements at different temperatures and times during material processing. Therefore, a holder was developed to place the samples in the furnace chamber (Fig. 1b). The resistance of different geometries was measured using various alternating currents between 1 and 100 mA to evaluate interactions with the new setup and to compare the results with thermodynamic predictions from Thermo-Calc using the TCMg07 database.

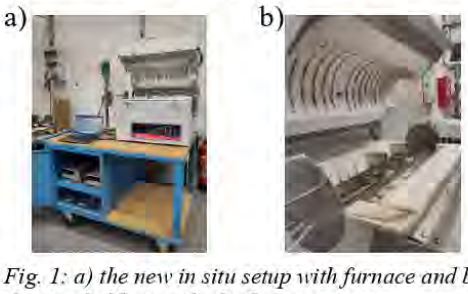

Fig. 1: a) the new in situ setup with furnace and b) the new holder inside the furnace.

RESULTS: Fig. 2 shows the resistivity values of pure Mg wire as a function of temperature. In the measurement shown in Fig. 2a, the results are not reproducible and do not match the calculated values. Compared to Fig. 2a, the trend of the measured values in Fig. 2b is similar to the calculated values. The main difference between the two experiments is the set measuring currents during the measurement in a) 1 mA and in b) 100 mA.

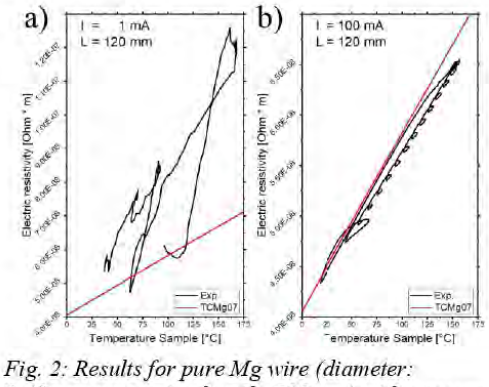

Fig. 2: Results for pure Mg wire (diameter: 0.65 mm, measuring length: 120 mm) with measuring currents of (a) 1 mA and (b) 100 mA, shown as a function of temperature.

DISCUSSION & CONCLUSIONS: In Fig. 2a, the strong deviation from reproducible measurement results can be attributed to susceptibility to errors caused by induced voltages from external electric fields or the furnace at low measuring currents. In Fig. 2b, two curves can be identified: (1) the heating curve with loops, and (2) the cooling curve, which appears as an approximately straight line parallel to the calculated values. The loops are caused by temperature differences between the thermocouple and the wire, as well as by the furnace's temperature control behavior. During cooling, the heating is switched off, resulting in a constant and uniform heat flow out of the furnace system, which eliminates significant temperature differences. When the correct measuring current is applied and values from the cooling phase are used, reliable resistivity values can be obtained. These values fall within the range of literature data [2] and calculated results, demonstrating that this setup is suitable for investigating new materials and validating thermodynamic predictions.

REFERENCES: [1] S. Meyer et al. (2022) *Abstract book 14th BIOMETAL*, Met-22. [2] S. Meyer et al. (2022) *Scripta Mater* **215**:114712.

European Cells and Materials Vol. NN. Suppl. N, 20xx (page htu) ISSN 1473-2262

Fe-Mn-C steel organic acid pickling as preliminary surface treatment for 3D printed devices

Lucena I[12], Paternoster C[1], Multigner M[2], Mantovani D[1]

[1]Lab. for Biomaterials and Bioengineering, CRC-I, Department of Min-Met-Materials Eng., University Hospital Research Center, Regenerative Medicine, Laval University, Québec, Canada; and [2]Dpto. de Matemática Aplicada, Ciencia e Ingeniería de Materiales y Tecnología Electrónica, ESCET, Universidad Rey Juan Carlos, España

INTRODUCTION: Fe–Mn–C biodegradable alloys are promising candidates for temporary biomedical implants. However, a thick and heterogeneous oxide scale forms during manufacturing, which can impact electrochemical performance and biological response [1]. To obtain a clean and homogeneous surface without compromising mechanical integrity, acid pickling was evaluated as a preliminary treatment. This study investigated the effects of various acids, temperatures, and immersion times on Fe–12Mn–1.2C alloy. Surface morphology and chemical composition was analyzed to optimize pickling parameters for future biomedical applications.

METHODS: A Fe-12Mn-1.2C (ISO GX120Mn13) alloy, also known as Hadfield steel, was used in the form of hot-rolled plates in the annealed, quenched, and austenitic states. Acid pickling was performed using various organic acid solutions, and mixes with striger ones (e.g. CH_3COOH, HCOOH, CH_3CH_2COOH, $C_3H_6O_3$, HCl, HF, HNO_3), under different conditions of temperature (25, 40, and 60 °C) and exposure time (1, 10, and 30 minutes). The morphological and chemical characterization was carried out by scanning electron microscopy (SEM), energy dispersive X-ray spectroscopy (EDS), X-ray photoelectron spectroscopy (XPS), and profilometry.

RESULTS: Fe-12Mn-1.2C steel samples were subjected to a various pickling treatments using organic acids (acetic, formic, propionic, citric, malic, and lactic) alone or in combination with strong acids (HCl, HF, HNO_3, H_3PO_4, H_2SO_4, and $HClO_4$). SEM analysis revealed a clear influence of immersion time on surface morphology. Shorter exposure times (1–10 min) at room temperature led to smoother surfaces, while prolonged treatments resulted in increased roughness and localized pitting. Particularly, samples treated with organic acids or organic acids + HCl mixtures at 25 °C exhibited preferential oxide removal along grain boundaries, exposing the internal grain structure (Fig.1). These conditions produced a surface with low roughness and improved uniformity. EDS mapping confirmed an effective reduction in surface oxygen content, and XPS data supported these observations by revealing a distinct surface chemistry under these conditions.

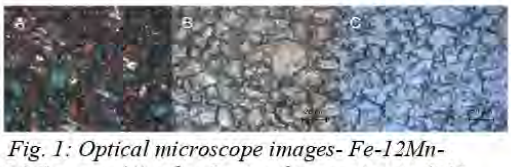

Fig. 1: Optical microscope images- Fe-12Mn-1.2C as rec (A), after 1 min of immersion in 40% vol. CH_3COOH,10% HCl (B); 10% CH_3COOH (C).

DISCUSSION & CONCLUSIONS: The results show that acid pickling is an effective pre-treatment for Fe–Mn–C biodegradable alloys, enabling the removal or controlled modification of the heterogeneous oxide scale formed during manufacturing. Organic acids, either alone or combined, offer a promising approach for achieving reproducible, homogeneous surfaces with reduced roughness—ideal conditions for subsequent processes like electropolishing. The surface morphology obtained under optimal conditions was characterized by low roughness and improved uniformity, suitable for subsequent biomedical surface treatments. In contrast, higher temperatures and prolonged immersion times led to increased surface roughness and localized degradation. EDS mapping and XPS analysis confirmed uniform surface modification without layered oxides—crucial for consistent biocompatibility. Overall, the study supports the use of tailored acid pickling protocols—particularly those involving organic acids—as sustainable and effective strategies to prepare Fe–Mn–C alloy surfaces for biomedical use.

REFERENCES: [1] de Andrade, L. M., et al. *Bioactive Materials*, *11* (2022).. , 166-180.

ACKNOWLEDGEMENTS: LBB, NSERC-Canada, Prima Quebec, and the CHU de Quebec Research Centre.

17th Biometal
25-30 AUGUST, 2025
Grand Hôtel San Michele,
Cetraro, CS, Italy

In-situ study of degradation controlled smart 4D actuator designs and their load-bearing capabilities for biomedical applications

Muzi Li[1], Guillermo Domínguez[1], William Solórzano-Requejo[2], Simon Pöstges[3], Alex Kopp[3], Conall Quinn[4], Jennifer Patterson[1] and Jon Molina-Aldareguía[1,2]

[1]*IMDEA Materials Institute, Getafe, Madrid 28906, Spain*

[2]*Department of Materials Science, Polytechnic University of Madrid, 28040 Madrid, Spain*

[3]*Meotec GmbH, 52068 Aachen, Germany*

[4]*National University of Ireland Galway, Galway, H91 TK33, Ireland*

The emerging field of 4D printing, which introduces time-dependent shape transformation into additively manufactured structures, offers unprecedented opportunities for dynamic biomedical applications. In this study, we explore the integration of biodegradable magnesium (Mg) and zinc (Zn) alloys—noted for their biocompatibility, mechanical properties, and controlled degradation profiles—into 4D-printed actuators designed for biomedical applications. Specifically, we focus on the application of these materials in addressing craniosynostosis, a congenital condition characterized by the premature fusion of cranial sutures, which impairs normal brain and skull growth. Traditional surgical interventions for craniosynostosis are invasive and often require repeated procedures. We propose a novel solution: 4D-printed, bioresorbable actuators composed of Mg/Zn alloys that can be implanted to apply gradual, controlled mechanical forces to promote cranial expansion over time, reducing the need for repeat surgeries.

In this work, the selected smart 4D actuator designs for the shape-morphing structures were evaluated and how the degradation of the different biodegradable metallic elements control the rate and extent of expansion of the 4D actuators were studied *in situ*, as well as the temporal evolution of their load-bearing capability. Three different actuator designs are evaluated: a serpentine spring actuator, a conical spring actuator, and an auxetic spring actuator. They are made of two different metallic alloys: nitinol, for the shape-morphing part of the actuator, and the Mg based WE43MEO alloy, for the biodegradable anchoring elements that hold the spring in its initial state. The degradation of the anchoring elements triggers the shape morphing over a period of time in multiple steps depending on their configuration and corrosion rates. The initial result of the serpentine actuator is shown in Figure 1. A Zn alloy (Zn1Mg) will replace nitinol in the next step, to make the actuator fully biodegradable.

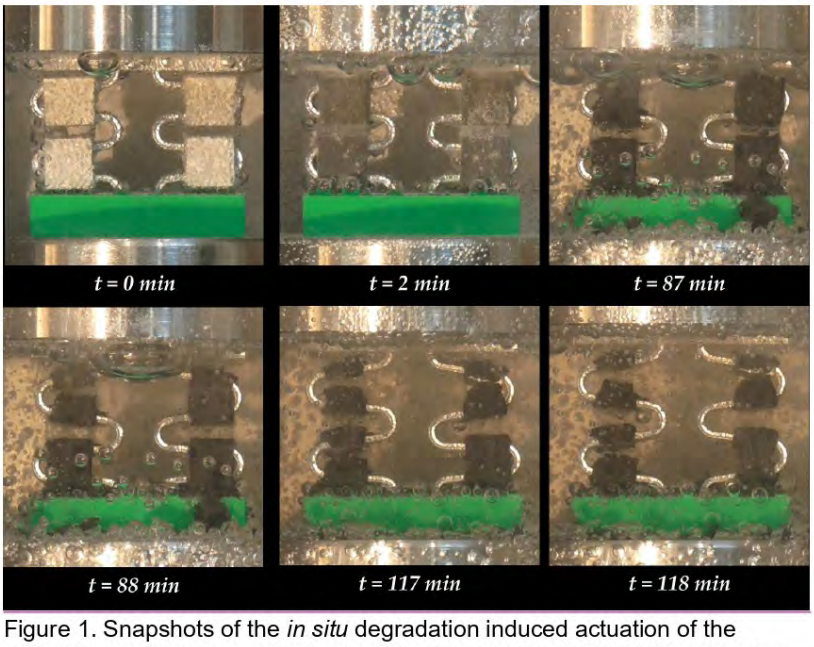

Figure 1. Snapshots of the *in situ* degradation induced actuation of the serpentine spring at specific time points. The top two WE43MEO anchoring brackets were 0.6 mm in thickness, while the bottom two were 0.8 mm thick.

European Cells and Materials Vol. NN. Suppl. N, 20xx (page htu) ISSN 1473-2262

Influence of texture on the mechanical performance of a wire-form bioabsorbable vascular scaffold

K MacLeod[1], D Nash[1], C MacLeod[2], M Steckel[2]

[1]University of Strathclyde, Glasgow [2]Lumenology Ltd., Glasgow

INTRODUCTION: Bioabsorbable vascular scaffolds (BVS) seek to improve the clinical outcomes for arterial disease relative to current drug eluting stents (DES) by elimination of the permanent foreign body implant. However, the relatively poor mechanical properties of available bioabsorbable materials, compared to the those applied in DES, has limited the success of BVS technology to date. To overcome the limitations of past BVS devices, a novel wire-form BVS device, manufactured from a Mg-Li-Y alloy is proposed. The influence that altering the material processing of the wire has on the microstructure and mechanical performance of the device is investigated herein.

METHODS: Mg-4Li-1Y alloy wire cold drawn to a diameter of 125µm was used in the manufacture of the wire-form BVS device (Figure 1a). The wire is formed through a sequential bending process into the shape of the BVS device and subsequently annealed. The device processing has then been modified to alter the dominant recrystallisation mechanisms during the required annealing step to tailor the texture for optimal mechanical performance

The microstructure of the device was characterised using SEM and EBSD analysis. Benchtop expansion and radial force testing were employed to assess its mechanical performance.

RESULTS: In the device manufactured using the original process, a split in texture is developed (Figure 1b). In contrast, the device manufactured using the modified process develops a more uniform texture distribution at the same location following the required annealing step (Figure 1c). During benchtop expansion testing, the modified device exhibits >20% increase in mechanical performance compared to the original process, whilst maintaining the same over-expansion limits.

DISCUSSION & CONCLUSIONS: The wire used to manufacture the device exhibits a typical basal texture, with the grains aligned with their c-axis perpendicular to the drawing direction. During device manufacture, tensile and compressive loading along the drawing direction of the wire results in compressive and tensile loading of the c-axis of the grains respectively. This promotes the activation of tensile twinning through regions of the wire deformed through compressive loading. Following annealing, the original device has a recrystallised microstructure dominated by grains nucleated from these tensile twins (Figure 1b+d). In contrast, using the modified process, a number of alternative nucleation sites were present in the device prior to annealing. Consequently, a range of nucleation sites are available, and a more uniform texture is developed following recrystallisation in the modified device (Figure 1c+e).

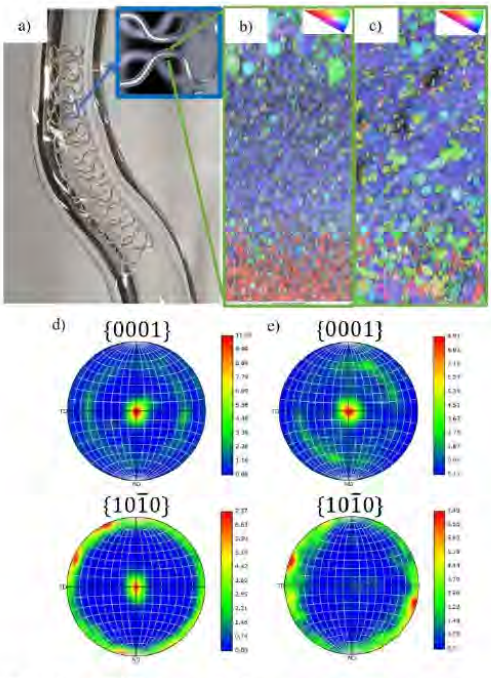

Fig. 1: a) BVS device b) Inverse pole figure map of device manufactured using original process c) Inverse pole figure map of device manufactured using modified process d) Pole figures for original process e) Pole figures for modified process

The texture developed in the modified device is more favourable for the activation of prismatic slip during device deployment. Consequently, it exhibits a >20% increase in mechanical performance compared to the original device.

ACKNOWLEDGEMENTS: This research was funded by the Medical Research Council

17th Biometal
25-30 AUGUST, 2025
Grand Hôtel San Michele,
Cetraro, CS, Italy

Liquid Ag, Zn, and Zn-based Alloys on Biodegradable Hadfield Steel for Biomedical Applications: Wettability and Interfacial Reactivity

S Gambaro[1,2], C Paternoster[2], A Bigos[3], M Janusz-Skuza[3], M Rancan[1], L Armelao[4], J Wojewoda-Budka[3], D Mantovani[2], F Valenza[1]

[1] *National Research Council, Institute of Condensed Matter Chemistry and Technologies for Energy, ICMATE, Italy*
[2] *Laboratory for Biomaterials and Bioengineering, Laval University, Quebec City, Canada*
[3] *PAS-IMMS – Polish Academy of Sciences - Institute of Metallurgy and Materials Science, Poland*
[4] *Department of Chemical Sciences, University of Padova, Italy*

INTRODUCTION: Fe-Mn steel is an interesting candidate for load-bearing biodegradable implants [1]. This kind of steel can be used together with other elements, added for specific purposes (e.g. Zn and Ag for antibacterial properties). Zn and Ag, known for antimicrobial and osteogenic properties, can be used as coatings to improve performance[2]. These alloys, which can be produced in many ways, has a strong tendence to oxidation, because of the high Mn amount; the presence of oxygen have strong effect on the formed phases when Zn and Ag are in contact. Understanding the wetting and interfacial behavior of a Fe-12Mn-1.2C with different surface chemistries (mechanically polished - MP, or oxidized under control with a plasma treatment-PO) is the key to optimize a series of processes and procedure in the fabrication of the multielement alloy.

METHODS: Fe12Mn1.2C coupons, after MP and PO, were used as two different substrates. Ag, Zn, Zn–Ag alloys were arc-melted into spherical buttons under Ar. Starting materials were characterized by SEM-EDS, XPS and 3D-profilometry before high-T tests. Wettability was assessed by sessile-drop tests in a custom alumina-tube furnace at selected temperature for each system. Microstructure and interfacial phases of cross-sectioned samples were assessed by SEM-EDS/TEM analysis.

RESULTS: XPS analysis, used to characterize the surface oxide, showed O a Fe layer. Unlike the native oxide on MP samples, which contains mixed oxides and metallic traces, the PO surface shows no metallic Mn or Fe. Depth profiling confirms a uniform oxide film ~ 100 nm thick. Zn and its alloys showed a reactive wetting on MP-Hadfield, with contact angles steadily decreasing and stabilizing after 200 s (Fig.1a). All exhibited similar slopes and symmetric drop profiles after 300 s, with final contact angles, $\theta < 20°$. In contrast, the liquids on PO-Hadfield failed to wet, maintaining $\theta > 140°$ (Fig.1b). Ag, however, behaved differently: on both substrates, θ quickly stabilized at ~ 65° after melting and remained constant to 300 s. The analyses of cross-sectioned samples showed that continuous interfacial layers of Fe-Zn and Fe-Zn-Ag intermetallic compounds formed at Zn-based liquid and MP-substrate. No metal diffusion nor interfacial layers were instead found for pure Ag/Hadfield system.

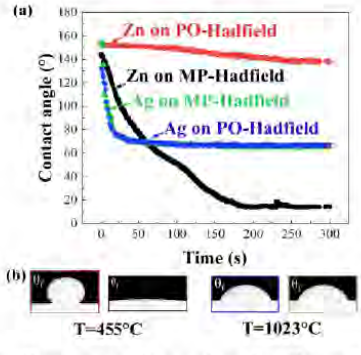

Fig. 1: Contact angle vs *time for Zn and Ag on MP- and PO-Hadfield (a); drop profiles after 300 s at the selected temperature (b).*

DISCUSSION & CONCLUSIONS: Zn and Zn–Ag alloys showed ideal wetting on MP-Hadfield, making them suitable for industrial use, but failed to wet the PO surface. In contrast, Ag wetted both substrates without forming a reactive layer, likely due to its ability to dissolve O in the liquid state. Due to the low contact angle and distribution of the intermetallic phases, Zn7Ag/MP-Hadfield interface seemed to be the most promising and its corrosion and biocompatibility need to be assessed.

REFERENCES: [1] S Gambaro et al (2021) Mater Today Commun 7. [2] M Hussain et al (2022) J Funct Biomater 14.

ACKNOWLEDGEMENTS: Memorandum of Understanding between CNR-ICMATE (Genoa, IT) and Laval University-LBB (Quebec, CA).

European Cells and Materials Vol. NN. Suppl. N, 20xx (page htu) ISSN 1473-2262

Microstructural and degradation evaluation of Fe-based biodegradable scaffolds fabricated using polyurethane templates

M Grodzicka[1], G Gąsior[1], A Radtke[1]

[1] *Nicolaus Copericus Univerity in Torun, Faculty of Chemistry, Poland*

INTRODUCTION: Biodegradable materials in biomedical engineering, such as iron alloys, represent a promising solution in orthopaedic implantology. Their advantage is that they can be degraded in a physiological environment, eliminating the need for surgical removal of the implant once it has fulfilled its function. Iron and its alloys have good biocompatibility and adequate mechanical properties, but their corrosion rate is relatively low, which may limit their use in implantology. The addition of elements such as manganese and copper allows the rate of degradation to be accelerated and regenerative processes to be actively promoted. Manganese stimulates angiogenesis by regulating growth factors (e.g. VEGF), stabilises the HIF-1α pathway and reduces oxidative stress in endothelial cells[1]. In addition, it promotes macrophage polarisation towards the M2 phenotype, promoting tissue healing and remodelling[2]. Copper exhibits anti-inflammatory and anticoagulant effects and promotes collagen synthesis and vascular regeneration[3]. Its presence in biomaterials benefits endothelial function, strengthens the structure of regenerating tissues and protects cells from oxidative stress. Fe-Mn and Fe-Cu alloys, due to their modified microstructure and electrochemical properties, degrade much faster than pure iron and represent a promising group of materials for temporary bone implants.

METHODS: The materials studied were: Fe, Fe35Mn, Fe1Cu and Fe35Mn1Cu (designations: Fe, FeMn, FeCu, FeMnCu). Alloys were produced from Fe, Mn and Cu powders using polyurethane (PU) foam as a template. The foams were moulded and dipped in a mixture of metal powders with a 5% polyvinyl alcohol solution (1:2 by weight), dried (95°C, 35 min) and then sintered in a tube furnace (Czylok). Morphology was analysed by SEM (Quanta 3D FEG), elemental composition by EDS (Bruker) and crystalline phases by XRD (Philips X'Pert, CuKα, incident angle 2°). Degradation was studied by potentiodynamic polarisation (BioLogic SP-200) in HBSS (37 ± 2 °C, range ±250 mV vs OCP, 0.5 mV/s). Three-electrode system: working electrode, counter electrode (Pt), reference electrode (Ag/AgCl). The corrosion current density was determined using the Tafel extrapolation method.

RESULTS: FeCu, FeMn and FeMnCu scaffolds were obtained using a polyurethane template, perfectly reproducing it. However, differences in alloy morphology can be seen. In the FeMn sample, the pore walls are thinner and smoother than in the FeMnCu sample. The FeMnCu foam shows the least homogeneous pore wall structure of all the samples analysed. The pore walls in the FeCu alloy are the smoothest. In the FeMn-PU samples, the manganese content was significantly higher than the assumed 35wt%. Local fluctuations in chemical composition were recorded, related to the tendency to form larger metal element clusters.

DISCUSSION & CONCLUSIONS: All analysed iron alloys obtained with the PU template showed a porous structure that reproduced the foam geometry well. FeCu stood out for having the thinnest, smooth walls. In the FeMn and FeMnCu samples, more variability in microstructure was observed, especially in the case of FeMnCu, where the structure was the least homogeneous. EDS analysis revealed an excess of the assumed manganese content (35 wt%) in the FeMn sample, indicating its local accumulation and uneven distribution in the material. This may affect the control of the degradation process and the mechanical properties of the implants. In conclusion, the PU template allows regular porous structures to be obtained. The inhomogeneous distribution of Mn in the scaffold requires further optimisation.

REFERENCES: [1]Wu Jinfu, Qin C *et al.* An immunomodulatory bioink with hollow manganese silicate nanospheres for angiogenesis. *Applied Materials Today*. 2021; 23: 101015.

[2] Wang J, Wang Y et *al.* A Bioinspired Manganese-Organic Framework Amelioratez Ischemic Stroke through its Intrinsic Nanozyme Activity and Upregulating Endogenous Antioxidant Enzymes. *Advanced Science*. 2023; 10: 2206854.

[3] Yue F *et al.* Dealloyed nano-porous TiCu coatings with controlled copper release for cardiovascular devices. *Biomaterials Advances*. 2024; 157: 213728.

17th Biometal
25-30 AUGUST, 2025
Grand Hôtel San Michele, Cetraro, CS, Italy

European Cells and Materials Vol. NN. Suppl. N, 20xx (page htu) ISSN 1473-2262

Natural ageing and static recrystallisation effects of additively manufactured biodegradable pure Zn and Zn-Mg alloys

H Abenayake[1], L Dieter[1], C Persson[1], F D'Elia[1]

[1] Division of Biomedical Engineering, Department of Materials Science and Engineering, Uppsala University, Sweden

INTRODUCTION: Powder bed fusion–laser beam (PBF-LB) processing of Zn-Mg alloys has gained attention as a promising approach for fabricating biodegradable, patient-specific implants[1]. Although alloying Zn with Mg contents ≤ 1 wt.% enhances tensile performance[2], natural ageing (NA) remains a persistent challenge[3]. This is due to Zn's low melting point, which enables significant atomic diffusion at low temperatures, resulting in an exceptionally low recrystallisation temperature and undesirable changes in mechanical properties over time. Studies on conventionally processed Zn-Mg alloys have reported increased tensile strength over time, accompanied by a significant reduction in ductility, attributed to Mg_2Zn_{11} precipitation[4]. To date, no comprehensive studies have examined the static recrystallisation (SRX) behaviour of pure Zn, or the NA characteristics of Zn-Mg alloys produced via PBF-LB. This work addresses that gap by evaluating the SRX and NA behaviour of PBF-LB processed pure Zn and Zn-1Mg (wt.%) at room temperature (RT) and body temperature (37 °C).

METHODS: Alloys were prepared by mechanical mixing of Zn and Mg powders. Constructs were fabricated using an Aconity Midi PBF-LB system with optimised process parameters (P_L = 60 W, v = 300 mm/s, h = 0.04 - 0.05 mm), achieving > 99.5% relative density. The evolution of mechanical properties of samples aged at RT and 37 °C was assessed by microhardness measurements and compression testing over 90 days. These changes were correlated with microstructural observations obtained via scanning electron microscopy (SEM) and energy dispersive X-ray spectroscopy (EDS). Grain size distribution and precipitation behaviour were examined using EBSD (electron backscattered diffraction) and Rietveld refinement of X-ray diffraction (XRD) patterns. Statistical analysis was performed using SciPy in Python.

RESULTS: The microhardness of pure Zn remained stable at RT but declined at 37 °C after 60 days (Fig. 1). Zn-1Mg showed stable hardness at RT for 30 days yet dropped significantly by 60 days. Similarly, Zn-1Mg exhibited a continuous decline in hardness at 37 °C, with a pronounced drop by 60 days. This trend correlates with the substantial reduction in the $MgZn_2$ phase fraction over time (Table 1).

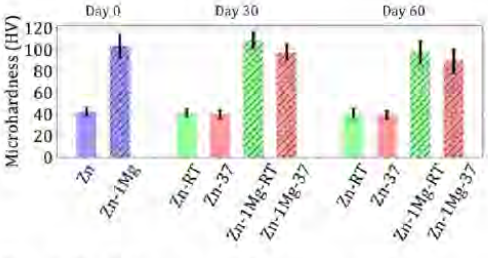

Fig. 1: Evolution of microhardness with time

Table 1. Variation of $MgZn_2$ phase fraction over time in PBF-LB Zn-1Mg alloy

T (°C)	$MgZn_2$ phase fraction (%)		
	0 days	30 days	60 days
RT	1.67 ± 0.06	1.51 ± 0.06	1.49 ± 0.06
37 °C		1.06 ± 0.06	0.98 ± 0.06

DISCUSSION & CONCLUSIONS: At RT, SRX has minimal impact on PBF-LB pure Zn, as indicated by stable microhardness over time. In contrast, the Zn-1Mg shows significant variations, reflecting pronounced natural ageing effect. The temperature-dependent trends in Zn-1Mg further confirm the strong impact of temperature on ageing, primarily driven by the transformation of the hard and brittle $MgZn_2$ intermetallic into more stable phases. In conclusion, PBF-LB Zn-Mg alloys show notable temperature-dependent natural ageing effects. Future works will focus on mitigating this issue through multi-component alloying and optimisation of printing parameters.

REFERENCES: [1]M Voshage et al., Mater Today Commun, 2022, 32, 103805. [2]E. Mostaed et al., Acta Biomater., 2018, 71, 1–23. [3]H. Jin et al., Mater. Sci. Eng., 2018, 84, 67–79. [4]M. S. Ardakani et al, Mater. Sci. Eng., 2020, 770, 138529.

ACKNOWLEDGEMENTS: This work is conducted within the AM4Life Competence Centre with financial support from VINNOVA, Swedish Research Council, and EU.

European Cells and Materials Vol. NN. Suppl. N, 20xx (page htu) ISSN 1473-2262

On the possibility of additive manufacturing of Mg-Zn-Ca biodegradable alloys

A.Dobkowska [1], J. Ciftci [2], Ł. Żrodowski [2], W. Święszkowski [1]

[1] Faculty of Materials Science and Engineering, Warsaw University of Technology, Warsaw, Poland [2] Amazemet Ltd., Warsaw, Poland

INTRODUCTION: The use of additive manufacturing for the production of biomedical Mg alloys addresses challenges associated with fabricating implants of complex shape and geometry using conventional methods such as extrusion or turning[1]. This approach can significantly reduce manufacturing costs, increase process efficiency, and potentially enhance the properties of Mg implants. Nevertheless, the additive manufacturing of Mg alloys requires a comprehensive understanding of both the process and the material, particularly the optimization of parameters that determine the alloy's final properties[2]. In this study, we attempted to fabricate Mg-Zn-Ca alloys using laser powder bed fusion (LPBF) with custom-made powder materials atomized via an induction method.

METHODS: The cast rods of ZX00, ZX50, and ZX50+Ag were atomized via ultrasonic atomization using a rePowder device (AMAZEMET, Poland). The alloy was melted in a graphite crucible. The molten alloy was poured using pressure differential pressure through nozzle on a plate-type sonotrode. The bulk materials in a cubic form 10×10×10 mm^3 were printed using AconityMIDI+ printer (Aconity3D, Germany). The particle size distribution was analyzed using Horiba LA-950 laser scattering particle size distribution analyzer. The printed materials were scanned using a microfocused X-ray tomographic system (MicroXCT- 400, Xradia - Zeiss), at 40 kV and 200 µA. The microstructure of the materials was characterized using scanning electron microscope (SEM, Hitachi SU70, Japan) equipped with Bruker EBSD detector. Afterwards, corrosion properties of the alloys were investigated using electrochemical methods and immersion tests. The antibacterial properties were tested.

RESULTS: As a result of the atomization process, powders with high sphericity were produced (Fig. 1). The average particle size varied depending on the chemical composition of the alloys, measuring 201 µm for ZX00, 107 µm for ZX50, and 118 µm for ZX50+Ag. Chemical composition analysis confirmed that no Zn evaporation occurred, and Ag was still present in the powder particles. The printed alloys exhibited a density of approximately 95%. Depending on their chemical composition, the resulting microstructures varied. As shown in Fig. 2, the addition of Ag to ZX50 affected microstructural recrystallization, leading to the formation of the equiaxed grains.

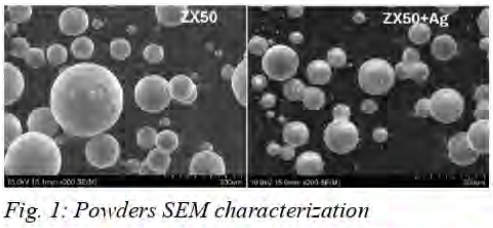

Fig. 1: Powders SEM characterization

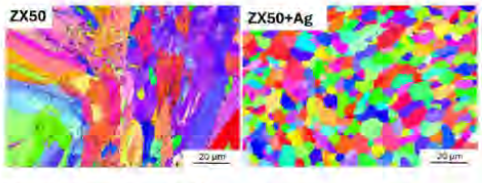

Fig. 2: Inverse pole figures maps

The electrochemical measurements and immersion tests demonstrated that corrosion behavior is highly dependent on the microstructure, with porosity playing a predominant role in the degradation performance.

DISCUSSION & CONCLUSIONS:

Modern powder production methods enable a broad research perspective on critically important biodegradable alloys for biomedical applications. The chemical composition of alloys can be tailored to impart desired properties, such as antibacterial activity. By mitigating porosity in additively manufactured magnesium alloys, their corrosion resistance can be significantly enhanced.

REFERENCES: [1]D. C. Martinez et al., Bioact. Mater., vol. 28, no. April, pp. 132–154, 2023, doi: 10.1016/j.bioactmat.2023.05.004. [2]A. Dobkowska et al., J. Magnes. Alloy., vol. 10, no. 12, pp. 3553–3564, 2022, doi: 10.1016/j.jma.2022.06.003.

ACKNOWLEDGEMENTS: The research founded by the Warsaw University of Technology within the Excellence Initiative: Research University (IDUB) programme.

European Cells and Materials Vol. NN. Suppl. N, 2025 (page htu) ISSN 1473-2262

Opioid-sparing non-surgical, bioresorbable nerve stimulator for pain relief

K Woeppel[1], T Emerick[1,2], XT Cui[1,3]

[1] Vanish Therapeutics, Pittsburgh, United States. [2] University of Pittsburgh Medical Center, Pittsburgh, United States. [3] Department of bioengineering, University of Pittsburgh, United States

INTRODUCTION: According to the 2012 Nation Health Interview Survey, an estimated 11.2% of the USA adult population suffers from daily chronic pain[1] with an economic burden exceeding $600 billion in the USA[1], and pharmaceutical treatments have fuelled the opioid epidemic. Neurostimulation offers an alternative to opioids, using electrical stimuli to modulate the perception of pain, and studies have shown that stimulation for as little as 60 days can produce long term relief.[2] However, neural stimulation is highly invasive, requiring surgical implantation, with a high risk of complications. Efforts have been made to produce minimally invasive forms of neural stimulation, but these devices often require a secondary removal operation and can fracture,[3] permanently leaving foreign materials in the patient and preventing participating in medical procedures like MRI. In response, we have developed non-surgical, fully bioresorbable peripheral nerve stimulation (PNS) device that provides analgesic stimulus for 60 days and rapidly degrades thereafter. Further, degradation can be activated at any time in the event of complications, reducing the need for secondary procedures.

METHODS: The bioresorbable PNS electrode is fabricated from zinc, a bioresorbable metal, and a custom bioresorbable polyurethane insulation. The insulation is applied to the zinc wire by dip-coating and a custom stimulator PCB is used to deliver analgesic pulses. For *in vitro* stimulation, we utilize a -20mA 200µs cathodic leading stimulus followed by a 10mA 400µs anodic phase. We measured the electrochemical impedance (EIS) and voltage transients after 1K, 250M, and 550M stimulations. We then demonstrated rapid degradation on command (DOC), applying a 100Hz on/off 1mA anodic stimulus to degrade the Zn wire. We then validated our device in a rat model, where stimulation was applied at an accelerated pace to examine the device performance, safety, and DOC efficacy *in vivo*.

RESULTS: Fabricated Zn leads were effectively insulated via the dip-coating procedure (*Fig. 1A*), and resulting electrodes were stable in both voltage transients and electrochemical impedance after 550M stimulations (*Fig. 1B,C*), the equivalent of 60 days under therapeutic conditions. DOC stimulation controllably degraded the Zn from the outside in, as shown by the elevated Oxygen detected in the outer layer under energy dispersive x-ray spectroscopy (EDS) (*Fig. 1D*). Unlike stainless steel, the DOC stimulation did not result in unsafe charge build-up, indicating the electrochemical safety of DOC (*Fig. 1E*).

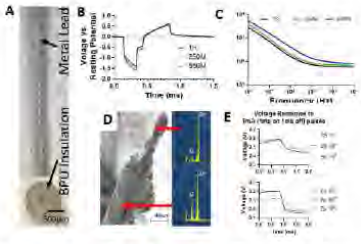

Fig. 1: A) insulated wire. B) and C) voltage transients and EIS of the wire during stimulation. D) EDS of DOC wire. E) Voltage during DOC

Following implantation in rats, the device was connected to a custom PCB which applied continuous therapeutic stimulation for up to 3 weeks and DOC (*Fig. 2A*). Rat behaviour was normal and electrodes rapidly degraded under DOC (*Fig. 2B*).

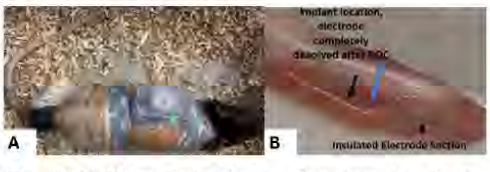

Fig. 2. A) Rat with implant and custom stimulator. B) explant electrode in tissue by sciatic nerve with electrode site degraded.

DISCUSSION & CONCLUSIONS: New methods of pain treatment are greatly needed. We have developed and validated a bioresorbable PNS device that can provide stimulation for 60 days of therapy and then rapidly degrade thereafter. The bioresorbable PNS platform hold great potential for non-pharmaceutical chronic pain treatment.

REFERENCES: [1]R. Nahin (2015) *J Pain.* [2]C. Gilmore et al. (2019) *Reg Anesth Pain Med.* [3]C. Gilmore et al. (2019) *Regional Anesthesia & Pain Medicine*.

ACKNOWLEDGEMENTS: This work was funded by the National Institute of Health R41NS132625 under the HEAL initiative.

European Cells and Materials Vol. NN. Suppl. N, 20xx (page htu) ISSN 1473-2262

Optimization of 3D printing parameters to densify the microstructure of FeMnC alloys for biomedical applications

C.A. Cuao-Moreu[1], Carlo Paternoster[1], Simon Gélinas[2], Paolo Mengucci[3], Carl Blais[2] and Diego Mantovani[1]

[1]Laboratory for Biomaterials and Bioengineering, CRC-1, Dept of Min-Met-Materials Engineering and Research Center of CHU de Québec, Division of Regenerative Medicine, Laval University, Quebec City, Canada; [2]Laboratory for Powder Metallurgy, Department of Min-Met-Materials Engineering, Laval University, Quebec City, Canada; [3]Department SIMAU & UdR INSTM, Università Politecnica Delle Marche, Ancona, Italy

INTRODUCTION: The demand for biomedical implants has increased recently, particularly for scaffolds to treat large bone defects or fractures and promote bone regeneration. Recent studies have focused on biodegradable ones (Mg, Zn, and Fe). Fe-based alloys exhibit superior mechanical properties but have a slower corrosion rate than Mg and Zn alloys. To overcome this challenge, different elements like Mn can be incorporated [1,2]. Also, non-conventional fabrication techniques, like 3D printing through Laser Powder Bed Fusion (LPBF) [3], lead to complex microstructural changes affecting the degradation rate, simultaneously allowing the fabrication of complex structures, and creating the wished microstructural features. Typically, LPBF employs pre-alloyed spherical powders ($Ø$ = ~20 ÷ 55 µm), but these are generally produced costly through atomization. Nevertheless, optimizing the 3D-printing parameters for using elementary powder to cut down the powder production cost is an important aspect that is proposed to keep the wished (microstructural, mechanical) properties, reducing the powder fabrication steps. The present work deals with the optimization of the fabrication process of a Fe-12Mn-1.2C alloy, its characterization, and evaluation of the performances through a fabrication process based on quasi-elemental powders.

METHODS: Commercial AISI 1025, Mn and graphite powders were mixed in appropriate amount, pre-sintered in an Ar-feed tubular furnace, and then milled, to improve their flowability. A laser power P in the range 50 – 140 W, and a laser speed in the range 270 – 1030 mm/s were used during the printing, to obtain a volumetric energy E_V in the range 60-200 J/mm^3. Powder morphology and chemical distribution were analyzed through scanning electron microscopy (SEM), and energy dispersive spectroscopy (EDS). Crystallographic structure information was gathered via X-ray diffraction (XRD) while the porosity and microstructure of the sintered samples were examined with optical microscopy.

Fig.1: Printed samples at 140 W (left). Optical micrograph for a (right) 101-W printed sample, (Nital 2 vol%.)

RESULTS & DISCUSSION: A relevant porosity decrease was obtained with increasing laser powers (Fig. 1 - left). After a certain E_V threshold, the particles completely melt, decreasing porosity during solidification: a laser power over 100 W was required to achieve denser samples. An irregular grain shape was obtained, for all the conditions (Fig. 1 – right). Due to the rapid melting process and high cooling rates during LPBF, a random arrangement of irregularly shaped grains was observed, organized in a hierarchal microstructure and with a fine cellular structure. All the investigated condition showed an austenitic microstructure, with traces of other phases (α-, α'-, and ε-Fe). The interdiffusion of elements was already relevant during the powder pre-sintering and milling of the starting powders.

CONCLUSION: The sintering process improved the flowability of the elemental powder, allowing the printing of homogeneous microstructures, whose porosity needs to be optimized. The used printing parameters were similar to those used for printing of prealloyed powders.

REFERENCES: [1]Razavi, M., et al. *Acta Biom.*, 2017. [2]Li, G., et al. *Mat. Sci. and Eng. C*, 2020. [3]Haverkamp, C., et al. *J. of Materials Mat. Res. and Tech.*, 2021.

ACKNOWLEDGEMENTS: This research was partially supported by the Laboratory for Biomaterials and Bioengineering, the Natural Science and Engineering Research Council of Canada, Prima Quebec, and the CHU de Quebec Research Center.

European Cells and Materials Vol. NN. Suppl. N, 20xx (page htu) ISSN 1473-2262

Oxygen Plasma Immersion Ion Implantation on AZ31B for Clinical Applications

Malvestiti L[1,2], Paternoster C[1], Beraldo C[1], Ceré S[2], Mantovani D[1]

[1]Lab. for Biomaterials and Bioengineering, CRC-I, Department of Min-Met-Materials Eng., University Hospital Research Center, Regenerative Medicine, Laval University, Québec, Canada; and [2]INTEMA-CONICET, Mar del Plata National University, Argentina

INTRODUCTION: Mg-based alloys have been extensively studied for temporary implants due to their biodegradability, biocompatibility, mechanical properties, and biological functions of Mg^{+2} [1]. However, their main limitation is its high corrosion rate in physiological environment triggering an immune response. To reduce the degradation rate and improve biological response, an oxygen plasma-immersion ion implantation (O-PIII) treatment has been proposed [2]. Through O-PIII, a relatively homogeneous magnesium oxide is generated on the alloy surface. Moreover, Mg topography, wettability and electrochemical behavior were also modified, enhancing the interface between Mg based alloy- physiological environment.

METHODS: A commercial AZ31B alloy (Al 3 wt.%, Zn 1 wt.%, Mg bal.) was treated. After chemical polishing, an O-PIII was performed in a PBII-300 system (Plasmionique, Varennes, CA) varying different working parameters, such as working pressure (P_W – 5 to 50 mTorr), plasma exposition time (t_d – 60 to 300 min.) and pulse repetition rate (f – 200 to 1000 Hz). The morphological, chemical and electrochemical characterization were carried out by scanning electron microscopy (SEM), X-ray photoelectron spectroscopy (XPS), static drop contact angle, X-ray diffraction (XRD), and potentiodynamic polarization curves in Hanks' solution.

RESULTS: The alloy was chemically polished before O-PIII (as-received condition, AR). The plasma treatment introduced different surface features depending on the used parameter values (Fig. 1), which affected the morphology, roughness, chemical composition, and corrosion resistance. In particular, after O-PIII, XPS revealed a general increase in surface oxygen content with increasing pressure, reaching values in the range of ~35–40 at. %; O was bound to the metallic substrate mainly in the form of metal oxides and hydroxides [3]. The hydrophilicity of the treated surfaces decreased, from ~40° for AR to a minimum value for lower P_W and shorter t_d (~100°). After O-PIII, the corrosion rate (CR), proportional to the corrosion current was reduced by half, modifying also the corrosion pattern of the material. XRD showed the presence of a modified alloy texture, after the implantation process, especially at high implant pressure, likely due to the heath exchange related to the process.

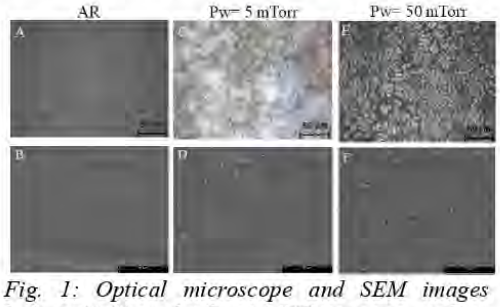

Fig. 1: Optical microscope and SEM images before (A-B) and after O-PIII varying working pressure (C-F).

DISCUSSION & CONCLUSIONS: The final surface morphology after implantation was modified in terms of surface chemical composition (O amount, presence of Mg oxide and hydroxide-related species), the roughness, and the physical properties (such as surface energy), being influenced by the alloy features (grain boundaries, precipitates, second phases, surface texture, etc.). The presence of a surface O-rich layer can also affect the formation of corrosion products. These results support the use of O-PIII technique and selected parameters as a potential surface modification, constituting a valid approach for clinical application. Biological tests related to cell viability (osteoblasts and neuronal cells) and hemocompatibility are carried out.

REFERENCES: [1]X. Zhang et al., J. Biomater. Appl. 35 (2021) 1275-1283. [2]M. Benčina et al., Molecules. 26 (2021). [3]S. Feliu et al., Appl. Surf. Sci. 347 (2015) 736-746.

ACKNOWLEDGEMENTS: LBB, NSERC-Canada, Prima Quebec, and the CHU de Quebec Research Centre. LM was awarded PhD scholarship from CONICET, Argentina.

17th Biometal
25-30 AUGUST, 2025
Grand Hôtel San Michele, Cetraro, CS, Italy

European Cells and Materials Vol. NN. Suppl. N, 20xx (page htu) ISSN 1473-2262

Powder-based precipitation simulation of a MgZnCa alloy

B. Alonso Rancurel[1,2], V. Shtender[1], D. Primetzhofer[3,4] F. D'Elia[1], M Fisk[5], C Persson[1,2]

[1]*Biomaterials System, Department of Material Science and Engineering, Uppsala University,* [2]*Wallenberg Initiative Materials Science for Sustainability, Department of Material Science and Engineering, Uppsala University,* [3]*Department of Physics and Astronomy, Uppsala University,* [4]*Tandem Laboratory, Uppsala University,* [4]*Department of Materials Science and Applied Mathematics, Malmö University*

INTRODUCTION: Developing biodegradable implants is of growing interest to help fight antimicrobial resistance. Magnesium alloys are candidates for orthopaedic applications, but there is a need for improving their corrosion resistance[1]. Alloying reduces corrosion rates, but further improvement could be achieved by microstructural tuning using additive manufacturing (AM). However, process parameter optimization is time and resource consuming, motivating the use of numerical modelling to accelerate alloy development. The aim of this study was to predict the microstructure-temperature relationship for a MgCaZn alloy using the CALPHAD method as input for a classical nucleation and growth theory (CNGT) simulation. To achieve this, raw powder feedstock was characterized, along with a minimal number of printed samples.

METHODS: The powder composition was identified as $Mg_{63.2}Zn_{32}Ca_{4.8}$ by Inductively Coupled Plasma – Optical Emission Spectroscopy (ICP-OES) and compared to the results of ToF-ERDA (Time-of-Flight Elastic Recoil Detection Analysis). The composition of printed samples was also measured to estimate evaporation rates during printing.

X-ray diffraction (XRD) was used for phase identification. Differential Scanning Calorimetry (DSC) was used to characterize phase transitions and generate Time-Temperature-Transformation (TTT) and Continuous-Heating-Transformation (CHT) diagrams.

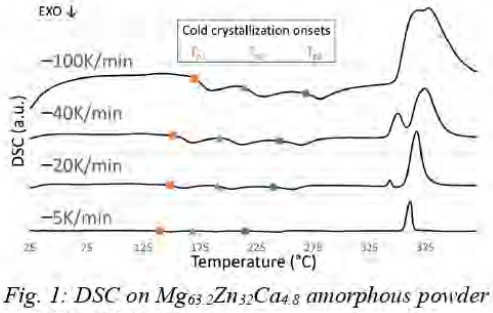

Fig. 1: DSC on $Mg_{63.2}Zn_{32}Ca_{4.8}$ amorphous powder at different heating rates.

RESULTS: Three cold crystallizations were distinguished (see Figure 1) and analysed by XRD. Kissinger analysis[2] was done on four heating rates and the results are shown in Table 1 together with the transformation onset temperatures. Metastable phases were formed at the first (T_{p1}, phase $Mg_{51}Zn_{20}$) and second crystallisation (T_{p2}, IM4). Thermodynamic data and unit cell parameters from experimental results and literature[3] were used in a Python code to simulate CHT and TTT diagrams for comparison with the experimental results. The experimental data was used to validate the numerical model.

Table 1. Transformation onsets in function of heating rates, and activation energy (E_a) results.

Heating rate [°C / min]	T_{p1} [°C]	T_{p2} [°C]	T_{p3} [°C]
5	139	168	215
20	149	190	240
40	152	193	245
100	171	214	268
E_a [kJ / mol]	132	111	117

DISCUSSION & CONCLUSIONS: The overall transitions and phases agreed with previous literature, with only significant differences in the obtained energies of activation. The first simulated TTT diagram to our knowledge has been generated for this composition and phases. Synchrotron studies and more compositions should be tested for proper validation of the methodology.

REFERENCES: [1]Radha, R., & Sreekanth, D. (2017), *J. Magnes. Alloy*, **5(3)**, 286–312. [2]Kissinger, H. E. (1957) *Anal. Chem.*, **29(11)**, 1702–1706. [3]Mezbahul-Islam, M. et al. (2014) *Calphad*, **46**, 134–147.

ACKNOWLEDGEMENTS: *This work was supported by the Wallenberg Initiative Materials Science for Sustainability (WISE) funded by the Knut and Alice Wallenberg Foundation and the Swedish Research Council (grant numbers 2019-00191 and 2023-00155) supporting the Ion Technology Center.*

European Cells and Materials Vol. NN. Suppl. N, 20xx (page htu) ISSN 1473-2262

Printability, microstructure formation, and material properties for L-PBF of binary Mg-Li alloys

S Kotiadis[1], C Persson[1], T Choma[2], F D'Elia[1]

[1]Division of Biomedical Engineering, Department of Materials Science and Engineering, Uppsala University, Uppsala, Sweden [2]Amazemet Sp. z o.o. [Ltd], Warsaw, Poland

INTRODUCTION: The biodegradation of magnesium (Mg) implants reduces the need for secondary surgeries, while the similar elastic modulus to bone prevents stress shielding [1]. Indeed, Mg alloys have been used in vascular stents and bone fixation implants. Additive manufacturing (AM) has allowed for advancement in biomedical implant design, primarily due to fabrication of custom components [1]. One disadvantage however, hindering the implementation of AM-fabricated Mg alloys is their limited ductility, given e.g., the propensity of texture formation during such processing. Magnesium-lithium (Mg-Li) alloys can aid in this regard, due to the formation of BCC at Li contents above 11.7wt.%. These alloys are also notable for their ultra lightweight and biocompatibity [2], and in alloys containing BCC Li-phases, improved corrosion resistance is seen through generation of a protective Li_2CO_3 layer. Nevertheless, AM processing of Mg-Li alloys is to the best of our knowledge, yet to be reported. Hence, the aim of this study was to investigate the processability of binary Mg-Li alloys using AM, specifically through laser-powder bed fusion (L-PBF). Both a single- (α-Mg) phase and dual-phase (α-Mg + β-Li) alloy were processed, and evaluated for mechanical properties and corrosion resistance.

METHODS: Laser surface remelting was first carried out on an EOS M100 (EOS GmbH, Germany) to evaluate the effect of rapid solidification on microstructure formation in both Mg-Li alloys. Here, laser tracks were deposited on cast substrates at powers ranging from 15 to 100 W at a speed of 80 mm/s. Melt pool microstructure was characterised by SEM and TEM, setting the stage for fabrication of bulk components by L-PBF.

For bulk printing, ultrasonic atomized powder (Amazemet, Poland) was used as feedstock on an Aconity Midi (Aconity GmbH, Germany) L-PBF printer. Process optimization was performed primarily by varying laser power and scan speed, and sample quality was characterised through density measurements using optical microscopy. Finally, microhardness and hydrogen evolution measurements were performed.

RESULTS: Micrographs in Fig. 1 depict the melt pool microstructure for both alloys at 50 and 65 W. Laser power did not impact the microstructure of the single-phase alloy, where columnar dendrites were predominant throughout. In contrast, a profound effect was seen in the dual-phase alloy, with a transformation from cellular-dendritic substructure at 50W (Fig. 1c) to that of eutectic nano-lamellae at 65W (Fig. 1d). Microhardness and hydrogen evolution were strongly influenced by alloy microstructure, with the dual-phase alloy showing a unique ability to tailor material properties through process-induced microstructural transformations.

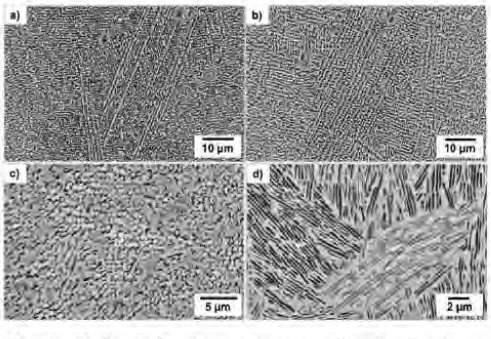

Fig 1. Melt pool microstructure of a single-phase Mg-Li alloy at a) 50W and b) 65W laser powers, and a dual-phase Mg-Li alloy at c) 50W and d) 65W laser powers.

DISCUSSION & CONCLUSIONS: The results demonstrate feasibility in processing Mg-Li alloys by L-PBF, highlighting the potential for the tailored fabrication of Mg-Li components, particularly for dual-phase alloys. Controlled processing of such alloys can enable enhanced versatility by tailoring material properties through unique microstructural transformations. Future work aims to further characterise mechanical and corrosion properties.

REFERENCES: [1] R. Karunakaran, S. Ortgies, A. Tamayol, et al (2020) *Bioact. Mater.* **5**:44-54. [2] W.R. Zhou, Y.F. Zheng, M.A. Leeflang, et al (2013) *Acta Biomater.* **9**:8488-8498.

ACKNOWLEDGEMENTS: This work is funded by the Carl Trygger Foundation (CTS 23-2980), and the EU Horizon 2020 Programme (Marie Curie - 101110609).

17th Biometal
25-30 AUGUST, 2025
Grand Hôtel San Michele,
Cetraro, CS, Italy

European Cells and Materials Vol. NN. Suppl. N, 20xx (page htu) ISSN 1473-2262

Shelf-life and stability of simulated body fluids used for in vitro tests biodegradable alloys

C. D. dos Reis Barros[1], J. A. C. Ponciano Gomes[1]

[1] *Labcorr, COPPE/UFRJ, Federal University of Rio de Janeiro, Rio de Janeiro, Brazil*

INTRODUCTION: In vitro biomaterials testing recommends the use of several simulate body fluids solutions. The literature reports a wide variety of formulations, from variable salinity inorganic to organic based complex solutions. The assessment of the same material in different media can yield varying results, as dissolution rates and formation of different corrosion products layers. The instability of these solutions, particularly when considering pH fluctuations and degradation in over extended test periods, may result in unreliable values of dissolution rates and surface morphologies [1-3]. This study aimed to characterize the physicochemical stability of the commonly used solutions for in vitro tests of biodegradable alloys, focusing both on their shelf-life stability, and their stability under long term experimental conditions.

METHODS: The solutions selected for this study were: Hanks Balanced Salt Solution (HBSS), Simulated Body Fluid (SBF), and Dulbecco's Modified Eagle Medium (DMEM). HBSS was evaluated in both commercial and prepared in laboratory. DMEM solution was evaluated with no supplementation, and with FBS and penicillin supplementation. The study period of 90 days was established, with analysis made at intervals of every 15 days. The shelf-life stability was conducted through pH, conductivity, and visual inspections. For shelf-life stability, aliquots obtained from storage conditions, 8±2°C, were analysed at 37±1 °C. The stability under testing conditions, was conducted in double-walled cells maintained at 37±1 °C during all study period, in setups like those used in immersion tests, also evaluated regarding pH, conductivity, and visual inspection at all proposed time points. In compliance with pH criteria, a range of 7.4 ± 0.2 was considered, as recommended by standards for in vitro evaluations aiming at simulating the human body environment.

RESULTS: SBF, commercial HBSS, and both DMEM solutions showed the ability to maintain pH values in accordance with the criteria, when stored under recommended conditions. Lab-prepared HBSS demonstrated shelf-life stability in pH for up to 60 days, when storage in similar recommended conditions to the commercial one. Under experimental conditions, such as immersion tests, with a continuous maintenance at 37 ±1°C, in the visual inspection only SBF remained without visual changes, HBSS solutions changed from reddish-orange colour to red, remained in this tone. DMEM solutions after 7 days, achieved a pinkish red tone shifted to purple, and increased turbidity, up to 30 days. This modification suggests the degradation of the environment. Only SBF showed the capacity to maintain pH for a long period within the required range. The commercial HBSS, as well as both DMEM exhibited an overall increase in pH over time, up to 15 days. The lab-prepared HBSS remained below the range in the period of 15 to 30 days, returning to the range in 60 days, thereafter, following at lower values than that, as disposal in Figure 1.

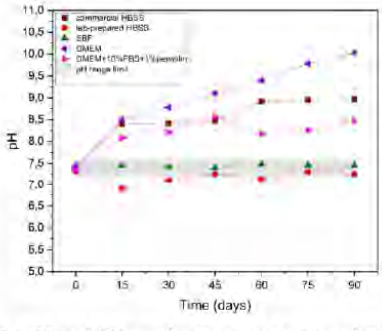

Fig. 1: pH stability under in vitro test conditions.

CONCLUSIONS: A shelf-life storage up to 90 days can be considered adequate for SBF, commercial HBSS and DMEM. Laboratory prepared HBSS exhibit lower shelf-life stability, 60 days. Under experimental conditions, the SBF solution showed better physical and chemical stability and was the best choice to perform long term in vitro tests.

REFERENCES: [1] J. Gonzalez et al. (2018) *Bioactive materials* **3**(2):174-185. [2] K. Törne, A. Örnberg and J. Weissenrieder (2017) *J Biomed Mater Res Part B* **105B**:1490–1502. [3] D. Mei et al. (2020) *Corrosion Science* **101**:182-192.

ACKNOWLEDGEMENTS: The financial support from the FAPERJ Brazilian research funding (E-26/204.450/2021).

European Cells and Materials Vol. NN. Suppl. N, 20xx (page htu)
ISSN 1473-2262

spray-deposited Ag nanoparticles on implant surface for enhanced bactericidal property and cytocompatibility

Dexin Chen, Peng Zhang, Zhentao Yu, Qiwei Wang

Institute of Advanced Wear & Corrosion Resistant and Functional Materials, Jinan University, 601 Huangpu Avenue West, Guangzhou 510632, China

INTRODUCTION: Metallic implants are highly expected in clinical applications because they can be individually designed and prepared with complex structures while taking into account the excellent corrosion resistance, biocompatibility and mechanical properties of metals. However, due to its surface biological inertness, the ability to promote bone regeneration and inhibit bacterial adhesion is insufficient. In addition, the occurrence of implant-related infections is still a challenge in clinical applications. Therefore, the surface modification of metallic implants to impart antibacterial properties is an urgent problem to be solved. In this work, silver nanoparticles (AgNPs) are deposited on the various surfaces of 3D printed Ti6Al4V by our self-developed spray deposition method. The surface feathers, in vitro biological activity, antibacterial ability, cytotoxicity and compatibility have been studied in details.

METHODS: Ti6Al4V substrates with a size of 10 mm×15 mm×5 mm were prepared by a BLT-S200 Selective Laser Melting System (Bright Laser Technology Co., Ltd). The specimens were firstly applied for surface grafting with silanes. After that, Tollen's reagent (0.1 mol/L $AgNO_3$ and 50 ml/L 25% $NH_3 \cdot H_2O$) and reducing agents (0.1mol/L $C_6H_{12}O_6$) were sprayed onto the TNTs of Ti6Al4V substrate surfaces by using simple spraying bottles, whose diameter of the spray nozzles (made of polymer) is 500 μm.

RESULTS: TiO_2/Ag composite coatings were prepared on these textures by merging anodic oxidation and spray deposition methods. The average diameters of TiO_2 nanotubes (TNTs) on all textures are about 100 nm. On the bottom side of these textures, there are nanopores closely arranged. These TNTs structures produced superhydrophilic properties for the Ti alloy surfaces. To investigate the antimicrobial capability of the samples, antimicrobial characterization was performed using Staphylococcus (S.) aureus and Escherichia (E.) coli, as shown in Fig. 1. The cytocompatibility of the prepared surfaces was tested by co-culturing with the MC3T3-E1 cell, as shown in Fig. 2.

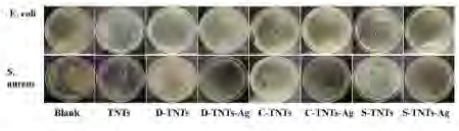

Fig. 1: Representative agar plate culture photos (E. coli and Staphylococcus aureus) of co-culture broth on the surface of samples with different textures after anodization and photografting and spray deposition of AgNPs after anodization

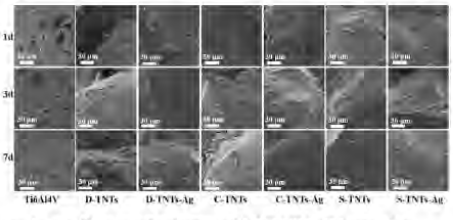

Fig. 1: Cell morphology of MC3T3-E1 on the surface of samples with different textures after anodization and AgNPs deposition

DISCUSSION & CONCLUSIONS: Compared with the untreated Ti surface, the surfaces with texture and TiO_2/Ag composite coatings show the best biological activity, which can promote the deposition of hydroxyapatite in Simulated Body Fluid. The antimicrobial experimental concluded that the texture structures have an enhanced antimicrobial effect. Compared to the planar TNTs, and the complete bactericidal effect was achieved by spray deposition of AgNPs on all different structural surfaces. The cells could adhere and proliferate well on all the surfaces. Interestingly, the AgNPs deposited on the surfaces had a positive role in promoting cell proliferation.

REFERENCES: [1] Y Li, D Chen, Y Sheng, et al (2021) *Surface Innovations* 2021, 9: 166-173. [2] D Chen, Y Li, H He, et al (2021) *Surf Coat Techn* **426**: 127773. [3] D Chen, Y Li, X Zhao, et al (2022) *Surf Coat Techn* **431**: 128010.

ACKNOWLEDGEMENTS: National Natural Science Foundation of China (52105186).

European Cells and Materials Vol. NN. Suppl. N, 20xx (page htu) ISSN 1473-2262

Stronger Absorbable Wire for Small Anatomies

Jeremy E. Schaffer, Adam J. Griebel
Fort Wayne Metals, Fort Wayne, IN, USA

INTRODUCTION: Stronger absorbable wire materials with good degradation profiles can enable valuable new interventions, especially in small vascular anatomies where relative device downsizing is important. Strength levels beyond 2 GPa are a critical ingredient to success in many medical interventions requiring thin gage wire elements. The strongest material used in medical intervention today is tungsten. This cold drawn microwire breaks at greater than 5 GPa with a modulus of elasticity of 400 GPa and is braided into devices such as neurovascular catheters to provide taut handling, elastic kink resistance, and x-ray visibility. Stainless steel with strengths exceeding 2.9 GPa are routinely used in guidewire cores and provide elastic tip navigation power in delivery of Co-Ni-Cr alloy self-expanding braids with strengths exceeding 2 GPa.

Among absorbable device candidates, magnesium alloys can be processed to achieve strength levels of up to 0.6 GPa with good elasticity on account of low stiffness. Monolithic iron alloys, such as FeMnN, can achieve strengths of more than 2 GPa and about 4x Mg-stiffness with a major drawback of localized breakup[1,2]. New strength levels with useful degradation profiles may be possible with alloy and composite strategies.

This paper highlights findings from work on FeMn with N and C additions as well as via composites of FeMn with molybdenum to prospect high strength solutions for eventual downsized device service, such as in neurovascular flow diverters.

METHODS: Molybdenum (Mo), Fe-30Mn-0.10N-0.08C (FeMnNC), FeMnN-DFT-30%Mo (N30Mo), Fe-35Mn-0.10N (FeMnN), and WE22 magnesium alloy were drawn and processed to near maximum strength through grain refinement and cold-working to a diameter of nominally 0.025 mm and then evaluated by tensile testing for strength comparison.

RESULTS: The highly drawn pure molybdenum wire withstood a stress of greater than 3.2 GPa before fracture. Strengths of other materials fell to FeMnNC, N30Mo, FeMnN, and WE22 respectively as 2.5, 2.4, 2.1, and 0.52 GPa. The elastic range of all wires was tested at greater than 1% strain to yield with wide variation in elastic moduli and good plastic yielding in all materials before rupture, indicating some ability to be formed.

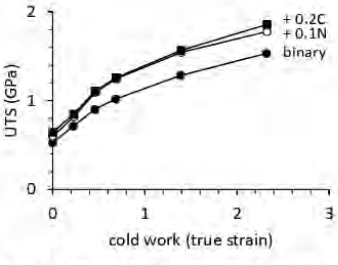

Figure 1. Ultimate tensile strength gains with cold work in Fe-Mn binary and with + 0.10 N or + 0.20 C (both wt.%) wire.

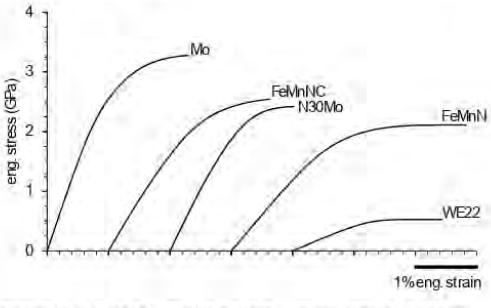

Figure 2. Actual engineering stress-strain curves for a variety of absorbable metal candidates processed to near maximum strength performance.

DISCUSSION: This study shows that certain cold-worked absorbable alloys can exhibit strengths on par with conventional high strength medical wire used in interventional service. Even greater strength and stiffness combinations should be possible with increasing molybdenum composite content while maintaining galvanic deterrent of fragmentation, with potential utility in future low-profile applications.

REFERENCES: [1]J.E. Schaffer, E.A. Nauman, and L. A. Stanciu, *Metal Mater Trans* B 43 (2012): 984-994. [2]A.J. Griebel, et al., *Bioactive Materials* 40 (2024): 74-87.

ACKNOWLEDGEMENTS: The assistance of Dale Herndon, Lane Bailey, Mario Gomez, and the FWM Metlab, is gratefully acknowledged.

European Cells and Materials Vol. NN. Suppl. N, 20xx (page htu) ISSN 1473-2262

Surface treated FeMnCSi biodegradable alloy for medical applications: in vitro study

MI Hankovits[1], JL Merlo[1], N Yasmeen[2], A-M Pappa[2], J Ballarre[1], SM Ceré[1]

[1] *Applied Electrochemistry, INTEMA-CONICET-UNMdP, Mar del Plata, Argentina.* [2] *Department of Biomedical Engineering, Khalifa University of Science and Technology, Abu Dhabi, UAE.*

INTRODUCTION: Biodegradable metallic materials, particularly Fe-based alloys, have emerged as promising candidates for orthopedic implants due to their mechanical strength and controllable degradation rates. However, pure iron's slow degradation and lack of antibacterial activity pose challenges for clinical translation. Alloying with elements like Mn and Si, and introducing surface modifications, may offer enhanced performance [1]. In this study, we investigate a dual-step surface treatment combining phosphate-carbonate pre-treatment with gentamicin-loaded silica nanoparticles (Si-Ge NP) [2] on a FeMnCSi alloy, aiming to improve antibacterial efficacy and blood compatibility.

METHODS: FeMnCSi discs (26.5% Mn, 1.14% Si, 0.50% C) were polished to 1000 grit-paper and subjected to a phosphate-carbonate pre-treatment. Si-Ge NP were synthesized via a modified Stöber method and deposited onto the pre-treated alloy surface. Surface roughness and contact angle measurements were performed for all conditions. Hemocompatibility and platelet adhesion were assessed according to ISO 10993-4:2002. Antibacterial activity against *E. coli* and *S. aureus* was evaluated after 6 h and 24 h. Cell adhesion assays were conducted using NCTC clone 929 mouse fibroblasts at 24 h. Uniaxial tensile tests on the bare metal were performed following ASTM D882-10.

RESULTS: The pre-treatment increased surface roughness (0.131 ± 0.004 µm) and improved wettability, with the lowest contact angle observed (36.4 ± 4.5 °). Hemolysis remained below 5 % in all cases, with the Si-Ge NP condition showing the best performance (3.4 ± 0.5 %), confirming good erythrocyte compatibility. Platelet adhesion displayed mainly activated morphologies with limited aggregation. Antibacterial assays (see Table 1) revealed strong early inhibition, sustained at 24 h only for Si-Ge NP samples. After 24 h, fibroblasts were observed in good density and healthy morphology across all surface conditions. Uniaxial tensile tests yielded a Young's modulus of 13.1 ± 0.05 GPa and a yield strength of 512.7 ± 6.1 MPa.

Table 1. Relative bacterial viability (%) at different times; where 'WM': Without material, 'P': polished, 'P-T': pre-treated, and 'P-T NP': pre-treated and Si-Ge NP.

Bacterial Strain	WM	P	P-T	P-T NP
E. coli (6 h)	100.0 ± 0.1	80.6 ± 10.9	59.1 ± 3.0	23.6 ± 0.1
E. coli (24 h)		151.7 ± 82.0	108.1 ± 33.0	22.8 ± 18.0
S. aureus (6 h)		67.9 ± 17.5	93.2 ± 4.0	93.2 ± 8.0
S. aureus (24 h)		184.4 ± 40.4	153.7 ± 39.0	60.2 ± 2.0

DISCUSSION & CONCLUSIONS: Surface roughness promoted fibroblast adhesion without compromising hemocompatibility. No desirable thrombus formation was observed despite platelet activation. The mechanical properties closely matched those of cortical bone, helping to minimize stress shielding effects. Moreover, the dual-step surface treatment significantly improved antibacterial behavior, particularly in the NP-coated condition, where the sustained release of gentamicin effectively inhibited bacterial growth over time.
These combined results highlight the potential of this functionalized FeMnCSi alloy as a biodegradable orthopedic implant material.

REFERENCES: [1] M. I. Hankovits et al. (2024) *FeMnCSi alloy for degradable pin implants: Surface and in vitro characterization*, Mater. Chem. Phys. 323 129565. [2] J. Ballarre et al. (2020) *Versatile bioactive and antibacterial coating system based on silica, gentamicin, and chitosan: Improving early-stage performance of titanium implants*, Surf. Coatings Technol. 381 125138.

ACKNOWLEDGEMENTS: PIP 2014-2016, PUE 073, PICT 2019-02760, ING652-15/G648, Tenax S.A., Dr. J. Malarría, Dr. A. V. Druker, Dr. D. Colombo, Biochem. L. Malvestiti, Dr. G. Martinez, and Dr. L. Di Meglio.

European Cells and Materials Vol. NN. Suppl. N, 20xx (page htu) ISSN 1473-2262

Tailoring surface quality and geometrical accuracy in additive manufacturing of biodegradable Mg/Zn alloys via powder quality and laser process control

S Pöstges[1], T Poel[1], F Fischer[2], M Voshage[2], A Kopp[1]

[1] *Meotec GmbH, Aachen, Germany.* [2] *Chair for Digital Additive Production DAP, RWTH Aachen University, Aachen, Germany*

INTRODUCTION: Biodegradable metals, especially zinc (Zn) and magnesium (Mg) alloys, hold considerable promise for biomedical uses, particularly in the development of temporary implants that naturally break down in the body. Recent research has shown that additive manufacturing (AM) can be effectively applied to these materials, enabling the creation of patient-specific implants with intricate and complex geometries[1,2]. This study explores the effect of powder quality and laser process control on the surface quality and geometrical accuracy of AM Mg/Zn parts in as-built state.

METHODS: Gas atomized, pre-alloyed Zn0.5Mg, conventional WE43 as well as medical grade WE43MEO powder is used to carry out the tests. All specimens are manufactured using a modified Laser Powder Bed Fusion system from *Aconity 3D GmbH* adapted to the use of biodegradable, low melting alloys. The effect of the powder quality is studied by comparing thin-walled lattice structures made out of conventional and medical grade powder whereas the influence of the laser parameters is investigated on both, full volume and thin-walled structures. A total of 18 specimens are fabricated with different volume energy density and spot diameter. Additionally, the overhang behaviour is studied by variation of the inclination.

RESULTS: In as-built state, the geometric accuracy is significantly increased when using medical grade WE43MEO powder as shown in Fig. 1. In the top view (Fig. 1 a) and c)), the strut size is decreased from 425,56 ± 17,38 µm for conventional WE43 to 387,11 ± 14,09 µm with WE43MEO. For the perpendicular planes (Fig. 1 b) and d)) this effect is even more visible.

The investigation on Zn0.5Mg demonstrated that a volume energy density of 133,33 J/mm³, when combined with a spot diameter of 80 µm, yields samples with high relative density. However, this parameter combination results in low geometric accuracy, particularly for samples with inclination angles below 45°, which cannot be reproducibly fabricated. By increasing the volume energy density to 170 J/mm³ and the spot diameter to 100 µm, samples with inclination angles of 30° and above are reliably fabricated.

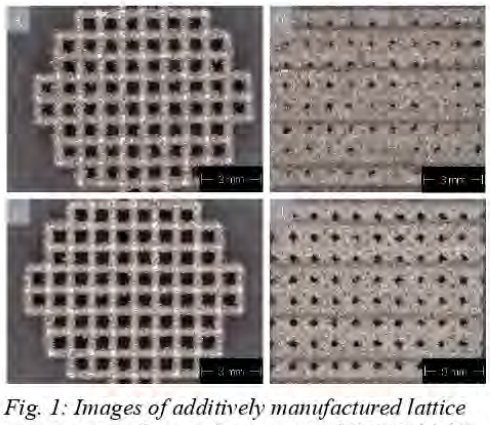

Fig. 1: Images of additively manufactured lattice structures made out of conventional WE43 (a)-b)) vs. WE43MEO (c)-d))

DISCUSSION & CONCLUSIONS: These results highlight the critical role of material selection and parameter tuning in balancing geometric precision and structural integrity for biomedical implants. While for Mg alloys the use of medical grade WE43MEO improves dimensional control, zinc alloys (e.g., Zn0.5Mg) require careful adjustment of energy density and laser intensity to overcome trade-offs between relative density and dimensional accuracy. This underscores the potential for patient-specific biodegradable implants but emphasizes the need for process optimization tailored to material behavior.

REFERENCES: [1]Y. Wu (2022) *Additive manufacturing of Zn-Mg alloy porous scaffolds with enhanced osseointegration: in vitro and in vivo studies*, Materials Science and Engineering: C, 134. [2]M. Voshage et al (2022) *Additive Manufacturing of biodegradable Zn-xMg alloys: Effect of Mg content on manufacturability, microstructure and mechanical properties*, Materials Today Communications 32: 1-9.

ACKNOWLEDGEMENTS: This work has received funding from the Federal Ministry of Education and Research funding indicator 03RU1U173A

European Cells and Materials Vol. NN. Suppl. N, 20xx (page htu) ISSN 1473-2262

Ultrasonic atomization of medical grade Mg alloys for additive manufacturing

J Cruz[1], F Wisotzki[1], A Mainguy[1,2], H Mescheder[3], S Pöstges[1], A Kopp[1]

[1]*Meotec GmbH, Aachen, Germany.* [2]*IMDEA Materials Institute, Getafe, Spain.*

[3]*Fraunhofer Institute for Production Technology IPT, Aachen, Germany*

INTRODUCTION: Additive manufacturing (AM) of magnesium alloys has gained significant attention in medical applications due to the ability to create complex, patient-specific structures[1]. Powder production plays a critical role in the outcomes of AM, as the properties of the powder directly impact the quality and precision of the manufactured parts[1,2]. Ultrasonic atomization (UA) enables the production of powders with a narrow size distribution, spherical particles, and minimal impurities. However, given their limited commercial availability, thorough characterization of the powders produced by UA-based systems is essential to ensure they meet the requirements of AM applications[2]. This study investigates the UA of WE43MEO and ZX00MEO powders using two different feedstock configurations (rod feeder and crucible) and evaluates their morphological and size distribution characteristics.

METHODS: The input materials used were 6.0 mm diameter rods of WE43MEO and ZX00MEO (Meotec GmbH, Aachen, Germany). Powder production was carried out using the ATO Lab Plus system with the Induction Melting System (IMS) module (3D Lab, Warsaw, Poland). The ZX00MEO powder was processed using the rod directly in the rod feeder setup, while the WE43MEO rod was cut to fit into the crucible. The reverse feedstock configurations will be tested to complete the study. The powders were sieved to below 90 µm prior to characterization. Morphology was characterized by using a 3D laser scanning microscope (Keyence VK-X100). The particle size distribution (PSD) was determined from Laser Scanning Microscopy (LSM) images using ImageJ (NIH, Bethesda, MD, USA), with D10, D50, D90, and span calculated, and the mean particle size and circularity also reported. Further characterization via Scanning Electron Microscopy (SEM) combined with Energy Dispersive Spectroscopy (EDS) is planned to provide a more detailed analysis of the particle size, morphology, and chemical composition of the powders.

RESULTS: WE43MEO powder showed D10 of 26.2 µm, D50 of 72.5 µm, and D90 of 91.4 µm, while ZX00MEO showed D10 of 20.7 µm, D50 of 65.6 µm, and D90 of 87.9 µm. The calculated span was 0.90 for WE43MEO and 1.02 for ZX00MEO. Mean particle sizes were 66.4 ± 22.7 µm (WE43MEO) and 62.4 ± 22.9 µm (ZX00MEO). Circularity analysis indicates high sphericity for both powders: 0.94 ± 0.04 (WE43MEO) and 0.95 ± 0.06 (ZX00MEO). LSM imaging (Fig. 1) confirmed generally spherical morphology, with some irregular particles observed.

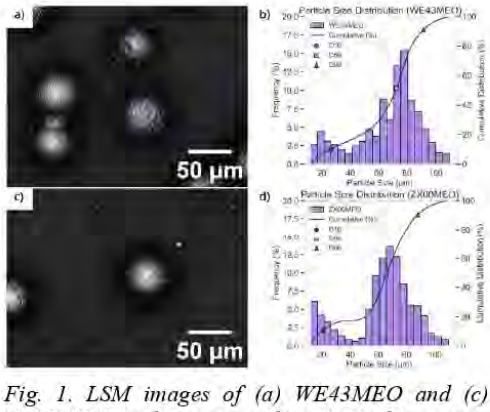

Fig. 1. LSM images of (a) WE43MEO and (c) ZX00MEO and corresponding PSD histograms with cumulative distribution plotted for (b) WE43MEO and (d) ZX00MEO.

DISCUSSION & CONCLUSIONS: The preliminary results demonstrate that UA via induction melting can produce fine, spherical Mg alloy powders suitable for AM applications. Both alloys exhibited high sphericity and acceptable PSDs. Completion of the full experimental matrix will allow further assessment of the influence of atomization setup and alloy type on powder properties. Planned SEM and EDS analyses will provide deeper insights into microstructure and compositional uniformity. Future work will also focus on process optimization.

REFERENCES: [1]Zeng, Z. et al. *J. of Magnes. Alloys* **10**, 1511–1541 (2022). [2]Khan, S. A. et al. *Powder Technol.* **455**, 120725 (2025).

ACKNOWLEDGEMENTS: This project has received funding from the European Union's Horizon 2020 research and innovation programme under Marie-Sklodowska Curie grant agreement ID no. 101120006.

17th Biometal
25-30 AUGUST, 2025
Grand Hôtel San Michele,
Cetraro, CS, Italy

European Cells and Materials Vol. NN. Suppl. N, 20xx (page htu) ISSN 1473-2262

A Finite Element Model for crimping and free deployment in the design of bioabsorbable metallic coronary stents

Diego Blunda[1], Ted J. Vaughan[1]

[1] *Biomedical Engineering, School of Engineering, College of Science and Engineering, University of Galway*

INTRODUCTION: Cardiovascular diseases (CVDs) are the leading global cause of death[1], with myocardial infarction, due to coronary artery occlusion, being a common manifestation[1]. Percutaneous Transluminal Coronary Angioplasty (PTCA) with drug-eluting stents (DES) is the current standard treatment to prevent infarction. While effective, DESs pose risks such as chronic inflammation, late thrombosis and restenosis due to their permanent presence in the body[2,3]. Bioresorbable stents, which degrade over time, offer a promising alternative by providing temporary support until the vessel heals and re-endothelializes[3]. Magnesium is a promising material for bioabsorbable stents, but its lower mechanical strength compared to DESs and manufacturing challenges necessitate innovative design solutions. This study focuses on the design and optimization of a thin-strut Mg/Zn bioresorbable coronary stent, with the first phase developing a crimping and free deployment finite element model (FEM) of an older Bare Metal Stent provided by B.Braun, Melsungen, to analyze the impact of geometric parameters on stent performance. Next steps include the optimization of novel stent concepts, and the usage of a corrosion model and its calibration on experimental data of magnesium components.

METHODS: To develop the crimping and free deployment FEM, the Abaqus finite element solver was used. Figure 1 illustrates the process, involving several components: an internal rigid shaft, a folded balloon, the stent (CoroFlex Blue, B.Braun), and crimping tools. The balloon's geometry, obtained by previous simulations similar to the one described by Geith et al.[4] was modelled using a hyperelastic (1st order Ogden) material, with parameters fitted from nylon testing.

The stent geometry, derived from data provided by B.Braun, featured a hybrid-cell design and was assigned an elasto-plastic material model to simulate the CoCr L605 alloy (E = 240.74 GPa, ν = 0.3). The crimping tools (n = 12) were modelled as rectangular rigid bodies.

The simulation consisted of five steps: in the first step, the crimping tools crimp the stent onto the folded balloon; in the second step, the crimping tools were removed; in the third step, the stent was deployed by inflating the balloon, in the fourth step, the balloon was deflated, allowing for the observation of stent recoil and, in the fifth, the stent was radially crimped. The simulation was performed using the SIMULIA Abaqus FEA explicit solver.

Experimental deployment and crimping studies were conducted to validate the model.

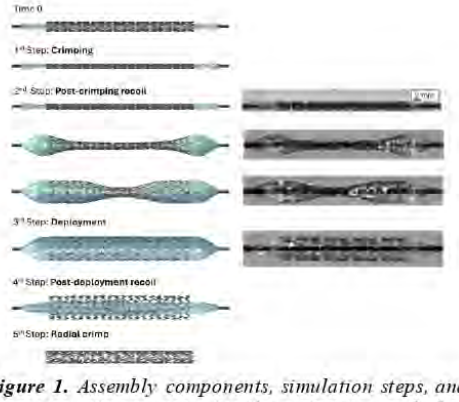

Figure 1. *Assembly components, simulation steps, and important time points in the crimping and free deployment simulation, compared to a study from literature*[5].

RESULTS: The simulation results (Figure 1) showed that the stent was effectively crimped onto the balloon, undergoing plastic deformation. In the second step, the stent recovered its elastic deformation. The stent was expanded to a maximum internal diameter of approximately 4 mm, which resulted in a peak von Mises stress of ~1750 MPa. Then, during the fourth step, the overall stent recoil was approximately 4.79%, which closely resembles the one obtained by B.Braun experimental test data (4.7%). Finally, the stent was radially tested to obtain the radial force-diameter curve. A qualitative comparison with a study from literature reveals an almost perfect agreement. The quantitative comparison against experimental data validates the model.

DISCUSSION & CONCLUSIONS: This study demonstrated an efficient and rigorous validated FEM for crimping and deployment, which will be utilized to design and optimize biodegradable coronary stent designs. As observed, the stent recoil value of 4.79% is almost identical to the 4.7% indicated by B.Braun experimental deployment test data. Also, the pressure-diameter curve during expansion and the radial force-diameter curve during the radial test validate the model.

REFERENCES: [1] WHO, Cardiovascular diseases (CVDs) Fact Sheet, 2021. [2] Kapoor *et al.*, Materials and Design, 2023. [3] Udriste *et al.*, Materials, 2021. [4] Geith *et al.*, International Journal for Numerical Methods in Biomedical Engineering, 2019. [5] Wiesent et al., PLOS ONE., 2019.

European Cells and Materials Vol. NN. Suppl. N, 20xx (page htu) ISSN 1473-2262

Development of bioabsorbable metals for endovascular medical devices: a presentation of the BIOMEND Doctoral Network

A Mainguy[1,2,3], K Mashoufi[1,2,3], J Cruz[1,4,5], M Thiel[6,7], S Schmidt[1,6], V Squartecchia[1,2,3], D Blunda[1,6,8], J Sygor[1,9,10], A Di Lorenzo[5,7,11], M Bittner[6,7], M Rodrigues[5,7,11], S O'Connell[6,12], A Fathy[13,14], A Panagi[15,16], T Vaughan[6], A Kopp[1,7,16]

[1]Meotec GmbH, Aachen, Germany, [2]IMDEA Materials Institute, Getafe, Spain, [3]Universitat Politecnica de Madrid, Madrid, Spain, [4]Lehrstuhl für Lasertechnik, Aachen, Germany, [5]RWTH University, Aachen, Germany, [6]University of Galway, Galway, Ireland, [7]Fibrothelium GmbH, Aachen, Germany, [8]B. Braun, Melsungen, Germany, [9]University of Eastern Finland, Kuopio, Finland, [10]Abiomed GmbH, Aachen, German, [11]BioTex – Biohybrid & Medical Textiles, Aachen, Germany, [12]Hydrumedical SA, Guimarães, Portugal, [13]Embocraft GmbH, Aachen, Germany, [14]OVGU, Magdeburg, Germany, [15]MERLN, Maastricht University, Maastricht, Netherlands, [16]Medical Magnesium GmbH, Aachen, Germany

INTRODUCTION: BIOMEND is a Doctoral Network focused on three major axes in bioresorbable devices. The first axis (WP1) is the development of alloying systems and manufacturing methods for the production of endovascular medical devices (EMD). The second axis (WP2) is focused on the design of EMD prototypes using experimental and analytical approaches. The third axis (WP3) consists in the preclinical validation of afore-mentioned EMD prototypes.

METHODS: PhD candidates of WP1 are focused on producing stent preforms. To achieve this, they are using gravity permanent mold casting of magnesium (Mg) and zinc (Zn) alloys are considered for their biocompatibility and favorable corrosion properties. This is followed by double extrusion of the cast material. After rods are produced with the first extrusion, the second extrusion is either a wire extrusion to achieve thin wires for wire-braided devices, or a microtube extrusion to produce laser-cut devices. Laser cutting and wire braiding are also explored within the scope of the BIOMEND project. Within WP1, the degradation behavior of these materials is also investigated, both in *in silico* simulations and in experimental setups.

Fig. 1: Graphical representation of WP1 workflow

In WP2, the devices developed by the PhD students are strongly interconnected with the methods investigated in WP1. A coronary stent, aortic stent-graft and large bore access closure will all benefit from the development of laser-cut preforms. A flow-diverting stent, intracranial stent and urethral stent will take advantage of the latest advances in wire braiding methods. A device for anastomosis, along with other devices, will also gain from the development of Mg alloys with increased corrosion resistance.

On one hand, some of these devices are developed with the help of simulations for mechanical performance, e.g. radial strength, crimping and crush resistance. On the other hand, experimental methods are used to validate simulations and conduct in-vitro biocompatibility studies. Bench testing will assess mechanical performance and corrosion behavior of devices.

WP3 focuses on testing the in-vivo biocompatibility and functional performance of devices developed within WP2. Small animal models will be used to assess the performance of endovascular devices and their bioresorbability. Histology and imaging techniques such as intravascular ultrasound (IVUS) and angiography are in the scope of the BIOMEND project.

RESULTS: Preliminary results will be presented individually by the PhD students present at the Biometals conference.

ACKNOWLEDGEMENTS: This project has received funding from the European Union's EU Framework Programme for Research and Innovation Europe Horizon. Grant Agreement n°101120006.

European Cells and Materials Vol. NN. Suppl. N, 2025 (page htu) ISSN 1473-2262

Colour-changing smart materials inspired by nature : Chameleon effect

Karine Mougin[1], Arnaud Spangenberg[1]

[1]*Institut de Science des Matériaux de Mulhouse, 15 rue Jean Starcky, 68057 Mulhouse, France*

INTRODUCTION: Nature's inventiveness often inspires human innovation. Indeed, numerous living organisms rapidly alter their appearance in response to changes in their environment. For instance, the most famous one is chameleon that is able to change color for camouflage, by adjusting the spacing of tiny, crystal-like cells called iridophores, which reflect light at different wavelengths. Cephalopods, like octopuses, have a similar behavior to hide from predators and use chromatophores—pigment cells controlled by muscles that allow for rapid color change. Inspired by these impressive examples, researchers have developed different strategies to create surfaces or materials able to adapt and change of color in response to their surroundings too. Actually, today, there are various sensitive, reactive, these so-called **intelligent compounds transform and change color in response of an external disturbance** such as the effect of temperature, optical excitation or mechanical stimulation (stretching, shock). Our approach was also inspired from nature and the idea was to create a novel hybrid material able to color change of surfaces at will [1]. The key element of this novel technology is based on the combination of two phenomena observed in the nature and transferable to material science: plasmonic and structural colors. The developed functional nanomaterial is composed of colloidal metallic nanoparticles (NPs) that are properly synthesized and assembled into polymer to ensure a variety of plasmonic colors under mechanical stresses.

METHODS: The matrix materials are different kind of polymers such as shape memory polymer (Tecoflex™) or polyvinylalcohol or elastomer. In a vial, polymer (ca. 100 mg) was dissolved in 1 mL of adapted solvent (water, DMF for instance) with the help of heating and stirring. Once done, 20 µL of a 100 mM aqueous gold solution was added with a micropipette. When the reducer has finished dissolving and the sample had its final color, the vial was placed in the oven where it was subjected to a dynamic vacuum.

RESULTS: In the world of nanomaterials, colloidal metallic nanoparticles (NPs) occupy a privileged position as their shape and size can be easily chemically tuned by varying the solution composition and relative reactant concentrations. In addition, one key component in the assembly of nanoparticles is their precise positioning to enable the creation of new complex structures. Controlling the nanoscale interactions is crucial for predicting and understanding of the behaviour of NPs in a matrix. Recently, Han *et al.* embedded nanoparticles into a polymer matrix and demonstrated that the sample color changed after a plastic deformation of the polymer as the distance between the nanoparticles changes in this way [2]. Plastic deformations, however, are hard to control. Therefore, our approach has been based on various polymer such as shape memory polymers and elastomers that allow comparable large deformations by a trigger like force, heat, humidity, electric and/or magnetic fields (Figure 1).

Fig. 1: Color changing material: a. Polyvinylalcohol polymer filled with Au NPs under mechanical stress b. 3D printed polyurethane polymer nanocomposite under hydric stress c. Scheme of photothermal activation of a nanocomposite.

DISCUSSION & CONCLUSIONS: The characteristics of this new hybrid material can be defined as an "***Intelligent***" material as it is able to achieve the required color on demand, "***Active***" as it responds quite instantaneously to a customer demand. Changing colors on demand is a new approach to modify consumer products. These impressive results in coloring have been motivated by combining plasmonic colors with different polymer and technologies to produce surface colors at will. These nature-inspired innovations are advancing applications in robotics, consumer products (inks, paints), wearable tech, sustainable packaging and medical products.

REFERENCES:. [1]K.Mougin et al. Advanced Functional and Structural Thin Films and Coatings, 74, 847–852, (2022), [2]X. Han et al. (2014), *Nano Letters* **14**, 2466.

ACKNOWLEDGEMENTS: The authors thank CNRS financial support.